THE EVOLUTION OF FUEL NITROGEN DURING THE VAPORIZATION OF HEAVY FUEL OIL DROPLET ARRAYS

by

SIMON PETER HANSON

S.B., Massachusetts Institute of Technology
(1974)

SUBMITTED IN PARTIAL FULFILLMENT
OF THE REQUIREMENTS FOR THE
DEGREE OF

DOCTOR OF SCIENCE

at the

MASSACHUSETTS INSTITUTE OF TECHNOLOGY

April 26, 1982

Sc.D. June 1982

Signature of Author _____
Department of Chemical Engineering, April 26, 1982

Certified by _____
Janos M. Beér, Thesis Supervisor

Certified by _____
Adel F. Sarofim, Thesis Supervisor

Accepted by _____
Glenn C. Williams, Chairman
Departmental Committee on Graduate Theses

THE EVOLUTION OF FUEL NITROGEN DURING THE VAPORIZATION OF HEAVY FUEL OIL DROPLET ARRAYS

by

SIMON PETER HANSON

Submitted to the Department of Chemical Engineering on April 26, 1982 in partial fulfillment of the requirements for the degree of Doctor of Science

ABSTRACT

The objectives of this investigation were to identify the significant factors influencing the vaporization of multicomponent fuel droplets, to show how these factors affect the rate of evolution of nitrogenous species from heavy fuel oils and to indicate the functional dependencies of the factors involved. Experiments were performed in a laminar flow drop-tube furnace on a linear array of 150 μm diameter fuel particles. The conditions to which the particles were subjected conformed to those found in the first stage of a multi-staged combustor.

Data on the evolution of fuel-nitrogen and rates of vaporization in an inert atmosphere at temperatures between 1000 K and 1400 K were obtained for a raw Paraho shale oil, a Gulf Coast No. 6 petroleum fuel oil, and Indo-Malaysian No. 6 Petroleum fuel oil, an SRC-II middle distillate fraction, an SRC-II heavy distillate fraction, an SRC-II 2.9:1 blend of middle and heavy distillate fractions, and n-dodecane doped with pyridine, quinoline or acridine. The evolution of fuel-nitrogen and residual carbon to hydrogen ratios of vaporizing droplet arrays of these fuels was compared with similar data obtained from equilibrium batch distillation experiments. It was found that the fuel-nitrogen evolution from vaporizing droplets differs significantly from that found from equilibrium batch distillation. The difference is due to diffusional resistance in the interior of the droplets which modifies the liquid surface composition, thereby changing the contribution of fuel components in the vapor phase.

The nitrogen evolution from droplets of fuels which contain their nitrogen primarily in the heavier fuel components was greater than batch distillation nitrogen evolution at equivalent extents of vaporization. However, for fuels in which the nitrogen content is associated with the intermediate molecular weight fuel species, the nitrogen evolution from vaporizing droplets is retarded in comparison to batch distillation nitrogen evolution, and the degree of retardation is temperature dependent. The observed behaviors during droplet vaporization result from an initial preference for the evolution of light, volatile, mobile components followed by an accelerated evolution of heavy fuel species. The extent of vaporization at which the change of prefrence occurs depends upon the fuel composition and the rate of vaporization.

A mathematical model of the internal concentration profiles of a multicomponent fuel droplet which obeys the "d^2-Law" of vaporization was developed and applied to the doped n-dodecane fuels. Agreement between the experimental data and theoretical results confirmed the difference between droplet vaporization and batch distillation results to be due to competition between diffusion in the liquid phase and vaporization at the phase boundary. The concentration profiles are given by the equation

$$\frac{m-m_o}{m_f-m_o} = G(\tau) + \sum_{\text{all } a} B_a \, M(a,\tfrac{3}{2},Z) \, (G(\tau) + H_a(\tau))$$

where

$$G(\tau) = 1 - e^{-b\tau}$$

and

$$H_a(\tau) = (1+K\tau)^a - 1 + \sum_{\text{all } a} (-1)^r \left(\frac{K}{b}\right)^r \left\{\prod_{q=0}^{r-1} (a-q)\right\} \left((1+K\tau)^{a-r} - 1 + G(\tau)\right)$$

The equation is in a normalized (Z, τ) reference frame which incorporates the effect of surface regression. The values for 'a' are all negative and unique for a particular (λ/D). The value of 'b' is a time constant in $G(\tau)$ for the rate of change of surface concentration of a fuel component and is a consequence of the coupling of mass transfer in the liquid phase and heat transfer in the gas phase by the thermodyanmic vaporization driving force (m_s-m_v). Increasing the rate of vaporization, or having a fuel component with lower diffusivity i.e. larger (λ/D), causes the vaporization to be more diffusionally limited. However, the point at which diffusional limitation controls is determined when $G(\tau) + H_a(\tau) = 0$ which is strongly dependent upon component volatility, 'b'. Nevertheless, for binary mixtures volatility initially controls the vapor composition during droplet vaporization, following which diffusional limitation controls, the extent of vaporization for this transition being smaller for large values of (λ/D) and 'b'.

Thesis Supervisors: Janos M. Beér
Professor of Chemical Engineering

Adel F. Sarofim
Professor of Chemical Engineering

MASSACHUSETTS
INSTITUTE OF TECHNOLOGY

DEPARTMENT OF
CHEMICAL ENGINEERING

Room number: 66-419

Cambridge, Massachusetts
02139

Telephone: 3-6479

April 26, 1982

Professor Newton
Secretary of the Faculty
Massachusetts Institute of Technology
Cambridge, Massachusetts 02139

Dear Professor Newton:

In accordance with the regulations of the faculty, I herewith submit a thesis, entitled, "The Evolution of Fuel Nitrogen During the Vaporization of Heavy Fuel Oil Droplet Arrays," in partial fulfillment of the requirements for the degree of Doctor of Science in Chemical Engineering at the Massachusetts Institute of Technology.

Respectfully submitted,

Simon Peter Hanson

SPH/sjk

ACKNOWLEDGEMENTS

The author would like to express his gratitude to the many people who made this thesis possible. In particular he would like to thank:

Professor J.M. Beér

Professor A.F. Sarofim

Dr. A.K. Gupta

No words are able to express my debt to these three, who so generously gave of their wisdom, time and friendship. Thanks are also due to:

Mr. A. Pukt, whose advice and skill helped create impossible designs in the machine shops of M.I.T.

Ms. L. Fong who patiently assisted in every way possible during the developmental stages of the equipment.

Mr. T.P. Tsang, Mr. E. Yu, and Mr. A. Mitra, who assisted in the acquisition of experimental data.

Ms. S. Kreuz, for her excellent typing of this thesis.

This research was funded under EPA grant No. 805552030 and EPRI contract No. RP1412-6.

During the course of any research project innumerable people play a role, and thus the author wished to include thanks to those who, due to failing memory, were not mentioned.

In memory of my father.

TABLE OF CONTENTS

Page

LIST OF FIGURES

Figure No. Page

LIST OF TABLES

CHAPTER 1

SUMMARY

It is expected that in the near future, fossil fuels to be burnt in the United States will have high nitrogen content and high carbon to hydrogen atomic ratios. The nitrogenous components of these fuels are preferentially converted to nitric oxide during fuel-lean combustion. The most effective methods for limiting the formation of nitric oxides from the fuel-nitrogen require the fuel-nitrogen to be evolved, and undergo gas phase reactions, in an oxygen deficient environment.

The evolution of fuel-nitrogen from multicomponent fuel droplets is controlled by the coupling of transport processes in the gas and liquid phases through the thermodynamic equilibria between phases. The objective of this investigation has been to identify those factors of significance during the vaporization of multicomponent fuel droplets, to show how these factors may influence the rate of evolution of nitrogenous species from heavy fuel oils, and to indicate the functional dependencies of the factors involved.

By comparison of the equilibrium distillation composition history of a fuel with composition variation of linear arrays of 150 micrometer fuel droplets subjected to high temperature (1000 K - 1400 K) helium environments, the importance of mechanisms that cause species differentiation is indicated. Equilibrium batch distillations at atmospheric pressure are performed using conventional techniques. The acquisition of time resolved pyrolysis data at various rates of vaporization is accomplished using a laminar flow drop tube furnace, Fig. 1.1. The furnace has a vertical uniformly heated test section 300 mm long and 50 mm in diameter with optical access. The droplet array is introduced downwards on the long-

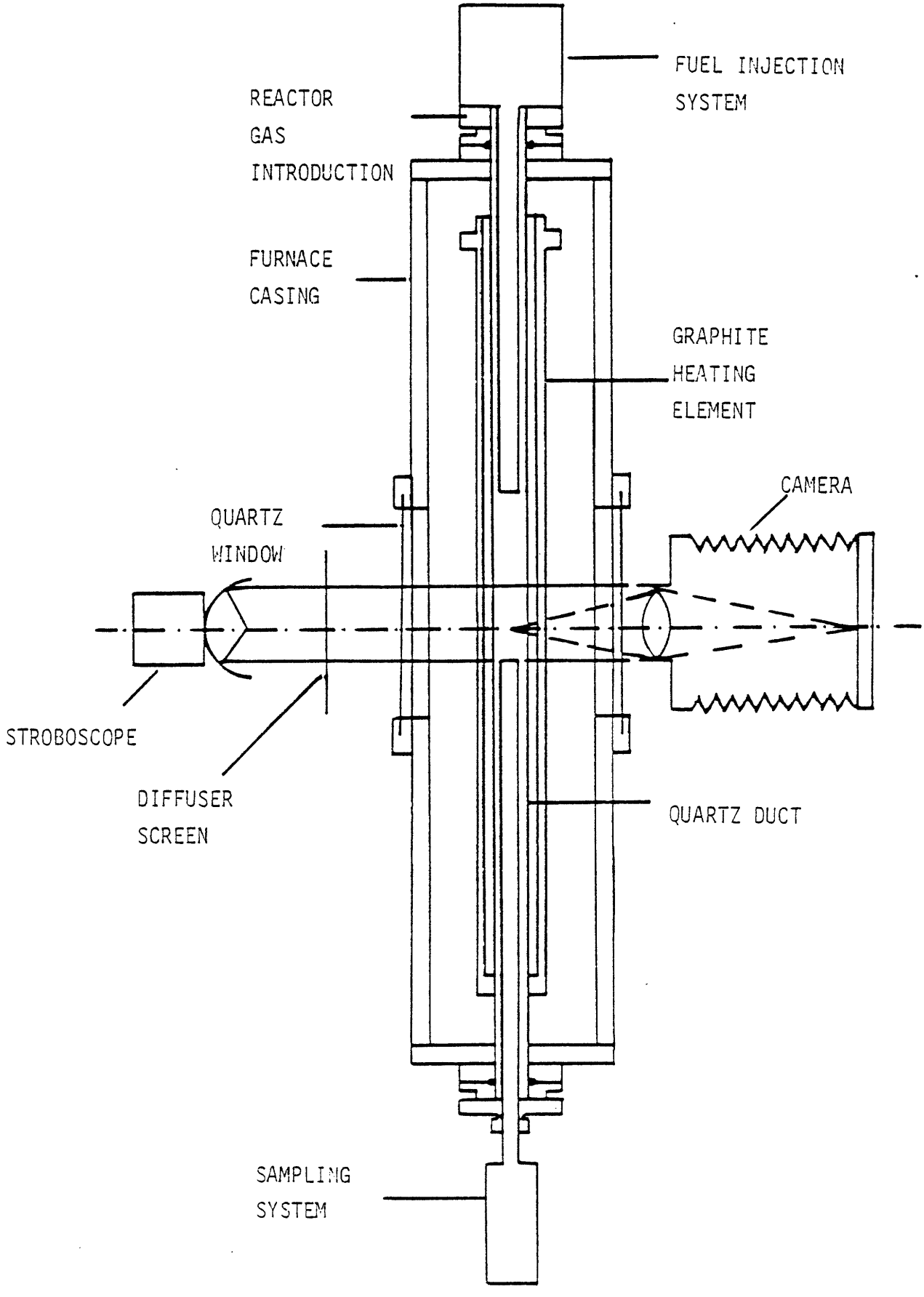

FIGURE 1.1 Schematic of Experimental System

itudinal axis by means of a vibrating orifice droplet generator, concurrently with the ambient helium. The droplet stream is interrupted at several positions in its trajectory by a sampling probe inserted through the base of the furnace. The probe quenches and transports the entire flow of the furnace to a sampling train which recovers the fuel droplet residue for analysis. A record of droplet size and velocity is obtained photographically to provide a measure of residence time and droplet surface regression for correllation against mass recovered.

The fuel oils studied in the aforementioned fashion include: a Gulf Coast No. 6 petroleum fuel oil; an Indo-Malaysian No. 6 fuel oil; a raw Paraho shale oil; and three solvent refined coal liquids (SRC-II), a light distillate fraction, a heavy distillate fraction, and a 2.9:1 blend of light and heavy distillate fractions. The results of experiments with these fuels showed the nitrogen evolution from pyrolysing droplets to differ significantly from that obtained by batch distillation at atmospheric pressure. This difference in behavior is a consequence of the diffusional resistance within the droplets. In order to more clearly observe the effect of liquid phase diffusion on the evolution of nitrogenous compounds having different volatilities, experiments were performed using n-dodecane doped with pyridine, quinoline or acridine. The results obtained from the model fuels were complemented by a theoretical description of the liquid phase temporal and spatial concentration of a fuel component in a vaporizing droplet for which the size varies according to a "d^2-law". The mathematical description confirmed the importance of diffusion, and moreover that liquid phase concentration profiles were determined by the ratio of surface regression velocity and diffusive velocity as represented by λ/D, and the relative volatility of each component at the droplet surface with respect to the other

fuel compounds.

The properties and compositions of fuel oils studied are presented in Table 1.1. Data for the equilibrium evolution of fuel-nitrogen for these fuels are displayed in Figs. 1.2 and 1.3. The petroleum based fuels retain most of their nitrogen in the residue, thus the nitrogen containing components are associated with the higher molecular weight species. The shale oil and SRC-II fuels all evolve their nitrogen more or less uniformly with mass vaporized.

The data for fuel-nitrogen evolution from rapidly vaporizing droplet arrays, Fig. 1.4 to 1.7, show a variety of behaviors. In all cases a departure from equilibrium nitrogen evolution is observed. The petroleum based fuels show a strongly accelerated nitrogen evolution which is not influenced by the rate of vaporization as indicated by furnace temperature. The shale oil exhibits an initially prefential evolution of nitrogen free material which increases with increasing rate of vaporization. The light distillate fraction SRC-II evolves nitrogen in a manner similar to the shale oil. The heavy distillate fraction SRC-II and 2.9:1 blend SRC-II show a slightly increased rate of nitrogen evolution without any obvious effect of furnace temperature. Generally, those fuels having most of their nitrogen associated with heavier fuel species evolve their nitrogen more rapidly, and those fuels having nitrogen associated with intermediate molecular weight species evolve their nitrogen less rapidly and exhibit a temperature dependent nitrogen evolution.

The differentiation of fuel species, over that affected by volatility differences, represented by the equilibrium distillation data, results from diffusional resistance in the liquid phase. The droplets are spherical, and due to their small size and rapid rates of vaporization, internal circula-

	(i)	(ii)	(iii)	(iv)	(v)	(vi)
Ultimate Analysis, %:						
Carbon	88.29	87.50	83.63	83.82	89.11	86.28
Hydrogen	12.31	12.41	11.81	9.07	7.49	8.83
Nitrogen	0.44	0.23	2.21	0.97	1.21	0.96
Sulfur	0.47	0.22	0.69	0.20	0.39	0.26
Oxygen	0.86	1.04	1.18	5.43	1.90	4.18
Ash	0.01	0.04	0.09	0.00	0.06	0.01
Water and Sediment	none		1.6	0.00		0.04
Flash Point, °C	149	99	102	64	129	66
Pour Point, °C	8	16	29	<-30	-13	<-30
Gross Heat of Combustion, MJ/kg	43.89	44.36	42.86	39.54	39.82	39.80
Specific Gravity @ 15°C	0.9309	0.9230	0.9279	0.9765	1.0655	0.9972

TABLE 1.1

Fuel Properties of (i) Gulf Coast No. 6 Petroleum Fuel Oil, (ii) Indo-Malaysian No. 6 Petroleum Fuel Oil, (iii) Raw Paraho Shale Oil, (iv) SRC-II Middle Distillate Fraction, (v) SRC-II Heavy Distillate Fraction, and (vi) SRC-II 2.9:1 Blend Middle and Heavy Distillate Fractions

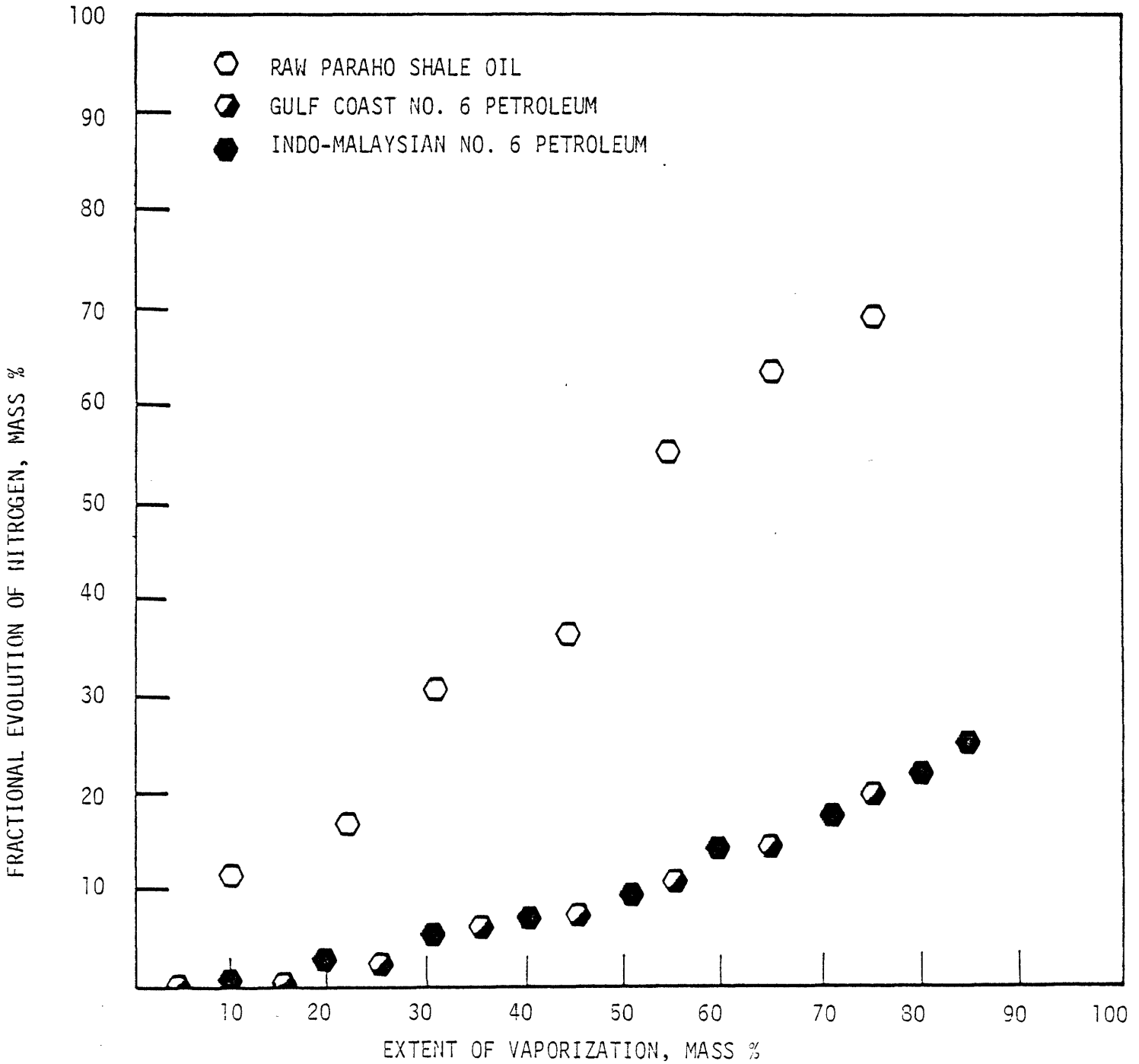

Figure 1.2 Nitrogen Evolution During Equilibrium Batch Distillation of Gulf Coast No. 6 Petroleum Oil, Indo-Malaysian No. 6 Petroleum Fuel Oil, and Raw Paraho Shale Oil

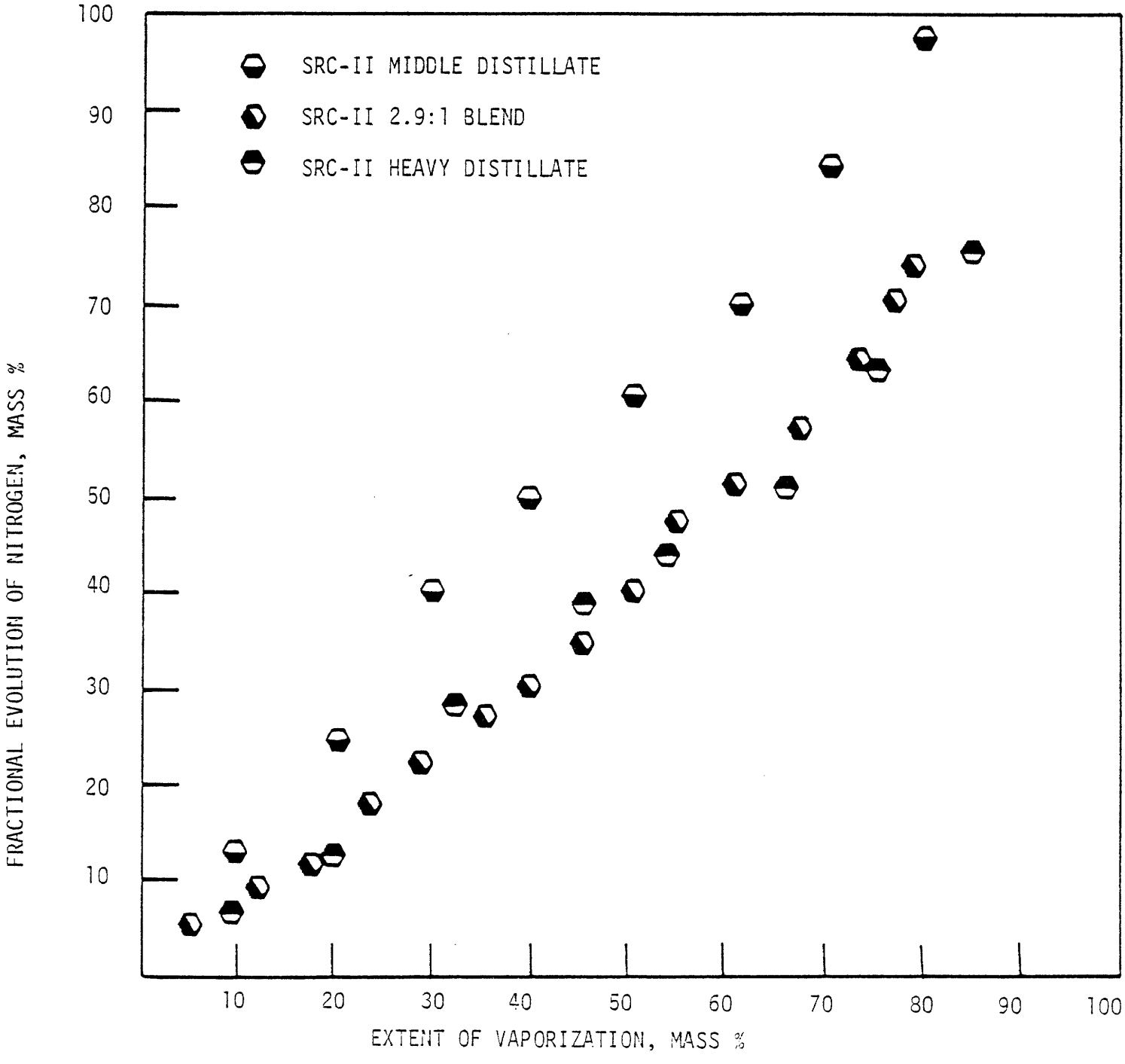

Figure 1.3 Nitrogen Evolution During Equilibrium Batch Distillation of SCR-II Middle Distillate Fraction, SRC-II Heavy Distillate Fraction, and SRC-II 2.9:1 Blend Middle and Heavy Distillate Fractions

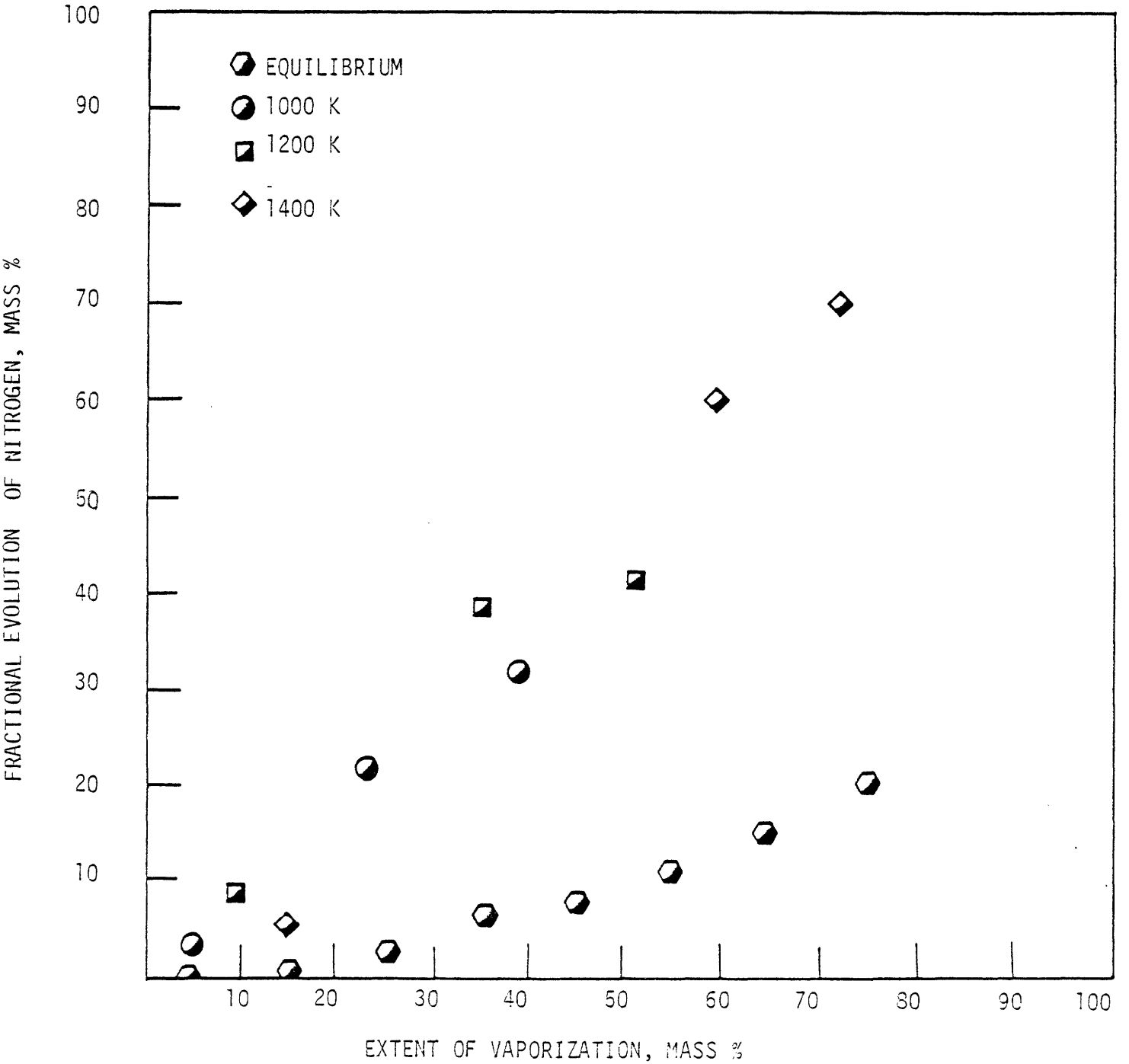

Figure 1.4 Nitrogen Evolution from Pyrolysing 150 μm Droplets Arrays of Gulf Coast No. 6 Petroleum Fuel Oil

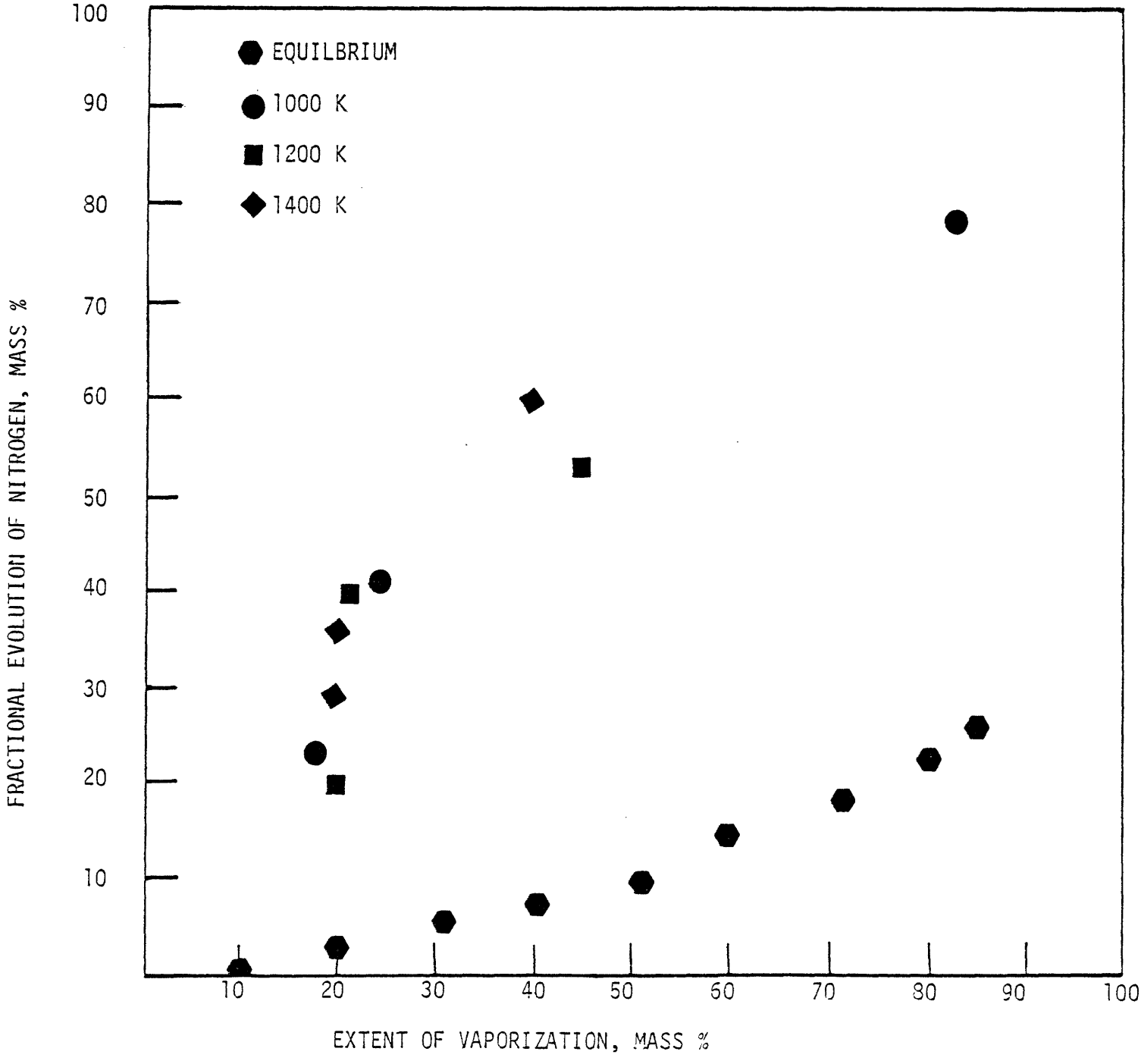

Figure 1.5 Nitrogen Evolution from Pyrolysing 150 μm Droplets Arrays of Indo-Malaysian No. 6 Petroleum Fuel Oil

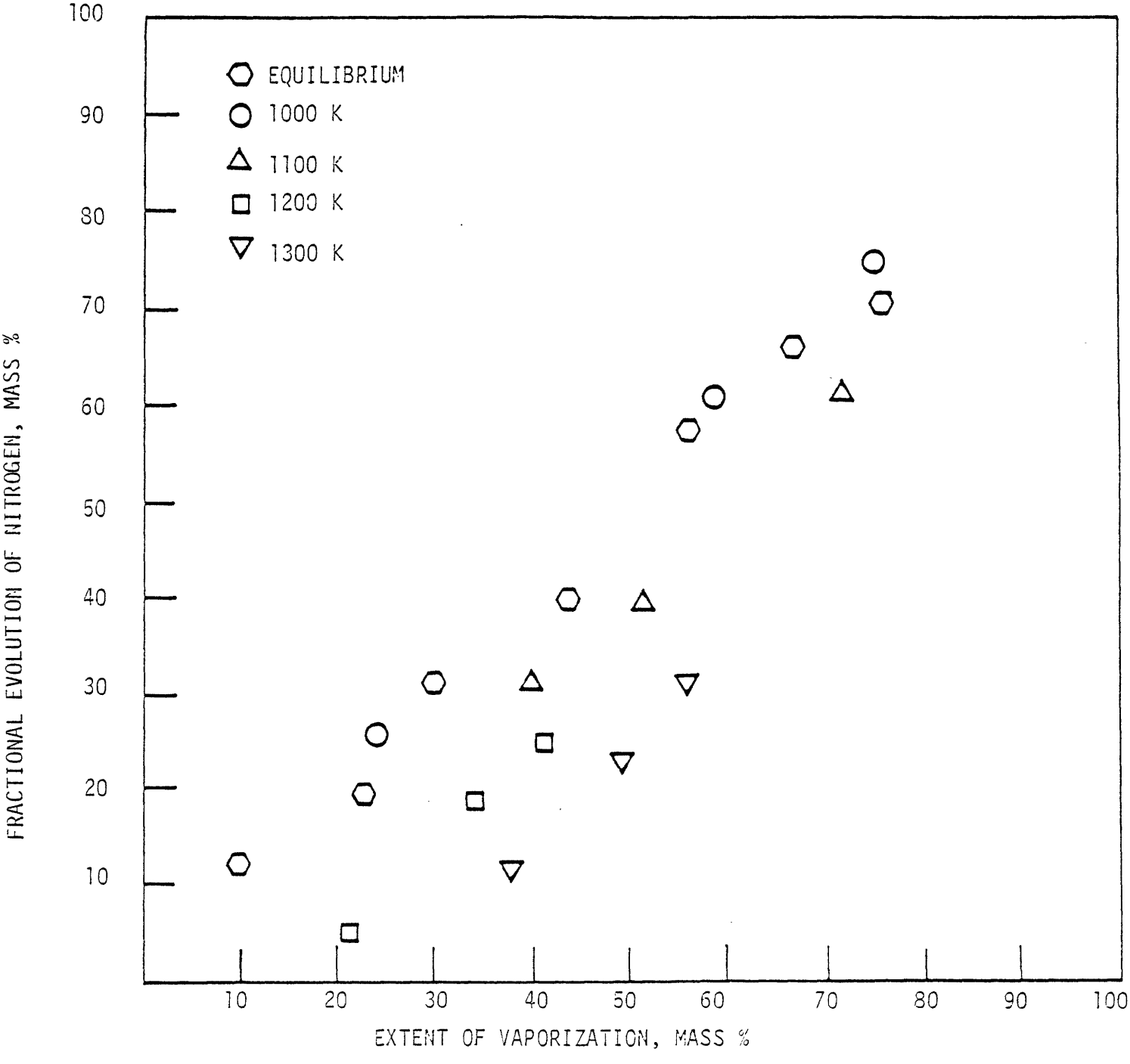

Figure 1.6 Nitrogen Evolution from Pyrolysing 150 μm Droplet Arrays of Raw Paraho Shale Oil

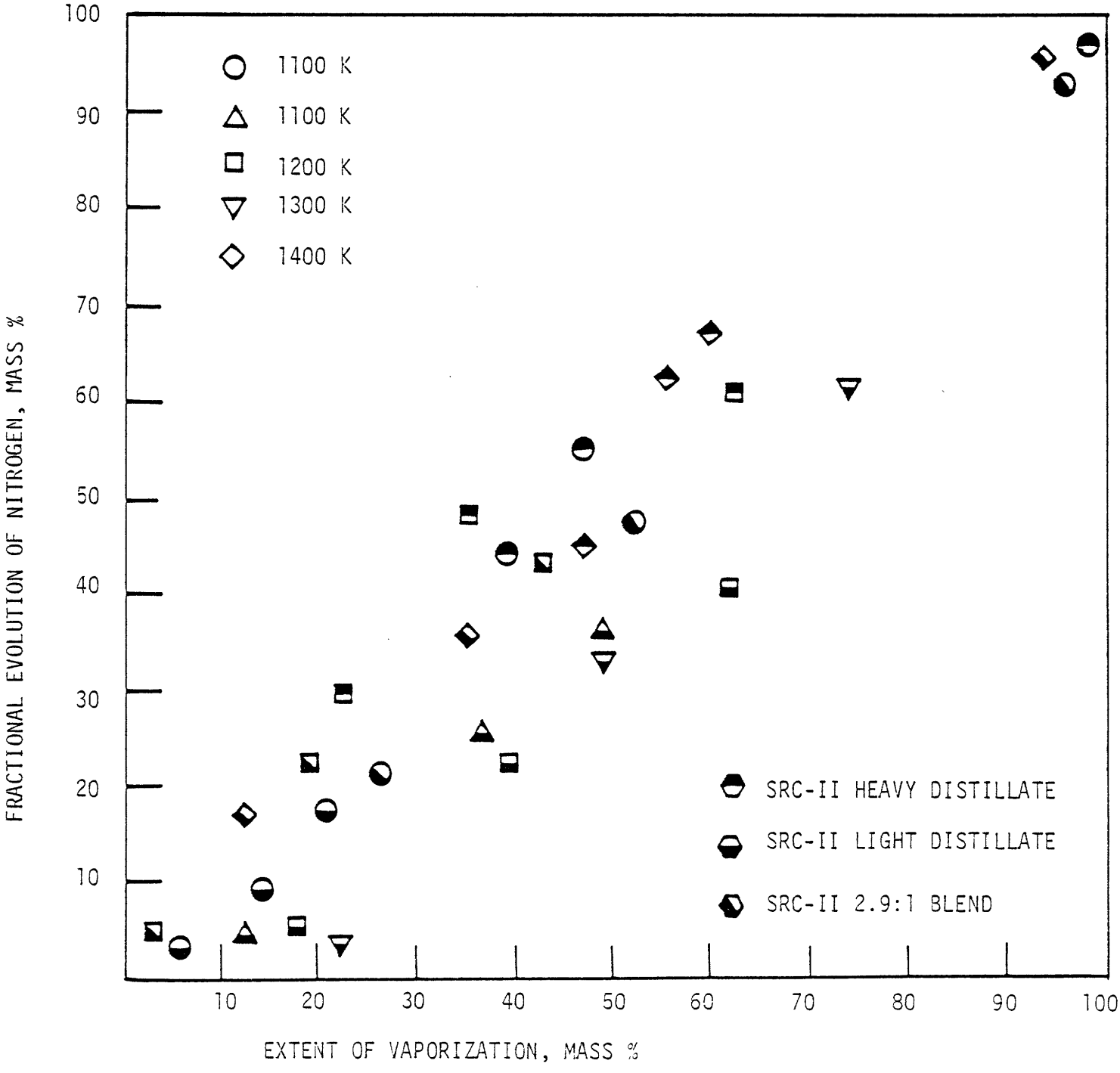

Figure 1.7 Nitrogen Evolution from Pyrolyzing 150 μm Droplet Arrays of SRC-II Middle Distillate Fraction SRC-II Heavy Distillate Fraction, and SRC-II 2.9:1 Blend Middle and Heavy Distillate Fractions

tion is of secondary importance. Temperature gradients within the droplets are small, but concentration gradients cannot be neglected (Le>20). Thus the rate of vaporization is controlled by gas phase energy transport processes, whereas the rate of evolution of a particular fuel component is determined by liquid phase mass transport processes modified by the rate of vaporization, i.e. surface regression, and changing surface volatility, represented by surface concentration and temperature.

When a droplet of fuel oil is introduced to a hot oxygen deficient environment, the droplet will heat up until its surface attains the initial boiling point of the fuel; internally, to a lesser or greater extent depending upon the droplet size, a thermal gradient will be established. At the droplet surface, the more volatile compounds are preferentially envolved. In the gas phase, the radial convective flux thickens the boundary layer surrounding the droplet reducing heat transfer rates and drag experienced by the droplet. With continued vaporization the temperature profile in the boundary layer adjusts to provide the enthapy required at the surface for vaporization. A transient persists throughout the vaporization of a multicomponent fuel, since the surface temperature is always rising with changing surface composition. In the liquid phase, the loss of light species from the surface establishes a concentration profile for each component. The lighter compounds, being depleted at the surface, diffuse from the center of the droplet, and the heavier compounds, being concentrated at the surface, diffuse to the center of the droplet. The combined effects of vaporization and diffusion determine the surface composition, and thereby, the surface temperature. This combination of temperature and composition determines the relative volatilities of the species present at the surface, and hence the vapor phase composition.

Following the arguments presented, an adequate explanation of the behavior of the fuel oils is possible. However, the data presents a summation of nitrogen evolution contributed by many components. Identification of the controlling transport phenomena was complicated by the multicomponent nature of the fuel. Thus, experiments using n-dodecane as a model fuel, and pyridine, quinoline, or acridine as dopant materials, were performed.

The properties and compositions of the model fuels used are presented in Table 1.2. The equilibrium distillation data from these mixtures Fig. 1.8, agree well with those expected from calculations based on ideal binary mixtures. The pyridine, being particularly volatile, has been totally evolved when the extent of vaporization is 40%. At the other extreme, acridine is barely beginning to evolve at an extent of vaporization of 80%. The quinoline, having a boiling point not much greater than n-dodecane, is uniformly evolved as expected for a component having moderately lower relative volatility than n-dodecane. The fractional evolution of nitrogenous component from 150 μm droplet arrays is shown in Fig. 1.9. The dopants all exhibited improved rates of vaporization compared to their equilibrium rates. The pyridine and acridine showed no observable effect of vaporization rate. However, the quinoline data display a temperature dependent behavior. The experimental results showed the model fuels to follow a "d^2-Law" with no observable effects of composition, having a vaporization rate constant of 0.35, 0.51, and 0.62 mm^2/s for furnace temperatures of 1000 K, 1200 K, and 1400 K respectively.

The pyridine, being a highly volatile and mobile compound relative to n-dodecane, is able to escape the surface, and be transported to the surface with great ease, thereby being depleted more rapidly than during

	n-Dodecane	Pyridine	Quinoline	Acridine
Molecular Weight	170.3	79.1	129.2	179.2
Normal Boiling Point, °C	216.3	115.4	237.7	346.0
Mole Fractions Mixture 1	0.874	0.126	-----	-----
Mole Fractions Mixture 2	0.867	-----	0.133	-----
Mole Fractions Mixture 3	0.984	-----	-----	0.016

TABLE 1.2

Fuel Properties of n-Dodecane Doped with Pyridine, Quinoline and Acridine

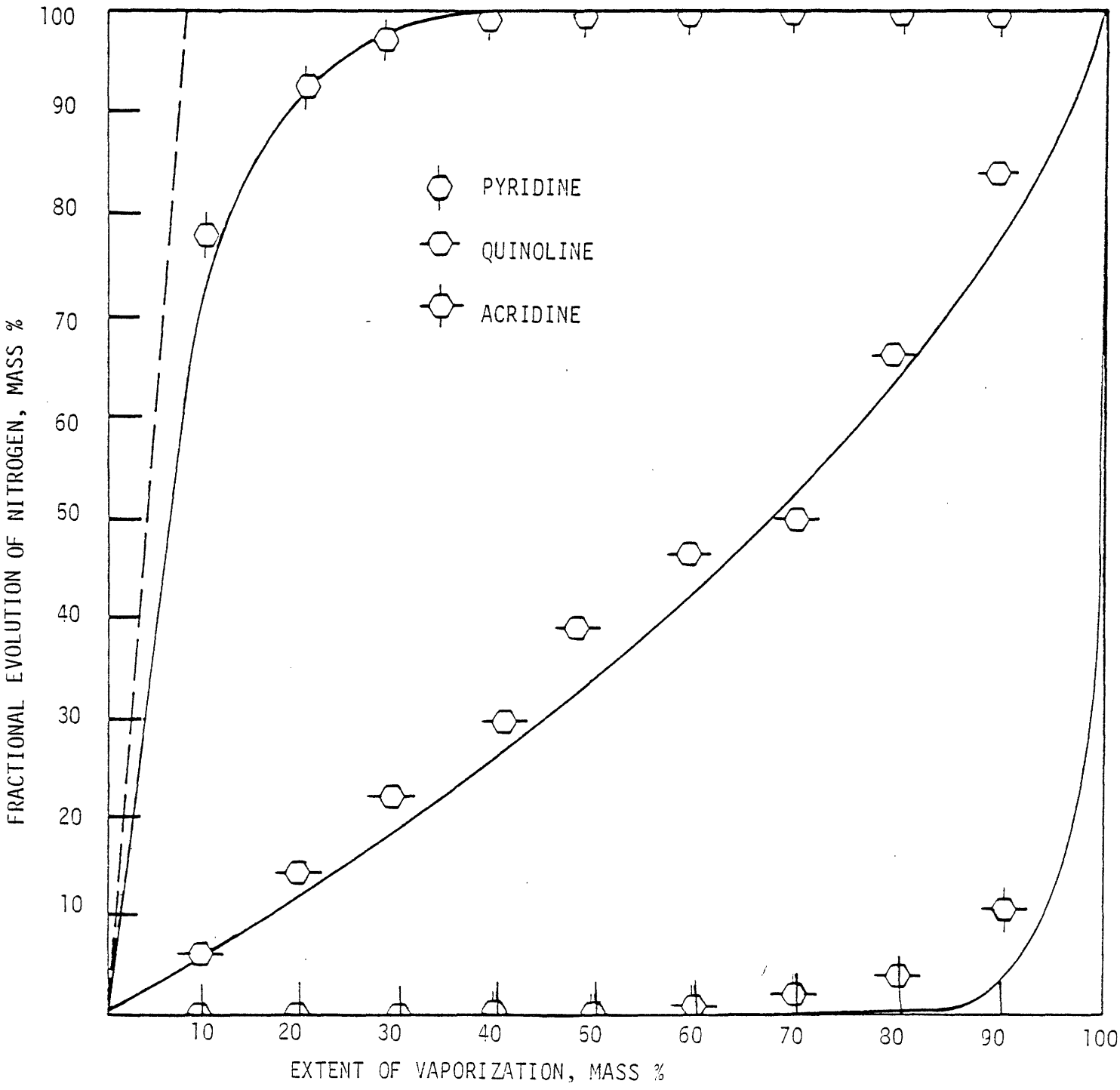

Figure 1.8 Nitrogen Evolution During Equilibrium Batch Distillation of n-Dodecane Doped with Pyridine, Quinoline or Acridine (Data Points are Experimental, Solid Lines are Calculations from Theory)

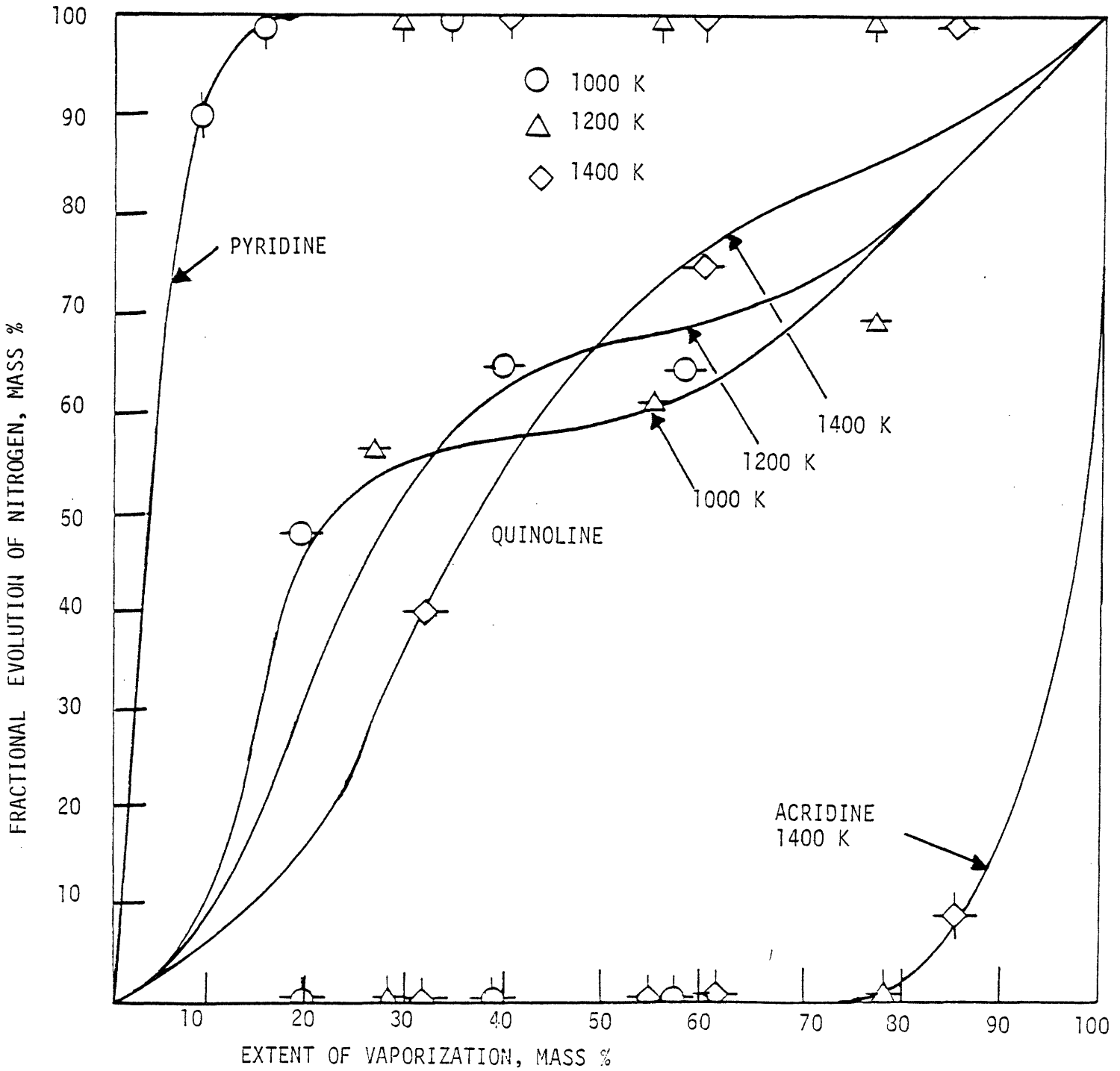

Figure 1.9 Nitrogen Evolution from Pyrolysing 150 μm Droplet Arrays of n- Dodecane Dopes with Pyridine, Quinoline or Acridine (Data Points are Experimental, Solid Lines are Calculations from Theory)

equilibrium distillation, especially since the surface temperature is as high as that found at a much greater extent of vaporization during equilibrium distillation. There is a limit to this behavior represented by the dashed line in Fig. 1.8 which represents the total evolution of pyridine with no loss of n-dodecane.

If diffusion is not able to transport enough material to the surface to satisfy the vaporization requirement, the surface composition will shift towards the heavier molecular weight component, increasing its relative volatility. This is seen to happen for the case of acridine, where its high molecular weight results in a smaller diffusivity and lower volatility, so that the acridine is unable to dissipate itself by diffusion, nor is it able to vaporize readily. Thus, the surface concentration increases until its relative volatility, enhanced by the higher concentration and temperature at the surface, is such that the acridine participates in the vaporization process. This takes place at an extent of vaporization less than that found for equilibrium distillation.

The quinoline doped fuel exhibits a transitional behavior due to the competition between surface regression, diffusional resistance, and relative volatility. The discussion for pyridine bounded the fractional evolution between the maximum evolution constraint and the equilibrium constraint. This is valid when the surface concentration remains low or constant throughout the vaporization, but if an intermediated build-up of surface concentration takes place, then a new equilibrium curve must be considered, and if any loss of the compound has taken place a new maximum limit must be designated. The separation of the contributions of the competing effects can only be revealed by a more complete analysis.

Assuming spherical symmetry, and overall rate of vaporization controlled

by thermal processes in the gas phase, the equations and constraints governing mass species diffusion in the droplet are

$$\frac{\partial m}{\partial t} = \frac{D}{r^2} \frac{\partial}{\partial r} \left(r^2 \frac{\partial m}{\partial r}\right) \tag{1.1}$$

$$t = 0, \quad m = m_o, \quad 0<r<R_o \tag{1.2}$$

$$r = 0, \quad \frac{\partial m}{\partial r} = 0, \quad t>0 \tag{1.3}$$

$$r = R, \quad \frac{\partial m}{\partial r} = \frac{\dot{m}''}{D} (m-m_v), \quad t>0 \tag{1.4}$$

and

$$R^2 = R_o^2 - \frac{\lambda t}{4} \tag{1.5}$$

In order to remove the moving boundary condition (Eq. 1.4), and nondimensionalize the equation variables, the following new variables

$$K = \frac{\lambda}{4D} \; ; \; Z = \frac{K}{4} \left(\frac{r}{R}\right)^2 \; ; \; \tau = \frac{Dt}{R^2} \; ; \; W = \left(\frac{m-m_o}{m_s-m_o}\right) Z^{1/2} \tag{1.6}$$

are introduced causing the original equations to assume the form

$$Z \frac{\partial^2 W}{\partial Z^2} + \left(\frac{1}{2} - Z\right) \frac{\partial W}{\partial Z} + \frac{W}{2} = \frac{(1+K\tau)}{K} \frac{\partial W}{\partial \tau} \tag{1.7}$$

$$\tau = 0 \quad W = 0 \quad 0<Z<\frac{K}{4} \tag{1.8}$$

$$Z = 0, \quad \frac{\partial W}{\partial Z} = \frac{W}{2Z}, \quad \tau>0 \tag{1.9}$$

$$Z = \frac{K}{4},\ \frac{\partial W}{\partial Z} = \frac{W}{2Z} + \frac{\rho_\ell}{2}\left(\frac{K}{Z}\right)^{1/2}(W-W_v),\ \tau>0 \qquad 1.10$$

The solution of these equations 1.7 - 1.10 for a constant surface concentration, m_s, is

$$\frac{m-m_o}{m_s-m_o} = 1 + \sum_{\text{all } a} B_a M(a,\tfrac{3}{2},Z)\ (1+K\tau)^a \qquad 1.11$$

The characteristic values of "a" are defined by the equation $M(a,\frac{3}{2},\frac{K}{4}) = 0$, where M is Kummer's function which has only negative solutions for "a". The values of the series constants, B_a, are given by

$$B_a = -\frac{\int_0^{K/4} Z^{1/2}e^{-z}M(a,\frac{3}{2},Z)dZ}{\int_0^{K/4} Z^{1/2}e^{-z}M(a,\frac{3}{2},Z)^2dZ} \qquad 1.12$$

The case for variable surface concentration may be generated by application of the Duhamel superposition theorem. It may be shown that the surface composition varies according to the equation

$$G(\tau) = \frac{m_s-m_o}{m_f-m_o} = 1-e^{-b\tau} \qquad 1.13$$

where the constant b is a unique value obtained from the boundary condition at r = R. The general solution is

$$\frac{m-m_o}{m_f-m_o} = G(\tau) + \sum_{\text{all } a} B_a M(a,\tfrac{3}{2},Z)(G(\tau) + H_a(\tau)) \qquad 1.14$$

where

$$H_a(\tau) = (1+K\tau)^a - 1 + \sum_{r=1}^{\infty} (-1)^r \left(\frac{K}{b}\right)^r \left\{ \prod_{q=0}^{r-1} (a-q) \right\} \left((1+K\tau)^{a-r} - 1 + G(\tau) \right) \qquad 1.15$$

In order to compare the theory with experimental results, one must average over the drop volume, thus

$$Y = 1 - (1-X)\left(1 + \frac{m_f - m_o}{m_o} \sum_{\text{all } a} B_a F_a H_a(\tau)\right) \qquad 1.16$$

where

$$F_a = \frac{3}{2}\left(\frac{4}{K}\right)^{3/2} \int_0^{K/4} Z^{1/2}\, M(a, \tfrac{3}{2}, Z)\, dz \qquad 1.17$$

and (X, Y) corresponds to the coordinates used in Fig. 1.8 and 1.9. The value of 'b' determines how rapidly surface concentration approaches its terminal value. In the simple binary systems that are being considered here, this terminal value would be zero, one or some stable azeotropic value. If 'b' is large, Eq. 1.14 reverts to the form of Eq. 1.11. Incorporated in 'b' is all the surface volatility effect, whereas 'a', which is indirectly derived from the ratio (λ/D), includes the combined effects of vaporization rate and diffusion resistance in the liquid phase. The competition between volatility and mass transport in the particle is clearly seen in the repetative combination of $\{(1+K\tau)^a - 1 + G(\tau)\}$. A dominant $G(\tau)$ controls the droplet vaporization through volatility effects. When the term $\{(1+K\tau)^a - 1\}$ is dominant the vaporization is mass transfer limited in the liquid phase. There is always a shift from one regime of control to the other, the extent of vaporization at which this occurs being de-

pendent upon the characteristic values of 'a', that is (λ/D), and the value of 'b' which is indirectly coupled to (λ/D) through Eq. 1.4. The coupling is through the thermodynamic equilibrium which determines the relative volatility of surface species. Since for a given liquid phase composition a unique equilibrium vapor phase composition exists, a vaporization driving force may be generated as a function of (m_s-m_o) as done for the model fuels in Fig. 1.10. The temporal variation of the abscissa is derived from Eq. 1.13. Thus 'b' is a scaling parameter for the (m_s-m_o) scale. The pyridine vaporization driving force continuously declines throughout the droplet vaporization. The quinoline and acridine have a maximum in their vaporization driving force. Differences between the quinoline and acridine evolution are because quinoline passes through this maximum (m_s-m_v) at intermediate extents of vaporization, where as acridine does not achieve its maximum (m_s-m_v) until large extents of vaporization. The non-dimensional time scales for quinoline and acridine are approximately the same, that is 'b' is approximately the same for both and is of the order 1. The value of 'b' for pyridine is of the order of 10^2. Thus surface concentrations for quinoline and acridine vary gradually from m_o to one over the lifetime of the droplet, whereas the pyridine surface concentration rapidly declines from m_o to zero.

Generally, the evolution curve of dopant from a droplet (Fig. 1.9) is initially tangent to the equilibrium evolution curve Fig. 1.8 and terminates with a slope of unity. If the dopant is more volatile than the fuel, its evolution curve shifts away from the diagonal drawn through the origin, whereas for a less volatile dopant, it shifts towards the diagonal. The case for quinoline is an example of a fuel in which mass transfer and volatility effects are of comparable magnitude. Thus the quinoline

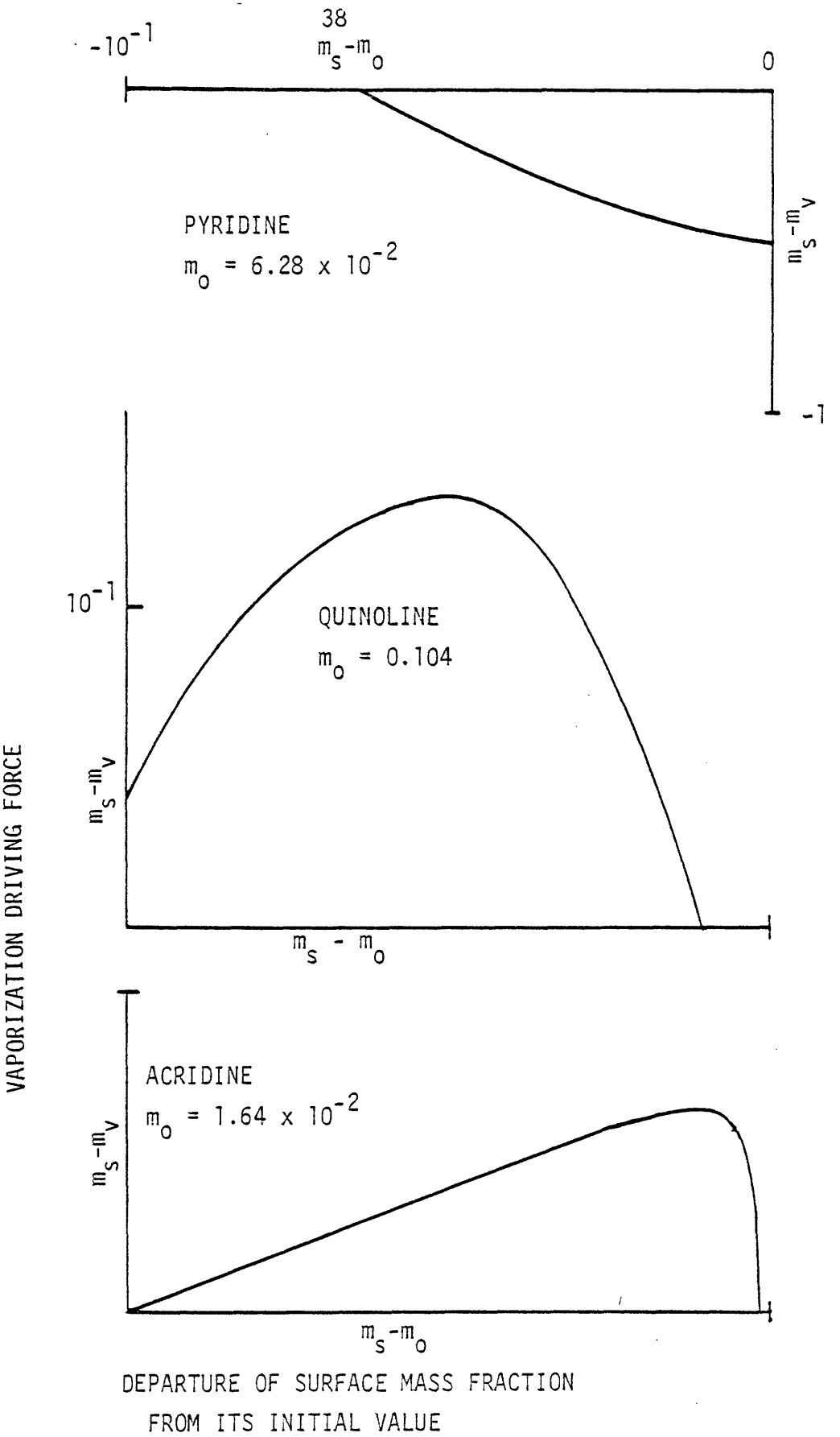

Figure 1.10 Vaporization Driving Force as a Function of Surface Mass Fraction for n-Dodecane Doped with Pyridine, Quinoline or Acridine

evolution is sensitive to the rate of vaporization causing mass transfer and volatility effects to alternately dominate.

Although the model has been applied in this instance to a binary system, there is no practicle distinction between the processes described here and those to be found in complex fuels. The only obstacle to the prediction of species evolution from a real fuel, is the lack of detailed information on fuel composition, and material properties in complex mixtures.

CHAPTER 2

INTRODUCTION

The demand for energy in the United States is growing at an ever increasing rate, as shown in Fig 2.1. At the termination of World War II, coal and oil contributed equally about 40% each to the energy supply.[1] Since 1950, oil and the natural gas associated with it, has been the preferred energy source. This has been due to the superior combustion characteristics of these fuels, greater demand of liquid fuels for transportation[2], and government regulations mandating higher health and safety standards for coal mining, and environment restrictions on the burning of high-Sulfur coal and the strip mining of coal[3]. Currently, oil accounts for half the energy supply, three times that contributed by coal[1]. During the 1960's, a declining discovery rate for exploration oil wells drilled in the United States, and the availability of inexpensive imported oil from established oil fields discouraged investment in extensive oil exploration[4].

American oil production reached a maximum in 1970. By 1976, 44% of oil consumed in the United States was imported, and it is estimated that by 1985 imported oil may account for almost 53% of oil consumed[2].

The considerable consumption of imported oils may be defended as a means to conserve domestic reserves, and to improve refining efficiency by allowing the selection of optimum quality fuels that give product yields compatible with market demands[5]. However, the continuing demand for oil in the industrialized nations, the reduced domestic oil production and discovery rate, and the politico-economic impact of agreements between oil exporting nations, has demonstrated American dependence on imported oil. In order to supplement domestic petroleum production,

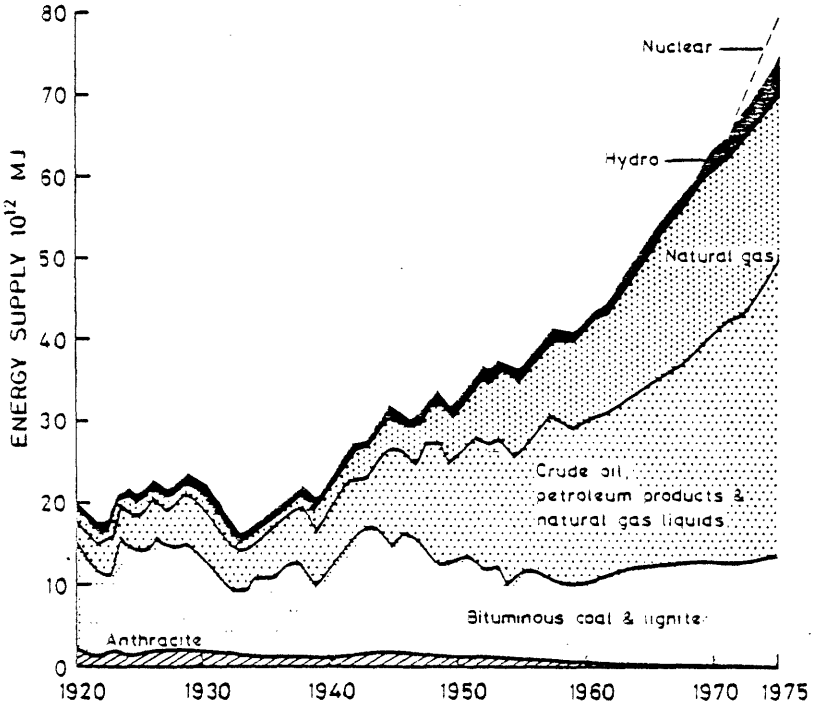

2.1 Energy Supply in the United States[1]

it is necessary to develop alternative liquid fuels from abundant energy resources which include coal, oil shale, tar sands, and low grade petroleum crudes and residuum previously considered unusable.

Since the C/H ratio of conventional liquid fuels is about 0.53, while the C/H ratio in coals is about 1.33, as shown in Table 2.1, the manufacture of synthetic fuel from coal hinges upon reducing this ratio[6]. The required hydrogen alone is estimated to cost $33 per barrel at current prices. An additional cost is due to the increased thermal losses in the refining process relative to petroleum fuels. Table 2.2 shows estimates of the overall thermal efficiency of several synthetic fuel processes. Thermal efficiency translates directly to cost, thus there is a significant benefit in being able to cope with fuels of higher C/H ratio.

During the 1980's alternative liquid fuels are expected to displace fuels currently used in utility boilers, industrial boilers and industrial furnaces, where conversion to direct coal combustion is not practicable. The crude oils from which the displaced fuels originated may then be refined with an emphasis on the lighter fractions[7].

The alternative fuels under consideration are usually found to have high nitrogen content. Figure 2.2 shows the contribution of various stationary sources to NO_x emissions. It is seen that the very systems in which the alternative fuels are to be used already contribute a major portion of the NO_x emissions from stationary sources. The NO_x emissions with respect to fuel type, shown in Fig. 2.3, increases with increasing fuel-nitrogen content. In order to successfully use these fuels, they must be burnt under controlled conditions that restrict the oxidation of fuel-nitrogen to NO_x without the formation of carbonaceous particulates.

Approximate U.S. Remaining Resources

	10^{12} MJ	Approximate Net Ratio C/H
Petroleum	740	0.50
Tar sands	110	0.57
Oil shale	21,000	0.53
Coal	95,000	1.33

Current liquid fuel consumption $\sim 42 \times 10^{12}$ MJ/YR

Table 2.1

Abundance and Carbon to Hydrogen Atomic Ratios of Energy Resources in the United States[6]

Type of Refinery		Energy Consumption -- Percent of Heating Value of Oil Refined
Petroleum low conversion		3 +
Petroleum U.S. high conversion		8-12
Synthetic coal liquid--	(C/H = 0.80)	28-31
high conversion	(C/H = 0.67)	18-21
Shale oil -- hydrogenated	(C/H = 0.52)	11-15

Table 2.2

Energy Consumption for Fuel Refining[6]

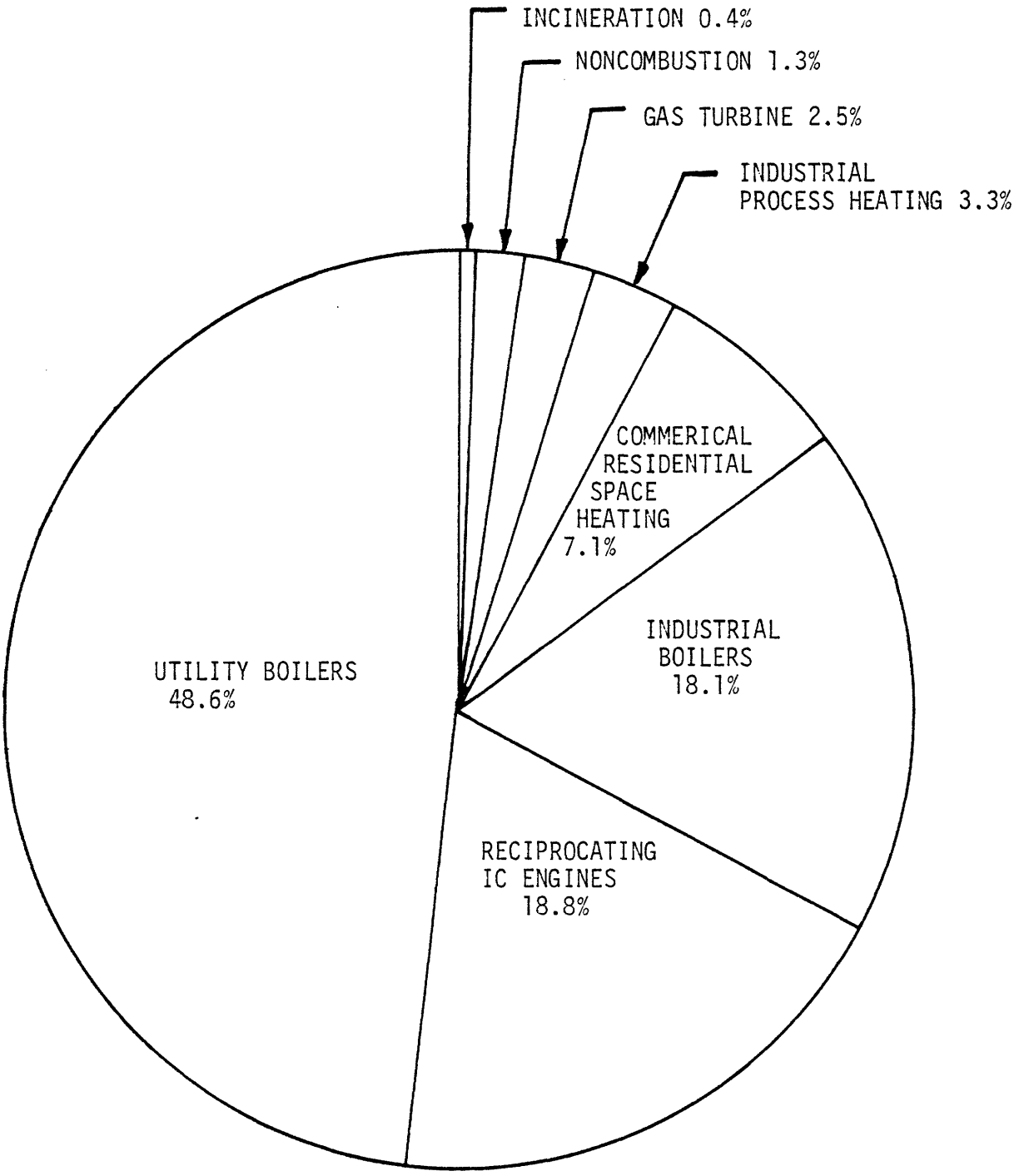

Figure 2.2 Nitrogen Oxide Emission from Stationary Sources in 1972[8]

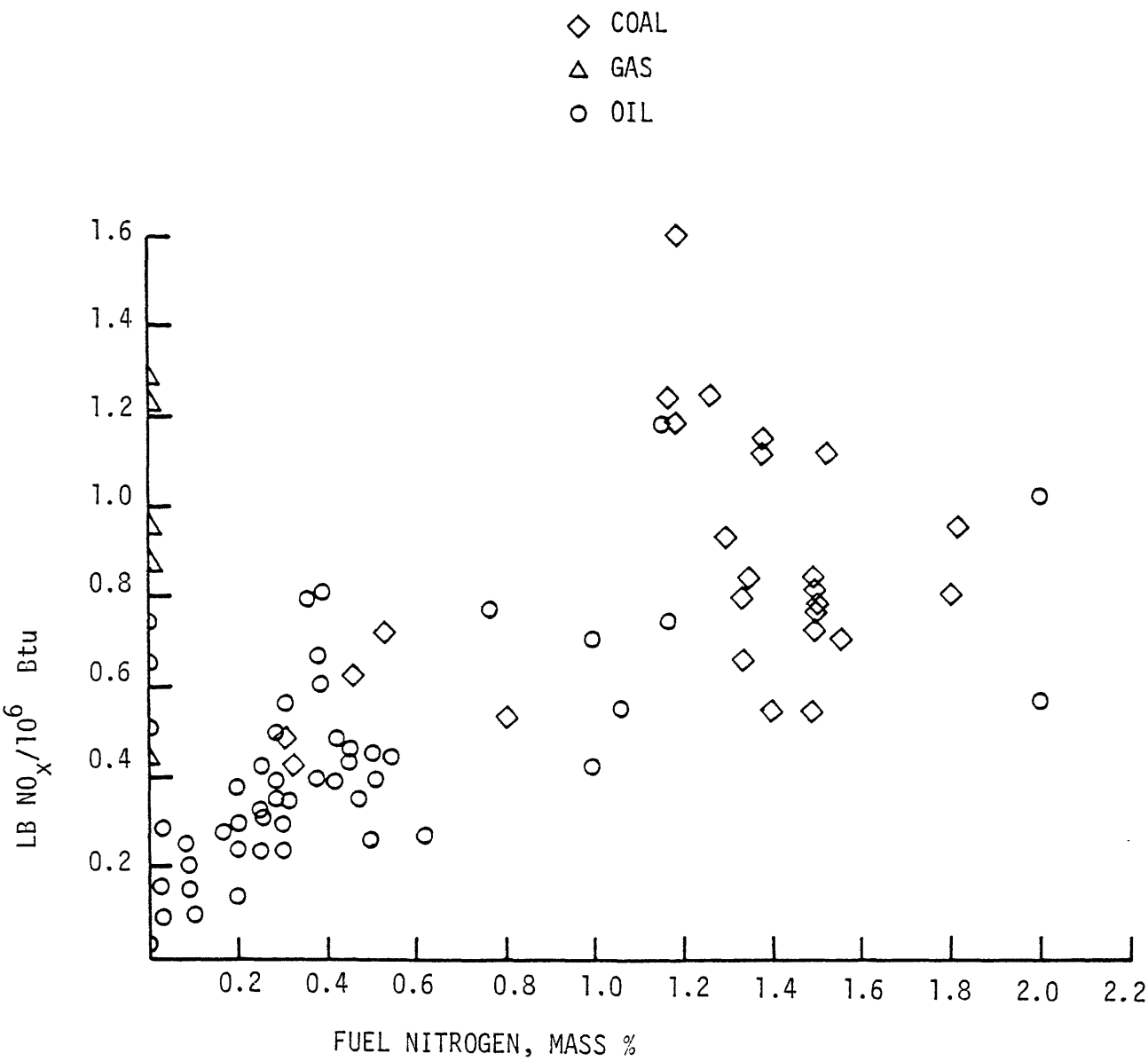

Figure 2.3 Nitrogen Oxide Emissions from Uncontrolled Combustors as a Function of Fuel-Nitrogen Content[9]

2.1 Combustion of Liquid Fuels

Oil may be burned homogeneously or heterogeneously. Homogeneous combustion is applicable only to volatile fuels which can be vaporized prior to ignition so that they burn like a gaseous fuel. Heterogeneous combustion requires that the fuel be broken into fine droplets which are injected into a combustor where they vaporize and react in the gas phase with oxidant. The alternative fuels are most suitable for heterogeneous combustion.

2.1.1 Atomization[22-33]

The breaking-up of a liquid into small droplets in order to produce an extensive interface between a liquid and a gas is a technique employed to enhance the transfer of momentum, energy, and mass, and the uniform distribution of liquid over large areas. The energy required for the creation of new surface by atomization is small and inversely proportional to the diameter of the droplets. However, the efficiency of atomization is typically less than one percent, considerable energy being required to achieve a high degree of atomization. The most important physical characteristic in the combustion of an oil spray is the average droplet size, whereas the breadth of the size distribution determines the time required for complete vaporization of the spray. The factors which affect drop size distribution are the atomizer design, the liquid properties, and the spraying atmosphere. Atomizers used for the disintegration of fuel oils in practical applications (fig. 2.4) are mostly of the swirl spray or twin fluid type, and to a lesser extent of the spinning cup type, although impact nozzles, fan sprays, and rotary atomizers may be used for particular applications. In order to remove the complexities

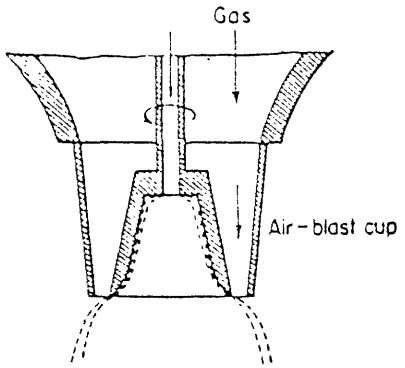

(a,1) Air-Blast Rotary Cup Atomizer[30]

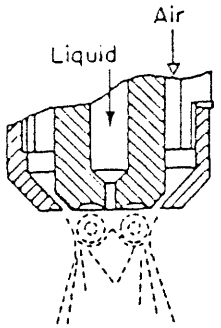

(a,2) Twin-Fluid Atomizer[30]

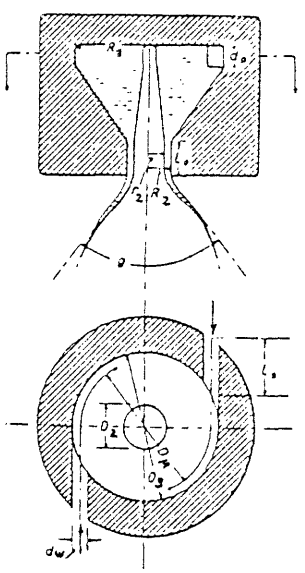

(a,3) Swirl Spray Nozzle[30]

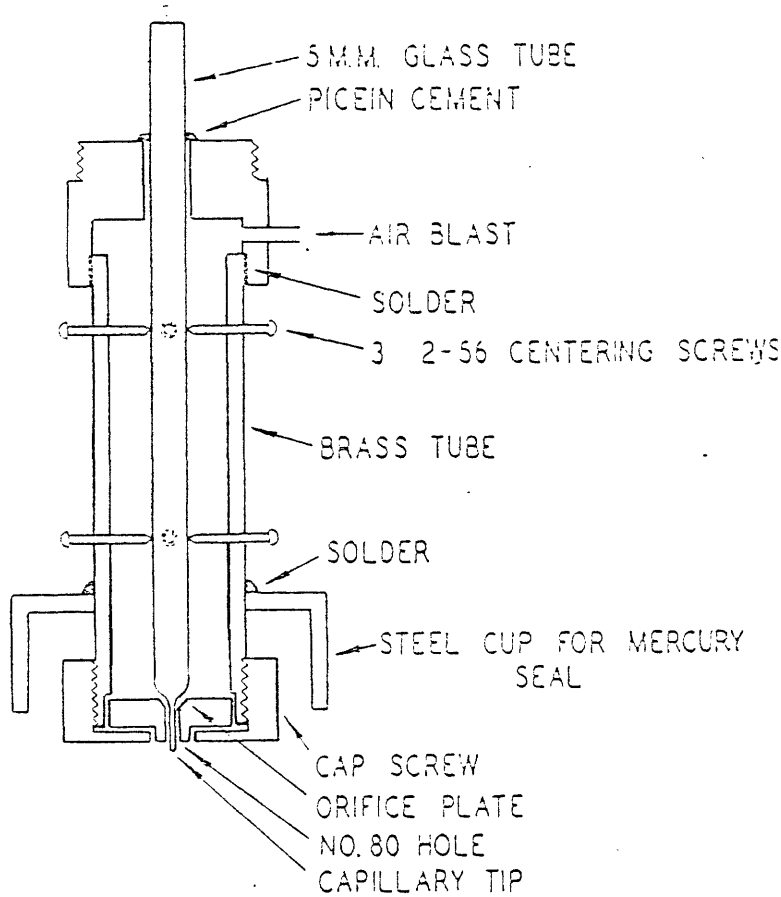

(b,1) Chang Drop Generator[31]

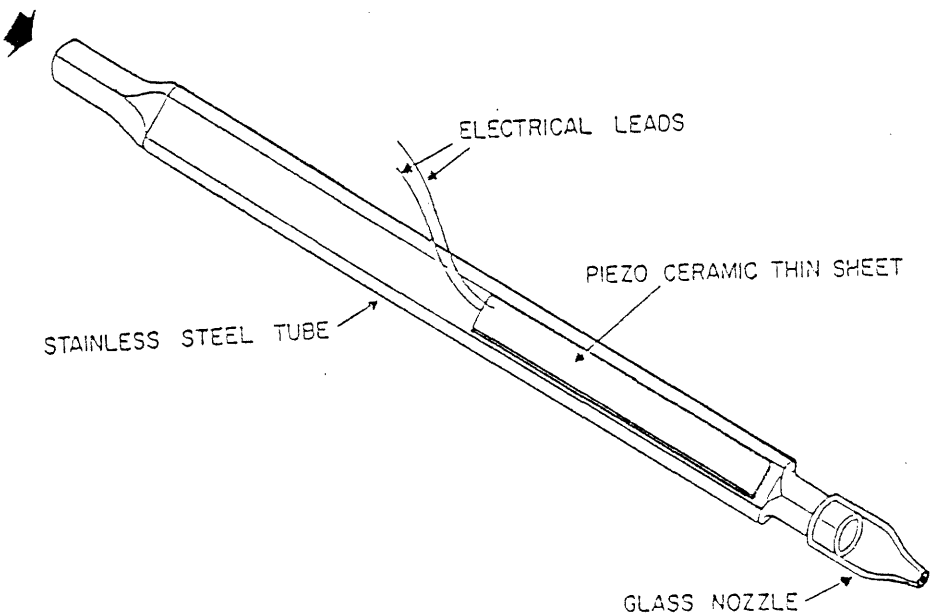

(b,2) Impulse Atomizer[33]

Figure 2.4 Liquid Atomization Devices for (a) Practical and (b) Research Applications [30-33]

of interpreting data obtained from poly-dispersed spray systems, several methods of generating a uniform particle size have been developed for research purposes. The physical process of atomization is an extremely complicated one. The modelling of the mechanism of atomization has been restricted to simple systems of liquid sheets and jets resembling the systems used for experimental research. The operation of practical atomizers is explained by analogy to these simple systems and dimensional analysis.

2.1.2 Vaporization

The combustion of liquid fuels takes place in the gas phase alone, and is thus limited by the rate of mass transfer from the liquid to the vapor phase. The rate of mass transfer is proportional to the interfacial area which increases as the average particle size decreases. In order to sustain high combustion intensities, and obtain reasonable combustor residence times, rapid vaporization is an absolute necessity.

Fuel injected into a furnace is heated to reduce its viscosity enough to permit adequate atomization. The fuel droplets must undergo further heating until they attain their initial boiling point after which they dissipate most of the heat received as latent heat of vaporization. Because of the preferential vaporization of light components, the boiling point of the fuel will increase, requiring sensible heat to be conducted into the droplet such that the liquid may sustain continued vaporization. Due to the increased liquid temperature and reduced surface area the mass rate of vaporization for a particular droplet is reduced. For a poly-dispersed spray, the small droplets will vaporize completely much sooner than the large droplets. Thus, even though all droplets diminish in size, the mean droplet size and the overall rate of vaporization will initially increase and later diminish.

Mass and energy transport in the gas phase of a vaporizing droplet is influenced by its velocity and the environment through which it travels. This interaction of the droplet with its environment is system specific, generalities of the vaporization rate of the droplet being limited to increased transport rates resulting from boundary layer thinning by the relative velocity of the droplet and its environment.

In the liquid phase there is less certainty as to the transport processes taking place. Whether circulation within the droplet is important depends upon particle size, viscosity, velocity and vaporization rate, and the importance of liquid phase reactions is subject to fuel composition and the contribution of radiation to the heat transfer to the droplet.

2.1.3 Mixing

Intimate contact between the vaporized fuel and oxidizing environment must be accomplished for combustion to proceed. This mixing process is usually the rate limiting step of heterogeneous combustion and involves a complex interaction of molecular diffusion and the flow field in the combustor. Macroscale mixing is accomplished by the turbulent fluid motion whereas microscale mixing is governed by molecular diffusion.

2.1.4 Chemical Reaction

The energy released by the reaction of fuel and oxidant is the desired product of a combustor. The reaction takes place in the gas phase creating combustion products that may be innocuous or undesirable. In the liquid phase polymerization and cracking reactions may occur resulting in the formation of a char.

2.1.4.1 Gas Phase Reactions [34-37]

The intimately mixed hydrocarbon vapors and oxidant undergo a complex series of reactions. The number of species and reactions involved increases with the molecular weight of the fuel. In fact, even for the simplest of hydrocarbons, methane, the reaction scheme is only partially known and the situation for heavier hydrocarbons is known with even less certainty. However, one may generalize that at flame temperatures vaporized hydrocarbons fragment into smaller species that are common to all hydrocarbon fuels, although the composition will differ with the carbon to hydrogen ratio of the fuel.

The thermal decomposition of hydrocarbons is initiated by unimolecular disintegration of the parent hydrocarbons. Synthesis reactions occur during combustion, leading to the formation of complex hydrocarbon molecules in the post flame region. The basic reaction paths for hydrocarbon species in flames are:

(i) Oxidative dehydrogenation of an aliphatic hydrocarbon molecule to form ethylene and acetylene

(ii) Chain lengthening of acetylene to form various unsaturated radicals

(iii) Dehydrogenation of these radicals to form polyacetylenes

(iv) Cyclization of polyacetylenes to form aromatic compounds

(v) Synthesis of cyclic polyacetylenes to form polycyclic organic compounds.

The oxidative mechanisms that dominate the combustion process would ideally result in the formation of carbon dioxide and water alone. A reaction scheme for the combustion of methane (Table 2.3) illustrates the type of reactions taking place. However, the additional pyrolysis

$$CH_4 + M \rightarrow CH_3 + H + M$$
$$CH_4 + O_2 \rightarrow CH_3 + HO_2$$
$$O_2 + M \rightarrow O + O + M$$
$$CH_4 + O \rightarrow CH_3 + OH$$
$$CH_4 + H \rightarrow CH_3 + H_2$$
$$CH_4 + OH \rightarrow CH_3 + H_2O$$
$$CH_3 + O \rightarrow H_2CO + H$$
$$CH_3 + O_2 \rightarrow H_2CO + OH$$
$$H_2 CO + OH \rightarrow HCO + H_2O$$
$$HCO + OH \rightarrow CO + H_2O$$
$$CO + OH \rightarrow CO_2 + H$$
$$H + O_2 \rightarrow OH + O$$
$$O + H_2 \rightarrow OH + H$$
$$O + H_2O \rightarrow OH + OH$$
$$H + H_2O \rightarrow H_2 + OH$$
$$CH_3 + O_2 \rightarrow HCO + H_2O$$
$$HCO + M \rightarrow H + CO + M$$

Table 2.3

Methane Oxidation Reactions[38]

reactions that a high molecular weight hydrocarbon undergoes (as presented in the preceding paragraph) inadequate mixing of fuel and oxidant, and the inclusion of nitrogen, sulfur, and other materials in the fuel, result in the formation of pollutants of which those of current concern are:

(a) Carbonaceous particulates

(b) Unburned hydrocarbons

(c) Polycyclic aromatic hydrocarbons

(d) Carbon monoxide

(e) Sulfur oxides

(f) Nitrogen oxides

(g) Volatile inorganics, e.g. lead and arsenic compounds

2.1.4.2 Liquid Phase Reactions[39-42]

The liquid phase temperature of a fuel droplet is regulated by vaporization of material from the surface. For heavy fuel oils, the vaporization occurs at temperatures high enough to cause heavy fuel components to undergo pyrolysis reactions. If the droplet includes radiation absorbing sites, it is possible that "hot spots" will occur in the liquid which act as centers for cracking. The products of pyrolysis are gaseous, liquid and solid. The solid residue may form as an amorphous mass, but more frequently as a cenosphere. These carbonaceous residues have burnout times that are many times greater than the vaporization times of the droplets, usually exiting the combustion chamber intact with the combustion gases as an undesirable emission that must not be exhausted to the atmosphere.

2.2 Nitrogenous Components of Liquid Fuels

The nitrogen associated with fossil fuel is organic in origin. The type of nitrogenous contaminant reflects the organic source from which it was derived.

2.2.1 Coal Liquids[44,45]

Nitrogen is found in the organic structure of coal in amounts generally less than 2 1/2% by weight dry (ultimate analysis). Nitrogen compounds of coal liquids are aromatic, and occur in an abundance commensurate with the coal source. The type of compounds found are derivatives of those in Table 2.4. Other compounds, such as acetonitrile and benzonitrile, have been detected, and are probably produced by degradation of larger aromatic compounds. Compounds that have been identified in coal tar, listed in Table 2.5, have molecular weights exceeding 150. Thus, although the nitrogen contained in the compounds may not be great, the total weight contribution is significant.

2.2.2 Petroleum[43]

Nitrogen contaminants in petroleum range in amount up to almost 1% by weight. However, after refining, these compounds are usually found to have concentrated in the high boiling resin and asphaltene fractions as shown in Table 2.6. The nitrogen compounds in crude oil are classified as basic or nonbasic. A representative sample of nitrogenous petroleum contaminants is presented in Table 2.7 using this classification.

2.2.3 Shale Oil[43]

The nitrogen content of shale oil is typically high compared to that of petroleum. Distillation of shale oil, Table 2.8, shows an

Acridines

Anilines

Carbazoles

Coronene

Fluoranthene

Indoles

Perylenes

Pyridines

Pyroles

Quinolines

Table 2.4

Types of Nitrogenous Compounds in Coal Liquids [43]

Structural Types	Molecular Weight	Total Weight[a] percent	Total Weight[b] percent
Carbazole	167	4.6	0.1
Acridine	179	2.5	0.8
4H-Benzo [def] carbazole	191	1.6	0.6
Dibenz [cd, g] indole	203	1.6	1.6
11H-Benzo [a] carbazole	217	3.6	o.6
Benz [c] acridine	229	1.3	1.0
1H-Anthra [2,1,9-cde indole	241	0.7	---
Indeno [7,1-ab] acridine	253	.6	1.4
Dibenz [b,h] acridine	279	.1	0.5
9H-Phenathro [4,5-abc] carbazole	291	Trace	---
X-Azabenzo (ghi) fluoranthene	227	---	0.6
Z-Azabenzo (ghi) perylene	277	---	0.6
Anthra (1,9=ab) carbazole	303	---	0.4
X-Azacoronene	301	---	0.1
Total		15.0	7.7

Table 2.5

Nitrogen Compounds in (a) Creosote Oil and (b) Coal Tar Pitch[43]

Field	Nitrogen in Crude Oil, percent by weight	Percentage of Nitrogen in Residuum
Schuler, Ark.	0.06	88
Heidelberg, Miss.	0.11	106
Deep River, Mich.	0.12	91
Midway-Sunset, Calif.	0.58	85
Wilmington, Calif.	0.65	86
Velma, Okla.	0.27	89
Yates, Texas	0.16	88
Chromo, Colo.	0.03	100
Dallas, Wyo.	0.28	96
Derby, Wyo.	0.25	96
Pilot Butte, Wyo.	0.22	95
Keri, Greece	0.17	94
Circle Ridge, Wyo.	0.23	96
Winkleman Dome, Wyo.	0.23	91
Sage Creek, Wyo.	0.28	93
Steamboat Butte, Wyo.	0.16	88

Table 2.6

Residuum Nitrogen Retention of Crude Oils[43]

Basic	Non-Basic
2,4 - Dimethylbenzo [h] Quinoline	Acridine
4,6 - Dimethyl (2,6,6-Trimethylcyclohexyl) Pyridine	Benz-2-Quinolone
Indoloquinoline	Carbazole
3-Methylpyridine	Indole
Quinoline	Pyrrole
	2-Quinolone
	2-Thioquinolone
	Vanadium - Porphyrin Complex

Table 2.7

Basic and Nonbasic Nitrogen Compounds in Petroleum Products [43]

Fraction	Boiling Range, C	Amount in Shale Oil, volume percent	Nitrogen in Fraction, weight percent
Naphtha	Below 200	3	1.17
Lithe distillate	200-310	16	1.24
Heavy distillate	310-430	34	1.60
Residuum	Above 430	47	2.04

Table 2.8

Nitrogen Distribution Shale Oil Fractions[43]

increased nitrogen content with increased temperature of the distillate fraction. The residuum contains 62% by weight of the total nitrogen. The principal nitrogenous species are pyridine and pyrrole type compounds. Nitrogen distribution in cyclic compounds by weight is 35% single ring compounds, 25% two-ring compounds, and 40% multiring compounds. Other nitrogen compounds that occur in small amounts in shale oil are amides, arylamides, and nitriles. Porphyrins are also found in trace amounts.

2.2.4 Tar Sands[43,46]

The elemental analysis of tar sands yields nitrogen concentrations of 1/2 to 3% by weight. The nitrogen is primarily contained as amides and carbazoles. The exploitation of tar sands has not yet reached a stage that detailed studies of the nitrogen content has been warranted.

2.3 Nitric Oxide Emissions[38,47]

Nitrogen oxides are formed in combustion processes by either the high temperature oxidation of atmospheric nitrogen (thermal NO), the oxidation of fuel-bound nitrogen compounds (fuel NO), or the fixation by hydrocarbons and subsequent oxidation of atmospheric nitrogen ("prompt" NO). The mechanism of thermal NO formation is the better known. The generally accepted model is that of the "atom shuttle" reaction by Zeldovich. In contrast to thermal NO, the rate of formation of which is a strong function of temperature, the formation rate of nitric oxide from fuel-bound nitrogen is only slightly dependent upon temperature, but increases markedly with increased oxygen concentrations. It is thought that this is due to the competition between reactions, involving nitrogen containing species, to produce nitric oxide or

nitrogen. The exact mechanism of fuel nitrogen conversion is not known, but a significant body of knowledge now exist for general conclusions to be drawn with respect to the major parameters, and some details of the reaction mechanism also emerge. The mechanism of "prompt" NO formation is still being formulated, although the oxidation of nitrogen containing fragments formed in this way is considered to be the same as for any other fuel-bound nitrogen.

2.3.1 Thermal NO

The mechanisms inovlving thermal NO were first described by Zeldovich[48] and later modified to what is referred to as the extended Zeldovich mechanism[36].

$$N_2 + O \longrightarrow NO + N \qquad 2.1$$

$$N + O_2 \longrightarrow NO + O \qquad 2.2$$

$$N + OH \longrightarrow NO + H \qquad 2.3$$

The contribution of Eq. 2.3 is small since both reacting species are radicals and present in low concentrations. Equilibrium concentrations predicted by this mechanism are greater than actually measured. The high activation energy of Eq. 2.1, 317 kJ/mole, controls the system and it is apparent that the oxygen radical concentration is a critical parameter in this system. Oxygen atoms are formed from the dissociation of oxygen molecules, or by hydrogen atoms reacting with oxygen molecules. In order to prevent formation of nitric oxide, one must inhibit the formation of oxygen atoms or limit the rate of reaction in Eq. 2.1. From measurements of nitric oxide formation in heated mixtures of nitrogen, oxygen and argon[49], an equation of nitric oxide concentration as a function of time has been derived.

$$[NO] = A[N_2][O_2]^{1/2} \; t \exp(-E/RT) \qquad 2.4$$

Equation 2.4 shows that thermal NO can be restricted by reducing residence time, reactor temperature, and concentrations of nitrogen and oxygen. Because the reaction of Eq. 2.1 is so slow, Eq. 2.1 is only valid in the hot post flame region. However, measurements on flat flame burners showed that when nitric oxide concentrations were extrapolated to the flame front the concentration did not go to zero as expected from Zeldovich kinetics.

2.3.2 "Prompt" NO

The finite concentration of nitric oxide in the flame region prevailed in nitrogen free hydrocarbon fuel-air systems but did not occur for carbon monoxide-air or hydrogen-air systems. The nitric oxide generated in this fashion was called "prompt" NO[50]. The "prompt" NO mechanism is believed to be initiated by hydrocarbon radicals attacking molecular nitrogen. The most important reaction is probably that which involves the CH radical

$$CH + N_2 \longrightarrow HCN + N \qquad 2.5$$

The production of "prompt" NO as affected by air-fuel ratio can be seen from the formation of nitric oxide from diffusion and premixed gas flames. The air-fuel ratio of the premixed flame is the same throughout the flame zone, whereas in the diffusion flame fuel-rich and fuel-lean zone will exist whatever the overall stoichiomtry of the system may be. The formation of nitric oxide, Fig. 2.5, is seen to peak for a premixed flame at a slighly fuel-lean composition, whereas the diffusion flame, which is never fuel-lean at the flame front, continues to yield increasing amounts of nitric oxide as the system

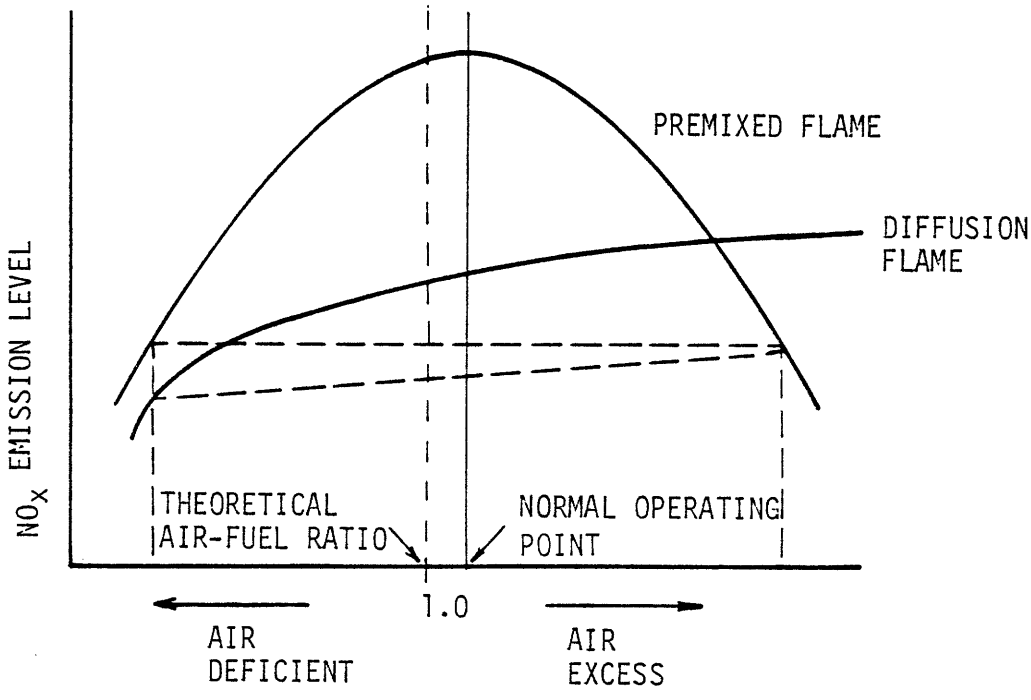

Figure 2.5 Nitrogen Oxide Emissions for Premixed and Diffusion Flames as a Function of Air-Fuel Ratio[51]

becomes more fuel-lean[52]. Whether this result is primarily due to composition is not certain since experiments have been performed relating the "prompt" NO formation to system temperature for similar air-fuel ratios, which suggests that a high temperature, high activation energy, and a low temperature, low activation energy mechanism may exist[52]. It appears that "prompt" NO may occur in the flame zone by both the Zeldovich mechanism on the fuel-lean side of the flame and the CH radical mechanism on the fuel-rich side of the flame[53].

2.3.3 Fuel NO

Fuel NO is formed early in the flame from nitrogen compounds in the vapors surrounding a burning fuel particle. Fuels doped with various nitrogenous compounds showed that the form of the nitrogen compound does not significantly influence the conversion to nitric oxide [7,18]. However, this conclusion was reached using relatively low boiling point additives and there is doubt that it would be valid for heavy nitrogenous compounds that are present in residual fuel oils. Increasing the fuel-nitrogen yields increasing nitric oxide emissions [15,18], but the conversion efficiency declines and at high nitrogen concentrations approaches an asymptotic value[50] (Fig. 2.6). Data from premixed and diffusion flames show a decrease in conversion efficiency with declining air-fuel ratio, and is particularly significant under fuel-rich conditions [15,18,50,54]. Studies of gaseous, liquid and solid fuels showed temperature to have only a slight effect on fuel nitrogen conversion[7,18]. Thus, composition effects in the ambient control the gas phase kinetics of fuel-nitrogen conversion to nitric oxide.

The nitrogen containing compounds released by the fuel particle to the gas phase undergo pyrolysis to form N, NH or CN. In lean flame

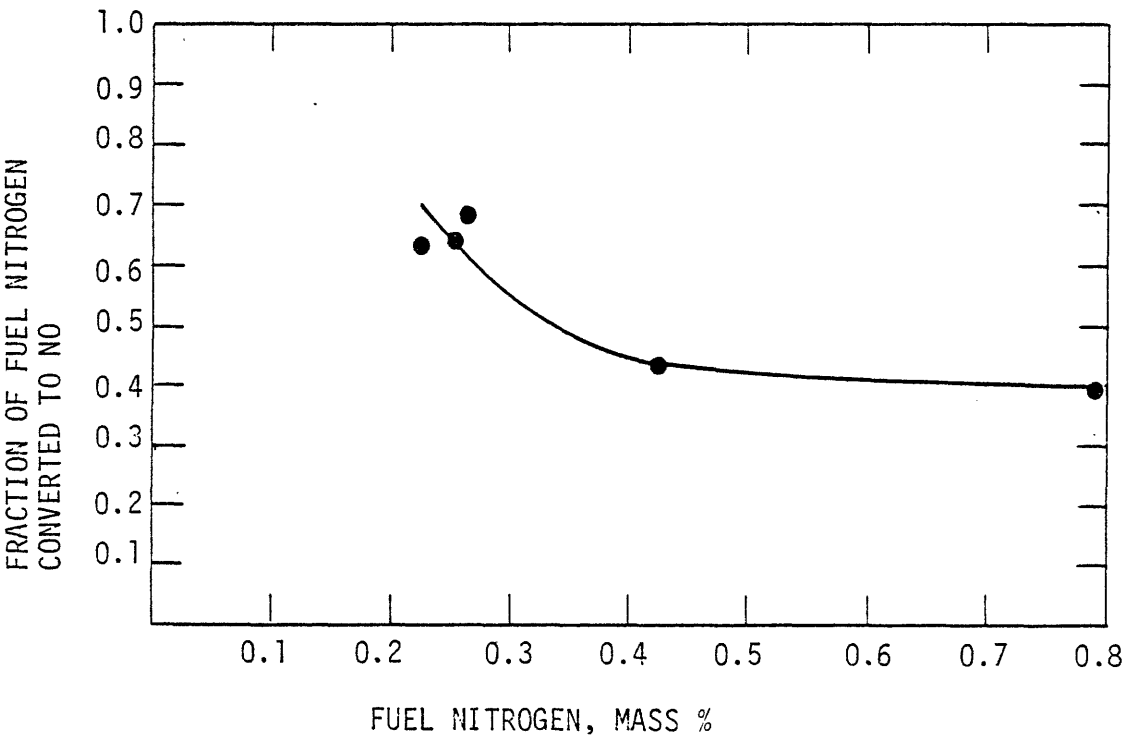

Figure 2.6 Effect of Fuel-Nitrogen Concentration upon the Efficiency of Conversion to Nitric Oxide[15]

zones these nitrogen containing fragments are converted with high efficiency to nitric oxide by the N and NH reaction paths[36,55]

$$NH + O \longrightarrow NO + H \qquad 2.6$$

$$NH + O \longrightarrow N + OH \qquad 2.7$$

$$N + O_2 \longrightarrow NO + O \qquad 2.8$$

$$N + OH \longrightarrow NO + H \qquad 2.9$$

and CN reaction path

$$CN + O_2 \longrightarrow OCN + O \qquad 2.10$$

$$OCN + O \longrightarrow NO + CO \qquad 2.11$$

For fuel-rich flame zones, the fuel-nitrogen is thought to convert rapidly to HCN, which is then oxidized to nitric oxide. The mechanism for this oxidation is in doubt due to the poor availability of the traditional oxidizing species O_2, O, and OH; however, there is evidence that the rate of HCN consumption is a mixed first and second order reaction with respect to OH concentration. Thus the reaction

$$HCN + OH \longrightarrow HNCO + H \qquad 2.12$$

appears to represent an important pathway in the fuel-rich oxidation of HCN. The resulting oxycyanogens may react with hydrogen to form amines that participate in reactions with OH or oxygen to produce nitric oxide, which may then be reduced by the high amine concentration to molecular nitrogen. Because of the low OH concentration it has been suggested that for fuel-rich system CN may be oxidized by CO_2[56]. It is difficult to discredit any reaction showing reasonable thermodynamic driving forces unless a complete description of reaction pathways is determined. The most probable result is that all reactions of the sort considered are significant.

2.4 Nitric Oxide Emissions Control[57]

Most nitric oxide control strategies are designed to minimize the residence time at peak temperatures, to operate at reduced peak temperatures, and restrict the availability of oxygen for reactions to nitric oxide. Techniques for accomplishing reduced nitric oxide emissions include

(1) Flue-gas scrubbing

(2) Flue-gas recirculation

(3) Burner design modification

(4) Low excess air combustion

(5) Staged combustion

2.4.1 Flue-gas Scrubbing[58]

Because nitric oxide is a relatively stable gas it is difficult to remove from flue-gas. The amount of nitrogen oxides in flue-gas is typically 700 ppm, about one-third that of typical sulfur oxide concentrations. Wet scrubbing limestone processes remove about 20% of the nitrogen oxides, and a better scrubbing agent designed for nitrogen oxides does not appear to be forthcoming.

2.4.2 Flue-gas Recirculation[11]

The return of oxygen deficient and partly cooled combustion gases to the combustion chamber reduces the peak temperature and oxygen concentration. Many large steam boilers employ flue-gas recirculation as a control technique under changing load conditions. Recirculation of combustion products may also be accomplished by introducing swirl into the flow field in the combustor. This will reduce oxygen concentrations, improve mixing near the burner, and help volatiles escape

from the fuel particle while still far from the flame.

2.4.3 Burner Design Modification[59,60]

Burner configuration influences the nitric oxide emission by the efficient use of combustor space. Tangentially fired burners are located at the corners of a boiler and directed so that the flames from each imping upon a circle on the axis of the combustion chamber. In this way the flame is more uniformly distributed in the combustion volume, thus reducing specific energy output, and improving radiative transfer to the boiler walls. The spiralling path of the reactants increases the residence time in the boiler improving heat transfer. The resultant effect is to lower peak temperatures and thereby nitrogen oxide emissions

2.4.4 Low Excess Air Combustion

Most combustion processes use excess air to ensure the burnout of carbonaceous particulates, carbon monoxide, and unreacted hydrocarbons. The cause of the poor combustion is poor mixing of the fuel and oxidant. By proper design, mixing may be improved allowing a reduction in the excess air. The reduced oxygen availability is seen to reduce nitrogen oxide emissions. The technique has been applied most successfully to gas and oil fired boilers, although coal fired boilers have shown reduced nitrogen oxide emissions.

2.4.5 Staged Combustion[57]

By the partial combustion of a fuel in a fuel-rich first stage oxygen concentrations are maintained at minimal levels, and peak combustion temperatures are limited, thereby limiting the conversion of

atmospheric and fuel-nitrogen. The remaining oxidant to complete combustion is added in a second stage which is prevented from generating excessive amount of thermal NO by inter-stage cooling of the combustion gases. Staged combustion appears to be the most promising, method for controlling fuel-nitrogen.

2.5 Conclusion

The combustion of liquid fuels has long been a problem of rapid kinetics and heat extraction. The processes involved in the combustion of liquid fuels had been developed to a level that the problems of producing energy from liquid fuels were for all intents and purposes, solved. The advent of the age of expensive energy has compelled consumers to consider sources of energy containing high concentrations of nitrogen. The most promising method for controlling the conversion of fuel nitrogen to nitric oxide appears to be staged combustion. In light of the restrictions imposed by the technique of staged combustion it is necessary to re-evaluate ones abilitiy to burn high carbon to hydrogen ratio fuels having high nitrogen content, under conditions limiting the conversion of fuel-nitrogen, without excessively increasing the formation of other pollutants.

If the fuel-nitrogen is evolved into the gas phase with sufficient time for mixing and reaction, then staged combustion seems to work well. However, the evolution of the fuel-nitrogen is limited by equilibirum, and mass transport constraints during the vaporization of the fuel droplet. Moreover, if the fuel-nitrogen is concentrated in the residuum, as distillation studies of alternative liquid fuels suggests, and that this residuum is composed of high molecular weight, high carbon to hydrogen ratio molecules, which tend to pyrolyse to chars that burn out slowly,

then it is conceivable that these nitrogen containing chars will not have sufficient residence times in the first stage, thus releasing their nitrogen in the oxygen rich second stage.

CHAPTER 3

PREVIOUS WORK

Most research on droplet combustion has been performed on single droplets and mono-size arrays, in that it is easier to model these systems, thereby obtaining insight into the physical and chemical processes. Research on polydisperse spray systems is limited to parametric studies which provide useful information for a particular combustor-burner-fuel combination. Laboratory research on sprays has usually been confined to mono-disperse one-dimensional flow systems in order to confirm the applicability of mathematical models.

Fuels used for laboratory studies have been pure liquids or light distillates. Only recently has it become necessary to take into account details of the peculiar behaviors of heavy fuels oils, in particular the alternate fuels. Experiments performed using heavy fuels oils have so far provided general observations of mass rates of vaporization, particle size variation, and char formation.

Modelling of liquid fuel vaporization and combustion is founded on models of single particle systems. These models are then extended to include the interactions between neighboring particles in simple arrays. The problem of droplet vaporization requires consideration of the simultaneous heat, mass, and momentum transport in the liquid and gas phases, and the coupling between the phases by thermodynamic constraints at the interface. If combustion is taking place in the gas phase, the effects of the reaction must be included. It is also possible that reactions in the liquid phase are also of importance. Because of the great difficulty in accounting for all these effects within a single comprehensive description, the models of droplet vaporization and combustion are greatly simplified. The most

successful models have been spherically symmetric quasi-steady state energy transport descriptions. Analysis of unsteady state systems, systems involving finite chemical kinetics or variable physical properties, have only served as guides for the validity of the spherically symmetric quasi-steady state models. Non-spherical models to describe flame contours, drag coefficients, and the enhanced gas phase transport processes, and circulation within the liquid phase due to slippage at the droplet surface, require solutions of the Navier-Stokes equations or boundary layer approximations of them. As a result, aspheric systems are corrected for deviations from spherical models either empirically or by analogy to solutions for hard sphere models.

3.1 Spherical Quasi-Steady State Models (Fig. 3.1)

Godsave [62-65] was one of the first to attack the problem of droplet combustion, although the problem of particle vaporization had been considered already by Maxwell[66], Nusselt[67], and Fuchs[68]. Godsave obtained the following expression for the mass rate of vaporization of a single component droplet under steady state conditions with spherical symmetry:

$$\dot{m} = \frac{2\pi\, k\, d\, \ln\left\{1 + c\left(\frac{T_f - T_s}{Q - R_a}\right)\right\}}{c\left(1 - \frac{d}{d_f}\right)} \qquad 3.1$$

No consideration of flame position, d_f, from gas phase composition is included in Eq. 3.1 and thus must be found experimentally. However, for the case of a droplet vaporizaing in a hot atmosphere without combustion, $d_f \to \infty$, and the parenthetical term in the denominator may be ignored.

Long rectified Godsave's neglect of flame position to obtain an

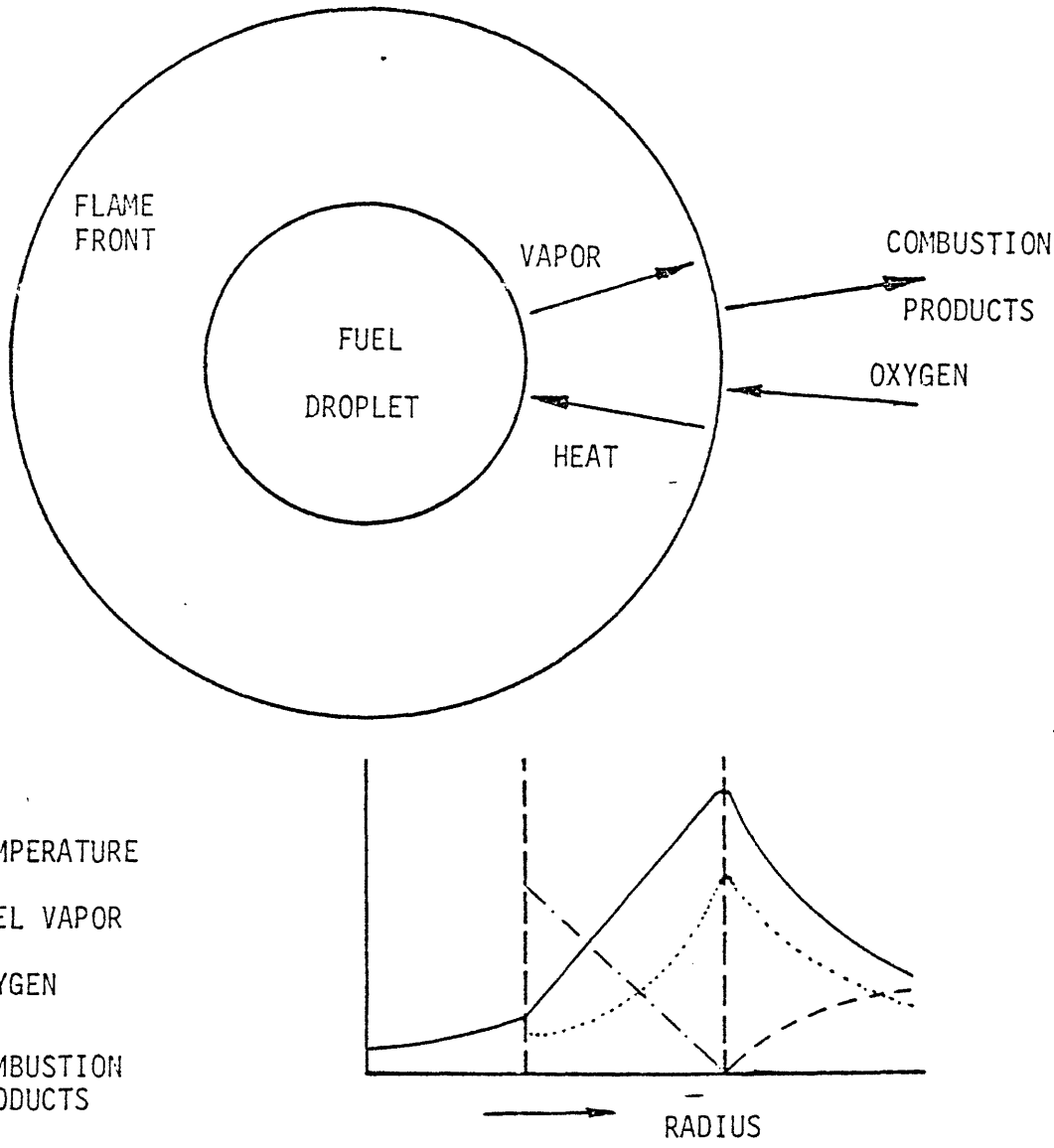

ASSUMPTIONS:

(1) SPHERICAL GEOMETRY
(2) GAS PHASE TRANSIENT BY DIFFUSION
(3) CHEMICAL REACTION IS INSTANTANEOUS
(4) LIQUID PROPERTIES UNIFORM AND EQUAL TO SATURATED CONDITIONS
(5) BODY FORCES, PRESSURE GRADIENTS, THERMAL RADIATION, AND BULK VISCOSITY, SORET, AND DUFOUR EFFECTS ARE NEGLIGIBLE

Figure 3.1 Spherically Symmetric Model of Droplet Vaporization[13]

expression for $\dot{m}$ without d_f.

$$\dot{m} = \frac{2\pi\ k\ d}{c} \ln \left\{1 + c\left(\frac{T_f - T_s}{Q}\right)\right\} + \frac{\pi\rho D\ d}{16\chi} \ln \left(1 + \frac{\chi\ N_\infty}{\Omega}\right) \qquad 3.2$$

Goldsmith and Penner[70] repeated Godsave's analysis, but allowed k, and c, to be linear functions of temperature. Wise et al.[71] assumed D and c/k to be constant, whereas, Hottel et al.[72] used a log mean value of k/d. Wise et al.[71] also derived expressions for flame temperature, mass fraction of fuel at the droplet surface, and the ratio of flame to droplet diameters. Goldsmith and Penner[70], and Wise et al.[71] also deduced the temperature and composition profiles surrounding the droplet.

Spalding [73, 74] postulated that combustion occurs in a boundary layer surrounding the droplet, and that the thickness of the layer may be predicted by analogy with heat and mass transfer coeficients. By solving the transport equations for heat and oxidant surrounding the droplet, Spalding[74] obtained expressions for T_f, d_f, and $\dot{m}$, the last being

$$\dot{m} = \frac{2\pi\ d\ k}{c} \ln (1 + B) \qquad 3.3$$

where B is called a transfer number,

$$B = \frac{H}{Q}\frac{M}{i} + c\left(\frac{T_g - T_s}{Q}\right) \qquad 3.4$$

Since the only time dependent term of Eqs. 3.1, 3.2, and 3.3 is d, by expressing $\dot{m}$ in terms of d, a relationship for the temporal size variation is found:

$$d_o^2 - d^2 = \lambda t \qquad 3.5$$

In Eq. 3.5, λ is termed the vaporization rate constant, and is related to the mass rate of vaporization, $\dot{m}$, by the equation

$$\lambda = - \frac{4 \dot{m}}{\pi \rho_{\ell} d} \qquad 3.6$$

3.2 Non-Steady State Models

While Eq. 3.5 has been found adequate for simple fuels burning at near atmospheric pressures, the vaporizing droplets are actually in a transient state which is evidenced by changes in the ratio of flame to droplet diameters that, according to the quasi-steady analysis of Goldsmith and Penner[70], should be constant. Kotake and Okazaki[75] undertook a numberical analysis of these effects, and Krier and Wronkiewicz[76] were able to express the "d^2-law", Eq. 3.5, in terms of (d_f/d). Rosner and Chang[77] studied the non-steady effects of droplet vaporization at near critical conditions. Crespo and Liñan[78] perfomed an asymptotic analysis of the non-steady effects in the gas phase. Hubbard et al.[79] considered in numerical study the effects of transients and variable properties. The results showed that temporal storage of mass species, energy, and radial pressure variations in the gas phase to be negligible, the initial transient behaviour being due to sensible heat accumulation in the droplet and related variations in the surface vapor pressure. The transient evaporation is also claimed to be independent of the initial size, but to follow a "d^2-law" behavior. Law[80] also found liquid phase heating to be the primary cause of transients following a lumped parameter analysis of the droplet. Wise and Abolow[81] derived temperature distributions within the droplet as a function of $\lambda/8\alpha$ and found that liquid phase temperature profiles to be significant if $\lambda/8\alpha$ is greater than unity.

There is still a great deal to be desired in the analyses of transient effects. It is still uncertain as to the importance of transport property variations, or whether the numerical analyses are generally valid. The

effects of multicomponent distillation are covered in a separate section.

3.3 Considerations of the Influence of Convection

It has already been stated that convection effects are difficult to model because of the complex momentum equations involved. As a result little theoretical progress has been made. The usual attack[82-85] is to assume similarity to solid sphere models and empirically fit constants to a correction factor for the static case:

$$\dot{m}_c = \dot{m} \quad (1 + a\ Re^{1/2}\ Pr^{1/3}) \qquad 3.7$$

The value of expressions of this type is limited, since they lack any correction for the radial velocity at the surface of the particle. Some attempts have been made to predict flame shape under these conditions but all rely on arbitrary simplifying criteria.

Generally, it is known that convection increases the vaporization rate, that the thermal flux is not uniform over the droplet surface, that a boundary layer of finite thickness exists, and that flame shape is deviated from spherical or even that the flame may become detached and burn in the wake of the droplet.

Because of the vaporization, a moving droplet experiences a lower drag than a solid sphere[86]. This is due to thickening of the boundary layer, and, for a burning droplet, the expansion of gases in the flame helping maintain pressure gradients at the surface inhibiting the formation of a turbulent wake. Analyses of the effects of vaporization on the drag coefficients of spheres have been accomplished for low Reynolds numbers. The reduction in drag is found to be even greater for arrays of vaporizing particles which can travel in each others wake[87].

3.4 Models of Particle Interactions

Carstens et al.[88] analysed the effects of interactions due to two droplets growing in a supersaturated atmosphere of finite dimensions, and Zung has employed semi-empirical models for multidroplet systems. A more rigorous approach to multiparticle systems was developed by Labowsky[90] to analyse the nearest neighbor interactions on the evaporation rate of particle clouds. Labowsky[90] used a modified method of images to determine the vapor concentration field in arrays of upto nine quasi-steady state vaporizing particles. The method employed is unwieldy and does not account for unsteady state behavior. However, Labowsky[90] empirically correlates the efficiency of evaporation for an array of N particles having interdrop spacings, S, and diameters, d:

$$\eta_A = \tanh \{(S/d)^{0.025(N-1)+0.287 \ln [5.71/(N-1)^{0.582}]}\} \qquad 3.8$$

Except for Ray and Davis[91], other studies [92-94] of this problem have limited application. Ray and Davis[91] present a generalized treatment of combined heat and mass transport between an assemblage of particles and their environment. The unsteady-state diffusive transport is shown to depend upon the size and positions of the particles, and the rate processes are found to differ markedly from single particle rates due to particle interactions. The expression obtained for η_A equivalent to Eq. 3.8 is

$$\eta_A = \frac{2 - \frac{N}{(N-1)}\frac{S}{d} - \frac{1}{(N-1)}\sum_{n=1}^{N-2}\frac{S}{S_n}}{N\left[\frac{d}{S} - \frac{1}{(N-1)}\frac{S}{d} - \frac{1}{(N-1)}\sum_{n=1}^{N-2}\frac{S}{S_n}\right]} \qquad 3.9$$

where S_n is the distance of the nth particle to the end of the array.

3.5 Multicomponent Droplet Vaporization Models

It is acknowledged that diffusion in liquids is relatively slow[95]. The effect of internal diffusional resistance is to cause a concentration of the less volatile species in the surface of a vaporizing droplet. Wood et al.[96] uses an expression to average composition effects for the burning rate coeffcients of binary mixtures. Law[97-99] has discussed at length and performed some calculations to identify the best models for describing multicomponent droplet vaporization, and some calculations on the relative importance of internal boiling and superheating. Landis and Mills[100] found from numerical analysis that internal diffusion can cause large deviations in species evolution as compared with batch distillation, and internal boiling, due to excess vapor pressure of trapped volatiles in the droplet core, to be a reasonable expectation.

3.6 Liquid Phase Circulation

Savic[101] has presented a solution for the formation of Hill's vortices in a particle falling through a viscous medium. Prakash and Sirignano[102] support the existance of this circulation in low viscosity droplets. Law et al.[103] consider the problem without committing themselves. For heavy fuel oils there is no consideration at all, although, based on the analyses for low viscosity materials, it appears unlikely that internal circulation plays a major role. Never-the-less, it is suggested[104] that diffusional effects will still be present but with a reduced length scale.

3.7 Experimental Studies

3.7.1 Pure Fuels and Light Distillates.

Single droplet combustion has been investigated using:

(i) Suspended drops

(ii) Porous spheres

(iii) Single droplets and droplet arrays in free flight

Experiments have been performed to determine ignition times, to confirm the validity of the "d^2-law", Fig. 3.2, and the variation of the burning constant with temperature, pressure, and oxygen concentration, Fig. 3.3, and to obtain empirical correlations for the effects of convection, Table 3.1. Kumagai and Isoda[114] obtained a correlation for the enhanced vaporization of single droplets in vibrating air. Spalding[115] observed wake flames stabilized behind a droplet in a stream having a velocity in excess of the extinction velocity. Udelson[116] observed another stable flame type within the boundary layer at the side of a droplet. Eisenklam and Arunachalam[117] found drag coefficients to be greatly influenced by the type of flame. Measurements of droplet temperatures indicate that thermal equilibrium is not accomplished for much of the droplets lifetime.

Studies of monodisperse and polydisperse systems have shown "d^2-law" behavior apparently prevails. Burgoyne and Cohen[118] found droplets less than 10 micrometers in diameter to burn like a premixed gas. Also it was found that burning velocities increased with increasing particle size but reduced the lower limit of flamability. Other researchers[119-121] of polydisperse system have found similar results but for different fuels.

3.7.2 Heavy Fuel Oils

The first serious studies of heavy fuel oils were undertaken at M.I.T.[31, 72], and by Topps[122], Kobayasi[60] and Wood et al.[96]. No significant additional research was performed until the early 1970's when pollution and energy considerations prompted a number of investigations[33, 123-126]. The droplets frequently show swelling, Fig. 3.4, and do not

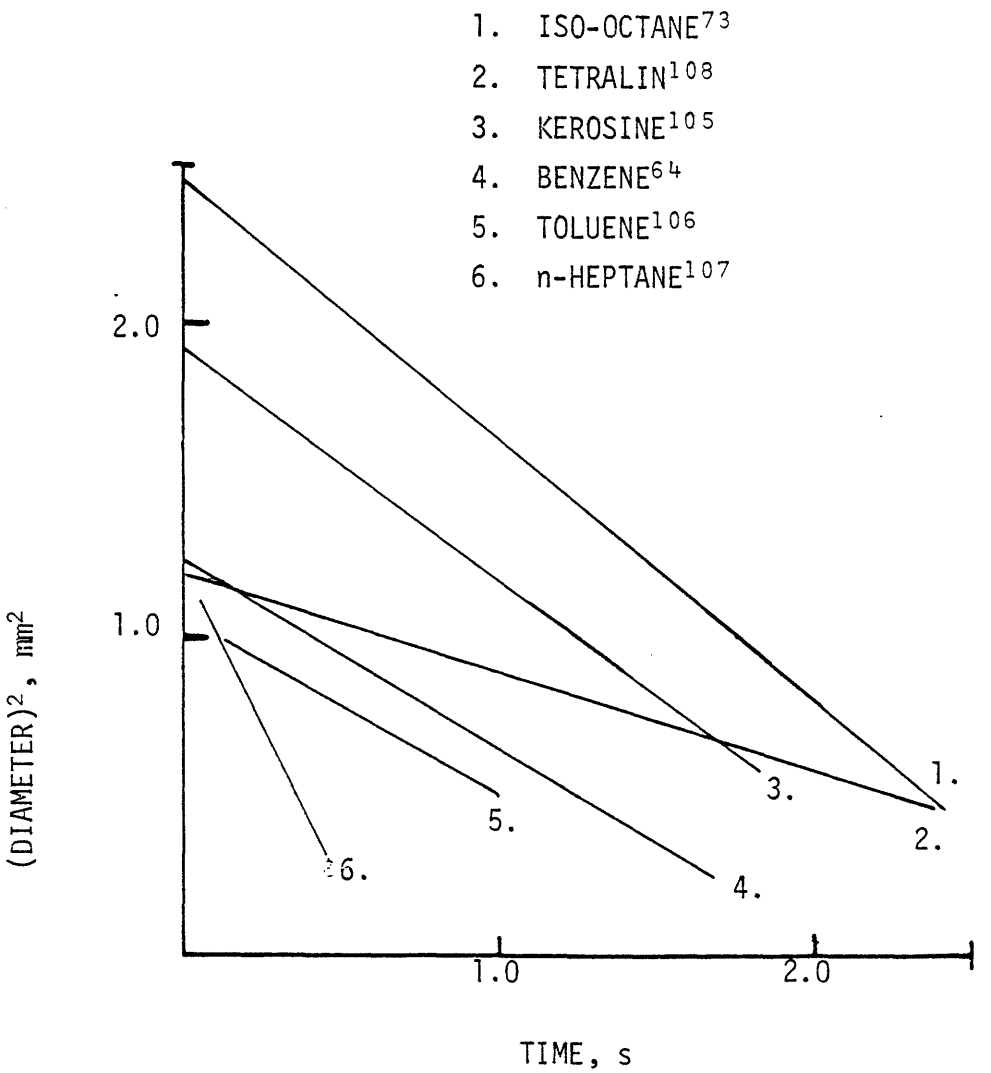

Figure 3.2 "d^2-Law" Dependence of Various Fuels

1. Amyl Acetate[108]
2. Benzene[64]
3. Cetane [106]
4. Diesel Oil[106]
5. Ethanol [110]
6. Furfuryl Alcohol[108]
7. n-Heptane[107]
8. Hexadecane.[83]
9. Iso-Octane[111]
10. Kerosine[105]
11. Tetralin[108]

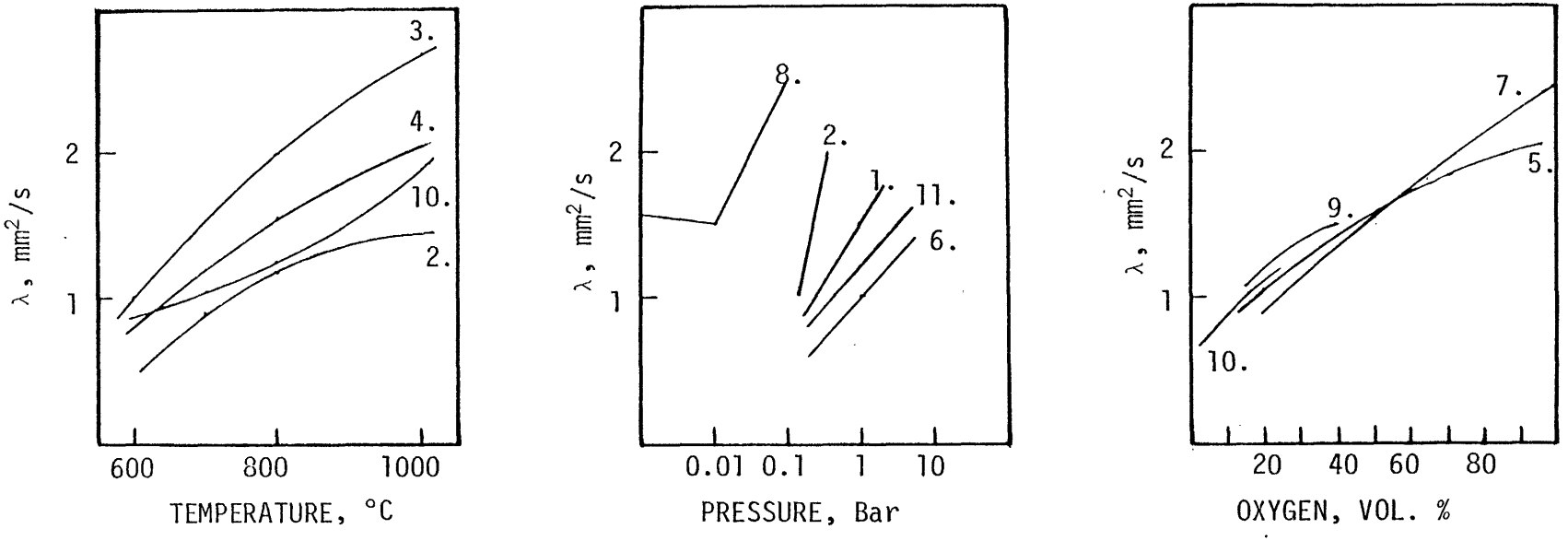

Figure 3.3 Variation of Vaporization Rate Constants with Temperature, Pressure, and Oyxgen Concentration for Burning Fuel Droplets

	Forced Convection
Ranz and Marshall[82]	$\dot{m}_c = \dot{m}\ (1 + 0.3\ Re^{1/2}\ Pr^{1/3})$
Agoston et al.[83]	$\dot{m}_c = \dot{m}\ (1 + 0.24\ Re^{1/2}), Pr = 1$
How[85]	$\dot{m}_c = \dot{m}\ (1 + 0.22\ Re^{1/2}), Pr = 1$
Spalding[73]	$\dot{m}_c = 0.53\ B^{3/5}\ Re^{1/2}\ \frac{\mu}{d}$

	Free Convection
Agoston[83]	$m_c = m\ (1 + \frac{0.20}{B^{0.44}}\ Gr^{0.3})$
Spalding[73]	$m_c = m\ \frac{k}{c}\ B^{3/4}\ (\frac{gd^3}{\alpha^2})^{1/4}$

Table 3.1

Convection Correlations for Droplet Vaporization

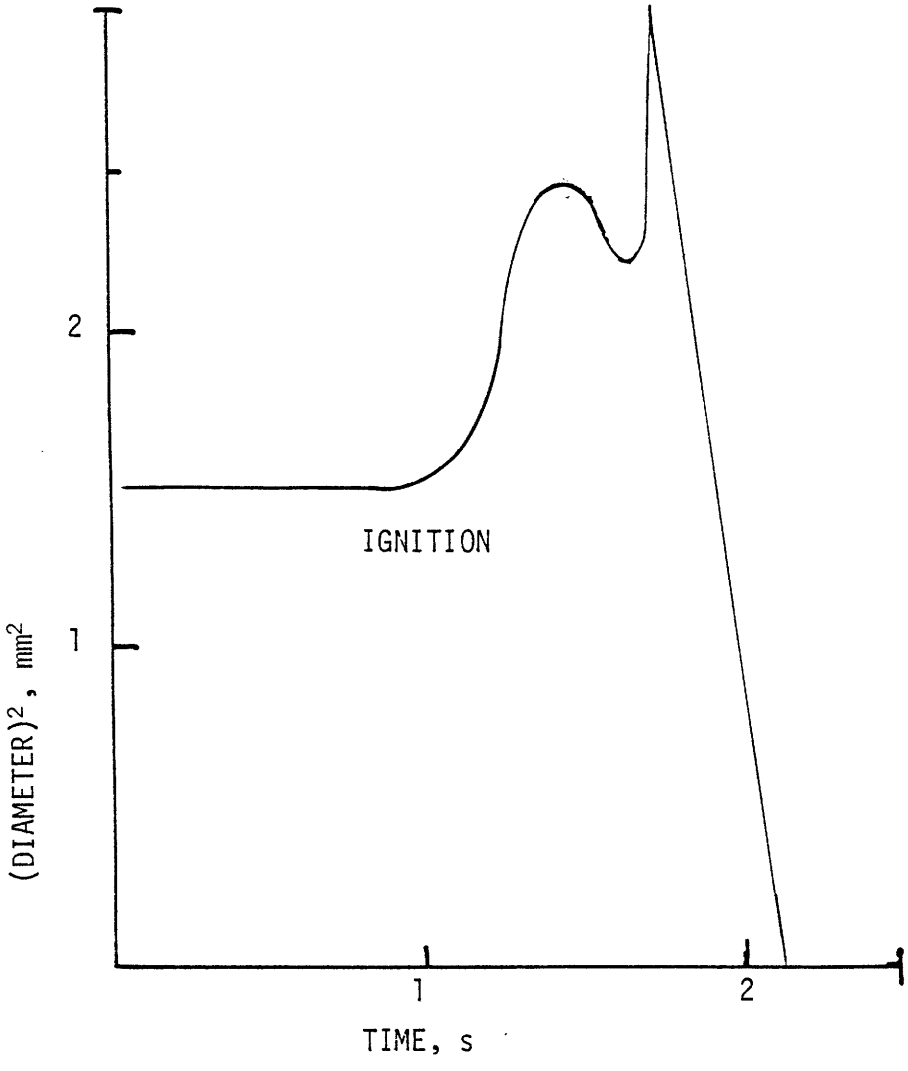

Figure 3.4 Surface Area Variation for Droplets of Residual Fuel Oil in Air at 1073 K

follow the "d^2-law" although based on weight loss, equivalent burning rate constants can be defined. Mardin and Thring[105] reported cenosphere formation and suggested, for the fuel used (pitch creosote), a relationship between cenosphere diameter and initial droplet diameter. Radiation appears to play a greater role in the vaporization of these fuels, and may be responsible for solids formation in the fuel droplet. Braide et al.[127] have been researching several alternative fuels including solvent refined coal, coal-oil mixtures and asphaltic residual fuels oils. Although containing much useful information, the interpretation of results is still poor.

CHAPTER 4

THESIS OBJECTIVES AND RESEARCH APPROACH

The objective of this thesis is to identify those factors of significance in the vaporization of multicomponent fuel droplets, to show how these factors may influence the rate of evolution of nitrogenous species from heavy fuel oil droplets under conditions of rapid heating, and by a theoretical analysis, to confirm experimental observations and indicate the functional dependencies of the factors involved. The investigation consists of three segments; an experimental study of the nitrogen evolution from heavy fuel oil droplets, an experimental study of average composition variations of binary model fuel droplets, and a theoretical description of liquid phase concentrations in a vaporizing droplet.

The experimental approach requires the acquisition of information on the time resolved pyrolysis products of a fuel droplet at various rates of vaporization. The apparatus selected was a laminar flow drop-tube furnace. A monosize linear array of fuel droplets is introduced into the furnace by means of a vibrating orifice droplet generator. The residue of the fuel droplets is collected through a transpiring wall sampling probe at several residence times. A record of droplet size and velocity is obtained photographically. The weights and compositional analyses of the residues are compared with the corresponding results obtained from batch distillation at atmospheric pressure. The photographic data provides a measure of residence times in the furnace, and the information on droplet surface regression necessary as an input for the theoretical description.

The heavy fuel oils considered in the experimental program are a raw Paraho shale oil, an Alaskan petroleum residual fuel oil, a Gulf Coast No. 6 petroleum fuel oil, an Indo-Malaysian No. 6 petroleum fuel oil, and

various distillate fractions and blends of SRC-II and H-coal liquids. The fuels were selected as being representative of the type of fuels that would be profitably burnt in a staged combustor and having a range of fuel-nitrogen concentrations. The furnace experiments are performed under conditions to simulate those encountered in the first stage of a two stage combustor. The droplets of fuel are injected with nominal diameters of 150 micrometers into an atmosphere of pure Helium at temperatures between 1000 K and 1400 K.

The model fuels were chosen to demonstrate a range of behavior similar to that of the heavy fuel oils, but without many of the complications found with complex multicomponent mixtures in order that the important effects may be readily indentified, interpreted, and theoretically described. The model fuels are binary mixtures of dodecane doped with pyridine, quinoline, or acridine. The experiments performed with the model fuels duplicate those performed with the heavy fuel oils.

The theoretical development describes the liquid phase temporal and spatial concentration of a fuel component in a vaporizing fuel droplet. The mathematical description is for the interpretation of the results obtained for the model fuels, and by extentsion the behaviors of the heavy fuel oils. The functional from of the equations may also provide a limited ability to predict the fuel-nitrogen evolution of fuels yet to be marketed, and thereby assist in the design of combustion systems.

CHAPTER 5

EXPERIMENTAL APPARATUS AND PROCEDURES

5.1 Description of Apparatus

A system, Fig. 5.1, for the study of liquid fuel vaporization was designed and assembled. The major components of the system are: a laminar flow furnace, having a uniformly hot reactor zone and optical access to the reactor zone; an isothermal fuel reservoir and atomizer; a multi-phase sampling probe and sampling train; a gas flow metering and control system for the reactor zone flow, and sampling probe quenching; a photographic device, including light sources and extension for high magnification. Each of these components is described in detail in the following sections.

5.1.1 The Furnace (Fig. 5.2)

The furnace was manufactured by Astro Industries, Inc. (Santa Barbara, CA) according to provided design specifications. The furnace shell is made from wrought aluminum tubing with an anodized finish. The end bulkheads are water-cooled nickel-plated aluminum. Between the inside diameter of the shell and the graphite felt insulation pack is a tube-traced copper heat sink. The water tubing is a continuous length with connections outside the furnace shell. This avoids the possibility of water leaks within the furnace. Overall furnace dimensions are 254 mm diameter by 1118 mm long.

Two windows, 13 mm wide by 305 mm long, are located on opposite sides of the furnace and symmetrically centered about the hot zone. The windows are sealed with one-eighth inch thick quartz plates. A port is provided at the center of the hot zone in a plane perpendicular to that of the

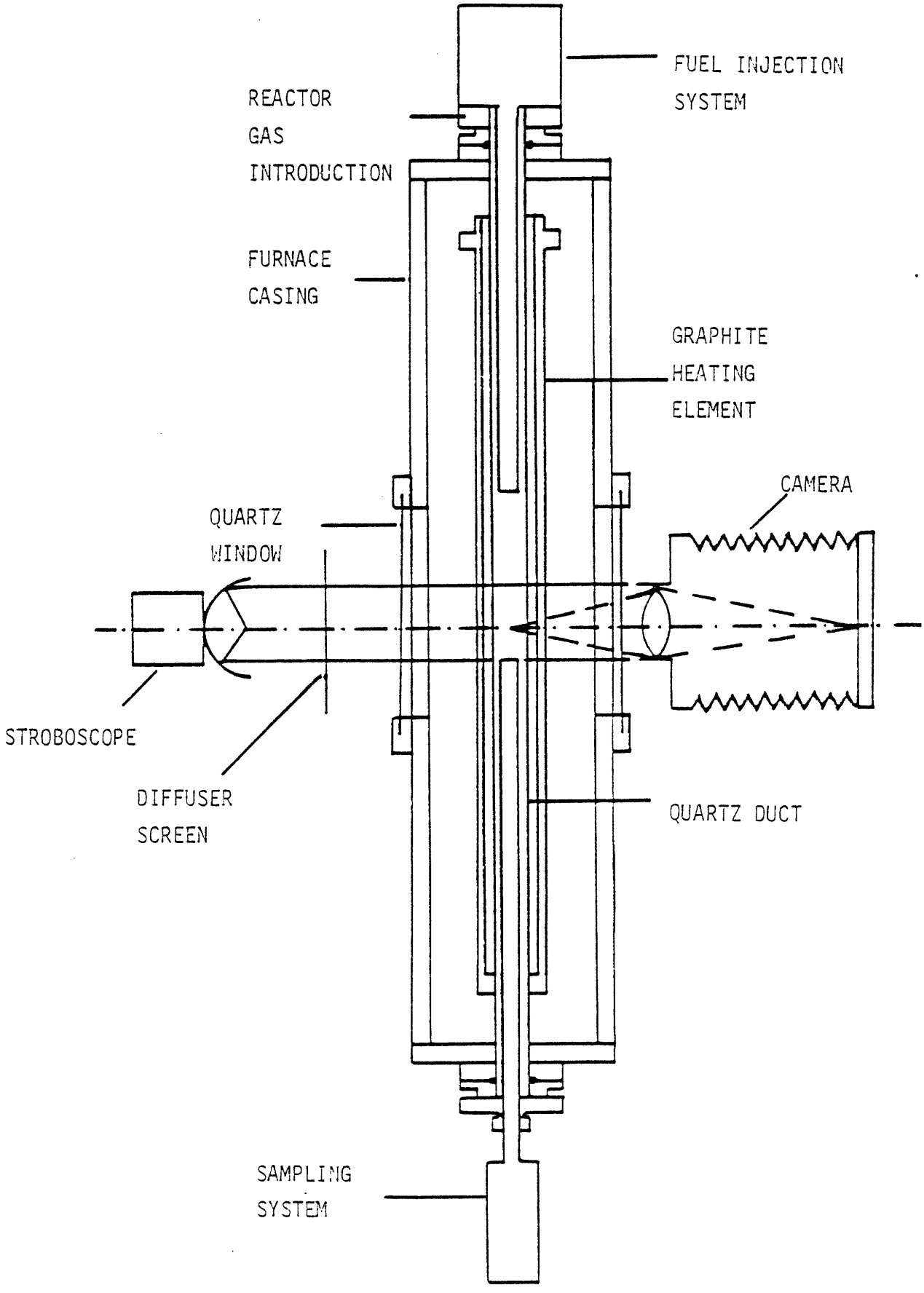

FIGURE 5.1 Schematic of Experimental System

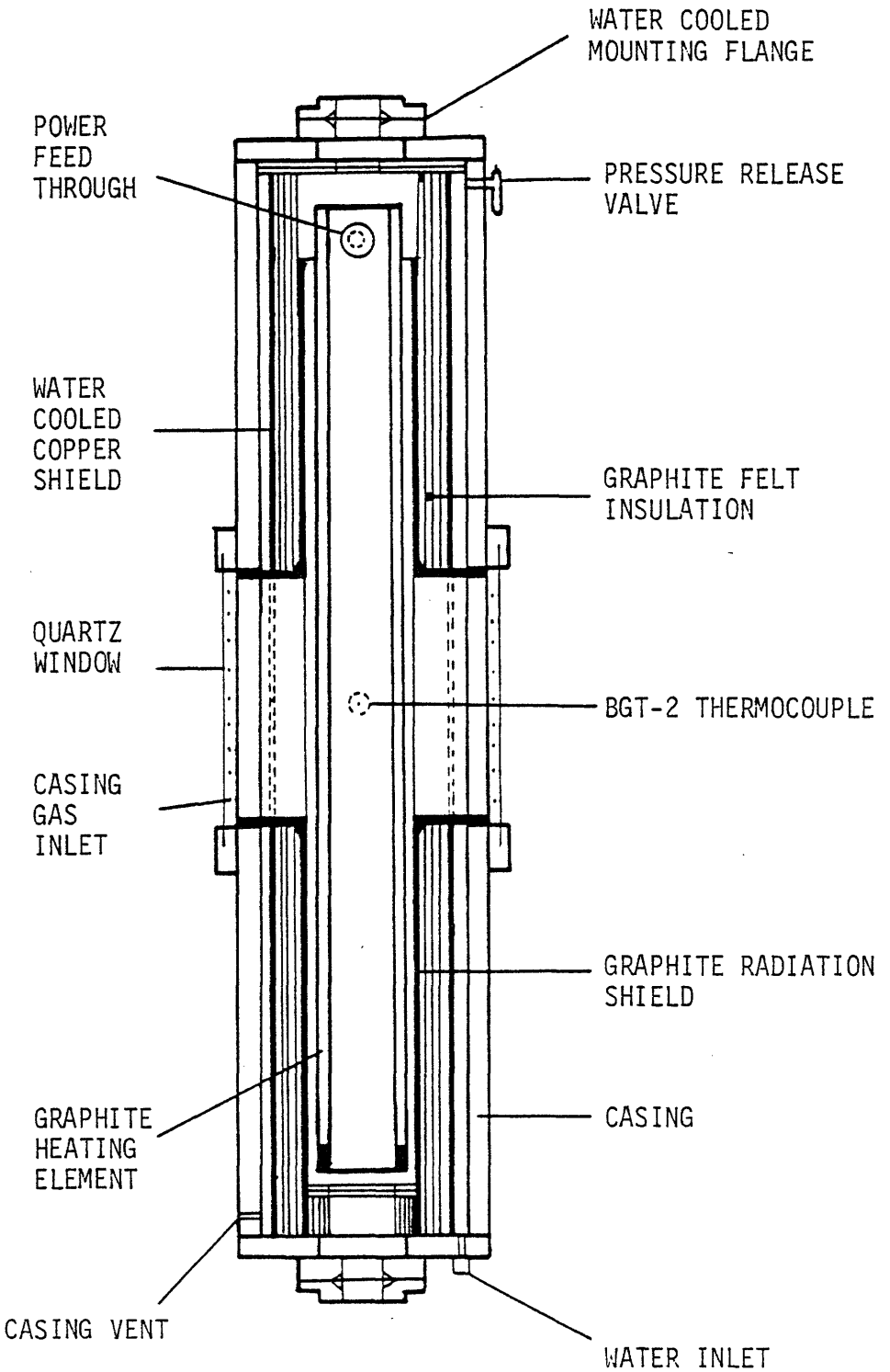

Figure 5.2 Laminar Flow Drop Tube Furnace

windows for a Graphite/Boronated Graphite thermocouple. A water-cooled 50 mm diameter O-ring seal assembly is provided at each end of the furnace to support a quartz tube that extends the length of the furnace.

The graphite heating element is supported from two power feed-throughs at one end of the furnace. This configuration limits the furnace orientation to a length-wise vertical position. The heating element is located between the quartz tube and the graphite radiation shield. The cavity containing the heating element is continuously flushed with helium, Fig. 5.3, which is introduced via a rotameter through orifices located in the window assembly and vented through a port in the casing at the lower end of the furnace. In the event of an over-pressurization of the casing, a pressure release valve is furnished through a port in the casing at the upper end of the furnace.

Power for the heating element is provided by a 20 k VA power supply consisting of a phase angle fired silicon controlled rectifier power regulator and a step-down load transformer. Power may be manually adjusted or automatically adjusted by a digital control programmer (Honeywell DCP-7700).

The digital control programmer is able to store upto nine separate programs or a total of 200 functions consisting of ramps, soaks, and event switches. The programmer is matched to the thermal stability characteristics of the furnace by proportional, integral and rate action. For the furnace system (this includes the influence of water-cooled devices in the quartz tube) it was found that the proportional gain constant was 1/2 mV (i.e. a difference of 1/2 mV between the input signal and the signal called for by the controller would cause a demand for 100% of available power to be provided to the heating element), the integral time was 1350 seconds per

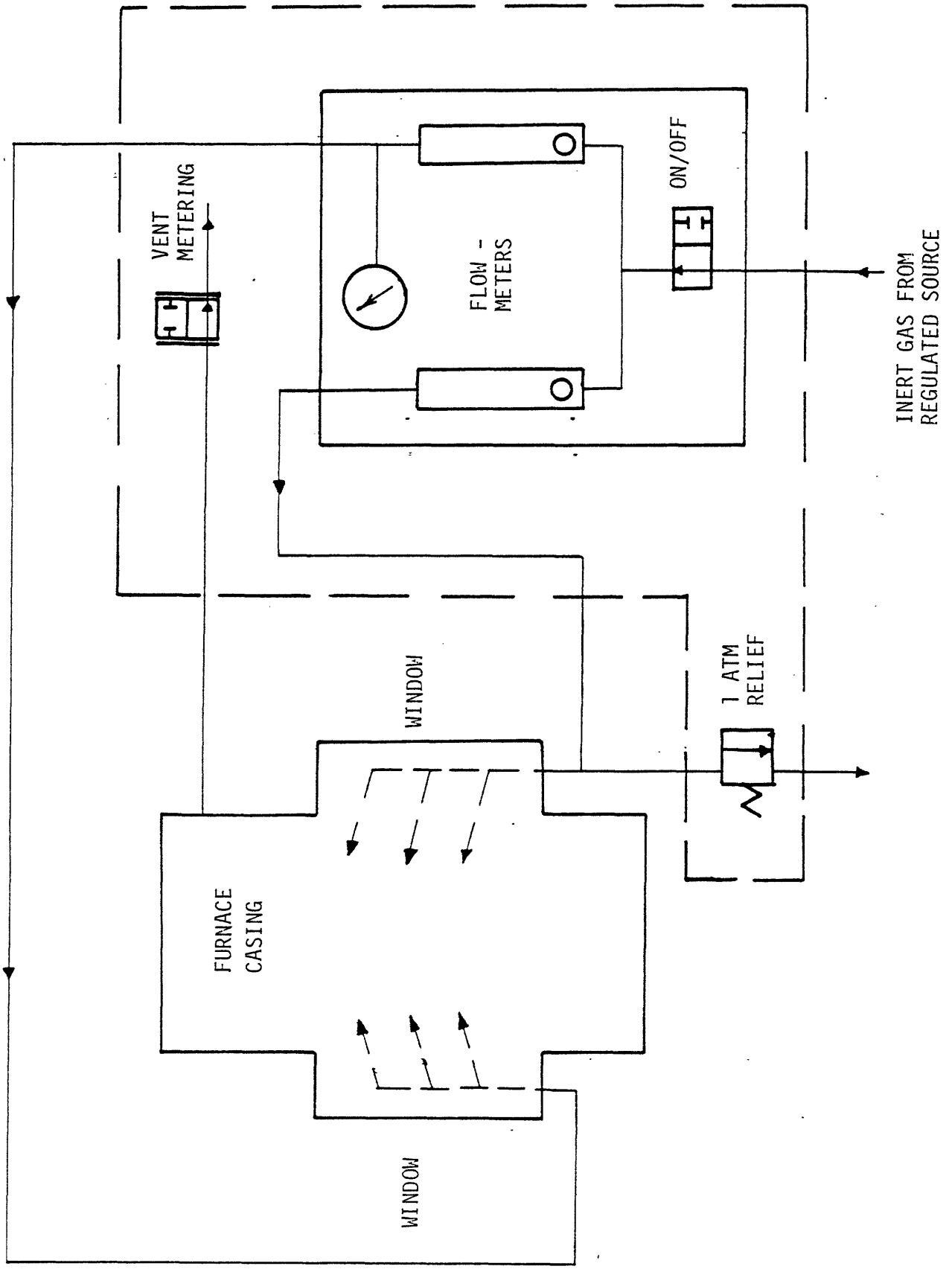

Figure 5.3 Schematic of Furnace Casing Gas Flows

cycle, and the derivative time was 240 seconds per cycle. Thus the system has a high thermal inertia. Once initiated, a program will control the rate of increase of furnace temperature, will hold the furnace at the desired temperature for any specified time, and will control the rate of cooling of the furnace.

The signal for the programmer is produced by the Graphite/Boronated Graphite thermocouple (Astro BGT-2) and transformed to a compatible programmer input by a signal transmitter (Rochester Instrument Systems model SC-1304). The BGT-2 thermocouple has an exceptionally high output and sensitivity throughout its entire operating temperature range, providing stable long-time operation to 2250K. All designs of this type of thermocouple have appreciable thermal mass and conduction losses along the graphite supporting elements to the water cooled cold-junction and thus must be calibrated.

The calibration is performed by sighting a "disappearing filiament" optical pyrometer (Pyro Micro-optical pyrometer model No. 95) through the furnace windows into a thermally equilibrated ceramic cavity (length to diameter ratio, 10) positioned at either end and the center of the uniformly hot zone which corresponds to the length of furnace having optical access. From these measurements it was found that maximum temperature differences within the uniformly hot zone did not exceed 8 celsius degrees at temperatures upto 1500 K. The calibration curve obtained from the center position is presented in Fig. 5.4. Sighting the optical pyrometer through the quartz plate necessitates a correction to the observed temperature due to adsorbtion of certain radiation wavelengths. This correction amounts to an additional 7 celsius degrees at 1400 K, 4 celsius degrees at 1200K, and 1 celsius degree at 1000 K.

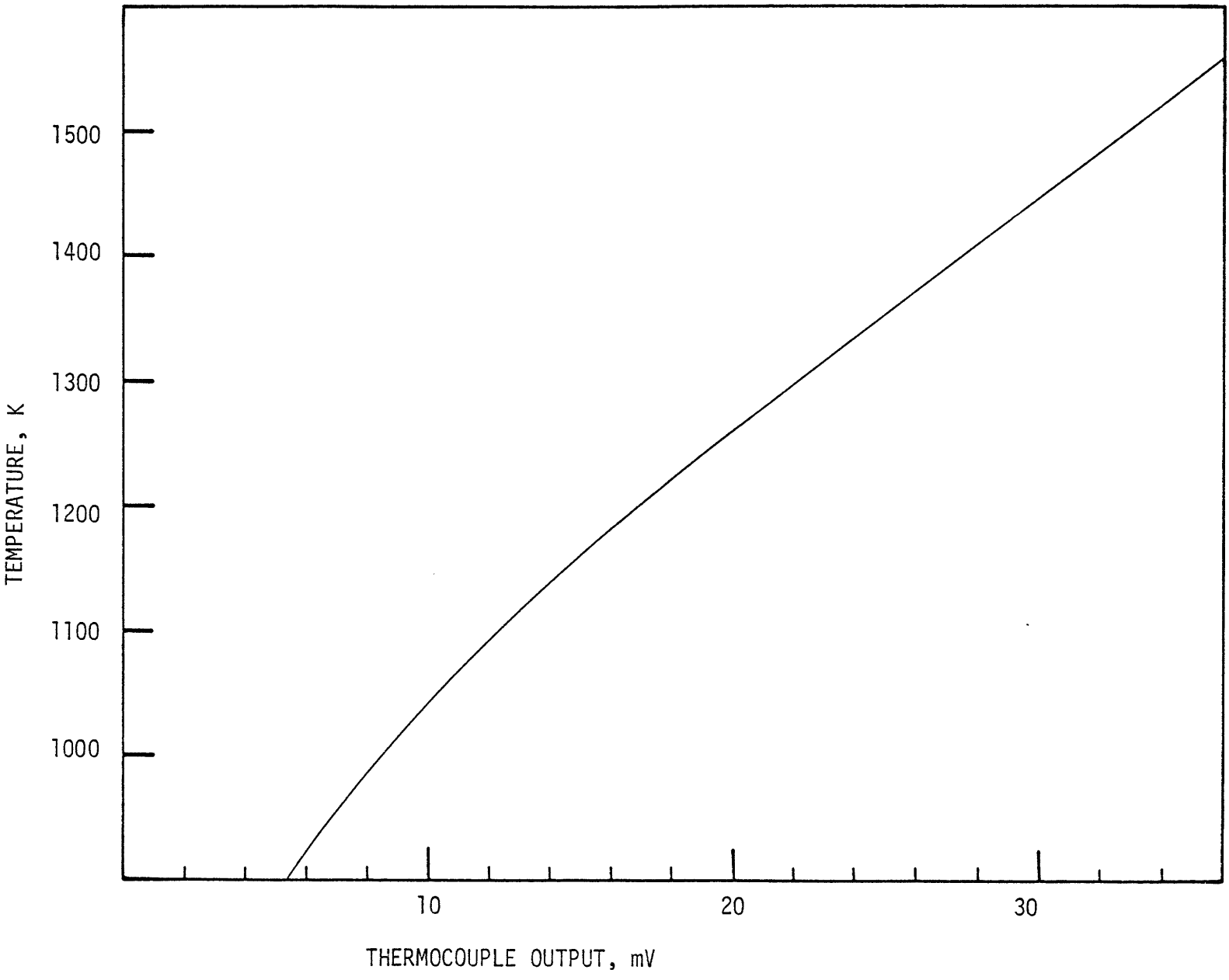

Figure 5.4 Calibration Curve for Furnace BGT-2 Thermocouple

The furnace is mounted on an elevating support stand, Fig. 5.5. The position of the furnace may be manually adjusted through a 305 mm vertical displacement. The furnace mounting bracket on the stand slides on hardened and ground shafts with linear ball brushings to provide smooth vibration free operation. Adjustment is by a hand crank driving a lead-screw through a right angle drive. The mechanical disadvantage of the gear is such that the furnace will remain steady in any position which may easily be set to within a millimeter.

5.1.2 Fuel Injection

The efficient atomization of a liquid requires that its viscosity be less than 20μ Pa.s (20 centipoise). For most heavy fuel oils this is accomplished when the fuel is heated to 100°C. In order to ensure uniformity of atomization the fuel temperature must be carefully held constant. The fuel introduction system designed for this investigation maintains a uniform temperature throughout the fuel system by allowing the boil-off of water. In Figure 5.6 the fuel reservoir and fuel lines are shown entirely surrounded by a water jacket. The lower probe-like section of the device is positioned inside the furnace (viz. Fig. 5.1) which provides the heat for the thermostat. In this lower section the water is a coolant, preventing excessive heating of the fuel from causing carbonization. The end section containing the atomizer is made from copper which calculations show will conduct heat rapidly enough so that even the extremities of this section exceed the coolant temperature by approximately only 2 celsius degrees. The heat from the lower section is carried by the coolant to the upper section where it heats the fuel in the reservoir. The temperature is controlled by adjusting the flow rate of coolant. In the case of heavy fuel oils, using water as coolant,

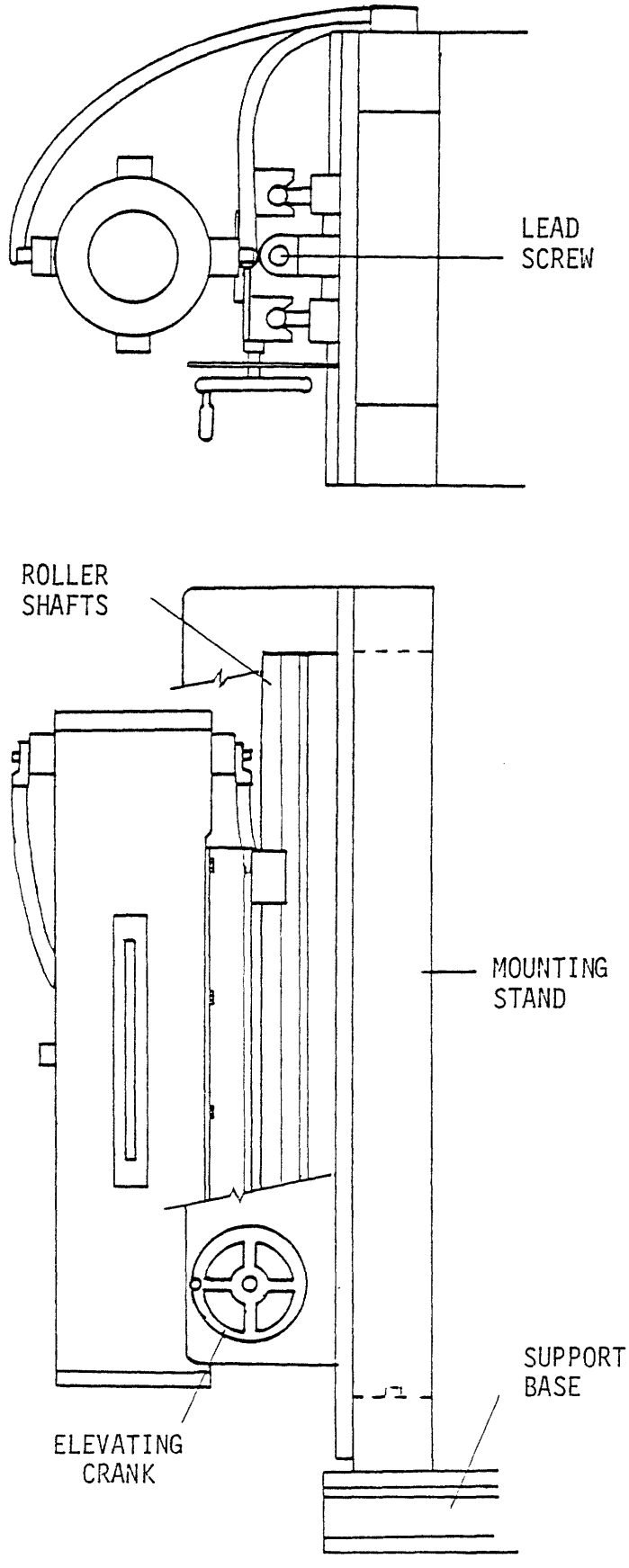

Figure 5.5 Furnace Elevating Support Stand

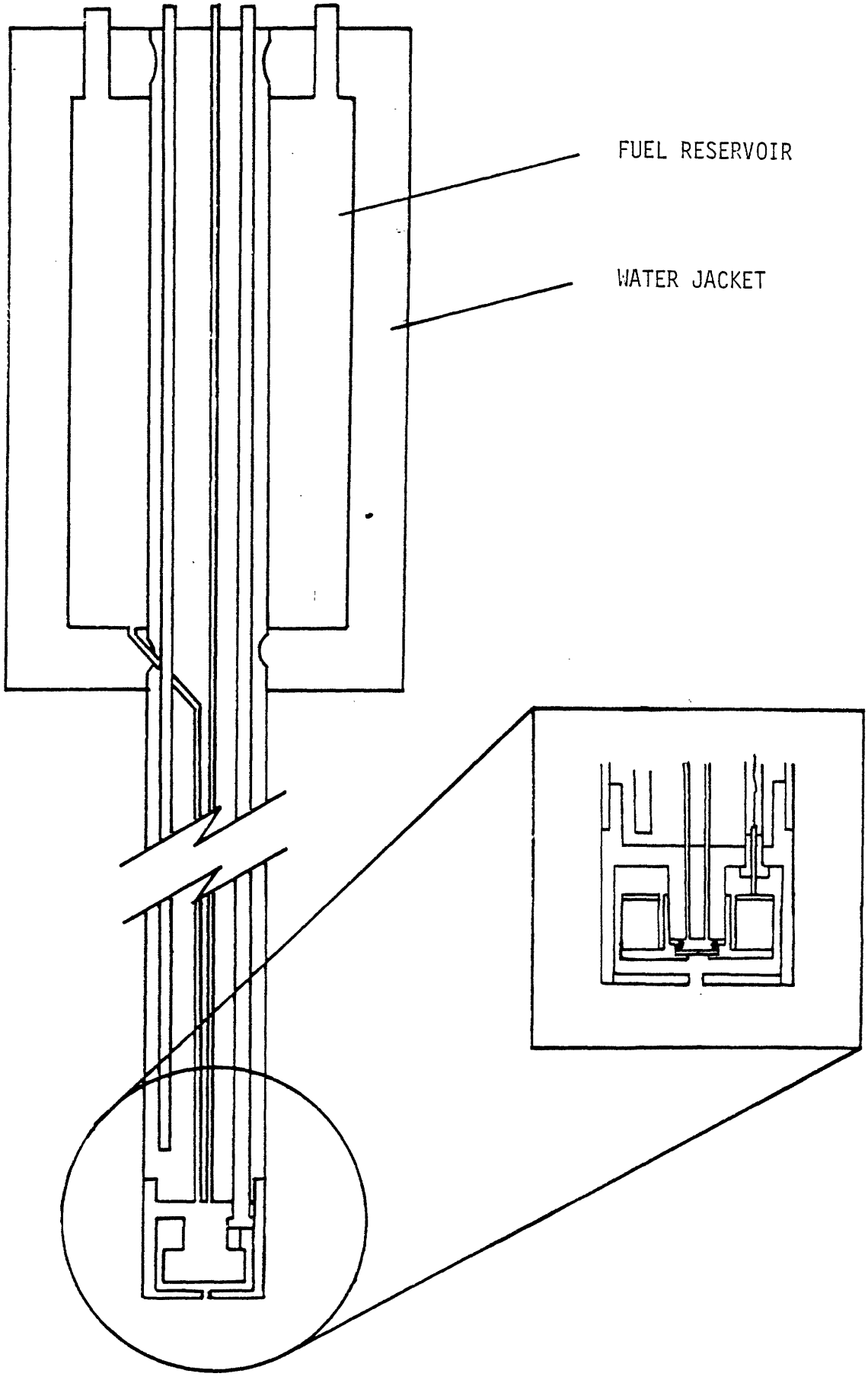

Figure 5.6 Fuel Injection System

the system is allowed to come to the boil, the water flow being only enough to maintain the fluid level. For fuels that do not require heating for atomization, a higher flow rate of water is maintained.

Pressurization of the fuel reservoir forces the fuel through the fuel feed lines to the atomizer. The fuel circuit is purged of any gas bubble by letting the fuel drive any gas out through the vent line. The fuel lines being completely filled with liquid, and the vent line valve closed, the only escape for the pressized fuel is through the atomizer orifice. The flow of fuel must be accurately and precisely controlled. This requires that a precision pressure regulator (Bellofram type 10B) be used in the pressurized gas line for the fuel reservoir. When the pressure is removed the static head of the fuel is sufficient to cause the orifice to leak, thus a slight vacuum is applied to the fuel reservoir to overcome the static head pressure, but not so much that the surface tension of the liquid in the orifice is overcome and gas drawn into the fuel system.

The atomizer, Fig. 5.7, is a vibrating orifice generator (TSI model 3050) driven by a piezo-electric ceramic stimulated by an electrical signal from a function generator (Tektronix model FG 503). The frequency of the signal is monitored by a frequency counter (Tektronix model DC 503).

A cylindrical liquid jet is naturally unstable and tends to break up into droplets. The optimum frequency of this process competes with a spectrum of allowable frequencies causing the break-up to produce non-uniform droplets. The application of an appropriate frequency will drive the system, forcing one size droplet to be produced. Moreover, as one droplet is produced per cycle of disturbance, the size of the

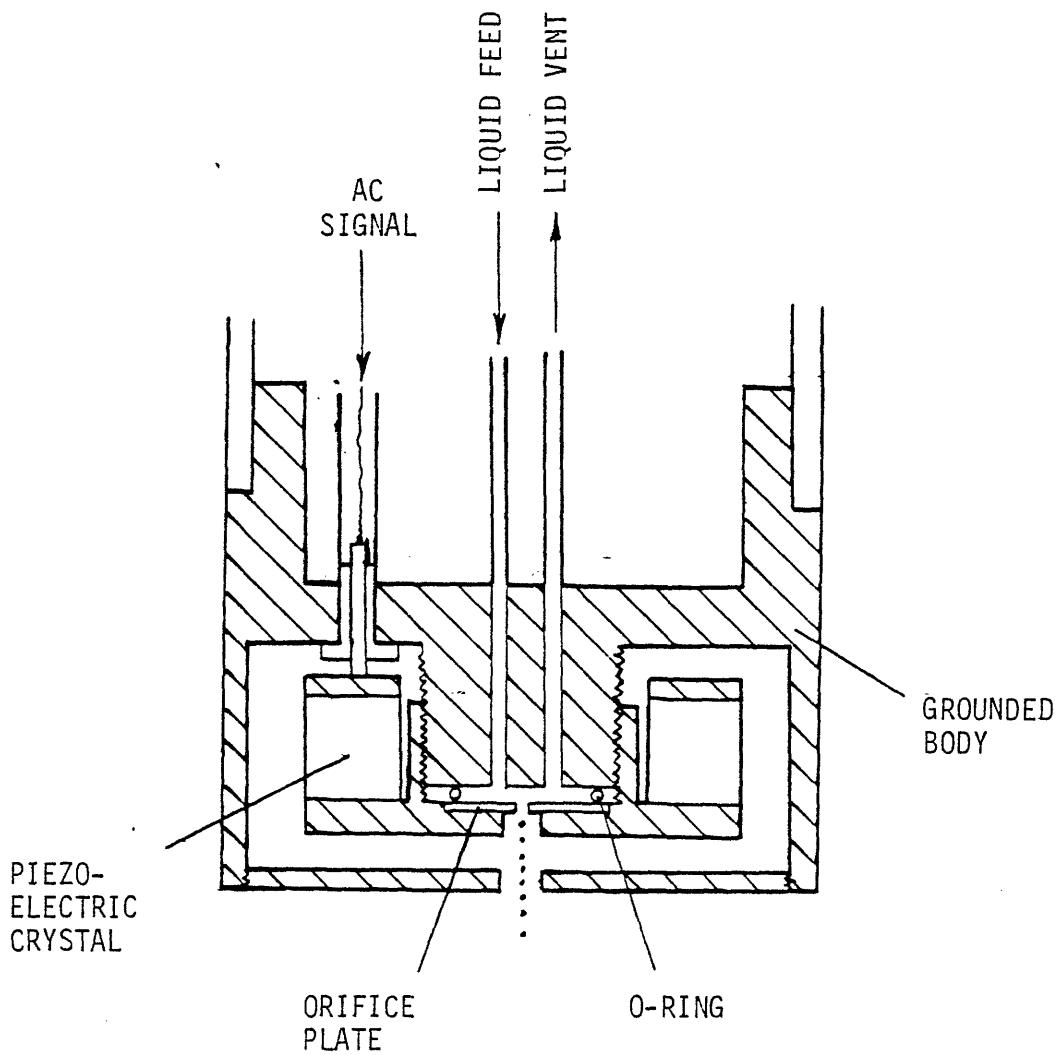

Figure 5.7 Piezo-Electric Atomizer

droplet and initial interdrop spacing are precisely determined by the fuel feed rate and the driving frequency,

$$d_o = \left(\frac{6}{\pi}\frac{\dot{v}}{\nu}\right)^{1/3} \qquad 5.1$$

$$S_o = \frac{4}{\pi}\frac{1}{D_o^2}\frac{\dot{v}}{\nu} \qquad 5.2$$

The stability with which a particular drop size is generated is determined from consideration of the jet diameter and velocity at the vena - contracta following the orifice. According to analyses by Schneider and Hendnicks[128], and Lindblad and Schneider[129], uniform droplets can be generated only by maintaining

$$1 < \frac{V_j}{3.5 D_j \nu} < 2 \qquad 5.3$$

and

$$V_j > \left(\frac{8\sigma}{\rho_\ell D_j}\right) \qquad 5.4$$

Instability may be introduced into the liquid jet from mechanical disturbances by the piezo-electric ceramic. The disturbances may result in the formation of poly-disperse, non-uniform, or satellite droplets. However, if the applied signal volatage is between 0.5 and 5 rms volts, the criteria of Eqs. 5.3 and 5.4, ensure uniform droplet generation.

5.1.3 Sample Collection (Fig. 5.8)

The sampling probe was constructed on similar lines to that used by

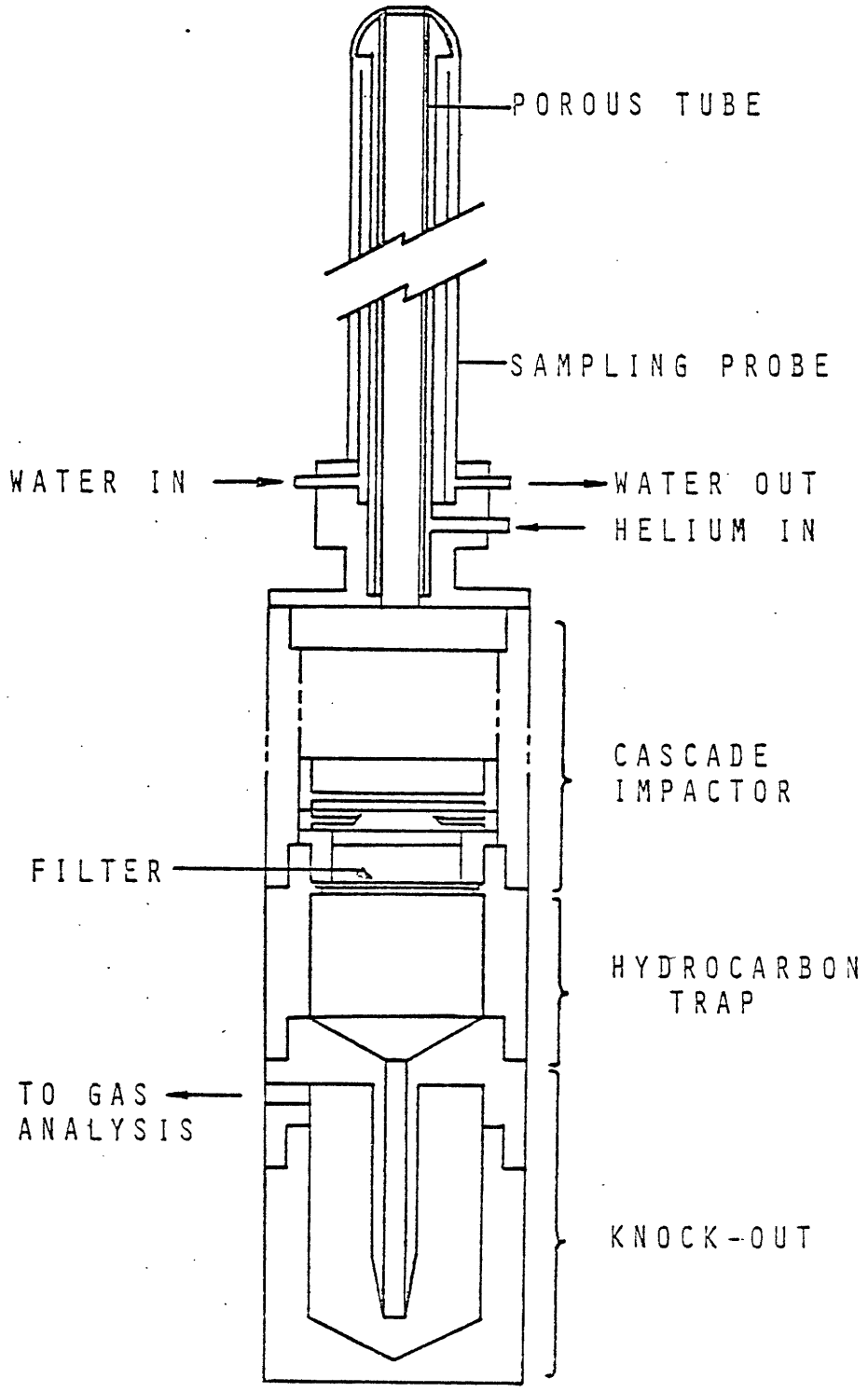

Figure 5.8 Sample Collection System

Mims[130]. The special capability of this sampling system is that it can co-currently recover a mixture of fuel residue, condensible vapor, gaseous products, and carbonaceous particulates with minimal interaction between the phases.

The sample is drawn into the water cooled sampling probe which is positioned coaxially (viz.Fig. 5.1) with the fuel particle array and the reactor gas flow. The probe draws in the entire flow from the reactor. The inside wall of the sampling probe is a sintered stainless steel tube (Mott Metallurgical Crop.) having an inside diameter of 6 mm and an average pore diameter of 5 micrometers. The low porosity of this material is such that it offers negligible resistance to gas flow. The ingested sample is quenched and diluted by Helium transpired through the porous wall. The mass of Helium transpired is typically an order of magnitude greater than the mass of the reactor gas flow, being about one liter per second at standard conditions. The sample is progressively diluted and accelerated during its course through the probe. The residence time in the probe is no greater than 70 ms. However, adequate quenching is accomplished within ten diameters or 15 ms. The transpiration gas prevents deposition of material on the walls of the probe, and the progressive dilution inhibits the interaction between fuel residues, carbonaceous particlates and condensed vapors.

Upon exiting the sampling probe, the fuel residue is segregated from the carbonaceous particulates and condensed hydrocarbons in a "Pilat Mark III Source Test Cascade Impactor". The cascade impactor separates aerosol particles into a number of size fractions. The separation of the aerosol particles is accomplished by passing the sample through jet orifices of progressively diminishing diameter and increasing gas jet velocity. The

aerosol particles of sufficient size are inertially collected on the first particle collection plate downstream of the first jet stage which is the single jet of the sampling probe exit. The particle diameter collected with 50 percent collection efficiency at a given stage is related to the impactor parameters by the equation[131]

$$d_{50} = \left(\frac{2.61 \, \mu \, D_o}{C \, \rho_p \, V_o} \right)^{1/2} \qquad 5.5$$

Samples collected during the course of this study are easily discriminated by this device (viz. Fig. 5.9). On the first stage collection plate essentially all particles above 20 micrometers are collected, thereby recovering the fuel residue. The second and third collection plates do not have any sample associated with them, but the fourth through seventh collection plates collect both soot and condensed hydrocarbons. The nominal collection size for these last four stages is from 10^{-1} to 1 micrometer.

Following the staged cascade is a glass fiber filter which removes any remaining aerosol. This is followed by a hydrocarbon absorbing resin (XAD-2) to remove uncondensed hydrocarbon vapors. The gas flow that leaves the system is clean and suitable for gas chromatographic analysis.

5.1.4 Reactor and Sampling Gas Circuit (Fig. 5.10)

Gas flows for the reactor and sampling probe are controlled by a bank of thermal mass flowmeters (Brooks models 5810 and 5811) which each activate a solenoid valve. The flow to the reactor is introduced through an annular ring of radial jets which has internal baffles (Fig. 5.11). The quench gas is introduced through the sampling probe wall. Both the duct gas and quench gas are drawn through the sample collection

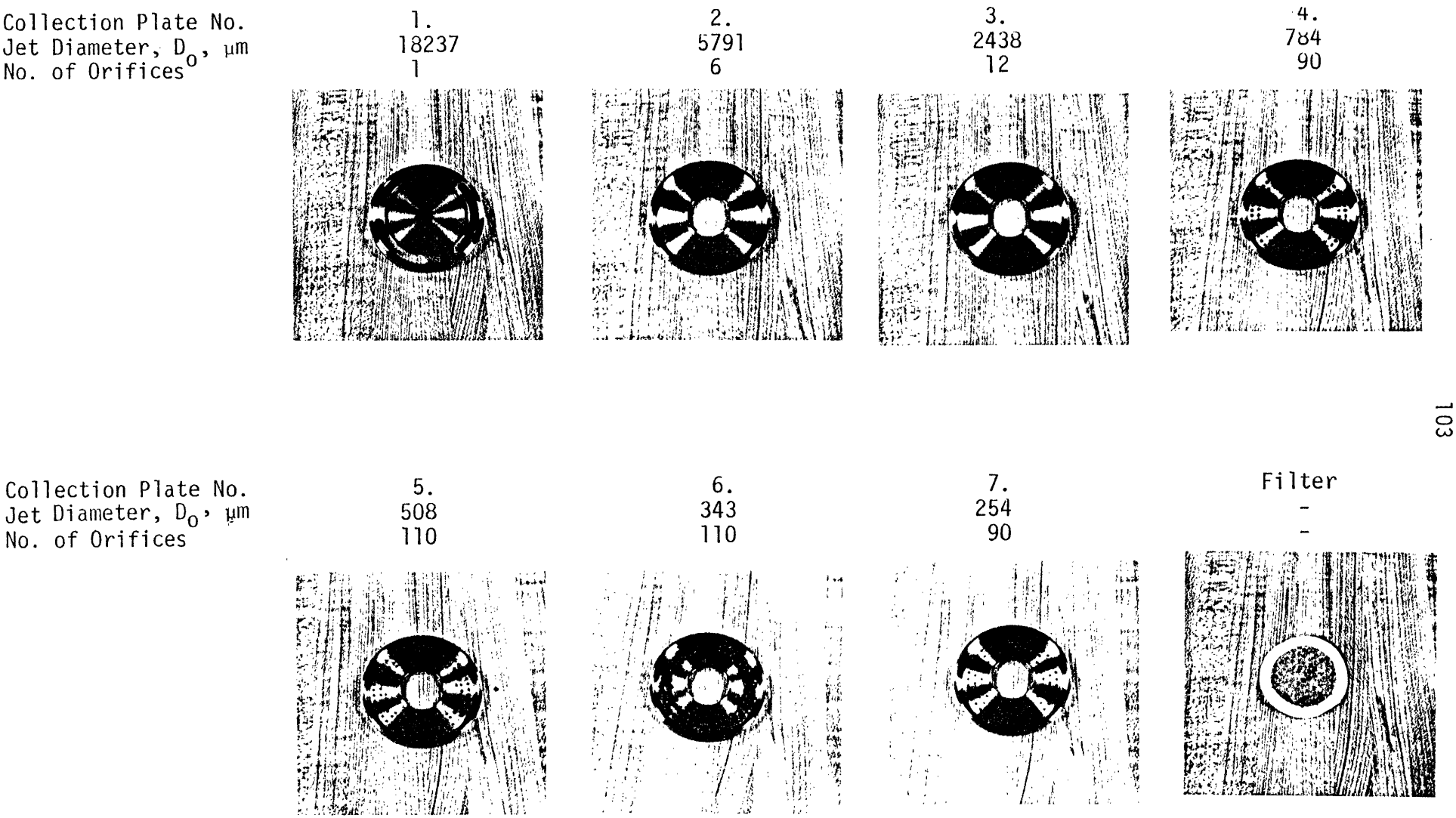

Figure 5.9 Sample Segregation in the Cascade Impactor

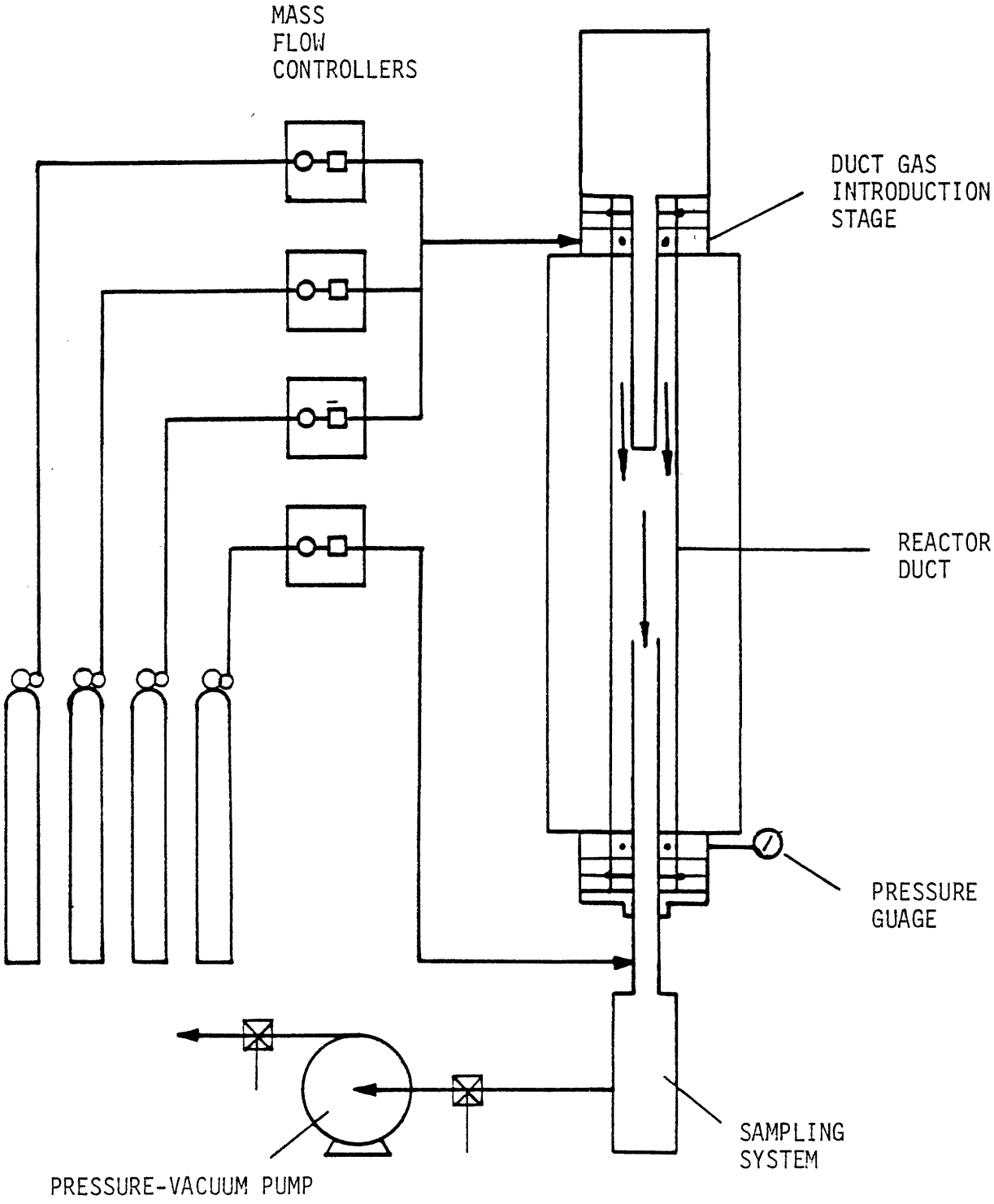

Figure 5:10 Schematic of Reactor Gas Flows

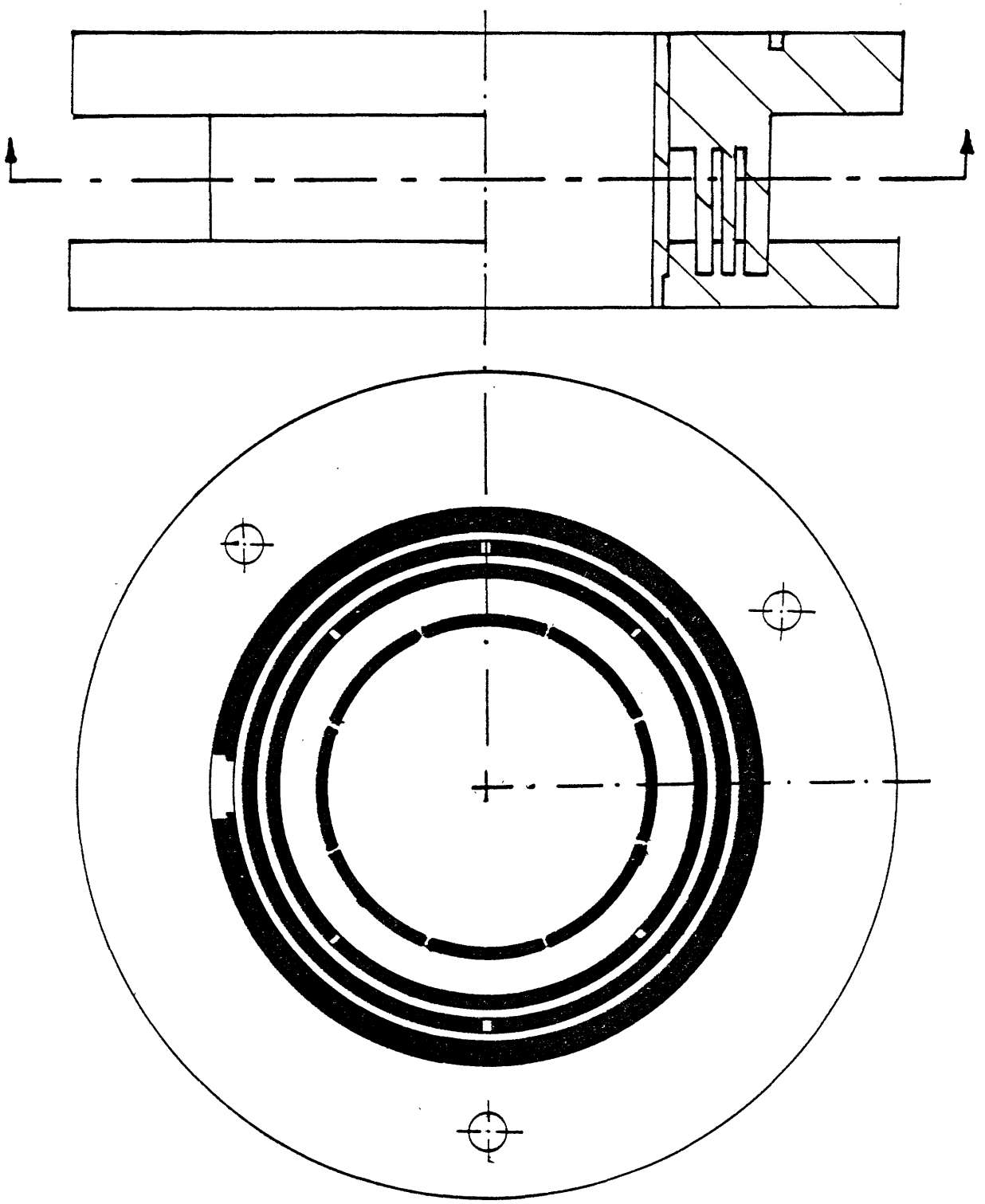

Figure 5.11 Radial Gas Introduction Distributor Plate

system by a vacuum pump (Gast Vacuum-Pressure pump model 0522-P2) which vents the gas to the atmosphere. The pressure in the reactor is measured with a water gauge manometer and adjusted to atmospheric pressure by a bleed valve on the inlet of the vacuum pump.

5.1.5 The Photographic Recording System

Non-intrusive techniques of measuring particle diameter larger than a few micrometers may be divided into light scattering techniques, and microphotography techniques. Microphotography offers several advantages and will certainly remain an important tool for investigating multiphase systems. Among these advantages are the simplicity and relative inexpense of photographic equipment, flexibility, the capability of detecting and analysing non-spherical particles, an insensitivity to optical properties of particles, derivation of particle velocity by multiple exposures and an exact knowledge of the geometry of particle distributions.

The optical system is shown in Fig. 5.12. An electronic stroboscope (Gen Rad model 1538-P3/P4) is positioned on the optical axis of the system, having a parabolic mirror to direct a parallel light beam along this axis. Between the stroboscope and test section is placed a diffusion screen to create a uniformly illuminated background. The camera lens is focussed on the particles to be measured. The particles in this system are observed as shadow-graphs.

The stroboscope is slaved to the shutter system such that upon opening the shutter the stroboscope emits a single high intensity flash. The system studied possesed a natural time standard in the generation of the fuel droplet array. Thus it was possible to "freeze" the motion of the droplet array by slaving the stroboscope to the signal generator

$$\frac{1}{u} + \frac{1}{v} = \frac{1}{F}$$

$$M = \frac{v}{u}$$

$$\Delta = \frac{2u(f/1720M)}{1-(f/1720M)^2}$$

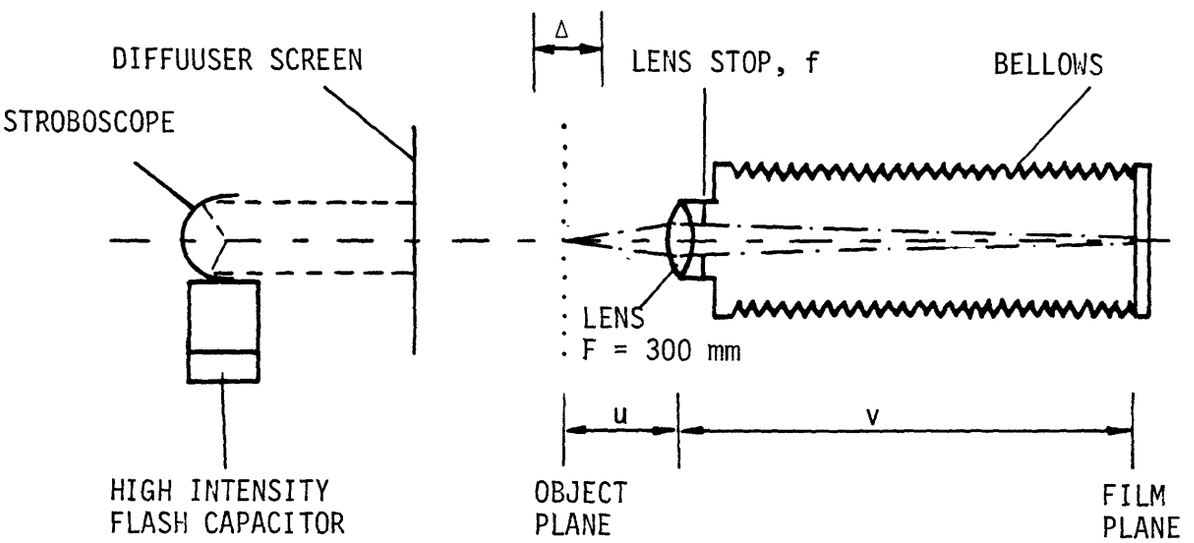

Figure 5.12 Schematic of Optical System

driving the fuel injection system. However, for random sprays a time standard may be artificially introduced by the double exposure of the particles using two light sources one of which is positioned off-axis and directed along the axis through a beam splitter positioned on the optical axis. The shutter triggers the first source which activates an electronic delay that triggers the second source after a precise time interval. The two images obtained on the emulsion thus contain a measure of velocity.

The ability to measure accurately the size of an object image from an emulsion is determined by the object velocity, the sharpness of focus, and the resolution of the lens-film combination. The motion of the object is minimized by a short duration flash and a compatible film sensitivity. The flash duration used was 8 microseconds, however, the time during which the flash intensity was capable of imprinting an image on the film (Kodak Technical Pan Film 2415) above gross fog was about 0.1 microseconds. Thus for an object having a velocity of the order 10 m/s, the motion will be a mere one micrometer. The ability to obtain a sharp focus depends primarily upon, Δ, the depth of field of focus. For an 4x5 inch plate camera this is determined by the formula[132]

$$\Delta = \frac{2u\ (f/1720\ M)}{1 - (f/1720\ M)^2} \qquad 5.6$$

A 300 mm focal length lens was used at an aperture f-number of 11. (The aperture was selected from resolution considerations). The image magification was 5 for which a object to lens distance of 360 mm is obtained. Thus Δ is calculated to be 1 mm. This value was confirmed by photographing a wire mesh positioned obliquely across the plane of focus. The camera adjustment at the film plane for a 1 mm change in object plane is 5 mm

and easily accomplished. The smallest resolvable object, d_m, is found from the formula[133]

$$d_m = \frac{1}{M}\left(\frac{1}{R_L} + \frac{1}{R_F}\right) \qquad 5.7$$

where R_L and R_F are the lens and film resolving powers. R_L is usually best at an aperture about two stops less than maximum. For the lens used this was an f-number of 11 which gave a resolution of about 125 lines per mm. The film was specified as having a high contrast resolving power of 63 lines per mm. Thus the smallest resovable object was 5 micrometers. The objects being measured were 100 to 150 micrometers in size. Applying normal sampling error to the measurement of the particle images, an object of 100 micrometers diameter would be measured with a 90% certaintainty to be between 97 and 103 micrometers.

Velocities were measured from interparticle distances, since the droplets were generated as a linear array at a fixed frequency. The velocities obtained are averages over the distance between particles. If the particles are numerous the actual velocities may be extracted from the average, or if the interparticle distance small, or the deceleration small, the actual velocities will not differ much from the average.

5.2 Experimental Procedures

5.2.1 Fuel Preparation

Heavy fuel oils tend to have a dispersion of very fine particulates which continually agglomerate to form particles that are able to precipitate. This process is accelerated by the presence of oxygen which forms a tarry substance by the slow oxidation of heavy fuel species. This behavior is particularly pronounced for "unstable" synthetic fuels such as

solvent refined coal.

Particulates in the fuel make it impossible to generate a continuous mono-size droplet array through an orifice of 100 micrometers or smaller. Thus immediately prior to performing a furnace pyrolysis experiment the fuel must be filtered. In order that no bias may be introduced, fuel samples that are used for other experiments which will yeild data for comparison with the furnace experiments, are also filtered.

The fuel is filtered at high pressure through a Millipore FGLP filter having a nominal pore diameter of 0.2 micrometers. The filter holder (Millipore model XX 4504700) and fuel reservoir, Fig. 5.13, are steam heated to facilitate fitration. The filtered fuel is transferred directly into the fuel reservoir of the fuel injection system. The fuel injection system should contain hot water (steam heated) in the coolant jacket, since repeated heating and cooling of heavy fuels was found to increase the rate of particulate formation.

The fuel injection system reservoir must be meticulously cleaned with solvents to remove any trace of particulates that form from residues that remain after prior experiments. The cleaning with solvents should always end with a volatile solvent that may be readily removed by heating and flushing with a dry inert gas. This is necessary mostly for the "unstable" synthetic fuels but to some extent for all heavy fuels, due to the solvent causing the less soluble species to precipitate out of solution.

5.2.2 Equilibrium Distillation

The equipment used for the atmospheric distillation of the experimental fuels consists of a 500 ml three-neck flask, a water-cooled bulb condenser, a magnetic stirrer, a heating mantle, and a rheostat. The vapor phase temper-

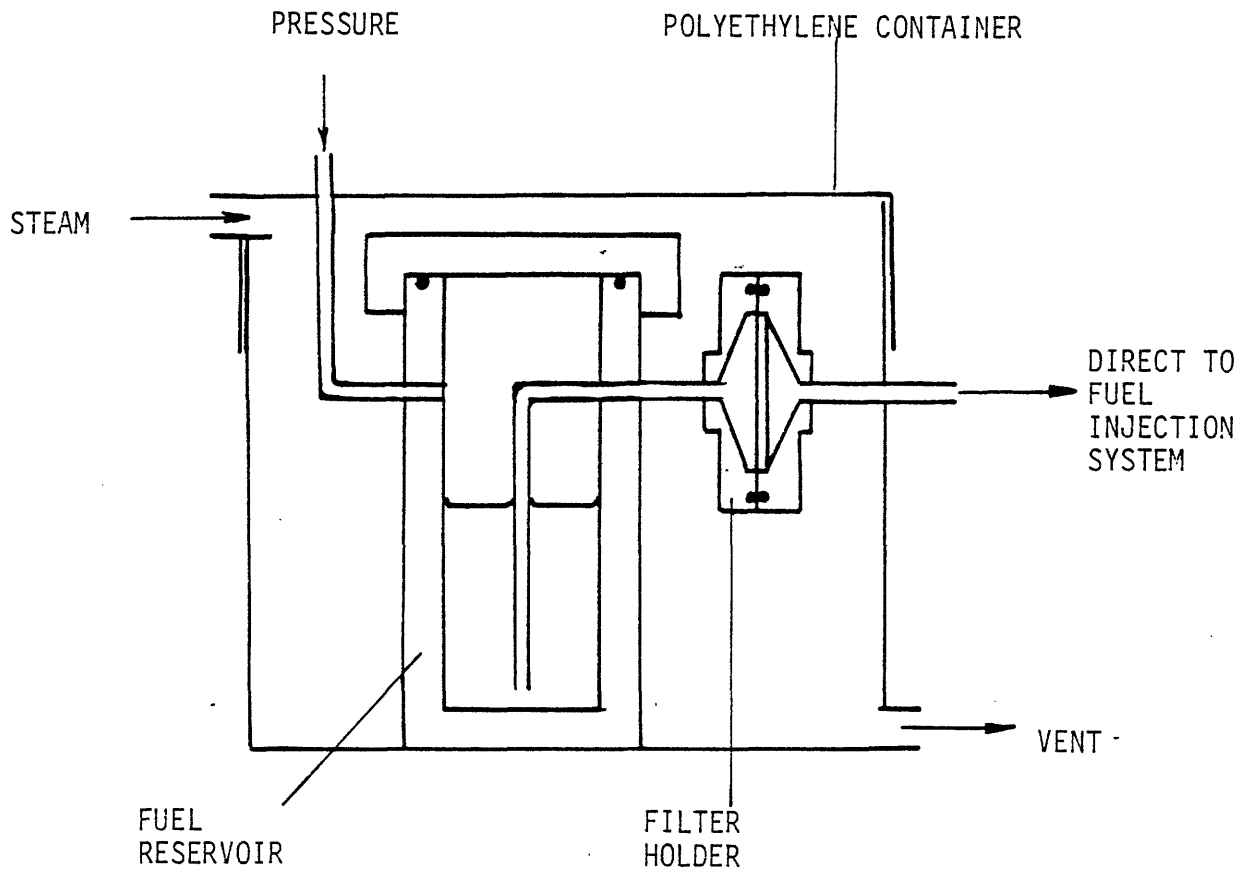

Figure 5.13 Fuel Filtration Equipment

ature is monitored by a glass mercury filled thermometer, whereas the liquid temperature is monitored by a chromel-alumel thermocouple. The normal considerations for a laboratory distillation[134] are observed.

A fuel sample of 100 ml is employed for the distillation. The heating rate is gradually increased such that the rate of distillate collection is about 1/4 ml per minute. Once 5 ml have been collected, this constitutes a sample and a new vial used to collect the next sample. Temperatures are recorded at the initial boiling point and after each sample is collected. The original fuel and the distillate fractions are analysed for Carbon, Hydrogen, and Nitrogen, or for compositional analysis by gas chromatography.

5.2.3 Furnace Pyrolysis

The furnace casing is evacuated to 200 micrometers of mercury pressure, for the removal of moisture and oxidizing gases, and backfilled with Helium to ambient pressure. A flow of 2.8 lpm Helium is established through the casing, and vented to the atmosphere. Cooling water, at least 5.7 lpm, for the furnace casing is turned on. With the aid of a laser, the sampling probe is aligned parallel to the furnace axis by the uneven compression of the O-ring seal in the probe mounting flange. Water cooling, 50 lpm, and a portion of transpiration Helium, 5 lpm, for the sampling probe is turned on and the temperature controller (section 5.1.1) is activated. When the furnace has reached the desired temperature, the fuel injection system is installed and aligned in a similar manner to the sampling probe by means of the laser light beam directed through the sampling probe. The reactor zone is vented through the base of the furnace and the sample collection system is assembled. The reactor zone is flushed with 5 lpm Helium, and the

probe transpiration gas flow is increased to 50 lpm Helium. With bleed valve wide open, the sampling system vacuum pump is turned on. The vacuum pump bleed valve is throttled so that the reactor zone pressure matches the ambient pressure. The reactor zone vent is then shut. The sampling probe is positioned so that its face concides with the lower extreme of the optical system's field of view. The height of the furnace is adjusted for the desired furnace sampling position. The apparatus is now ready.

The fuel injection system is switched from vacuum to pressure and timing of the fuel flow is begun. The optical system is activated by the camera shutter release. After 20 to 40 seconds of fuel flow, the fuel injection system is returned to vacuum. The reactor zone vent is opened. The sampling system vacuum pump bleed valve is opened and the vacuum pump turned off. The probe transpiration gas is reduced to 5 lpm Helium. The sample collection system is disassembled and the fuel particle residue recovered for weighing and elemental analysis for Carbon, Hydrogen, and Nitrogen, or for compositional analysis by gas chromatography. The procedure is repeated, omitting the preliminary steps that do not require duplication, for different furnace positions and temperatures, and different fuels.

5.2.4 Sample Analysis

The fuel residues and distillate fractions produced from experiments were analysed for their elemental content of Carbon, Hydrogen, and Nitrogen in the case of heavy fuels oils, but were analysed for their molecular composition by gas chromatography in the case of model fuels. The elemental analyses were performed by either Galbraith Laboratories, or at M.I.T.. In either case a Perkin-Elmer Elemental Analyser model 240 B was used. The compositional analyses were performed at M.I.T. using a Perkin-Elmer Sigma 1

gas chromatographic System.

CHAPTER 6

THEORETICAL ANALYSIS

6.1 Equilibrium Distillation[135]

Differential vaporization is the term used to describe the batch operation in which a uniform mixture is distilled by heating a sample in a still until it attains the bubble point. At the bubble point boiling starts and continues as the distillate is continuously removed. A gradual increase in boiling temperature of the liquid takes place as the more volatile components are distilled off. The vapor evolving at any instant from the boiling liquid mixture is assumed to be in equilibrium with it. Thus, the composition of the liquid changes continuously throughout the distillation process as does that of the vapor in equilibrium with it. A material balance for a component i, Fig. 6.1, yields the following expression when differential products are neglected:

$$\ln\left(\frac{L_o}{L_f}\right) = \int_{x_{if}}^{x_{io}} \frac{dx_i}{y_i - x_i} \qquad 6.1$$

Equation 6.1 is known as the Rayleigh[136] equation.

6.1.1 Ideal Binary Systems

$$x_1 + x_2 = 1 \qquad 6.2$$

$$y_1 + y_2 = 1 \qquad 6.3$$

From the ideal gas equation and Dalton's Law:

$$P_1 + P_2 = P_T \qquad 6.4$$

Assuming Raoult's Law to be valid, i.e. the component of interest is in low concentration

$$P_1 = x_1 p_1 \qquad 6.5a$$

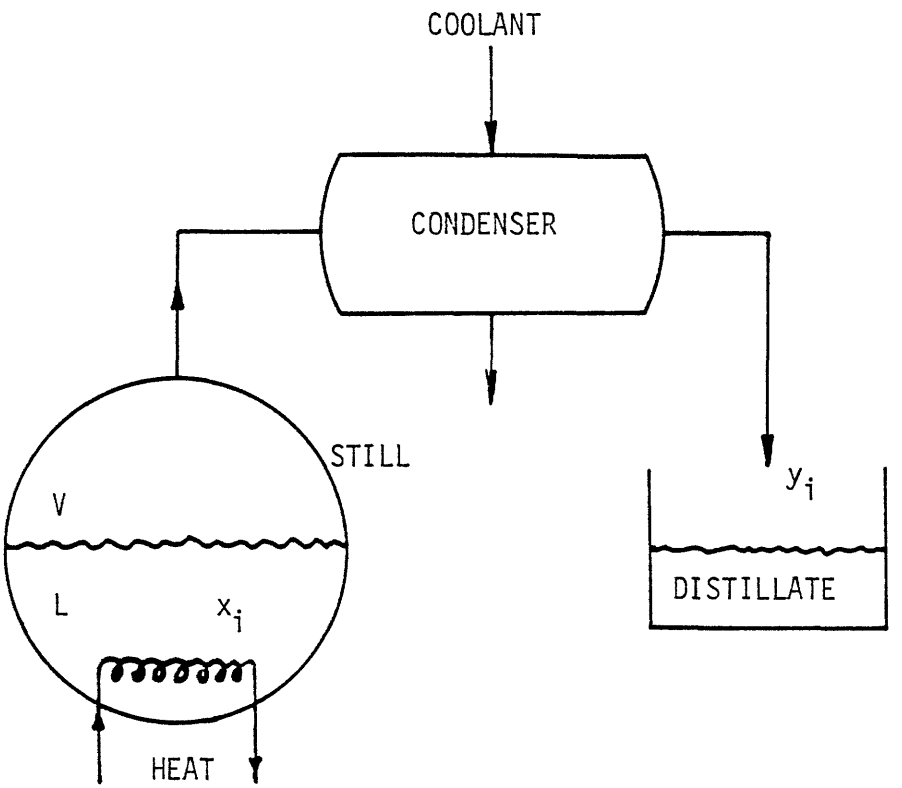

$$Lx_i = (L-dL)(x_i-dx_i)+(y_i+dy_i)dL$$

Neglecting differential products

$$(x_i-y_i)dL = Ldx_i$$

Figure 6.1 Schematic of Differential Vaporization

$$P_2 = x_2\, p_2 \qquad 6.5b$$

Combining Eqs. 6.2, 6.3, 6.4, 6.5a and 6.5b

$$x_1 = \frac{P_T - p_2}{p_1 - p_2} \qquad 6.6$$

$$y_1 - x_1 = \left(\frac{p_1}{P_T} - 1\right)\left(\frac{P_T - p_2}{p_1 - p_2}\right) \qquad 6.7$$

The vapor pressures, p_1 and p_2, are unique functions of temperature for each component. Thus Eq. 6.6 and Eq. 6.7 are also unique functions of temperature. Thus, introducing these equations into Eq. 6.1, an integration may be performed in terms of the single parameter, temperature, between limits corresponding to x_{10} and x_{1f}.

6.2 Droplet Vaporization

The model of droplet vaporization adopted follows the usual quasi-steady state assumptions applied to the gas phase energy equation, Fig. 6.2.

$$V_r \frac{\partial T}{\partial r} = \frac{\alpha}{r^2} \frac{\partial}{\partial r} \left(r^2 \frac{\partial T}{\partial r}\right) \qquad 6.8$$

$$V_r = \frac{\dot{m}}{4\pi r^2 \rho} \qquad 6.9$$

$$T = T_g \;,\; r \to \infty \qquad 6.10$$

$$T = T_s \;,\; r = R \qquad 6.11$$

Combining Eqs. 6.8 and 6.9, with rearrangement

$$r^2 \frac{\partial^2 T}{\partial r^2} + \left(2r - \frac{\dot{m}}{4\pi\rho\alpha}\right) \frac{\partial T}{\partial r} = 0 \qquad 6.12$$

Now the second term in the parentheses of Eq. 6.12 is a function of time alone and, according to the quasi-steady state assumption, is to be treated

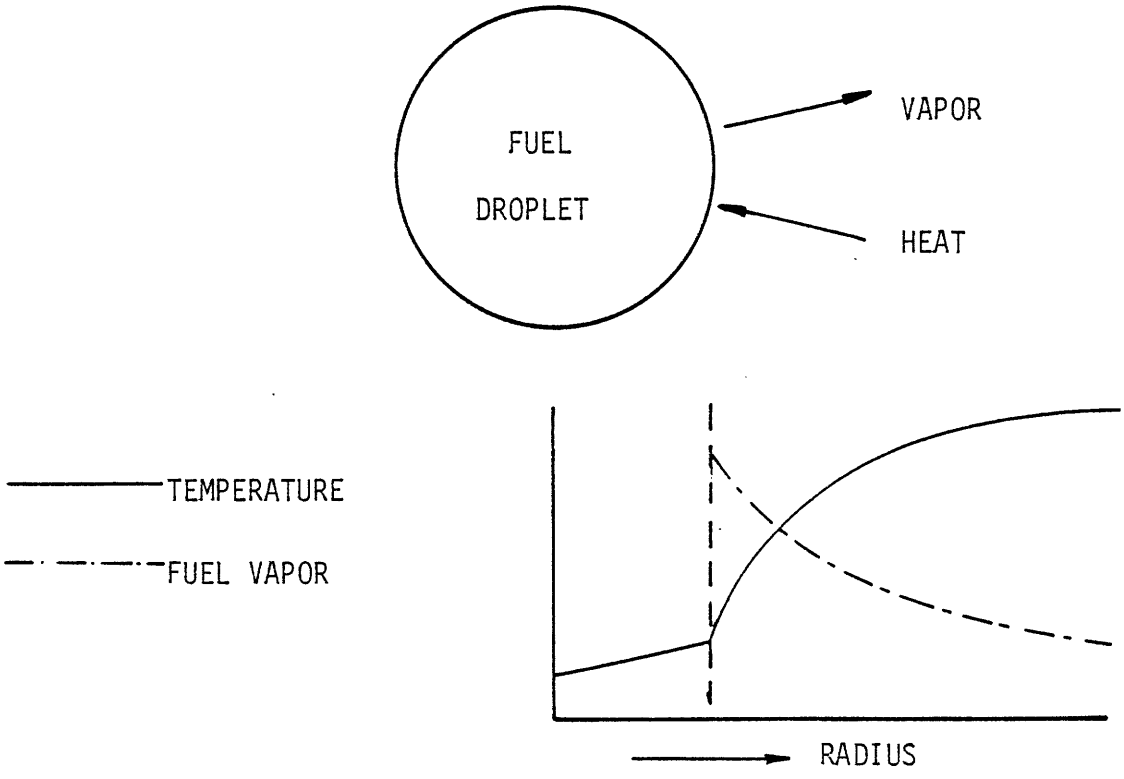

ASSUMPTIONS:

(1) SPHERICAL GEOMETRY
(2) ENERGY TRANSPORT IN THE GAS PHASE CONTROLLING
(3) LIQUID PROPERTIES UNIFORM AND EQUAL TO SATURATED CONDITIONS
(4) BODY FORCES, PRESSURE GRADIENTS, THERMAL RADIATION, AND BULK VISCOSITY, SORT, AND DUFOUR EFFECTS ARE NEGLIGIBLE

Figure 6.2 Quasi-Steady State Droplet Vaporization

as a constant. Solving Eq. 6.12 for the boundary conditions of Eqs. 6.10 and 6.11 produces the equations

$$\frac{T - T_g}{T_s - T_g} = \frac{1 - \exp\{-\dot{m}/4\pi\rho\alpha r\}}{1 - \exp\{-\dot{m}/4\pi\rho\alpha R\}} \qquad 6.13$$

$$Nu_d = \frac{2\,(\dot{m}/4\pi\rho\alpha R)}{\exp\{\dot{m}/4\pi\rho\alpha R\} - 1} \qquad 6.14$$

The temporal variation in diameter is obtained from coupling the energy and mass conservation equations.

$$\dot{m}\,Q = h\,\pi d^2\,(T_s - T_g) \qquad 6.15$$

$$\dot{m} = \rho_\ell\,\frac{\pi d^2}{2}\,\dot{d} \qquad 6.16$$

$$h = \frac{2k}{d}\,Nu_d \qquad 6.17$$

Combining Eqs. 6.15, and 6.17, with rearrangement

$$\dot{m} = 2\pi\rho\alpha d\,\ln\left(1 + \frac{T_g - T_s}{\rho\alpha Q}\right) \qquad 6.18$$

Substituting Eq. 6.16 and integrating, assuming the changing surface temperature to be of only secondary importance

$$d^2 = d_o^2 - \frac{8\rho\alpha}{\rho_\ell}\,t\,\ln\left(1 + \frac{T_g + T_s}{\rho\alpha Q}\right) \qquad 6.19$$

Equations 6.18 and 6.19 are equivalent to those obtained by Godsave, Eq. 3.1, but for the case of vaporization without a flame and neglecting radiation.

$$\lambda = \frac{8\rho\alpha}{\rho_\ell}\,\ln\left(1 + \frac{T_g - T_s}{\rho\alpha Q}\right) \qquad 6.20$$

The form of Eq. 6.14 would suggest a better form for the Nussult number under forced convection to be

$$Nu_{d,fc} = Nu_d + a\ Re^{1/2}\ Pr^{1/3} \qquad 6.21$$

Also, the functional form of Eq. 6.14 explains the empirical relationships obtained by Spalding[73] and Agoston et al.[83] for vaporization with natural convection, a possible form being

$$Nu_{d,nc} = a\ Nu_d\ Gr^{1/4} \qquad 6.22$$

The effect of interactions between droplets have been discussed in section 3.4. Accordingly, Eq. 3.9 is used to adjust rates of vaporization calculated from Eq. 6.18, and also the vaporization rate constant, Eq. 6.20, when these equations are used to model the experimental system.

The Lewis number for a hot gas is frequently taken to be unity. Under this condition concentration and temperature profiles are similar. Thus, Eq. 6.13 would describe the species concentration profiles of gas phase components when α is replaced by the diffusivity of the compound in the mixture. However, it must be recognized that, T_s, would be replaced by the gas phase concentration which, except for a pure fuel, is closely coupled to mass transport phenomena within the fuel particle.

The value of gas phase properties to be used when evaluating Eq. 6.18 is best weighted towards the liquid surface conditions. This is confirmed on consideration of Eqs. 6.13 and 6.14. As the mass rate of vaporization increases the boundary layer thickens and the average temperature about the droplet decreases. Comparison of solutions using various reference property schemes with those for variable properties show good agreement according to Hubbard et al[79], when properties are evaluated using a

simple 1/3 rule which is adopted for this study.

$$T_r = T_s + (1/3)(T_g - T_s) \qquad 6.23$$

6.3 Liquid Phase Species Transport in a Vaporizing Multicomponent Droplet

The physical interpretation of the following mathematical development are fully discussed in Chapter 8. The equations describing the concentration profile of a fuel component in the liquid phase of a droplet are not amenable to a quasi-steady state analysis. The simplifying assumptions, Fig. 6.3, are mostly the same as for the gas phase analysis except for a particular consideration that internal circulation is not of first order importance. The equation set is solved for a "d^2-law" vaporization as expected for the model fuels, but is not valid for a heavy fuel oil. However the equations may easily be formulated for a "d^n-law" vaporization.

$$\frac{\partial m}{\partial t} = \frac{D}{r^2}\frac{\partial}{\partial r}\left(r^2 \frac{\partial m}{\partial r}\right) \qquad 6.24$$

$$m = m_o \ , \ 0 \leq r \leq R_o \ , \ t = 0 \qquad 6.25$$

$$\frac{\partial m}{\partial r} = 0 \ , \ r = 0 \ , \ t > 0 \qquad 6.26$$

$$\frac{\partial m}{\partial r} = \frac{\dot{m}''}{D}(m - m_v), \ r = R \ , \ t > 0 \qquad 6.27$$

$$R^2 = R_o^{\,2} - \frac{\lambda}{4} t \qquad 6.28$$

Let

$$K = \lambda/4D \qquad 6.29$$

$$Z = \frac{K}{4}\left(\frac{r}{R}\right)^2 \qquad 6.30$$

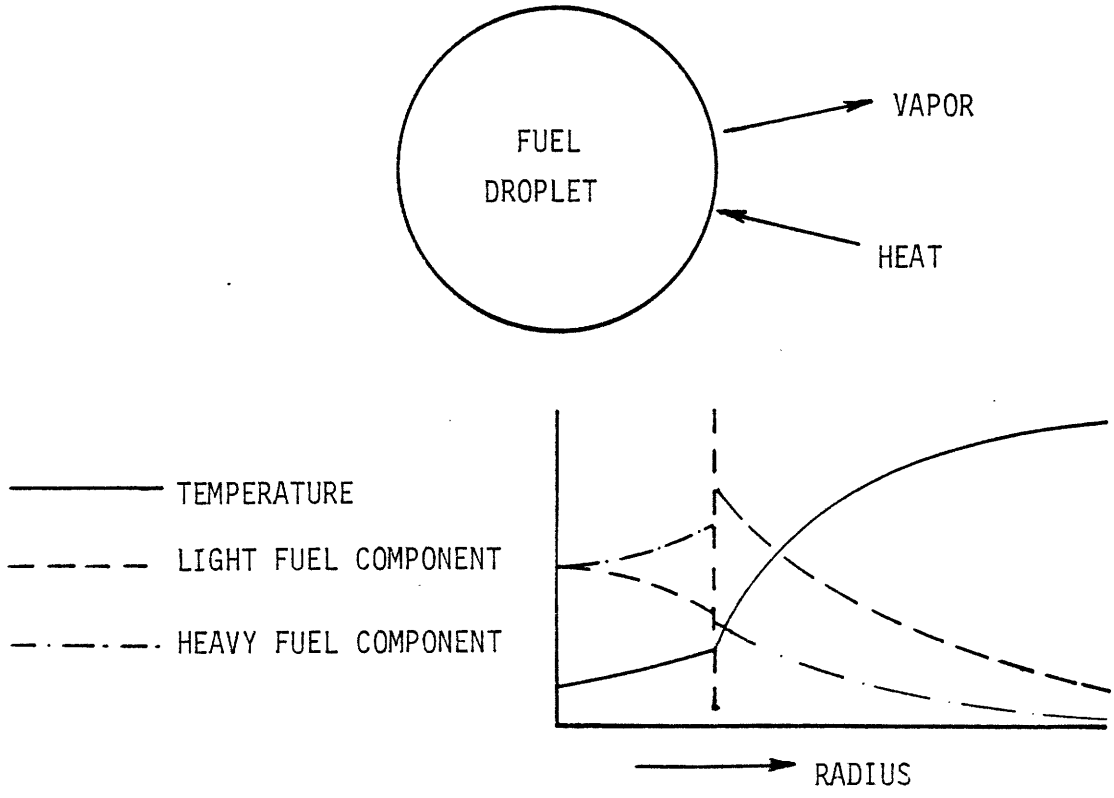

ASSUMPTIONS:

(1) SPHERICAL GEOMETRY
(2) TEMPERATURE PROFILES DETERMINED BY QSS MODEL VIZ. FIG. 6.2
(3) DROPLET PROPERTIES VARY RADIALLY ONLY
(4) EQUILIBRIUM CONDITIONS EXIST AT THE INTERFACE
(5) LIQUID-VAPOR COMPOSITION OBEYS RAOULT'S LAW
(6) DROPLET DIAMETER OBEYS "d^2-LAW"

Figure 6.3 Assumptions for Modelling Liquid Phase Species Transport

$$\tau = \frac{Dt}{R^2} \tag{6.31}$$

$$W = \left(\frac{m - m_o}{m_s - m_o}\right) Z^{1/2} \tag{6.32}$$

Transforming Eqs. 6.24 - 6.29 with Eqs. 6.29 - 6.32

$$Z \frac{\partial^2 W}{\partial Z^2} + \left(\frac{1}{2} - Z\right) \frac{\partial W}{\partial Z} + \frac{1}{2} W = \frac{1 + K\tau}{K} \frac{\partial W}{\partial \tau} \tag{6.33}$$

$$W = 0 \ , \ 0 \leq Z \leq \frac{K}{4} \ , \ \tau = 0 \tag{6.34}$$

$$\frac{\partial W}{\partial Z} = \frac{W}{2Z} \ , \ Z = 0 \ , \ \tau > 0 \tag{6.35}$$

$$\frac{\partial W}{\partial Z} = \frac{W}{2Z} + \frac{\rho_\ell}{2}\left(\frac{K}{Z}\right)^{1/2} (W-W_v), \ Z = K/4, \ \tau > 0 \tag{6.36}$$

Now $\frac{\partial W}{\partial Z}$ is finite and W is finite. Thus for Eq. Eq. 6.35 to be valid at $Z = 0$, $W = 0$. The boundary condition in Eq. 6.36 is a complex temporally dependent constraint. For an analytic equation set, assume $m = m_s$ at $Z = \frac{K}{4}$. The boundary conditions in Eq. 6.35 and Eq. 6.36 now become

$$W = 0, \ Z = 0 \ , \ \tau > 0 \tag{6.37}$$

$$W = \sqrt{K/4} \ , \ Z = K/4, \ \tau > 0 \tag{6.38}$$

Let $$W = \xi (Z) \ T (\tau) + \phi (Z) + \zeta (\tau) \tag{6.39}$$

Then by separation of variables

$$Z \ \xi'' + \left(\frac{1}{2} - Z\right) \xi' - \left(a - \frac{1}{2}\right) \ \xi = 0 \tag{6.40}$$

$$(1+K\tau) \ T' - a \ KT = 0 \tag{6.41}$$

$$Z\,\phi'' + \left(\frac{1}{2} - Z\right)\phi' + \frac{1}{2}(\phi - 2\ell) = 0 \qquad 6.42$$

$$(1 + K\tau)\,\zeta' - \frac{1}{2}K\,(\zeta + 2\ell) = 0 \qquad 6.43$$

where ℓ is an arbitrary constant.

When ξ is replaced by $(\phi-2\ell)$ Eq. 6.42 is equivalent to Eq. 6.40 when $a = 0$. When T is replaced by $(\zeta+2\ell)$ Eq. 6.43 is equivalent to Eq. 41 when $a = \frac{1}{2}$. Equation 6.40 is one case of Kummer's equation[137]

$$\chi\,y'' + (b-\chi)\,y' - a\,y = 0 \qquad 6.44$$

which has the general solution

$$v = A\,M(a, b, \chi) + B\,\chi^{1-b}\,M(1+a-b, 2-b, \chi) \qquad 6.45$$

where $M(a, b, \chi)$ is Kummer's function. Thus solving Eqs. 6.40-6.43

$$\xi_a = A_a\,M\left(a-\frac{1}{2}, \frac{1}{2}, Z\right) + B_a\,Z^{1/2}\,M\left(a, \frac{3}{2}, Z\right) \qquad 6.46$$

$$\phi = A_\phi\,M\left(-\frac{1}{2}, \frac{1}{2}, Z\right) + B_\phi\,Z^{1/2}\,M\left(0, \frac{3}{2}, Z\right) + 2\ell \qquad 6.47$$

$$T = C\,(1+K\tau)^a \qquad 6.48$$

$$\zeta = C_\zeta\,(1+K\tau)^{1/2} - 2\ell \qquad 6.49$$

Thus, noting $M\left(0, \frac{3}{2}, Z\right) = 1$ and absorbing C into A_a and B_a, the complete solution is

$$W = A_\phi\,M\left(-\frac{1}{2}, \frac{1}{2}, Z\right) + B_\phi Z^{1/2} + C_\zeta\,(1+K\tau)^{1/2} + \sum_{\text{all } a}\left[A_a\,M\left(a-\frac{1}{2}, \frac{1}{2}, Z\right) + B_a Z^{1/2}\,M\left(a, \frac{3}{2}, Z\right)\right](1+K\tau)^a \qquad 6.50$$

Applying the boundary condition, Eq. 6.37

$$A_\phi + C_\zeta (1+K\tau)^{1/2} + \sum_{all\ a} A_a (1+K\tau)^a = 0 \qquad 6.51$$

In order for Eq. 6.51 to be valid for all $\tau > 0$

$$A_\phi = 0 \qquad 6.52a$$

$$C_\zeta = 0 \qquad 6.52b$$

$$A_a = 0 \qquad 6.52c$$

Applying the boundary condition in Eq. 6.38, and Eqs. 6.52

$$B_\phi + \sum_{all\ a} B_a M\left(a, \frac{3}{2}, \frac{K}{4}\right) (1+K\tau)^a = 1 \qquad 6.53$$

In order for Eq. 6.53 to be valid for all $\tau > 0$

$$B_\phi = 1 \qquad 6.54$$

$$M\left(a, \frac{3}{2}, \frac{K}{4}\right) = 0 \qquad 6.55$$

Applying the initial condition, Eq. 6.34

$$\left[1 + \sum_{all\ a} B_a M\left(a, \frac{3}{2}, Z\right)\right] Z^{1/2} = 0 \qquad 6.56$$

Now $Z^{1/2} M(a, \frac{3}{2}, Z)$ is orthogonal over $0 \le Z \le \frac{K}{4}$ with a weighting function, derived from Eq. 6.40, of $Z^{-1/2}\, e^{-Z}$. Thus, multiplying Eq. 6.56 by $e^{-Z}\, M\left(a, \frac{3}{2}, Z\right)$ and integrating over $0 \le Z \le K/4$, B_a is determined.

$$B_a = -\frac{\int_0^{K/4} Z^{1/2}\, e^{-Z}\, M\left(a, \frac{3}{2}, Z\right) dZ}{\int_0^{K/4} Z^{1/2}\, e^{-Z}\, M\left(a, \frac{3}{2}, Z\right)^2 dZ} \qquad 6.57$$

Solving for m,

$$\theta = \frac{m - m_o}{m_s - m_o} = 1 + \sum_{all\ a} B_a M\left(a, \frac{3}{2}, Z\right) (1+K\tau)^a \qquad 6.58$$

To solve for a time dependent surface concentration, m_s, the Duhamel integral is used.

$$D(\tau) = m_s(\tau) - m_o \qquad 6.59$$

$$m - m_o = \int_o^\tau \theta\left(Z, \tau-s\right) \frac{d}{dt}\left[D(s)\right] ds \qquad 6.60$$

Substituting Eq. 6.58 into Eq. 6.60

$$m - m_o = D(\tau) + \sum_{all\ a} B_a M\left(a, \frac{3}{2}, Z\right) \int_o^\tau \left(1+K\{\tau-s\}\right)^a \frac{d}{dt}\left[D(s)\right] ds) \qquad 6.61$$

Integrating Eq. 6.61 by parts

$$m - m_o = D(\tau) + \sum_{all\ a} B_a M\left(a, \frac{3}{2}, Z\right) \left(D(\tau)+aK\int_o^\tau D(s)(1+K\{\tau-s\})^{a-1} ds\right) \qquad 6.62$$

The boundary condition under study, Eq. 6.27, is best rendered as

$$\frac{\partial m}{\partial Z} = \rho_\ell \left(m_s - m_v\right),\ Z = \frac{K}{4},\ \tau > 0 \qquad 6.63$$

Now $M'(a, b, Z) = \frac{a}{b} M(a+1, b+1, Z)$, thus

$$\sum_{all\ a} B_a \frac{2a}{3\rho_\ell} M\left(a+1, \frac{5}{2}, \frac{K}{4}\right)\left(D(\tau) + aK \int_o^\tau D(s)(1+K\{\tau-s\})^{a-1} ds\right) = m_s - m_v \qquad 6.64$$

As $\tau \to \infty$: $m \to m_f$, $0 \le Z \le \frac{K}{4}$; $D(\tau) \to D(\infty) = m_f - m_o$: $m_s - m_v \to 0$ 6.65

Applying Eq. 6.65 to Eq. 6.62 and Eq. 6.64

$$\sum_{\text{all } a} B_a \, M\left(a, \tfrac{3}{2}, Z\right)\left(D(\tau) + aK \int_0^{\tau} D(s)\left(1+K\{\tau-s\}\right)^{a-1} ds\right) \to 0 \qquad 6.66$$

$$\sum_{\text{all } a} B_a \, \frac{2a}{3\rho_{\ell}} \, M\left(a+1, \tfrac{5}{2}, \tfrac{K}{4}\right)\left(D(\tau) + aK \int_0^{\tau} D(s)\left(1+K\{\tau-s\}\right)^{a-1} ds\right) \to 0 \qquad 6.67$$

$D(\tau)$ does not have any dependence on 'a' which is a artifact of the problem for which $D(\tau) = 1$. Thus, from Eq. 6.66 and Eq. 6.67,

$$D(\infty) = \frac{-\sum_{\text{all } a} B_a \, M\left(a, \tfrac{3}{2}, Z\right) aK \int_0^{\tau \to \infty} D(s)\left(1+K\{\tau-2\}\right)^{a-1} ds}{\sum_{\text{all } a} B_a \, M\left(a, \tfrac{3}{2}, Z\right)} \qquad 6.68$$

$$D(\infty) = \frac{-\sum_{\text{all } a} a \, B_a \, M\left(a+1, \tfrac{5}{2}, \tfrac{K}{4}\right) aK \int_0^{\tau \to \infty} D(s)\left(1+K\{\tau-s\}\right)^{a-1} ds}{\sum_{\text{all } a} a \, B_a \, M\left(a+1, \tfrac{5}{2}, \tfrac{K}{4}\right)} \qquad 6.69$$

Equating Eq. 6.68 to Eq. 6.69 and rearranging

$$\sum_{\text{all } a}\left(\frac{B_a \, M\left(a, \tfrac{3}{2}, Z\right)}{\sum_{\text{all } a} B_a \, M\left(a, \tfrac{3}{2}, Z\right)} - \frac{a \, B_a \, M\left(a+1, \tfrac{5}{2}, \tfrac{K}{4}\right)}{\sum_{\text{all } a} a \, B_a \, M\left(a+1, \tfrac{5}{2}, \tfrac{K}{4}\right)}\right) aK \int_0^{\tau \to \infty} D(s)\left(1+K\{\tau-s\}\right)^{a-1} ds = 0 \qquad 6.70$$

$D(s)$ is a monatonic function, thus $aK \int_0^{\tau \to \infty} D(s)\left(1+K\{\tau-s\}\right)^{a-1} ds$ is zero only when $D(s) = 0$. The contents of the brackets in Eq. 6.70 cannot be zero when Z is unspecified. However, if $aK \int_0^{\tau \to \infty} D(s)\left(1+K\{\tau-s\}\right)^{a-1} ds$ is a constant, then the bracketed expression is identically zero. Applying this result to Eq. 6.68

$$D(\infty) = -aK \int_0^{\tau \to \infty} D(s)\,(1+K\{\tau-s\})^{a-1}\,ds \qquad 6.71$$

Let $$D(s) = D(\infty)\,G(s) \qquad 6.72$$

then $$1 + aK \int_0^{\tau \to \infty} G(s)\,(1+K\{\tau-s\})^{a-1}\,ds = 0 \qquad 6.73$$

Integrating Eq. 6.73 by parts

$$1 - G(\infty) + \int_0^{\tau \to \infty} G'(s)\,(1+K\{\tau-s\})^{a}\,ds = 0 \qquad 6.74$$

By repeated integration by parts Eq. 6.73 becomes

$$1 - G(\infty) - \sum_{n=1}^{\infty} (aK)^{-n} \frac{d^n}{d\tau^n} G(\infty) = 0 \qquad 6.75$$

'a' is not rational, is always negative, and may be arbitrarily large. $G(\tau)$ must be zero at $\tau = 0$, approach unity as $\tau \to \infty$, and be repeatedly differentiable. The only function satisfying these properties is

$$G(\tau) = 1 - e^{-b\tau} \qquad 6.76$$

Recalling Eq. 6.62, and Eq. 6.63

$$\frac{m - m_o}{m_f - m_o} = 1 - e^{-b\tau} + \sum_{all\,a} B_a\, M\left(a, \frac{3}{2}, Z\right) \int_0^{\tau} be^{-bs}\,(1+K\{\tau-s\})^{a}\,ds \qquad 6.77$$

$$\frac{m_s - m_v}{m_f - m_o} = \sum_{all\,a} B_a \frac{2a}{3\rho_\ell} M\left(a+1, \frac{5}{2}, \frac{K}{4}\right) \int_0^{\tau} be^{-bs}\,(1+K\{\tau-s\})^{a}\,ds \qquad 6.78$$

Eqs. 6.77 and 6.78 require the evaluation of $\int_0^{\tau} be^{-bs}\,(1+K\{\tau-s\})^{a}\,ds$. This is accomplished by the repeated integration by parts. Let this integral be designated I, thus

$$I = (1+K\tau)^a - e^{-b\tau} + \sum_{r=1}^{\infty} (-1)^r \left(\frac{K}{b}\right)^r \left(\prod_{q=0}^{r-1} \{a-q\}\right) \left(\{1+K\tau\}^{a-r} - e^{-b\tau}\right) \quad 6.79$$

Let $$I = G(\tau) + H_a(\tau) \quad 6.80$$

Then

$$H_a(\tau) = (1+K\tau)^a - 1 + \sum_{r=1}^{\infty} (-1)^r \left(\frac{K}{b}\right)^r \left(\prod_{q=0}^{r-1} \{a-q\}\right) \left(\{1+K\tau\}^{a-r} - e^{-b\tau}\right) \quad 6.81$$

and

$$\frac{m - m_o}{m_f - m_o} = G(\tau) + \sum_{\text{all } a} B_a M\left(a, \frac{3}{2}, \frac{K}{4}\right) (G(\tau)+H_a(\tau)) \quad 6.82$$

$$\frac{m_s - m_v}{m_f - m_o} = \sum_{\text{all } a} B_a \frac{2a}{3\rho_\ell} M\left(a+1, \frac{5}{2}, \frac{K}{4}\right)(G(\tau)+H_a(\tau)) \quad 6.83$$

For an equilibrium binary system, $m_s - m_v$, is a function of m_s alone, which is a function of τ, Eq. 6.76. Thus both sides of Eqs. 6.82 and 6.83 are functions of τ, requiring only that a value be determined for 'b'.

When analysing experimental data, only average concentrations are available so that the profiles of Eq. 6.77 must be averaged also.

$$\bar{m} = \frac{\int_o^r m\, 4\pi r^2 dr}{\int_o^r 4\pi r^2 dr} = \left(\frac{3}{2}\right)\left(\frac{4}{K}\right)^{3/2} \int_o^{K/4} m\, Z^{1/2}\, dZ \quad 6.84$$

$$\frac{\bar{m} - m_o}{m_f - m_o} = G(\tau) + \sum_{\text{all } a} B_a F_a (G(\tau)+H_a(\tau)) = \sum_{\text{all } a} B_a F_a H_a(\tau) \quad 6.85$$

where

$$F_a = \left(\frac{3}{2}\right)\left(\frac{4}{K}\right)^{3/2} \int_o^{K/4} Z^{1/2} M\left(a, \frac{3}{2}, Z\right) dZ \quad 6.86$$

For comparison of results, the data is formulated as fractional evolution of a component or element, Y, versus the extent of vaporization, X.

$$Y = 1 - \frac{\bar{m}}{m_o}\left(\frac{R}{R_o}\right)^3 \qquad 6.87$$

$$X = 1 - \left(\frac{R}{R_o}\right)^3 \qquad 6.88$$

Then

$$Y = 1 - (1-X)\left(1 - \frac{m_f - m_o}{m_o} \sum_{\text{all } a} B_a F_a H_a (\tau)\right) \qquad 6.89$$

When X is selected, τ may be obtained from Eqs. 6.28, 6.29, 6.31 and 6.88. Thus, eq. 6.89 is fully specified for the determination of the fractional evolution.

CHAPTER 7*

RESULTS

7.1 Fuel Characterization

The following fuels were employed for this study:

(i) Gulf Coast No. 6 petroleum fuel oil

(ii) Indo-Malaysian No. 6 petroleum fuel oil

(iii) Anvil Points raw Paraho shale oil

(iv) SRC-II, middle distillate fraction

(v) SRC-II, heavy distillate fraction

(vi) SRC-II, 2.9:1 blend, middle to heavy distillate fractions

(vii) n-dodecane doped with pyridine

(viii) n-dodecane doped with quinoline

(ix) n-dodecane doped with acridine

Other fuels considered, but found to be too viscous, or excessively prone to the formation of precipitate, thereby precluding their use for furnace pyrolysis experiments, include:

(x) Alaskan raw petroleum fuel oil

(xi) H-coal fuel oil, light distillate fraction

(xii) H-coal fuel oil, heavy distillate fraction

(xiii) H-coal fuel oil, full range

The results that were obtained for this latter set of fuels are contained in Appendix A.

The viscosity variation with respect to temperature for the heavy fuel oils is presented in Fig. 7.1. The petroleum based fuels exhibit a power law dependence with an exponent of 7/2, typical of petroleum fuels oils. The shale oil has a similar power law dependence, but a smaller exponent,

*Tables and figures are collectively assembled at the end of the chapter.

7/3. The smaller exponent and higher pour point, Table 7.1, of shale oil is attributable to the presence of wax. The solvent refined coal liquids (SRC-II) have an exponential dependence on temperature over the temperature range tested, their viscosities having for every 30 celsius degrees increase in temperature. The difference between the viscosity behavior of the petroleum type fuels and the solvent refined coal liquids is accounted for by the polar nature of the latter.

The compositions and other properties of the heavy fuel oils and those of the model fuels are presented in Tables 7.1 and 7.2 respectively. The carbon to hydrogen atomic ratios for the petroleum based fuels and the shale oil are all about 0.6, whereas for the SRC-II middle distillate, 2.9:1 blend, and heavy distillate they are 0.77, 0.81, and 0.99 respectively. The nitrogen content is particularly high for shale oil, 2.21% by weight, and lowest for the Indo-Malaysian petroleum fuel oil, 0.23% by weight. The solvent refined coal liquids were analysed by gas chromatography, using a nitrogen specific detector, for their nitrogen distribution, Fig. 7.2. The SRC-II middle distillate and heavy distillate both have mono-modal nitrogen distributions. The peak nitrogen concentration for the middle distillate occurred at a carbon number of 12, and that for the heavy distillate at a carbon number of 17. The SRC-II, 2.9:1 blend, has a bimodal nitrogen distribution, the maxima corresponding in carbon number and magnitude, to those expected from consideration of the blended fuels. Major components identified in the SRC-II middle distillate and heavy distillate, Table 7.3, are mostly derivatives of Naphthalene, and it is to be expected that the nitrogen is associated with compounds of this sort.

The fuels (vii) - (ix), are model fuels designed to simulate the heavy fuel oils. The mixtures of dodecane with nitrogen containing

additives were selected in order to simulate the real fuel average composition and to be yet simple enough to permit analysis of the transport phenomena in the liquid phase. The model fuels are based on n-dodecane, since it is a readily available, conveniently handled liquid, with a boiling point approaching that of the heavy fuels oils under investigation. The dopant compounds were selected as being representative of typical nitrogen containing species to be found in heavy fuel oils, and being members of a homologous series, their solvent interactions are similar, thus removing a possible mechanism of species differentiation. The amount of pyridine and quinoline added to the n-dodecane was such that the nitrogen content would be 1% by weight. The acridine has limited solubility in dodecane at room temperature thus the amount of acridine added to n-dodecane represents the maximum soluble.

7.2 Equilibrium Distillation Results

7.2.1 Boiling Curves

The Gulf Coast No. 6 petroleum, the Indo-Malaysian No. 6 petroleum, and the raw Paraho shale oil have boiling curves, Fig. 7.3, that range mostly between 600 K and 750 K for the first 80% extent of vaporization. The low initial boiling point of the Gulf Coast No. 6 petroleum fuel oil, and more rapid temperature increase is indicative of a broader spectrum of chemical species than associated with the Indo-Malaysian No. 6 petroleum fuel oil, and the shale oil.

The solvent refined coal liquids have boiling curves, Fig. 7.4, that generally fall below that of the petroleum No. 6 fuel oils and the shale oil. There is little temperature variation for the first 50% vaporization of the SRC-II heavy and middle distillate fractions however, above 50% extent of vaporization the heavy distillate fraction displays a rapidly increasing boiling temperature. The SRC-II blend only slightly increases

its temperature during the distillation, remaining within 50 degrees celsius of the corresponding boiling temperature of the middle distillate for the first 75% extent of vaporization.

The boiling curves for the model fuels, Fig. 7.5, are dominated by the contribution of n-dodecane. The observed liquid temperature closely approximates the boiling temperature of pure n-dodecane. Except for the acridine doped fuel, distillations were taken to completion. In the case of acridine, at great extents of vaporization, decomposition of the acridine would take place.

7.2.2 Residue Carbon to Hydrogen Atomic Ratios

The carbon to hydrogen atomic ratio of the fuel residue, normalized with respect to the carbon to hydrogen atomic ratio of the original fuel, offers an indication of the composition of the vaporized material. The normalized carbon to hydrogen atomic ratio for the petroleum fuels oils and the shale oil, Fig. 7.6, shows that the Gulf Coast No. 6. petroleum fuel oil undergoes a continual loss of the relatively lighter species, in agreement with the large and steep temperature change of its boiling curve, Fig. 7.3. The Indo-Malasian No. 6 petroleum fuel oil exhibits a similar behavior, but to a lesser degree, in agreement with its boiling curve. The raw Paraho shale oil, which has a boiling curve similar to the Indo-Malaysian No. 6 petroleum fuel oil, shows no tendency to increase its carbon to hydrogen atomic ratio during the course of equilibrium distillation.

The solvent refined coal liquids behave identically with respect to the normalized carbon to hydrogen ratio of their residues Fig. 7.7. During the first 70% extent of vaporization, there is an insignifant increase in the carbon to hydrogen ratio, but thereafter a large rate of increase ensues. The level portion of this data is reflected in the

boiling curves of these fuels, Fig. 7.4.

7.2.3 Nitrogen Evolution

Figure 7.8 shows the fractional evolution of nitrogen during the course of equilibrium atmospheric distillation for the petroleum fuel oils and shale oil. The Gulf Coast No. 6 petroleum and Indo-Malaysian No. 6 petroleum fuel oils have almost identical nitrogen evolutions, the bulk of their nitrogen being retained in the residue. Thus the nitrogen is primarily associated with the heavy species in these fuels. The raw Paraho shale oil evolves its nitrogen in proportion to its mass. Thus the nitrogen is either broadly distributed with respect to species molecular weight; or associated with intermediate molecular weight species in a mixture of many species, each in low concentration; or associated with a mixture of species having a narrow spectrum of molecular weights. The first of these descriptions is correct, as supported by shale oil analyses (viz. Section 2.2.3).

The nitrogen evolution from SRC-II fuels, fig. 7.9, is more or less in proportion to the mass vaporized. The middle distillate fraction evolves its nitrogen more rapidly than the heavy distillate and blend, which have similar nitrogen evolutions. The nitrogen distributions for these fuels, Fig. 7.2, are in agreement with the equilibrium nitrogen evolutions that were determined.

The nitrogen evolution for the model fuels, Fig. 7.10, corresponds to the evolution of the nitrogenous component. The equilibrium evolution of dopant is as expected for the distillation of binary mixtures having large vapor pressure differences between the components in the case of pyridine (high vapor pressure component) and acridine (low vapor pressure component), and small vapor pressure differences in the case of quinoline.

7.3 Furnace Pyrolysis Results

7.3.1 Variation of Droplet Size, Mass, and Velocity

Due to the possibility of internal boiling it is not practical to use particle size as a measure of mass when dealing with heavy fuel oils. Shale oil is a typical example. When 150 micrometer droplets of shale oil are injected into the helium atmosphere of the laminar flow furnace at 1000 K, they are seen to swell to three times their original diameter, Fig. 7.11, even though 50% of the mass has been vaporized.

The spatial mass variation, obtained when sampling, must be correlated against the particle velocity history in order to yield the temporal variation in mass for a vaporizing particle. The velocity is determined because of the highly ordered droplet array used for these experiments, by the particle injection frequency. The interdrop spacing is a function of the vaporization rate of the particle array[138], it being observed that the array initially increases its interdrop spacing as vaporization begins, and thereafter, gradually adjusts the interdrop spacing as the rate of vaporization and mass of the particles change. Thus the maximum residence time in the test zone of the furnace is determined by the injection frequency and vaporization rate of the array, given a constant initial praticle size. The particular velocity variation along a vaporizing droplet array is a function of fuel type, rate of particle generation, furnace temperature, and furnace gas composition.

Figures 7.12, 7.13 and 7.14 show the velocity profiles of the fuels investigated. The heavy fuel oils show a more gradual rise in velocity than the model fuels. The injection velocities differ in order that stable droplet arrays may be generated with each fuel. The increase in velocity for increasing furnace temperature is seen to be only slight when

compared at a single furnace location. However, the integrated effect of this velocity difference may reduce residence times at 1400 K to 90% that at 1000 K.

Of the petroleum fuels and shale oil, the Gulf Coast No. 6 petroleum is remarkable for its initially rapid vaporization, Fig. 7.15. The Indo-Malaysian No. 6 petroleum fuel oil and the raw Paraho shale oil have similar behaviors matching that typically observed[72] for heavy fuels. The solvent refined coal liquids appear, Fig. 7.16, to behave like the Gulf Coast No. 6 petroleum, rapidly evolving mass initially, but at a declining rate thereafter. The model fuels behaved almost as if they were pure n-dodecane, and their mass rates of vaporization, Fig. 7.17, followed a "d^2-law" irrespective of dopant material for the extents of vaporization sampled. Curve fitting the model fuel data yielded the following values for the "d^2-law", Eq. 3.5:

$$1000\ K \quad d_o = 146\mu m,\ \lambda = 0.354\ mm^2/s,\ r^2 = 0.98 \qquad 7.1$$

$$1200\ K \quad d_o = 147\mu m,\ \lambda = 0.514\ mm^2/s,\ r^2 = 0.96 \qquad 7.2$$

$$1400\ K \quad d_o = 144\mu m,\ \lambda = 0.622\ mm^2/s,\ r^2 = 0.93 \qquad 7.2$$

7.3.2 Carbon to Hydrogen Atomic Ratios of Vaporizing Particles

The Gulf Coast No. 6 petroleum fuel oil shows little change in its carbon content, Fig. 7.18, except at high temperatures and large extents of vaporization. The Indo-Malaysian No. 6 petroleum shows no variation in carbon to hydrogen ratio after an initial increase. The raw Paraho shale oil is strongly temperature dependent with respect to the carbon to hydrogen ratio of the vaporizing droplet array, becoming carbon rich to greater degrees and at lower extents of vaporization with increasing furnace temper-

ature. This above behavior is completely different from that observed for equilibrium bulk distillation.

The SRC-II fuels also exhibit a variation in carbon to hydrogen ratio, Fig. 7.19, that differs greatly from equilibrium bulk distillation results. The SRC-II heavy distillate fraction and 2.9:1 blend do not show any tendency to increase their carbon to hydrogen ratios, whereas the SRC-II middle distillate shows a temperature dependence similar to the shale oil.

7.3.3 Nitrogen Evolution from Droplet Arrays

The Gulf Coast No. 6 petroleum evolves nitrogen from a rapidly vaporizing droplet array in proportion to the mass vaporized, Fig. 7.20, without any apparent dependence on temperature. The Indo-Malaysian No. 6 petroleum, Fig. 7.21, exhibits an initial evolution of nitrogen free material, following which a rapid increase in nitrogen evolution occurs at about 20% extent of vaporization, which eventually lessens until the nitrogen is evolved at rate approximately proportional to the mass evolved. The raw Paraho shale oil has a temperature dependent nitrogen evolution, Fig. 7.22. At furnace temperatures below 1000 K, the fractional evolution of nitrogen is similar to that for equilibrium bulk distillation. However, as the furnace temperature increases, a progressively larger amount of nitrogen free mass is evolved. Thereafter the nitrogen appears to be evolved in proportion to the mass vaporized.

The temperature dependence of SRC-II middle distillate observed for its carbon to hydrogen ratio, is also exhibited in its nitrogen evolution, Fig. 7.23, which parallels that observed for raw Paraho shale oil. The SRC-II heavy distillate has increased its rate of nitrogen evolution, over that expected from distillation results, as has the SRC-II blend, but to a lesser degree. Comparison with the corresponding equilibrium distillation

curves, Fig. 7.9, shows that the heavy and middle distillate fractions have changed positions.

The model fuel nitrogen evolution, Fig. 7.24, is in all cases greater than that for equilibrium distillation. Since these fuels are binary mixtures it can be said that the evolution of n-dodecane lags that of the dopant. The pyridine doped fuel evolves its dopant so rapidly that except for the 1000K pyrolysis experiment no samples were collected with any significant pyridine content. The quinoline evolution data present a confusing temperature dependence that requires careful interpretation. The acridine evolution is not seen to depart from the equilibrium data except for large extents of vaporization at 1400 K.

7.4 Theoretical Calculations

7.4.1 Equilibrium Distillation

The evaluation of Rayleigh's equation, Eq. 6.1, for the differential vaporization of the model fuels is shown, Eqs. 6.6 and 6.7, to need only a knowledge of the vapor pressures of the components concerned. Vapor pressure data[26] of the model fuel compounds was curve-fitted with the following result, where the vapor pressure is mm Hg:

$$\text{Acridine} \quad p_A = 1.792 \times 10^8 \exp [-7635/T], \; r^2 = 1.00 \qquad 7.4$$

$$\text{n-Dodecane} \quad p_D = 2.507 \times 10^8 \exp [-6189/T], \; r^2 = 1.00 \qquad 7.5$$

$$\text{Pyridine} \quad p_P = 2.233 \times 10^8 \exp [-4855/T], \; r^2 = 1.00 \qquad 7.6$$

$$\text{Quinoline} \quad p_Q = 1.918 \times 10^8 \exp [-6328/T], \; r^2 = 1.00 \qquad 7.7$$

Applying Eqs. 7.4-7.7 to Eqs. 6.1, 6.6 and 6.7, where for example, in the case of pyridine $p_1 \equiv p_p$, $p_2 = p_D$, $P_T = 760$ mm Hg, $x_{10} = 0.126$ (viz.

Table 7.2), and $x_{1f} = 0$, the boiling curves, Fig. 7.5, and nitrogen evolution curves, Fig. 7.10, of the model fuels are generated.

7.4.2 Furnace Pyrolysis

Applying Eqs. 3.9 and 6.20 (viz. Appendix B) to the model fuel arrays, vaporization rate constants are calculated to be

1000 K	$\lambda = 0.406\ mm^2.s$	7.8
1200 K	$\lambda = 0.490\ mm^2/s$	7.9
1400 K	$\lambda = 0.570\ mm^2/s$	7.10

The evolution of dopant is evaluated using the equations developed in section 6.3. Assuming the liquid and vapor phase components to be always in equilibrium, the vaporization driving force at the surface used for the boundary condition, Eq. 6.78, may be defined as a function of the surface mass fraction, Fig. 7.25, employing Eqs. 7.4-7.7 and the equilibrium considerations of the preceeding section. The fractional evolutions of dopants, Fig. 7.24, is greater than the equilibrium calculations, matching well with the measured pyrolysis results. The quinoline calculations show a complex temperature dependence that was not evident for the pyridine and acridine doped fuels over the temperature range considered. The 1000 K curve for pyridine is shown alone for clarity, the higher temperature curves being almost coincident with the maximum rate of pyridine evolution represented by the dashed line in Fig. 7.10. Similarly, only the 1400 K curve for acridine is presented, lower temperature curves being close to the equilibrium curve, Fig. 7.10.

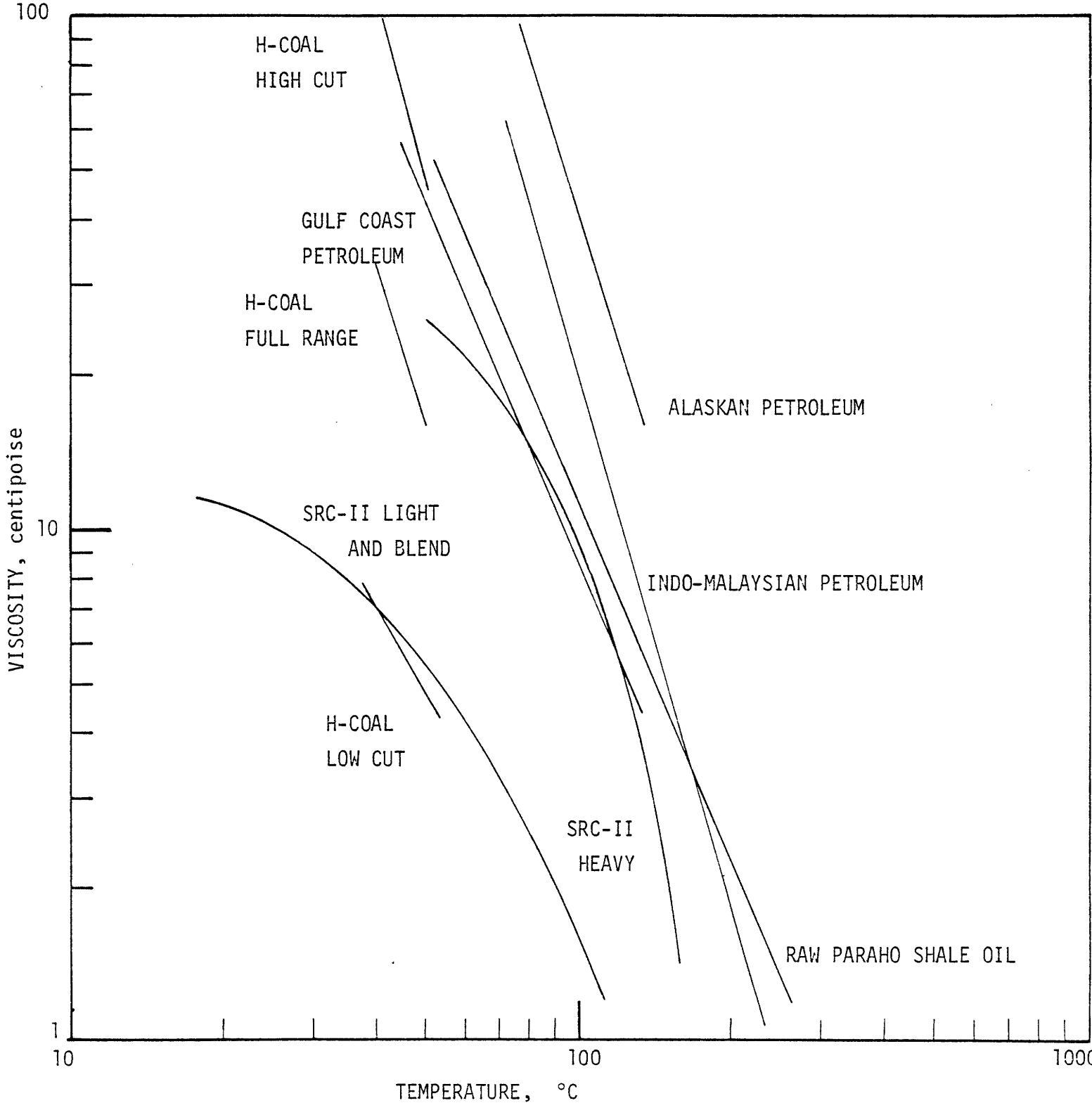

Figure 7.1 Viscosity Variation with Temperature for Gulf Coast No. 6 Petroleum Fuel Oil, Indo-Malaysian No. 6 Petroleum Fuel Oil, Raw Paraho Shale Oil, SRC-II Middle Distillate Fraction, SRC-II Heavy Distillate Fraction, SRC-II 2.9:1 Blend Middle and Heavy Distillate Fractions, Raw Alaskan Petroleum, H-Coal Low Cut, H-Coal High Cut, and H-Coal Full Range

	(i)	(ii)	(iii)	(iv)	(v)	(vi)
Ultimate Analysis, %:						
Carbon	88.29	87.50	83.63	83.82	89.11	86.28
Hydrogen	12.31	12.41	11.81	9.07	7.49	8.83
Nitrogen	0.44	0.23	2.21	0.97	1.21	0.96
Sulfur	0.47	0.22	0.69	0.20	0.39	0.26
Oxygen	0.86	1.04	1.18	5.43	1.90	4.18
Ash	0.01	0.04	0.09	0.00	0.06	0.01
Water and Sediment	none		1.6	0.00		0.04
Flash Point, °C	149	99	102	64	129	66
Pour Point, °C	8	16	29	<-30	-13	<-30
Gross Heat of Combustion, MJ/kg	43.89	44.36	42.86	39.54	39.82	39.80
Specific Gravity @ 15°C	0.9309	0.9230	0.9279	0.9765	1.0655	0.9972

TABLE 7.1

Fuel Properties of (i) Gulf Coast No. 6 Petroleum Fuel Oil, (ii) Indo-Malaysian No. 6 Petroleum Fuel Oil, (iii) Raw Paraho Shale Oil, (iv) SRC-II Middle Distillate Fraction, (v) SRC-II Heavy Distillate Fraction, and (vi) SRC-II 2.9:1 Blend Middle and Heavy Distillate Fractions

	n-Dodecane	Pyridine	Quinoline	Acridine
Molecular Weight	170.3	79.1	129.2	179.2
Normal Boiling Point, °C	216.3	115.4	237.7	346.0
Mole Fractions Mixture 1	0.874	0.126	-----	-----
Mole Fractions Mixture 2	0.867	-----	0.133	-----
Mole Fractions Mixture 3	0.984	-----	-----	0.016

TABLE 7.2

Fuel Properties of n-Dodecane Doped with Pyridine, Quinoline and Acridine

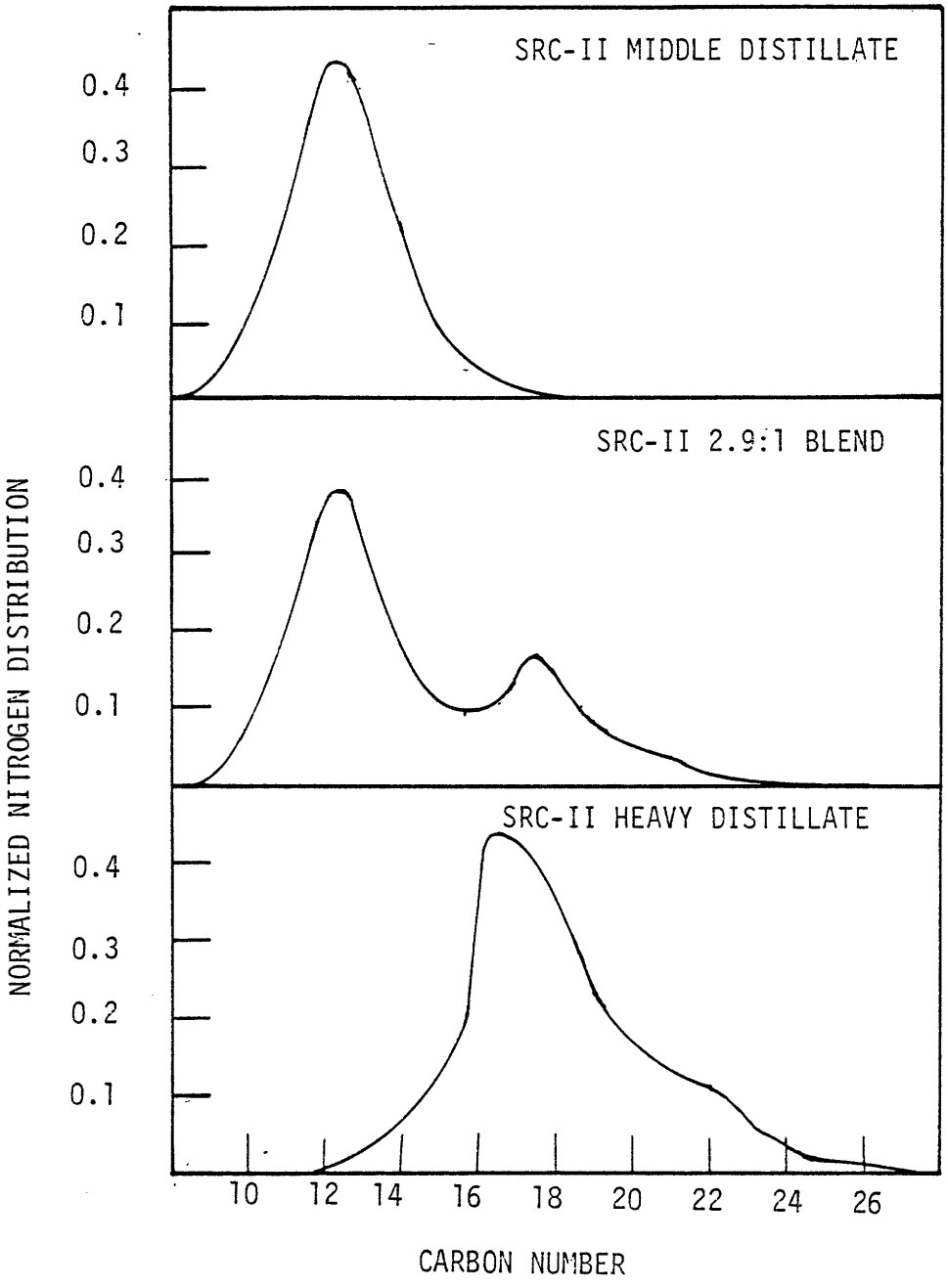

Figure 7.2 Normalized Nitrogen Distribution with Respect to Carbon Number for SRC-II Middle Distillate Fraction, SRC-II Heavy Distillate Fraction, and SRC-II 2.9:1 Blend Middle and Heavy Distillate Fractions

Middle Distillate	Heavy Distillate
1,2,3,4 tetrahydronaphthalene	C_3 naphthalene
Naphthalene	Acenaphthene
Methyl tetrahydronaphthalene	C_4 naphthalene
Dimethyl-(1,2,3,4) tetra-hydronaphthalene	Fluorene
	Methylacenaphthene
Methylnaphthalene	C_2 acenaphthene
Ethyltetrahydronaphthalene	Methylfluorene
	Anthracene
	Phenathrene
	Methyl phenanthrene
	Fluoranthene
	Pyrene

Table 7.3

Major Components Identified in SRC-II Middle Distillate Fraction and SRC-II Heavy Distillate Fraction

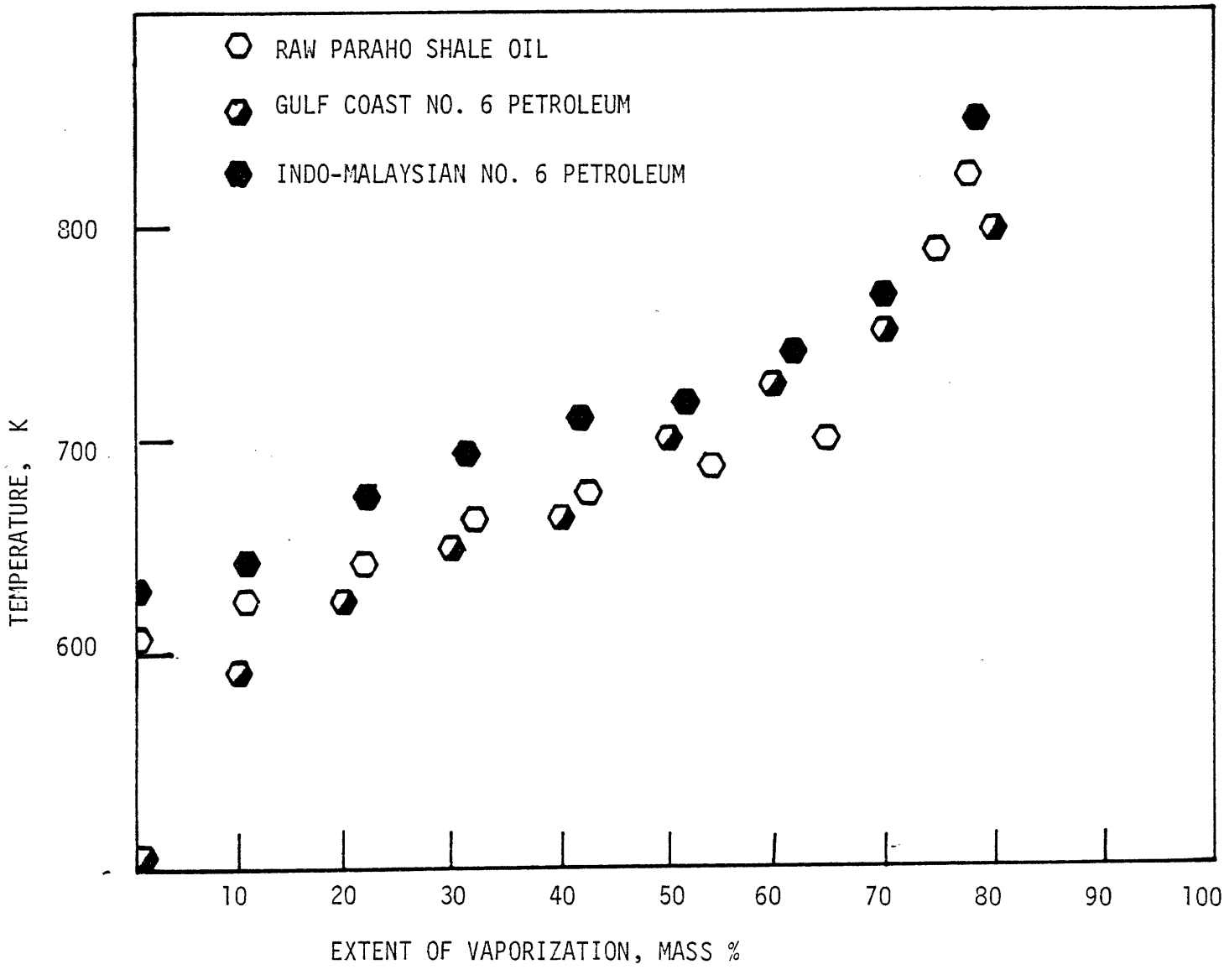

Figure 7.3 Engler-Type Boiling Point Curves of Gulf Coast No. 6 Petroleum Fuel Oil, Indo-Malaysian No. 6 Petroleum Fuel Oil, and Raw Paraho Shale Oil

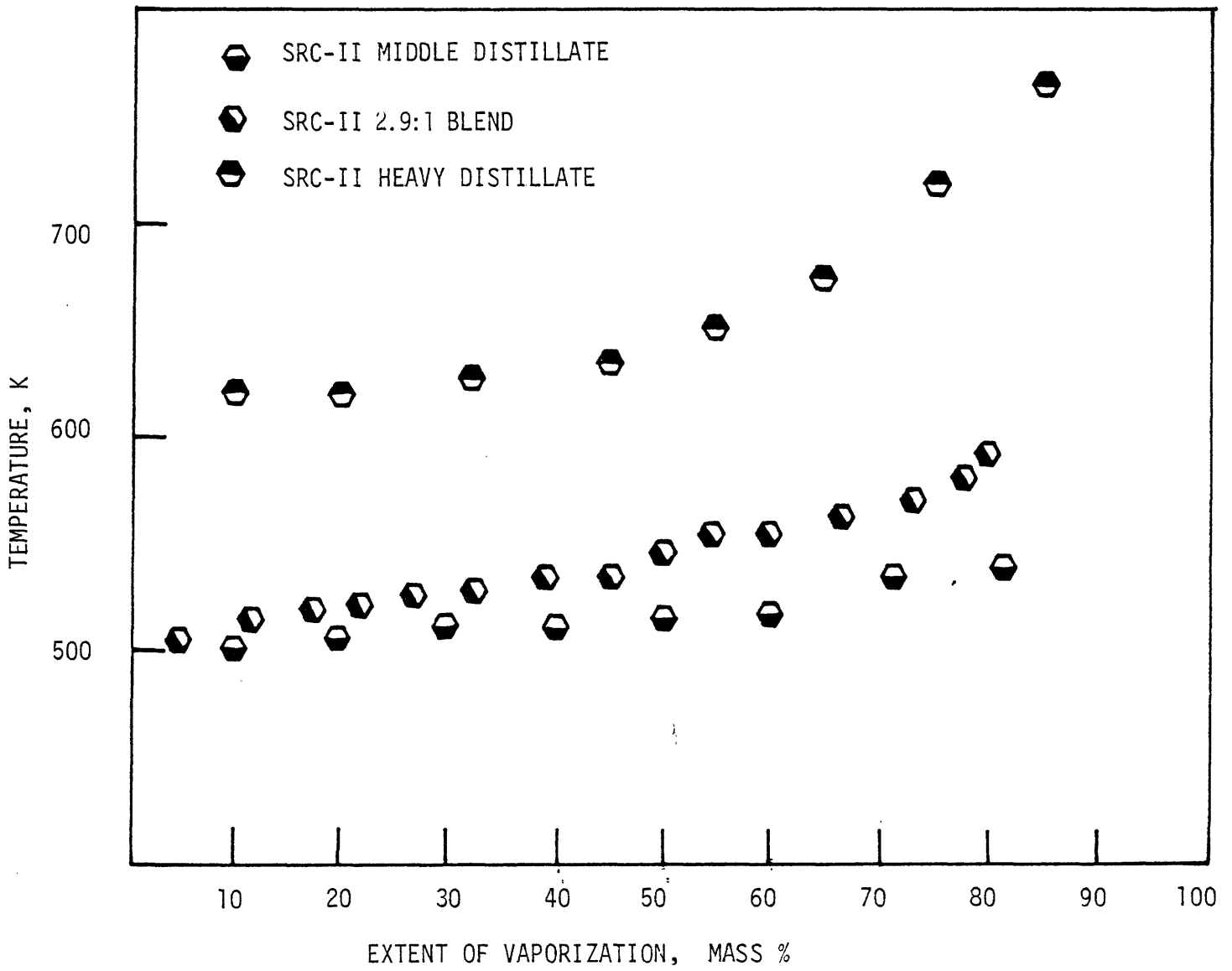

Figure 7.4 Engler-Type Boiling Point Curves of SRC-II Middle Distillate Fraction, SRC-II Heavy Distillate Fraction, and SRC-II 2.9:1 Blend Middle and Heavy Distillate Fractions

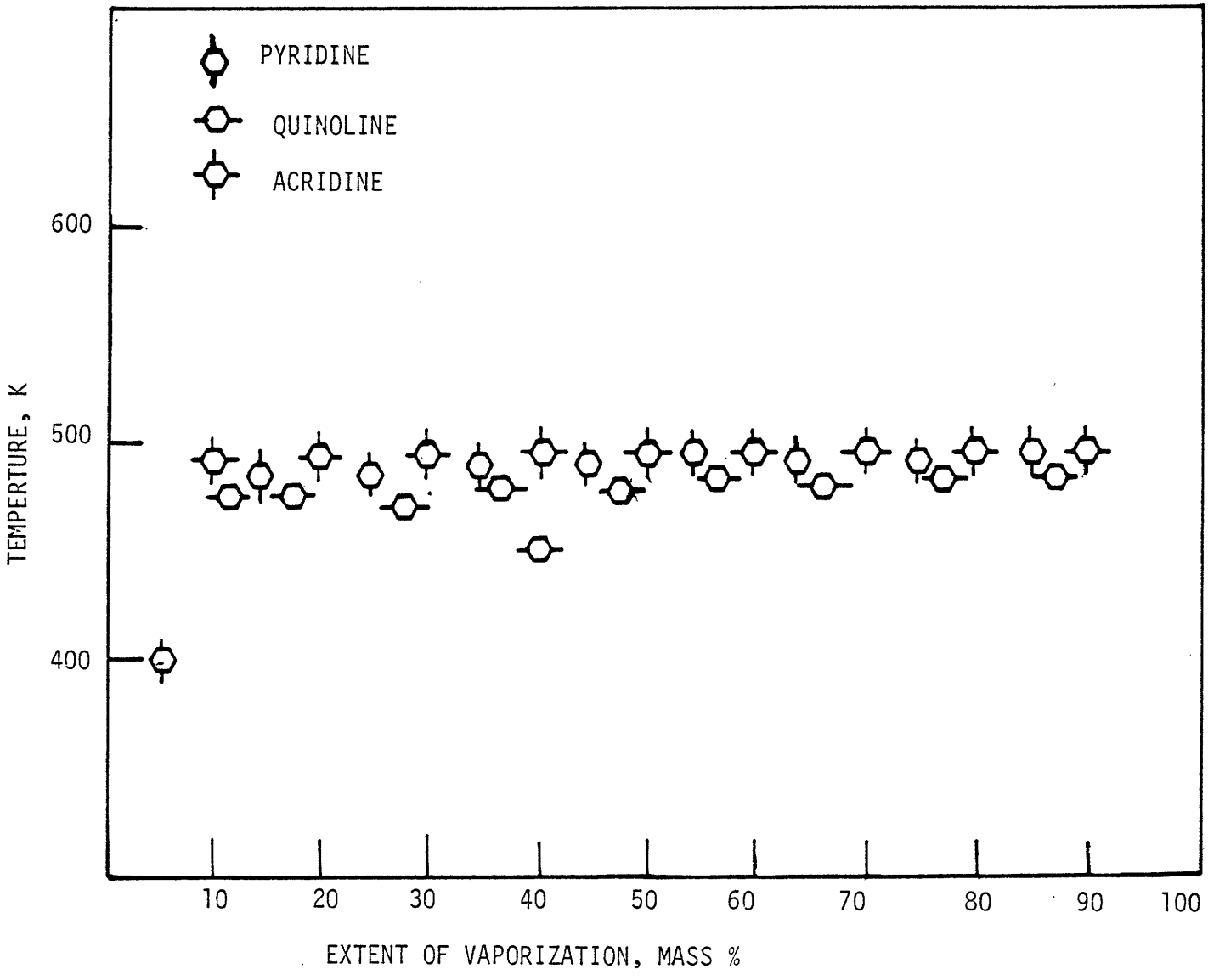

Figure 7.5 Engler-Type Boiling Point Curves of n-Dodecane Doped with Pyridine, Quinoline or Acridine

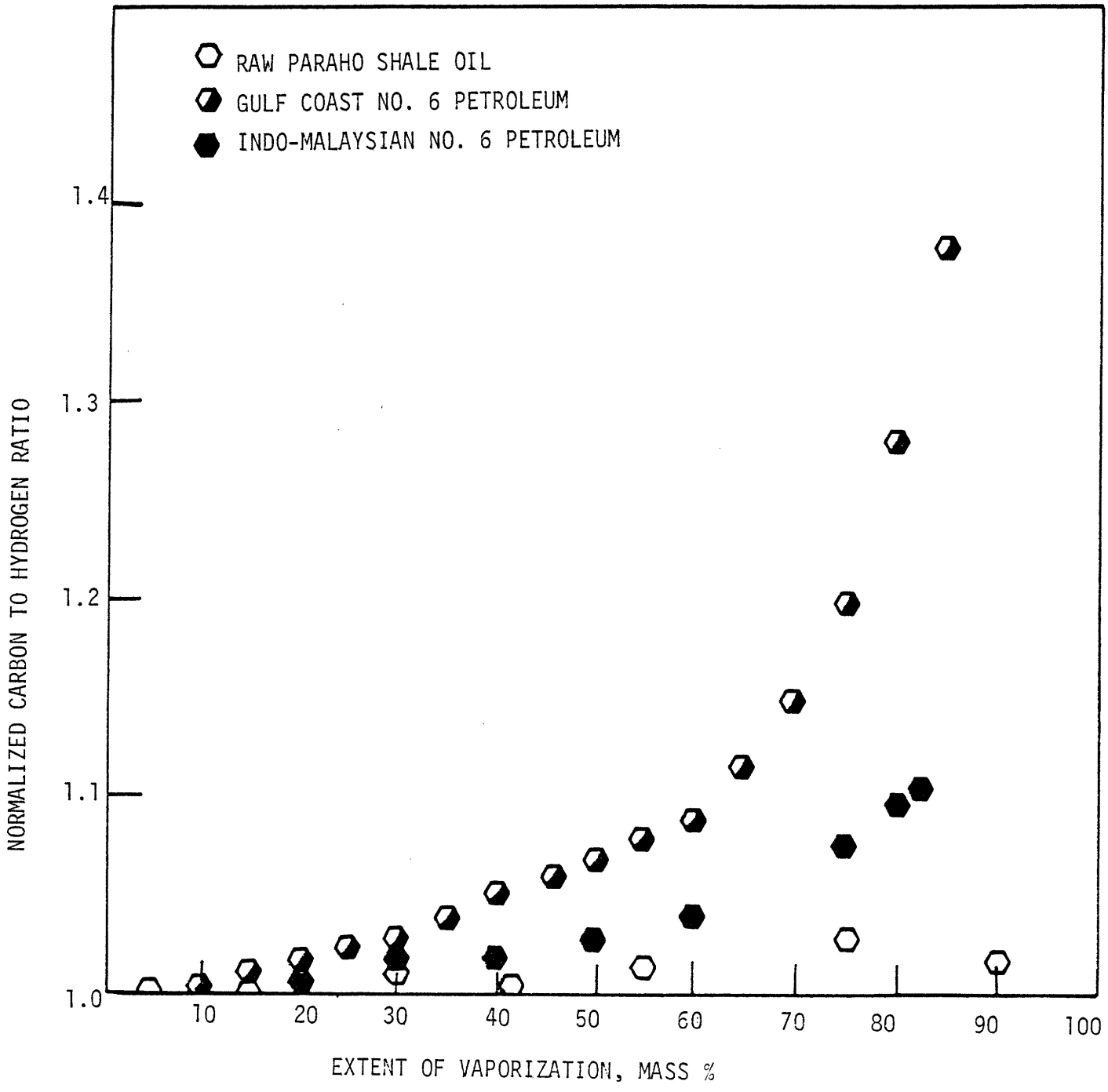

Figure 7.6 Normalized Carbon to Hydrogen Atomic Ratios of Fuel Residues During Equilibrium Batch Distillation of Gulf Coast No. 6 Petroleum Fuel Oil, Indo-Malaysian No. 6 Petroleum Fuel Oil, and Raw Paraho Shale Oil

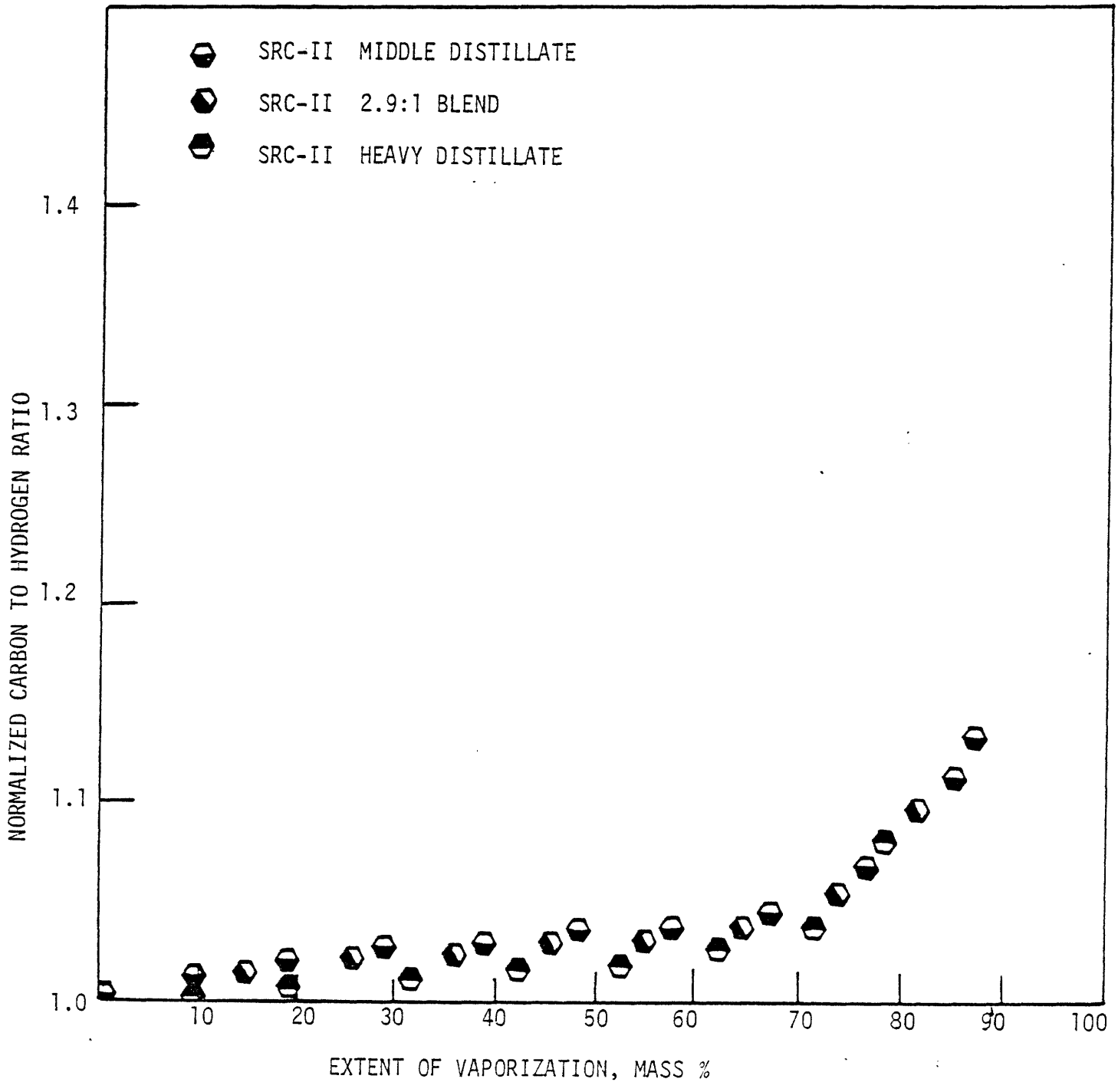

Figure 7.7 Normalized Carbon to Hydrogen Atomic Ratios of Fuel Residues During Equilibrium Batch Distillation of SRC-II Middle Distillate Fraction, SRC-II Heavy Distillate Fraction, and SRC-II 2.9:1 Blend Middle and Heavy Distillate Fractions

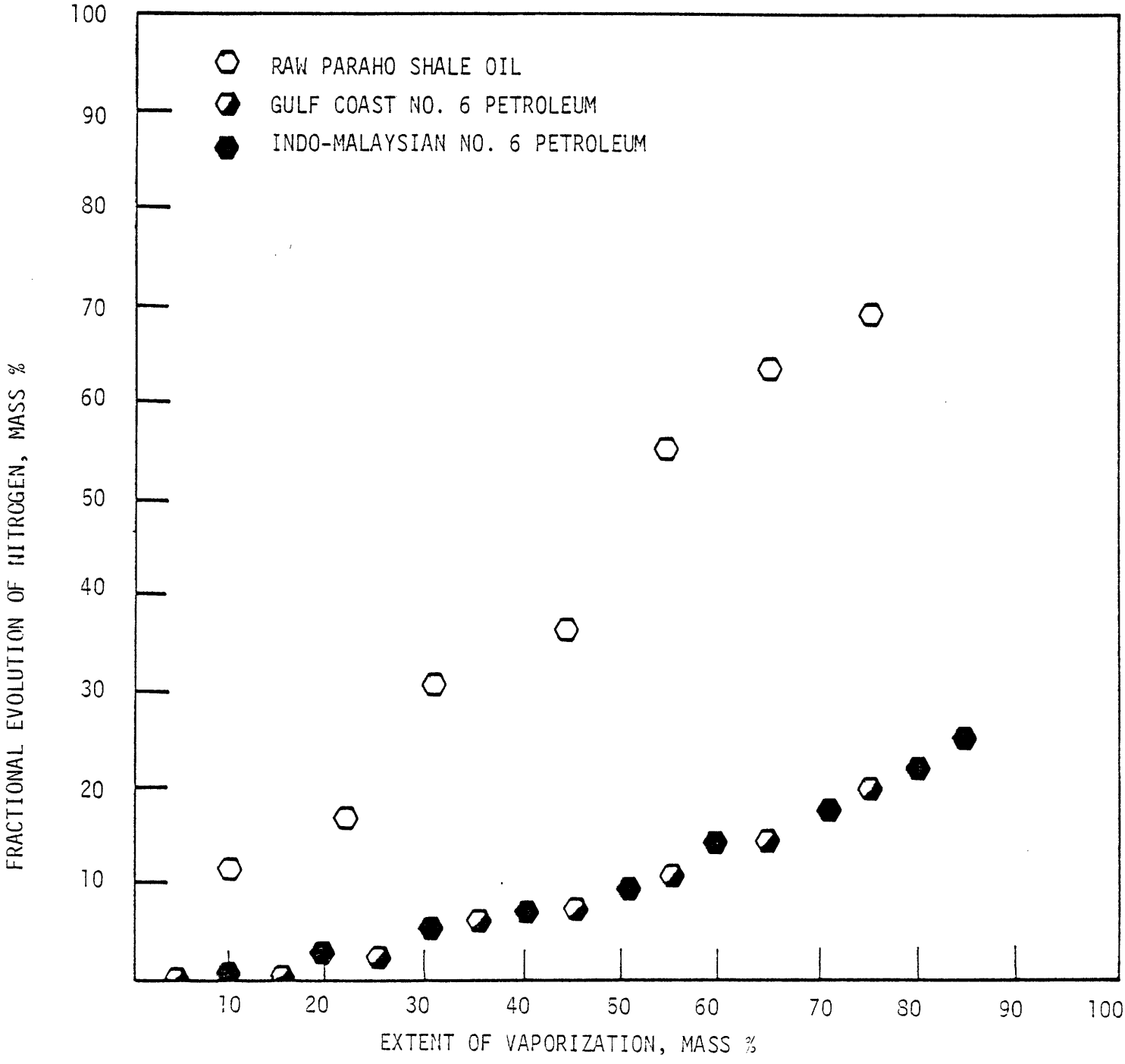

Figure 7.8 Nitrogen Evolution During Equilibrium Batch Distillation of Gulf Coast No. 6 Petroleum Oil, Indo-Malaysian No. 6 Petroleum Fuel Oil, and Raw Paraho Shale Oil

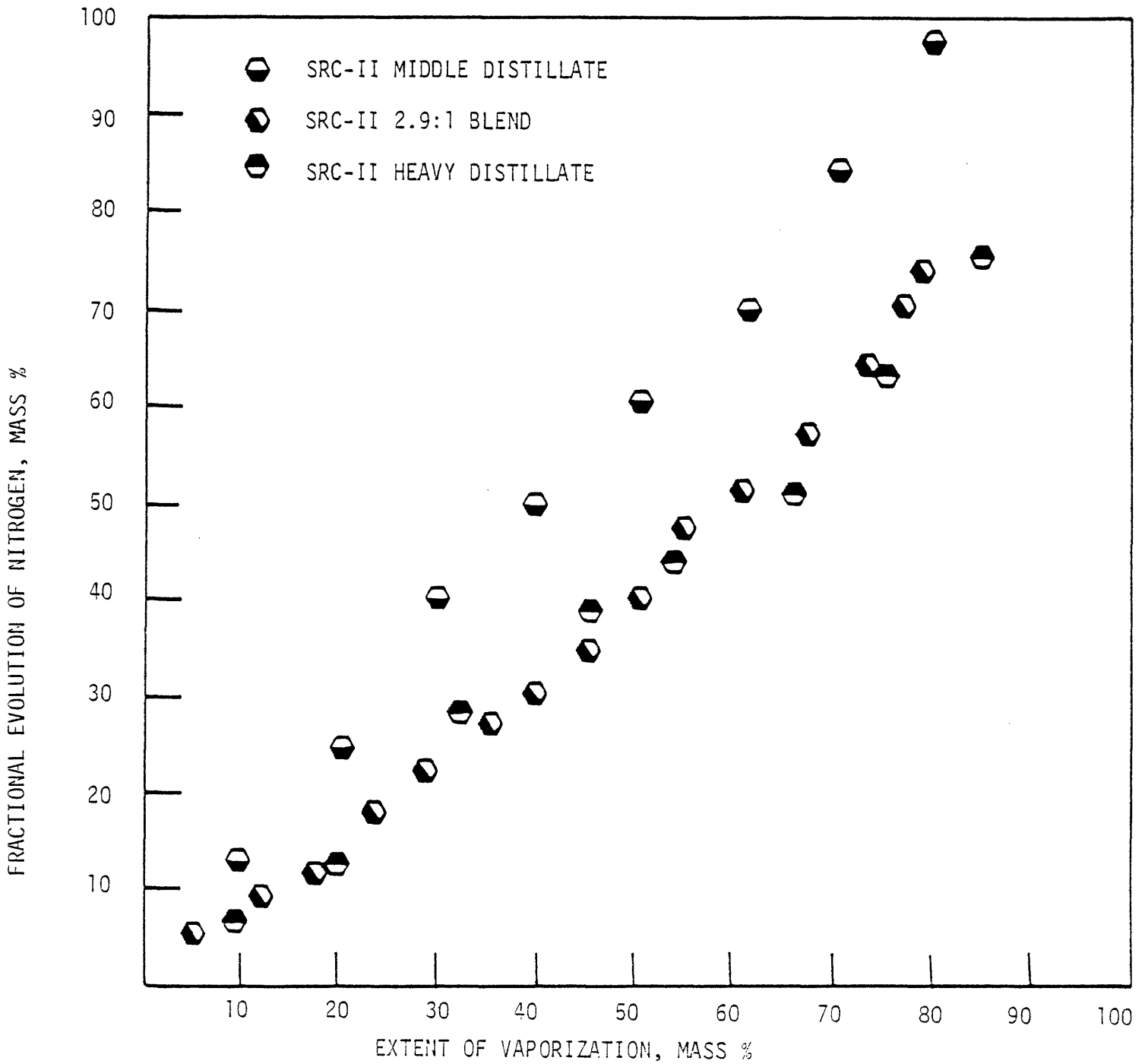

Figure 7.9 Nitrogen Evolution During Equilibrium Batch Distillation of SCR-II Middle Distillate Fraction, SRC-II Heavy Distillate Fraction, and SRC-II 2.9:1 Blend Middle and Heavy Distillate Fractions

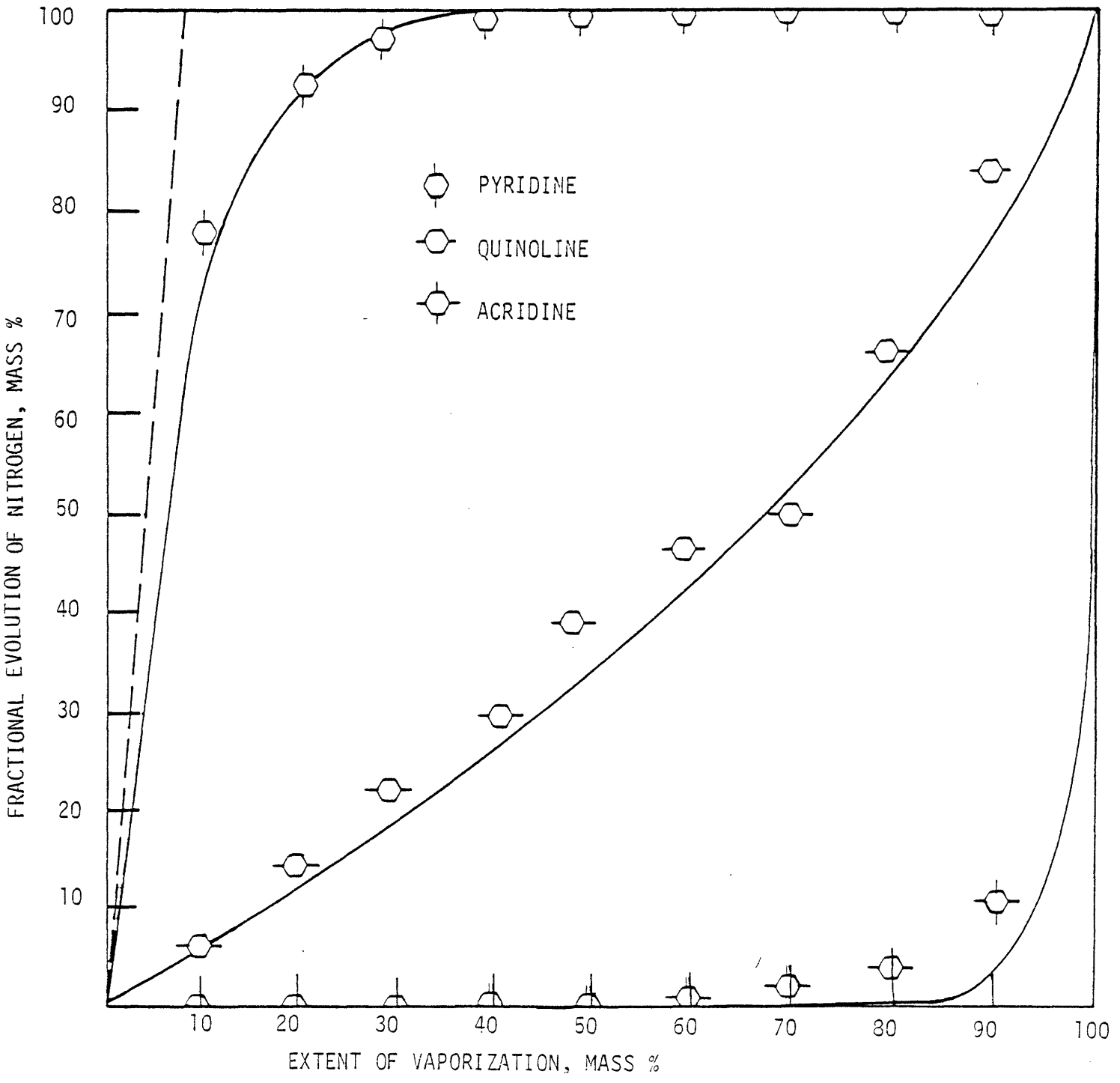

Figure 7.10 Nitrogen Evolution During Equilibrium Batch Distillation of n-Dodecane Doped with Pyridine, Quinoline or Acridine (Data Points are Experimental, Solid Lines are Calculations from Theory)

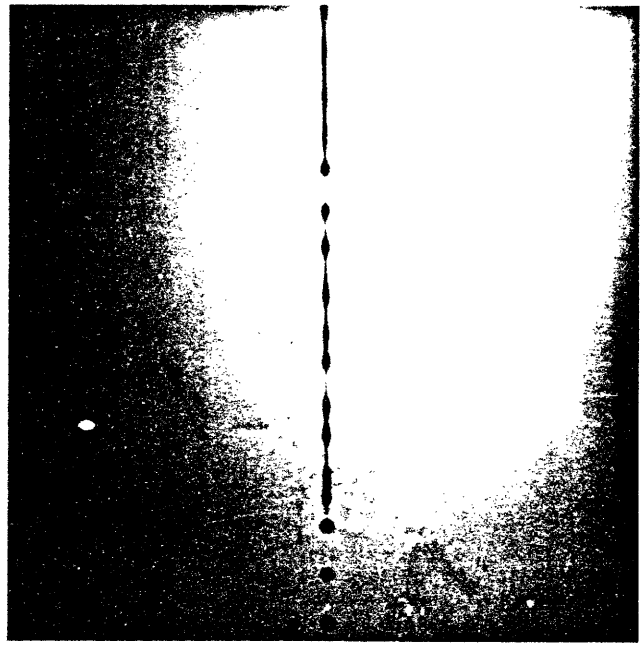

(a)

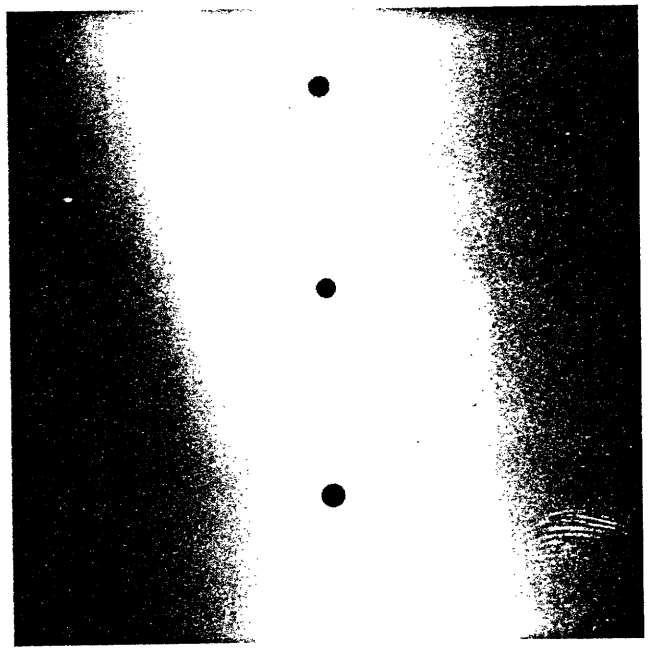

(b)

Figure 7.11 Raw Paraho Shale Oil Droplets Vaporizing in Helium Atmosphere at 1000 K (a) At Point of Introduction, 150 μm Diameter, (b) 115 ms Residence Time, 50 % Mass Loss, 450 μm Diameter

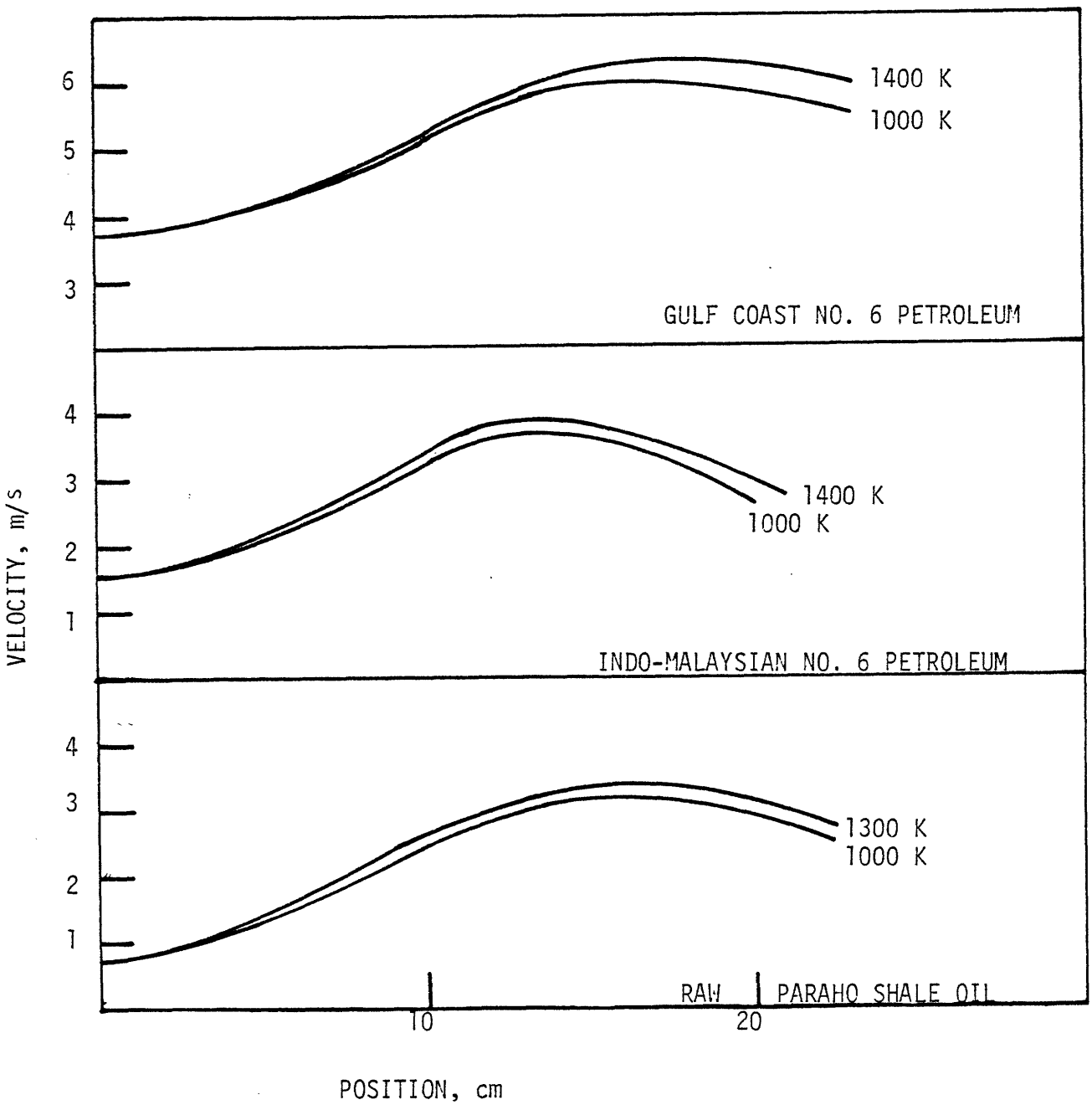

Figure 7.12 Particle Velocity versus Position in Furnace For 150 μm Droplet Arrays of Gulf Coast No. 6 Petroleum Fuel Oil, Indo-Malaysian No. 6 Petroleum Fuel Oil, and Raw Paraho Shale Oil.

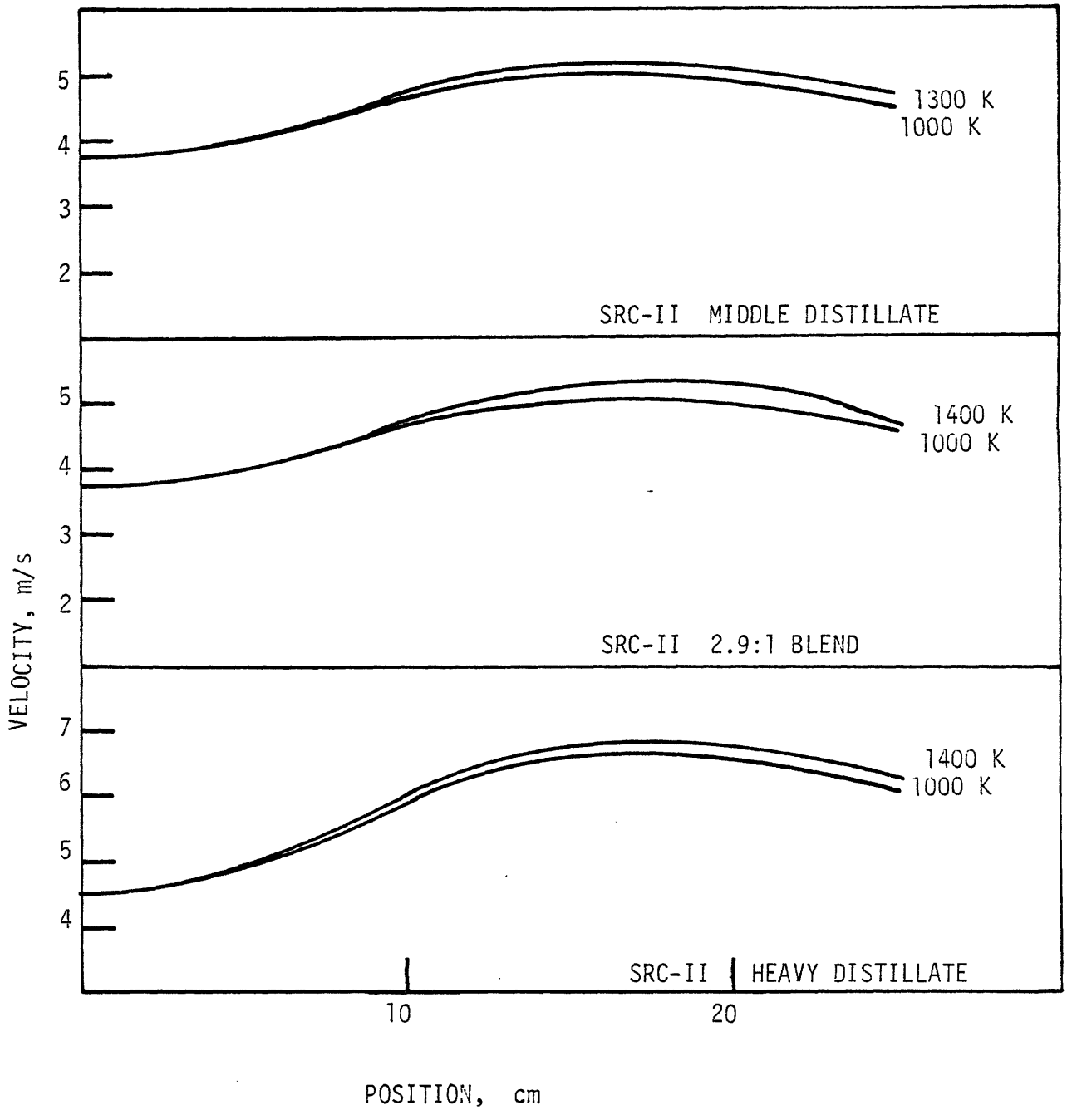

Figure 7.13 Particle Velocity versus Position in Furnace for 150 μm Droplet Arrays of SRC-II Middle Distillate Fraction, SRC-II Heavy Distillate Fraction, and SRC-II 2.9:1 Blend Middle and Heavy Distillate Fractions

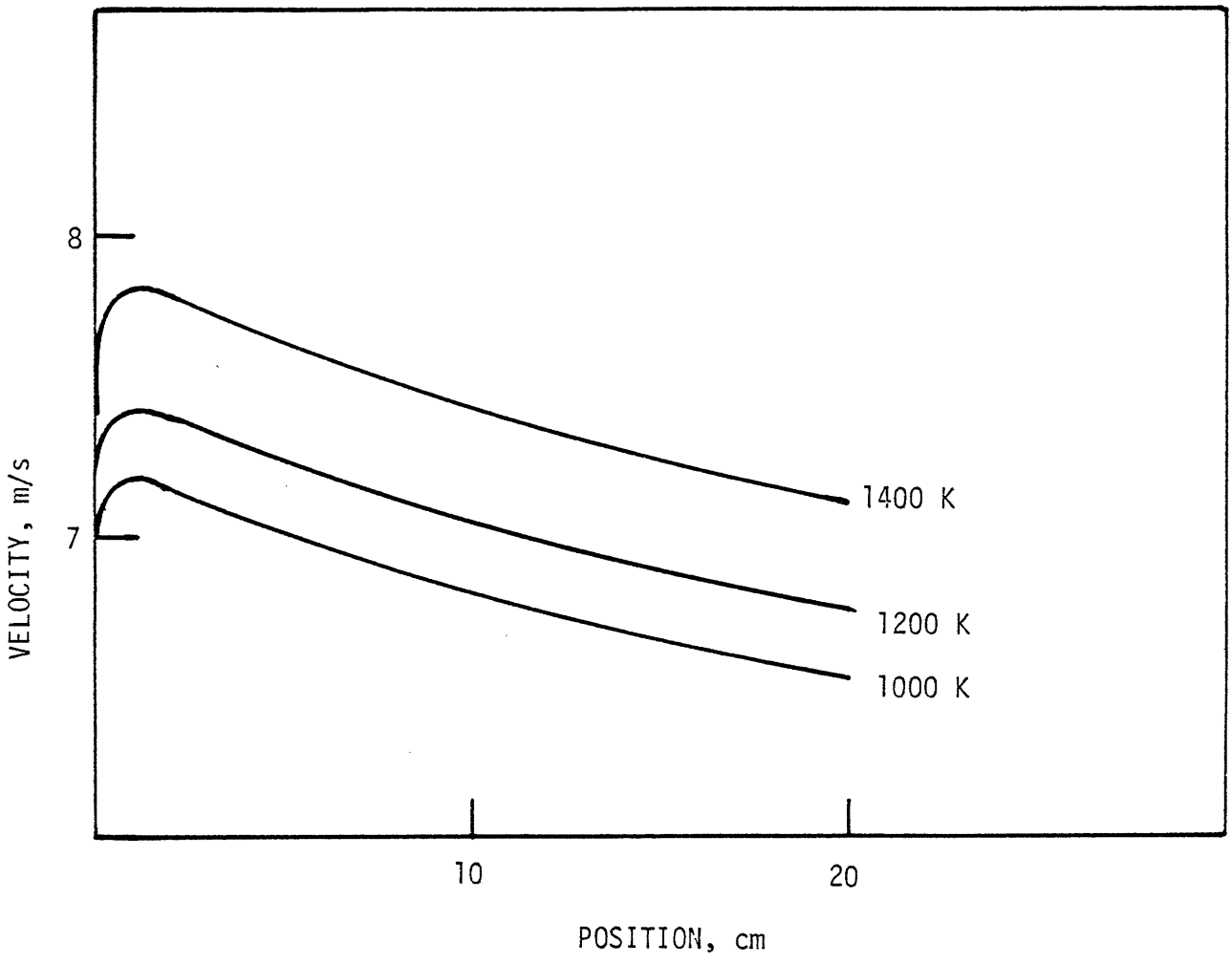

Figure 7.14 Particle Velocity Versus Position in Furnace for 150 μm Droplet Arrays of n-Dodecane Doped with Pyridine, Quinoline or Acridine

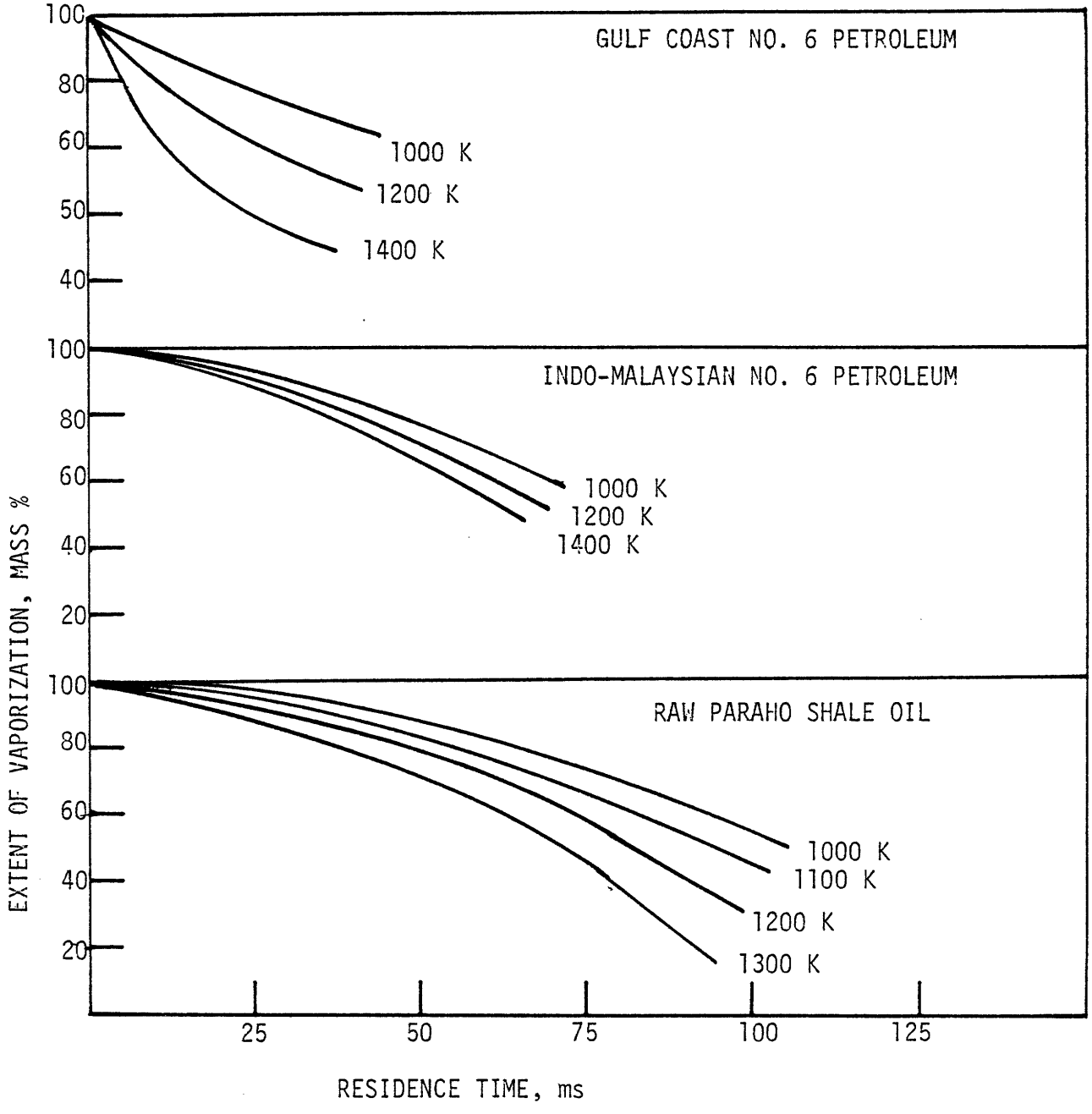

Figure 7.15 Extent of Vaporization versus Residence Time in Furnace for 150 μm Droplet Arrays of Gulf Coast No. 6 Petroleum Fuel Oil, Indo-Malaysian No. 6 Petroleum Fuel Oil, and Raw Paraho Shale Oil

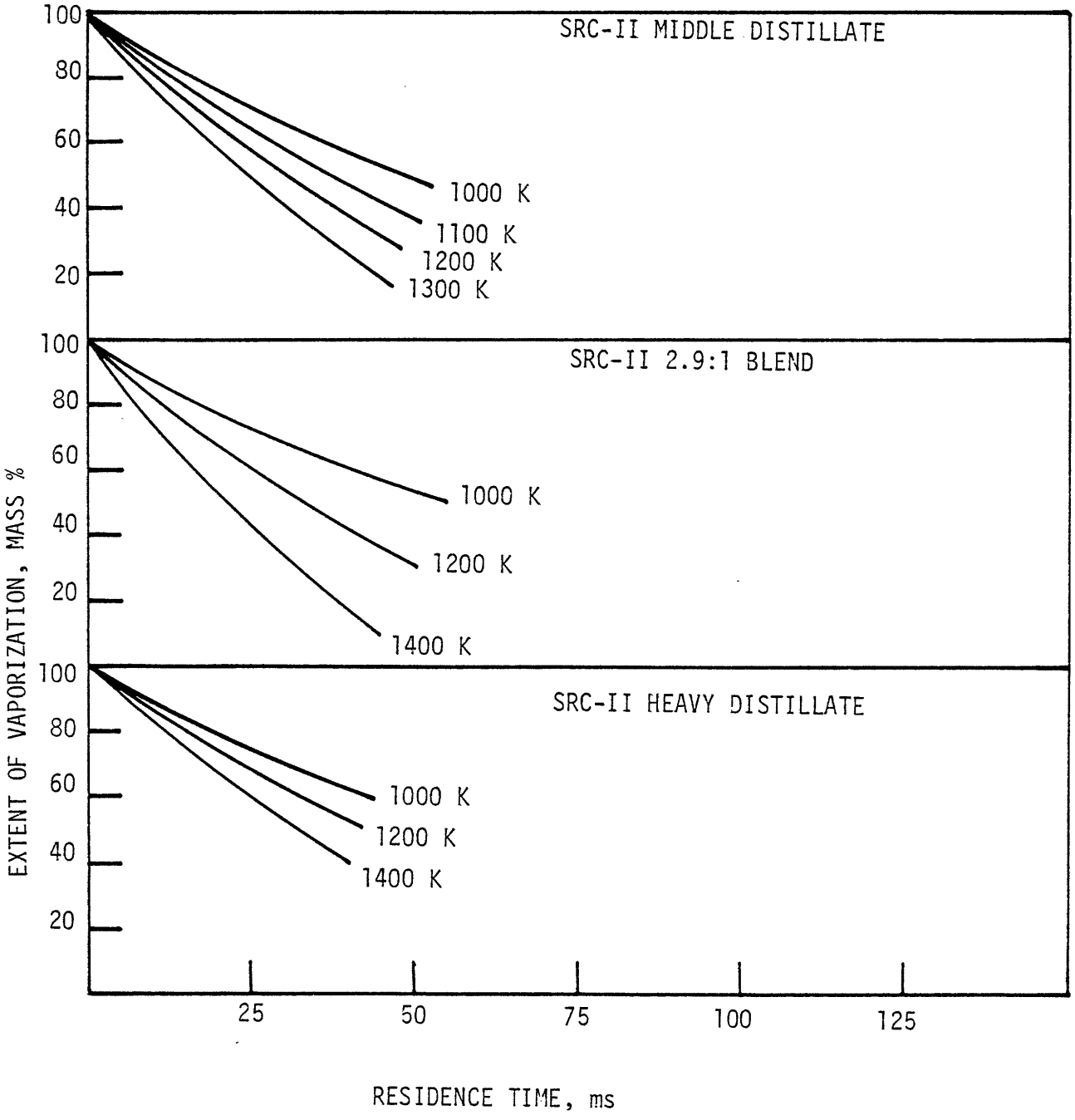

Figure 7.16 Extent of Vaporization versus Residence Time in Furnace for 150 μm Droplet Arrays of SRC-II Middle Distillation Fraction, SRC-II Heavy Distillate Fraction, and SRC-II 2.9:1 Blend Middle and Heavy Distillate Fractions

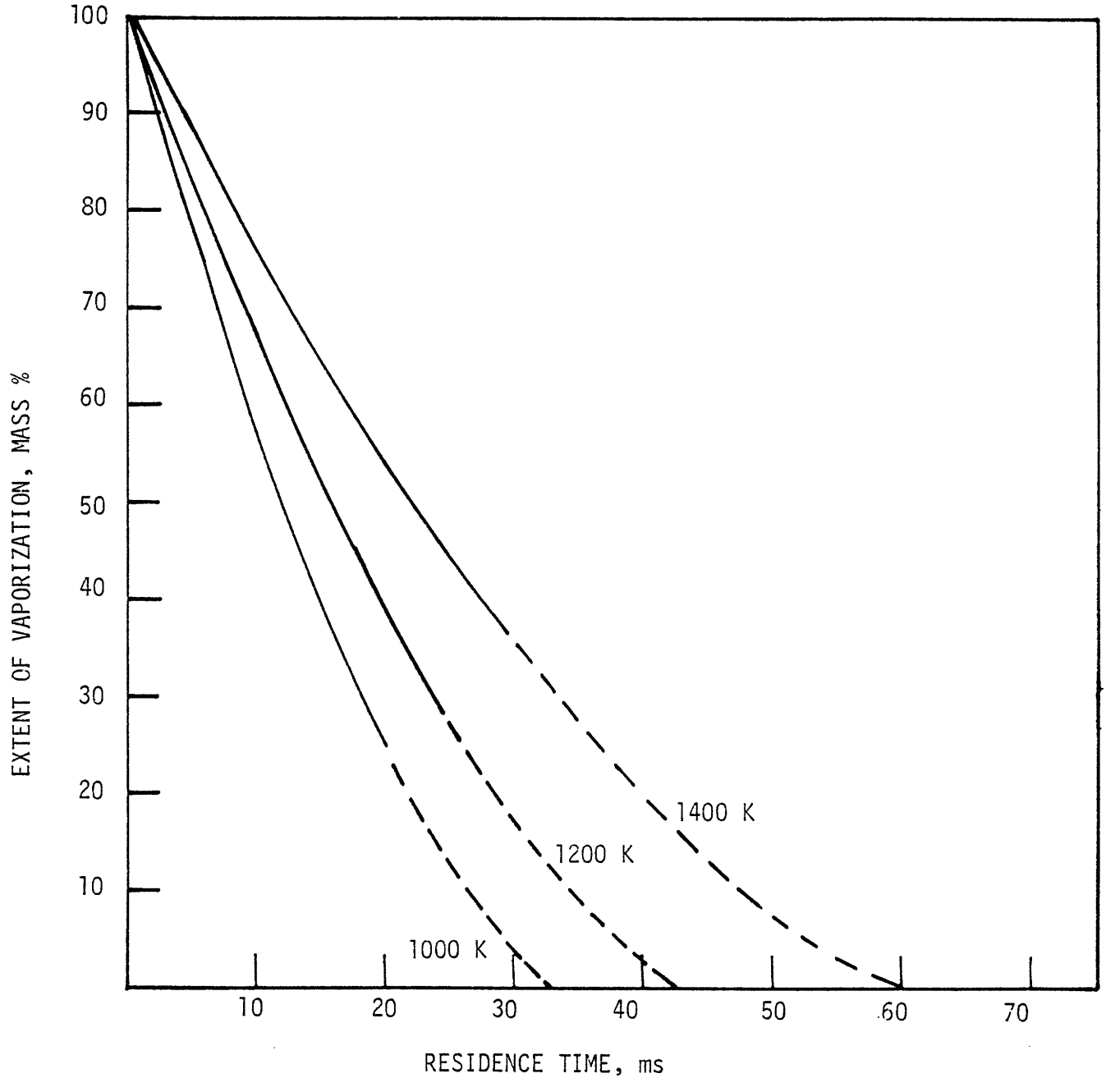

Figure 7.17 Extent of Vaporization versus Residence Time in Furnace for 150 μm Droplet Arrays of n-Dodecane Doped with Pyridine, Quinoline or Acridine

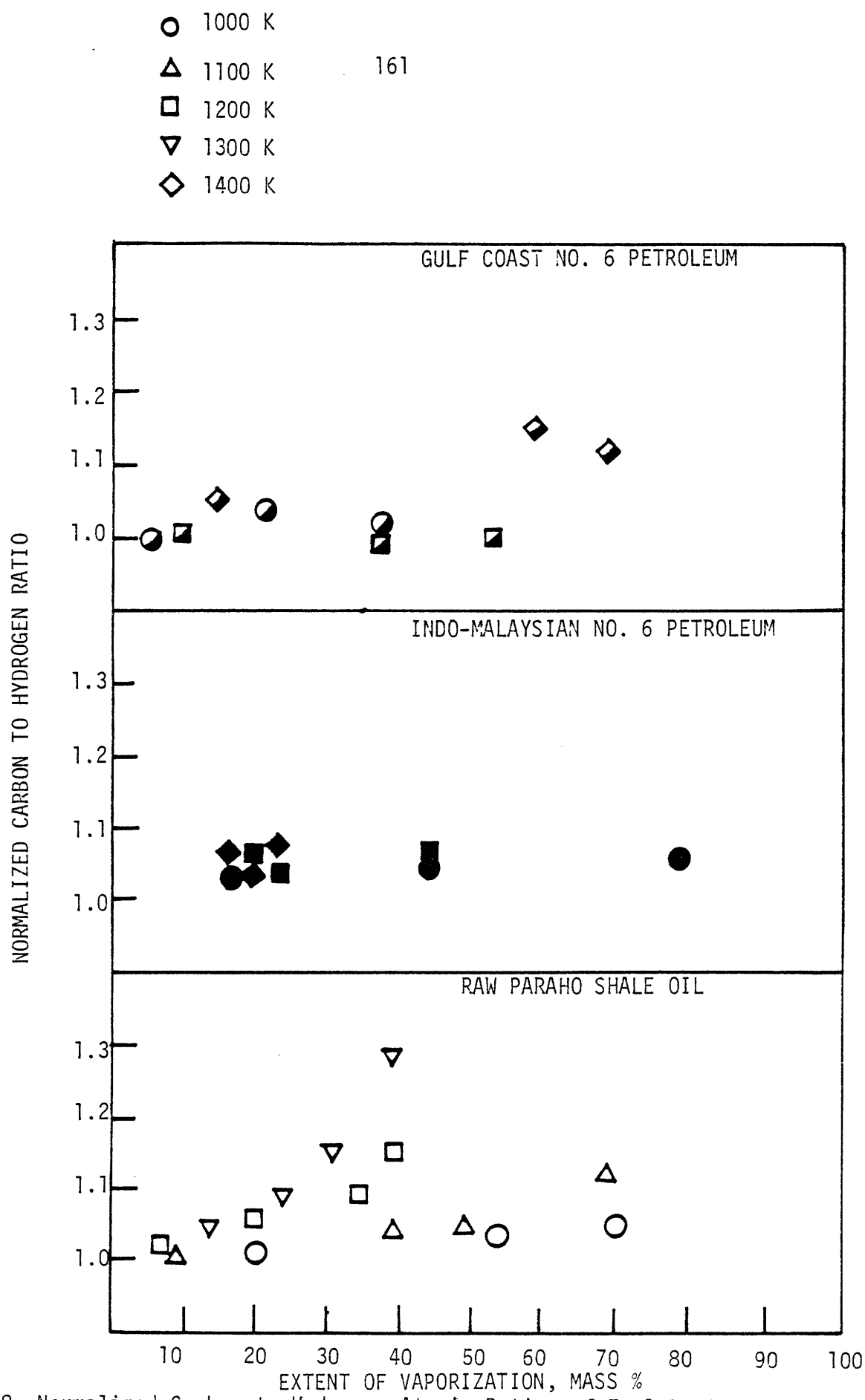

Figure 7.18 Normalized Carbon to Hydrogen Atomic Ratios of Fuel Residues from Pyrolysing 150 μm Droplet Arrays of Gulf Coast No. 6 Petroleum Fuel Oil, Indo-Malaysian No. 6 Petroleum Fuel Oil and Raw Paraho Shale Oil

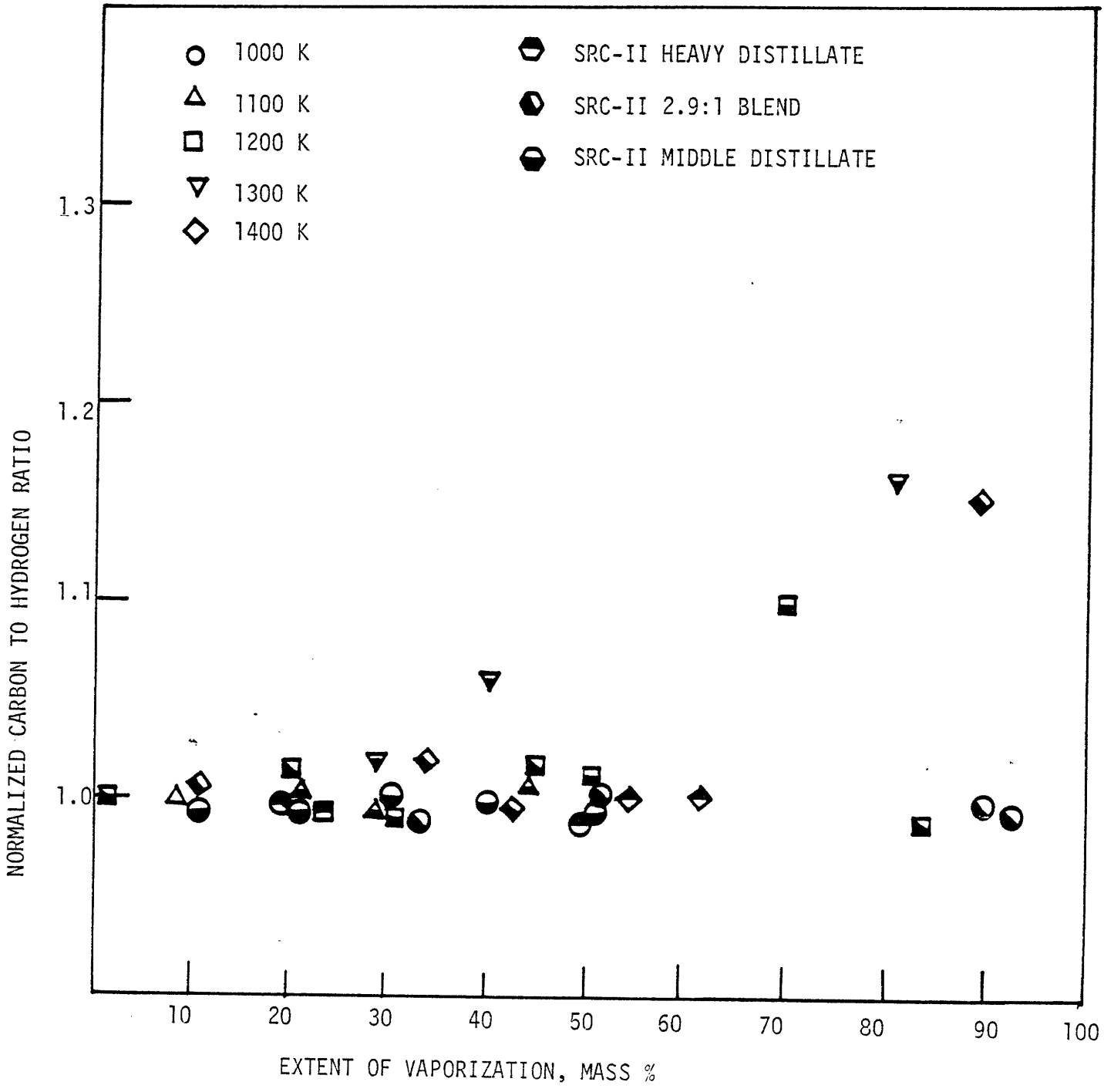

Figure 7.19 Normalized Carbon to Hydrogen Atomic Ratios of Fuel Residues from Pyrolysing 150 μm Droplet Arrays of SRC-II Middle Distillate Fraction, SRC-II Heavy Distillate Fraction, and SRC-II 2.9:1 Blend Middle and Heavy Distillate Fractions

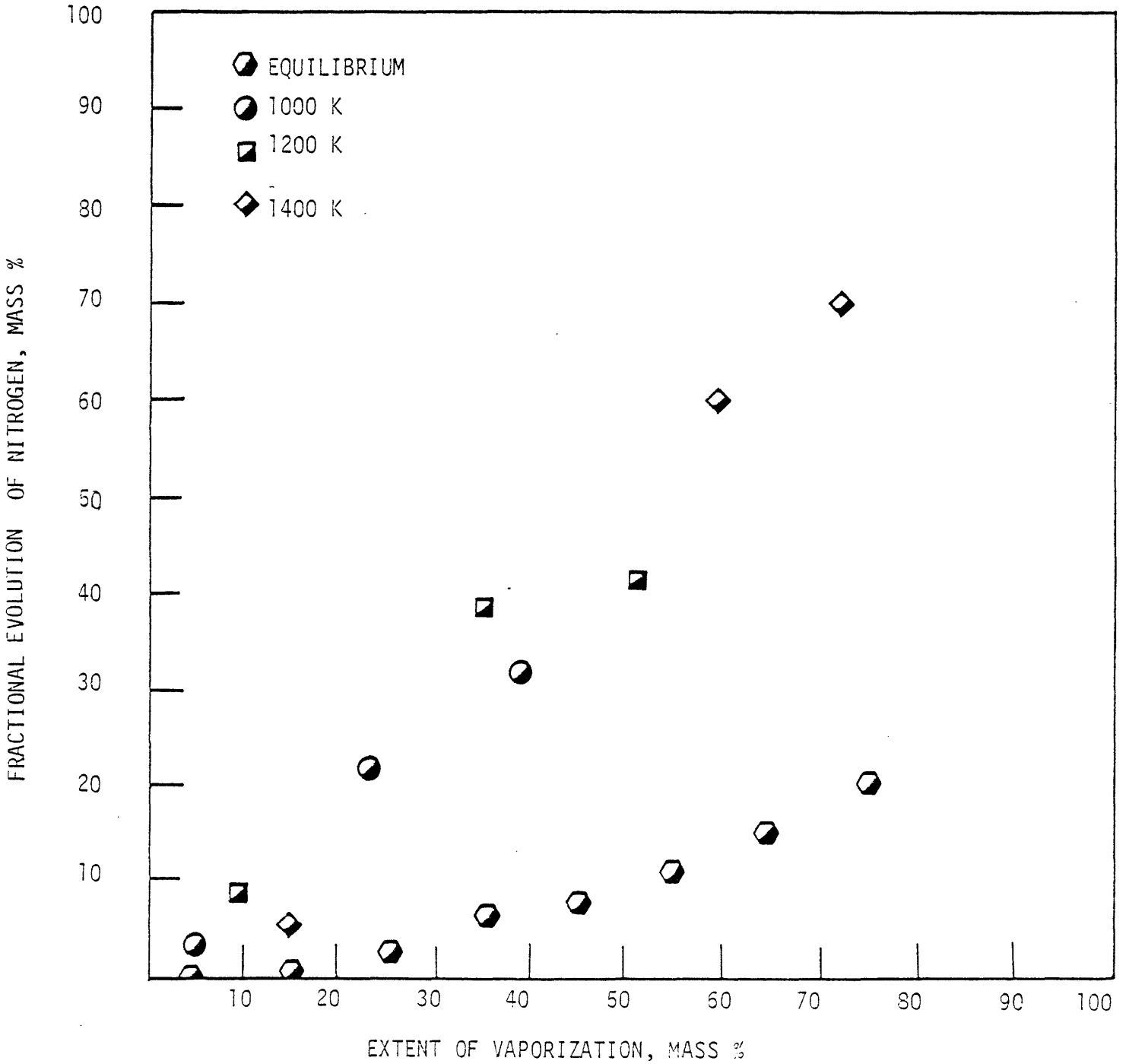

Figure 7.20 Nitrogen Evolution from Pyrolysing 150 μm Droplets Arrays of Gulf Coast No. 6 Petroleum Fuel Oil

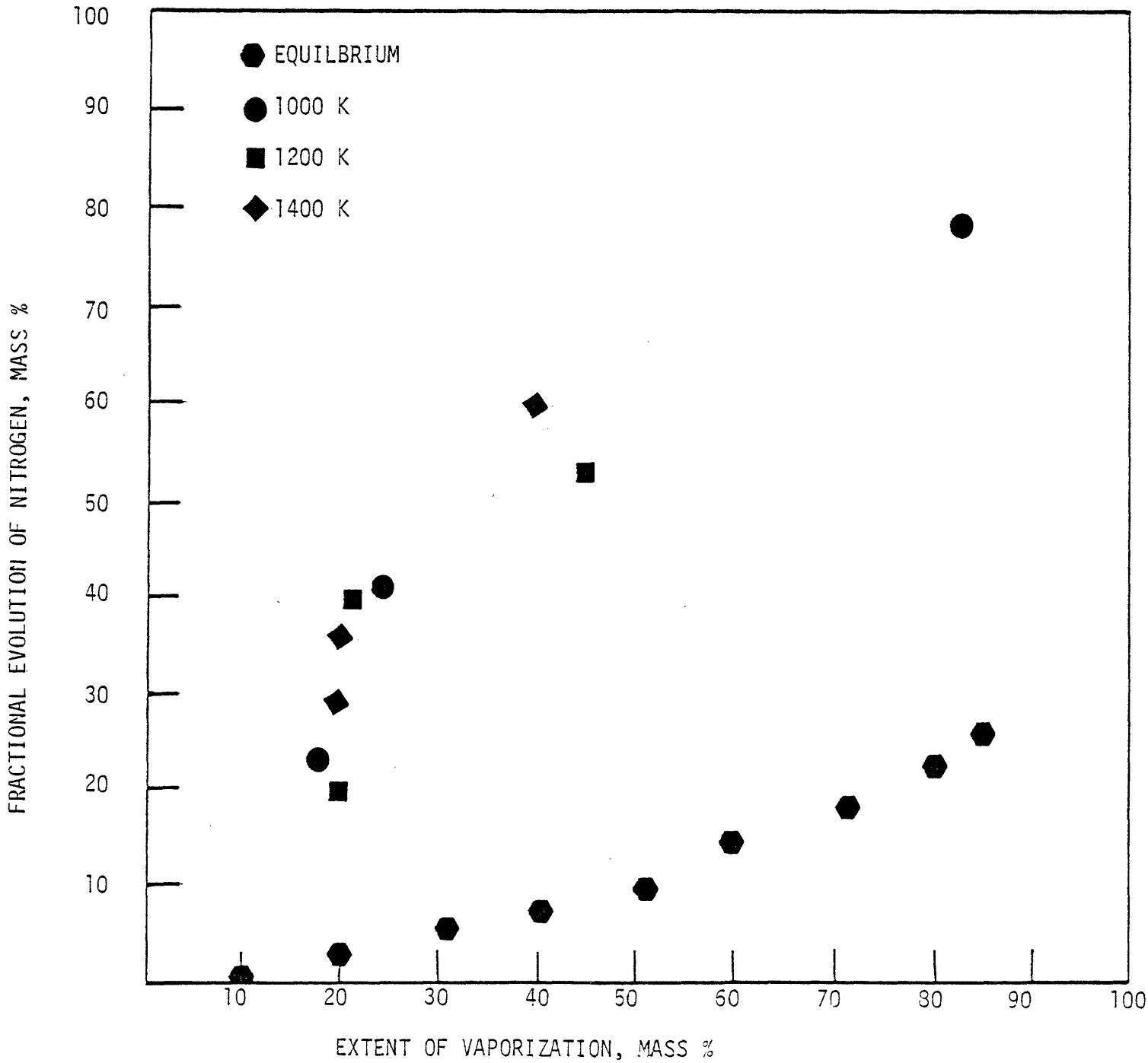

Figure 7.21 Nitrogen Evolution from Pyrolysing 150 μm Droplets Arrays of Indo-Malaysian No. 6 Petroleum Fuel Oil

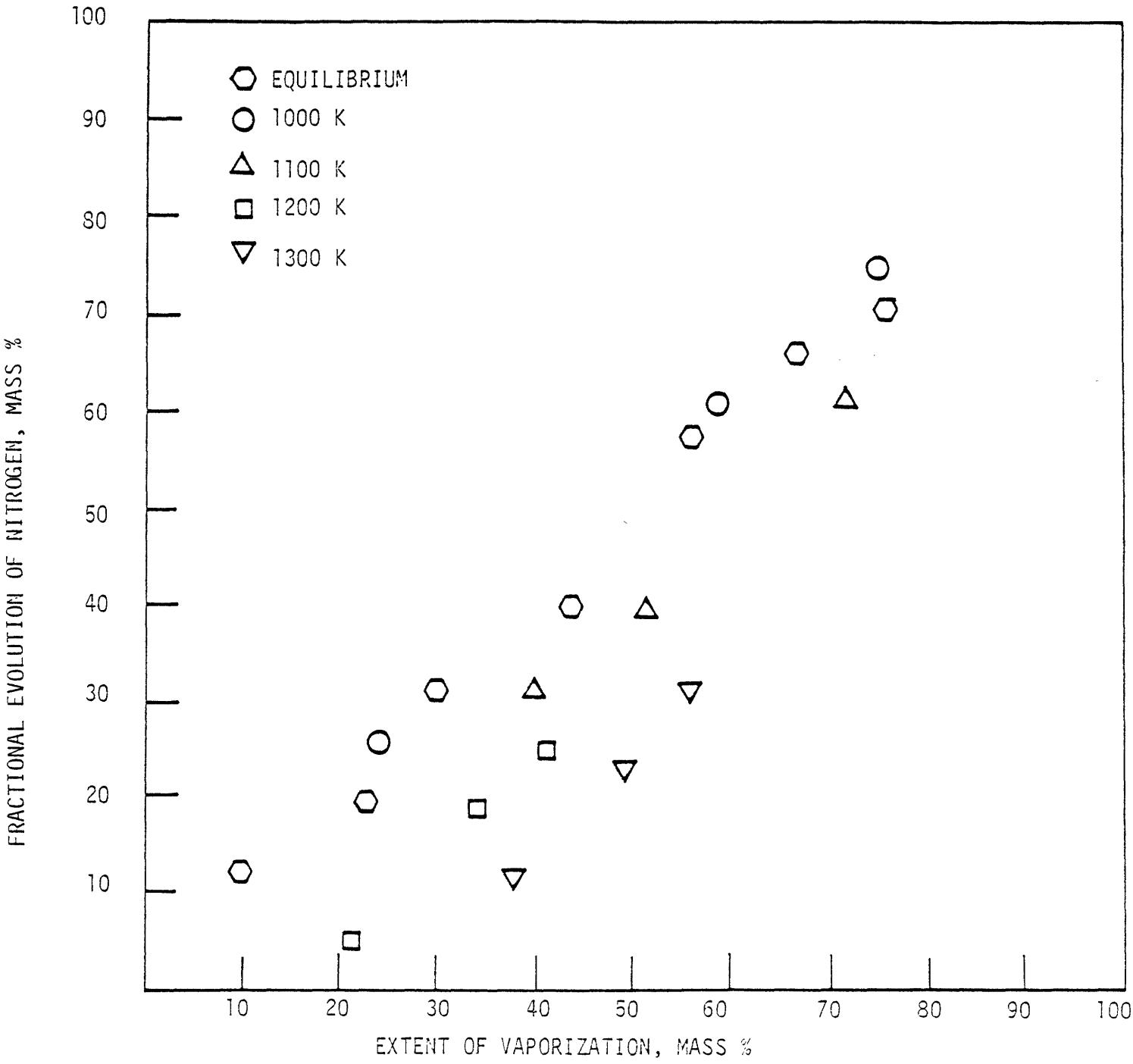

Figure 7.22 Nitrogen Evolution from Pyrolysing 150 μm Droplet Arrays of Raw Paraho Shale Oil

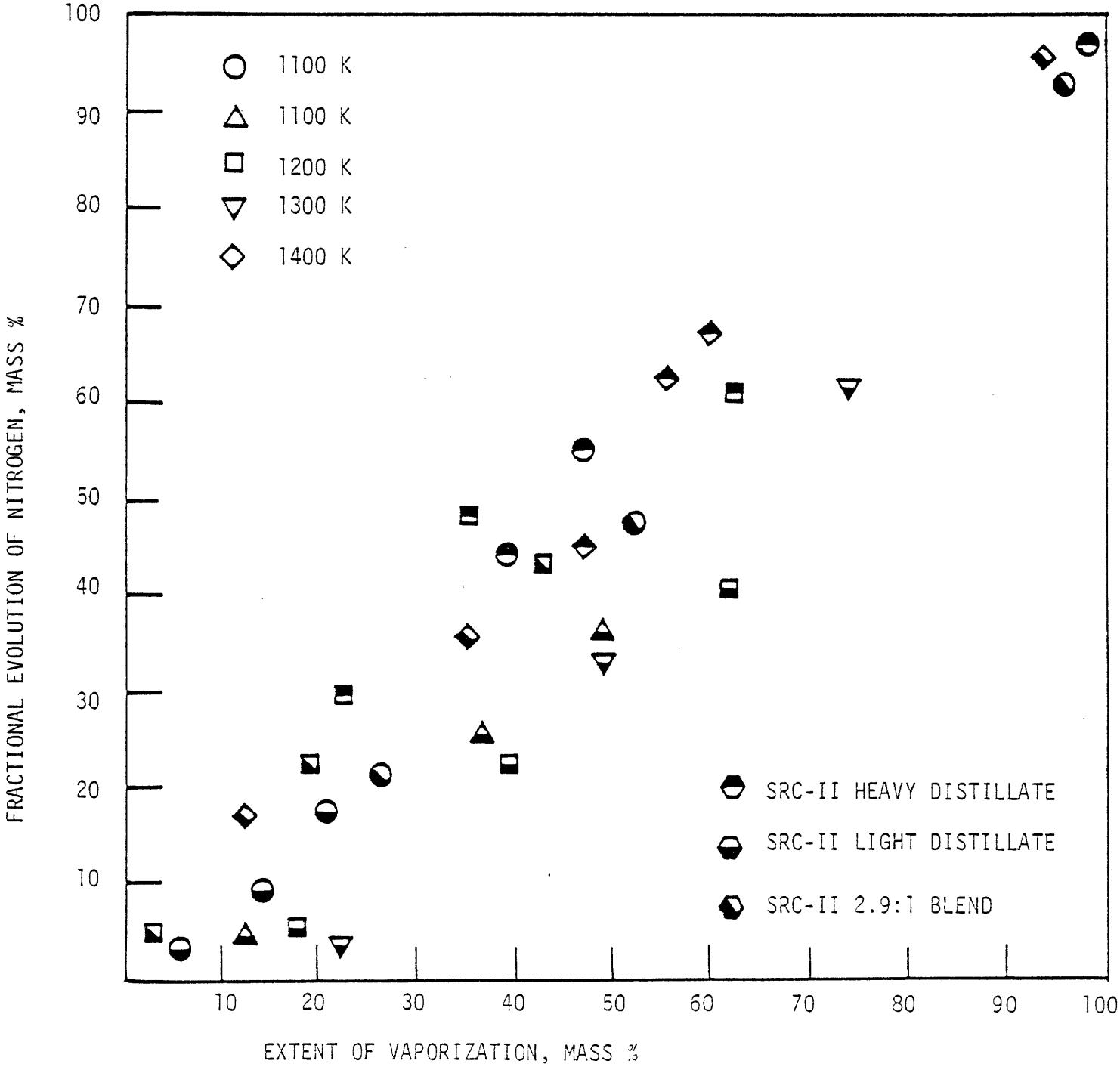

Figure 7.23 Nitrogen Evolution from Pyrolyzing 150 μm Droplet Arrays of SRC-II Middle Distillate Fraction SRC-II Heavy Distillate Fraction, and SRC-II 2.9:1 Blend Middle and Heavy Distillate Fractions

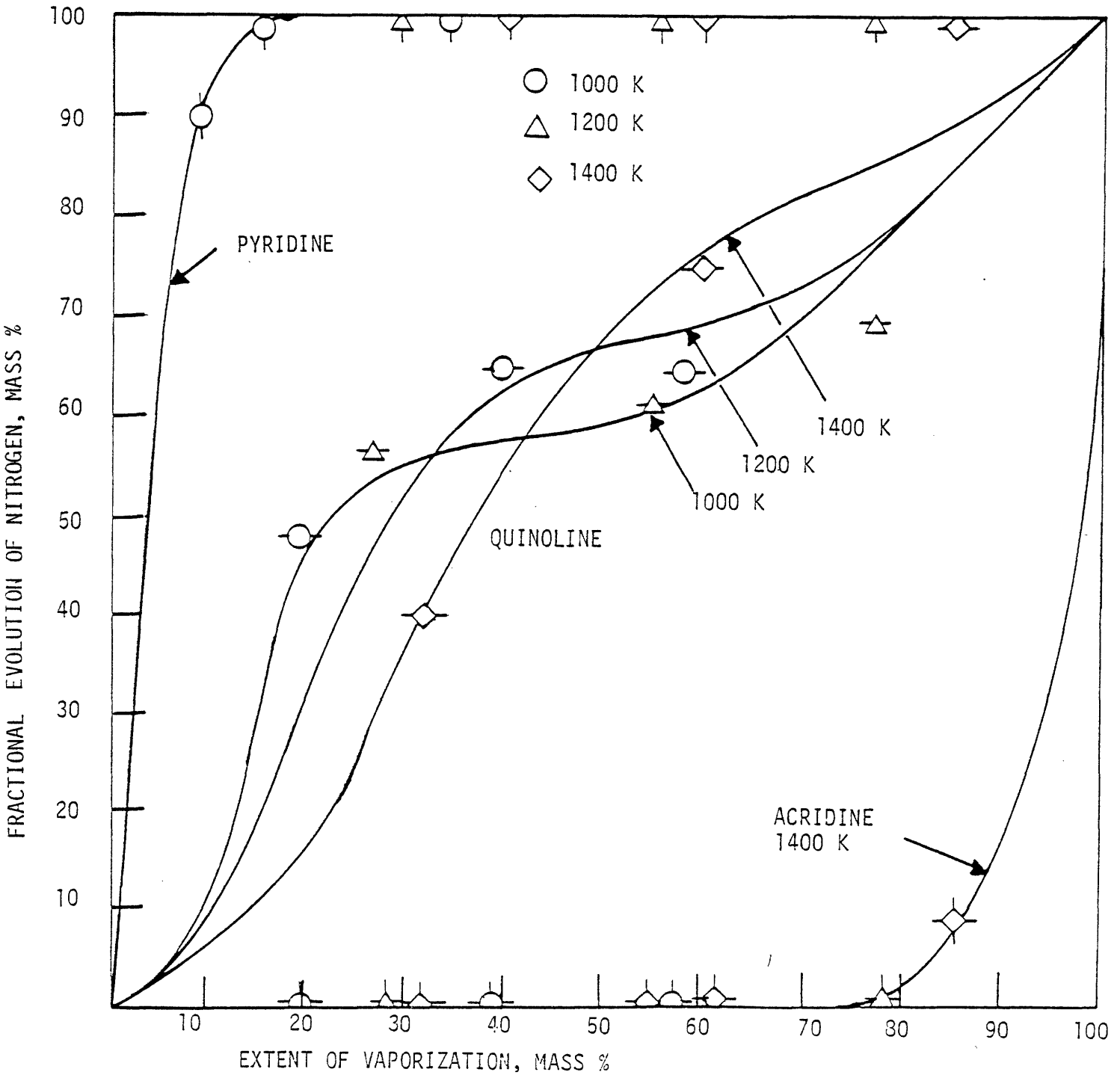

Figure 7.24 Nitrogen Evolution from Pyrolysing 150 μm Droplet Arrays of n- Dodecane Dopes with Pyridine, Quinoline or Acridine (Data Points are Experimental, Solid Lines are Calculations from Theory)

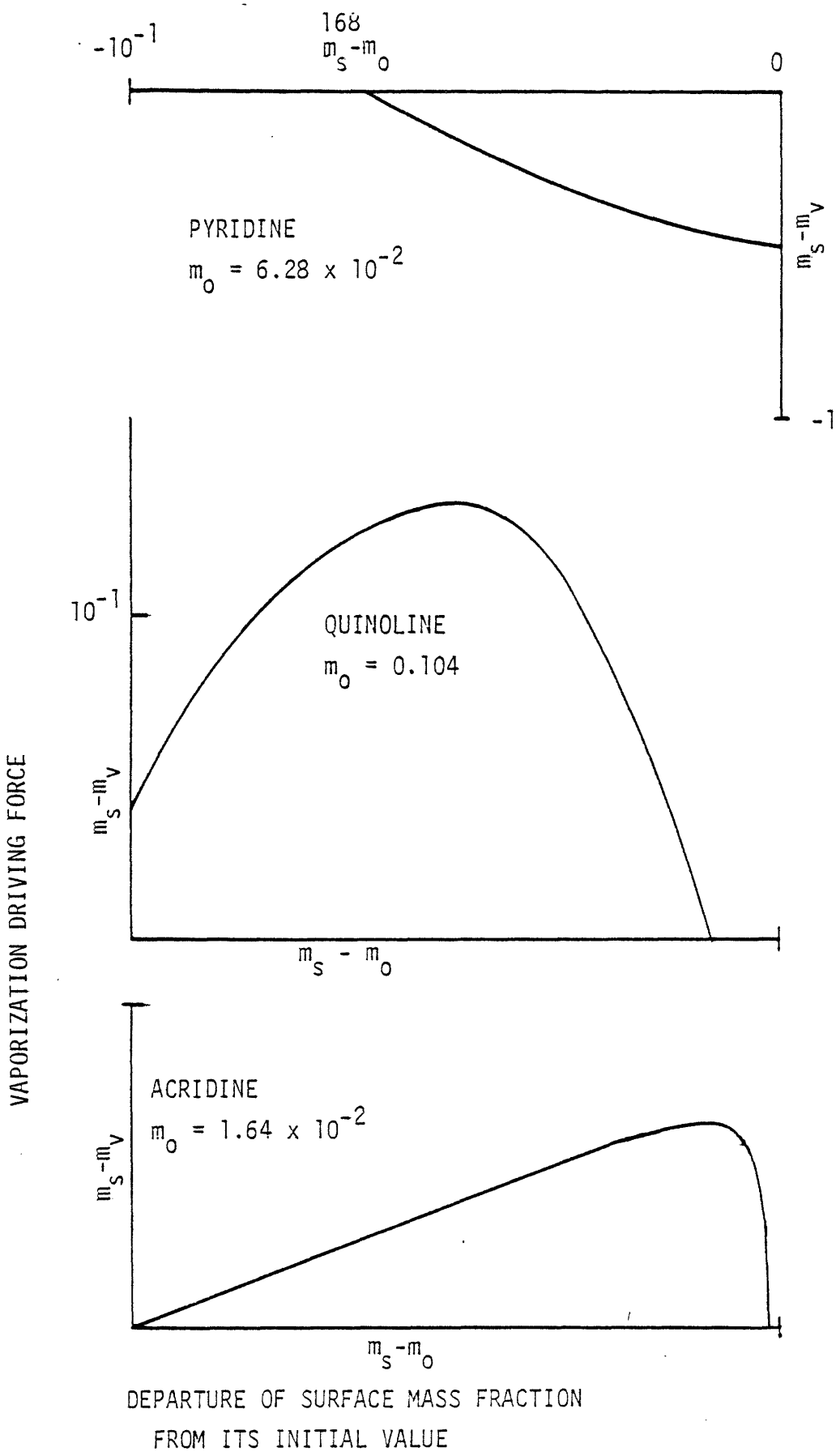

Figure 7.25 Vaporization Driving Force as a Function of Surface Mass Fraction for n-Dodecane Doped with Pyridine, Quinoline or Acridine

CHAPTER 8

DISCUSSION

When considering the evolution of fuel nitrogen during the vaporization of heavy fuel oils it must be remembered that the nitrogen is associated with many fuel components all of which are contributing to the total nitrogen evolution to some extent. The molecular weight of the compound in which the nitrogen is found influences the ability of the nitrogen to escape in several ways: the higher the molecular weight, the less volatile is the compound relative to the other fuel components at the surface and the less mobile is the compound relative to the other fuel components within the droplet; also, for a given nitrogen content, the mass of the fuel with which the nitrogen is associated increases.

8.1 Nitrogen Evolution: Batch Distillation versus Droplet Vaporization

The equilibrium batch distillation of a fuel reveals the nitrogen evolution under well mixed conditions. Data of this sort is often used as an indication of the nitrogen evolution from atomized fuels, however, it is better used as the vaporization rate limited case of droplet vaporization, i.e. internal mixing is rapid compared to the rate of droplet vaporization. The evolution of nitrogen from a rapidly vaporizing droplet does not match equilibrium nitrogen evolution after the initial few percent extent of mass evolution. This is because internal mixing is not rapid for droplets having diameters of the order of 100 micrometers, undergoing vaporization at rates typical of practical combustion systems. The differentiation of fuel species, over that affected by volatility differences, represented by the equilibrium distillation data, is due to diffusional resistance in the liquid phase, and droplet surface regression.

8.2 Heat and Mass Transport Phenomena Important to Vaporizing Droplets

Droplets of the size considered are spherical because of the overriding effect of surface tension and the reduced effect of impact deformation due to the strong momentum efflux at the surface caused by the droplet vaporization. Circulation inside the droplet is of secondary importance due to the small size of the droplets, the high viscosity of heavy fuel oils, and the reduced drag at the droplet surface due to boundary layer thickening by the mass evolved from the droplet. There is also the possibility that droplets rotate on an axis not parallel to the velocity vector, which would inhibit the formation of stable internal circulation. However, in the event that a circulation similar to a Hill's vortex is established, the effects of diffusional resistance and surface regression would still be significant but with a reduced length scale of between 1 and 1/3 radius. Temperature gradiants within the droplet are small, but concentration gradients cannot be neglected (Le > 20). The droplet temperature is not constant with time but follows the surface temperature, the center temperature lagging by an amount that varies with the surface temperature which is affected by the changing surface composition. For a 100 micrometer kerosine fuel droplet, the temperature lag was found to be about 2 celsius degrees[139], but for heavy fuel oils the lag would be greater, and subject to abrupt changes in surface temperature. Nevertheless, once vaporization has begun the heat capacity of the droplet is small compared to the latent heat content of the vaporized material. Thus the rate of vaporization is controlled by gas phase energy transport processes, whereas the evolution of a particular fuel component is determined by liquid phase mass trasport processes modified by surface regression and component volatility at the droplet surface. The resultant fuel-nitrogen evolution is the summation of the evolution of nitrogenous components, and is therefore highly dependent upon

the nitrogen distribution amoung the fuel components.

8.3 Nitrogen Evolution from Heavy Fuel Oils

The Gulf Coast No. 6 petroleum and Indo-Malaysian No. 6 petroleum fuel oils have most of their nitrogen associated with heavy fuel components and during equilibrium batch distillation retain much of this nitrogen in a non-distillable residue. The carbon to hydrogen ratio gradually increases due to the progressive loss of the lighter fuel components. The nitrogen evolution from the vaporizing droplet array is greatly in excess of the equilibrium data. The Gulf Coast fuel oil uniformly evolves its nitrogen with mass, and the Indo-Malaysian fuel oil, after an initial evolution of nitrogen free mass, behaves similarly. The carbon to hydrogen ratio of the fuel droplets do not vary significantly except for an initial rapid increase for the Indo-Malaysian fuel oil, which corresponds to the evolution of nitrogen free material. Apparently, after an initial period of conditioning, during which light fractions are vaporized, a surface composition is established having a higher temperature and higher concentration of heavy molecular weight compounds than the average composition would dictate. The higher relative volatility of the heavy species at the surface allows the nitrogenous compounds to be evolved together with the other fuel components, thus preventing the formation of a non-distillable nitrogen rich concentrate.

The raw Paraho shale oil presents a case in which the nitrogen species are distributed amoung the intermediate and heavy molecular weight fuel species. The broad distribution of nitrogen results in the uniform nitrogen evolution with mass during equilibrium batch distillation. The presence of a light nitrogen free fraction is not evident from batch distillation results. This is as a consequence of simultaneous evolution of a portion

of the intermediate molecular weight nitrogenous compounds, caused by the similarity of, or strong interaction between the fuel species as evidenced by the invariant carbon to hydrogen ratio. The nitrogen evolution from a vaporizing droplet at 1000 K is almost identical to the equilibrium evolution presumably due to the fuel species similarity or strong interactions. However, with increasing furnace temperature, the effects of diffusional resistance become evident, and light nitrogen free material is initially evolved until a surface composition is attained that permits the nitrogenous compounds to be envolved. The evolution of each nitrogenous compound is diffusionally limited to a different extent, thus although the nitrogen is evolved in proportion to the mass, the contributions of the nitrogenous compounds in the vapor differ from batch distillation composition and also differ with vaporization rate as reflected in the temperature dependent variation of carbon to hydrogen ratios for the droplet residues.

The SRC-II middle distillate behaves in a manner similar to the raw Paraho shale oil. The nitrogen distribution is primarily in the mid-molecular weights of this fuel, and the fuel species exhibit strong interactions. These characteristics are comparable to those described for the shale oil, which like SRC-II may be considered a synthetically manufactured fuel. The SRC-II heavy distillate contains its nitrogen in the heavier molecular weight fuel species. The interactions between fuel species are strong as manifested in the uniform equilibrium nitrogen evolution, however, the improved evolution of the heavy nitrogenous compounds, as observed for the petroleum fuel oils, is observed for vaporizing droplets, but less markedly due to the strong species interactions. The SRC-II 2.9:1 blend behaves more like the middle distillate for equilibrium distillation and more like the heavy distillate for the fur-

nace pyrolysis, the resultant effects being a composite of the two distillates and intermediate between them.

A droplet of fuel oil introduced to a hot oxygen defieient environment heats up until its surface attains the initial boiling point of the fuel; internally to a lesser or greater extent depending upon the droplet size, a thermal gradient is established. At the droplet surface, the more volatile compounds are preferentially evolved. In the gas phase, the radial convective flux thickens the boundary layer surrounding the droplet, moderating heat and mass transfer rates and reducing the drag experienced by the droplet. With continued vaporization, the temperature profile in the boundary layer adjusts to provide the enthalpy required for vaporization at the droplet surface. A transient persists throughout the vaporization of a multicomponent fuel since the surface temperature is always rising with changing surface composition. In the liquid phase, the loss of light species from the surface establishes a concentration profile for each component. The lighter compounds, being deficient at the surface, diffuse from the center of the droplet, and the heavier compounds, being concentrated at the surface diffuse to the center of the droplet. The combined effects of vaporization and diffusion determine the surface composition, and thereby, the surface temperature. This combination of temperature and composition determines the relative volatilities of the species present at the surface, and hence the vapor phase composition.

In light of the preceeding arguments, the behaviors of the heavy fuel oils studied may be explained. However, the data present only a summation of nitrogen evolution contributed by many components some of which may behave as a light and heavy component during the course of vaporization.

Identification of the controlling transport phenomena is hindered by the lack of adequate information on fuel composition and component properties in complex mixtures. Thus, in order to extract the fundemental nature of the processes involved it is necessary to resort to the simplified systems that may be mathematically described which are discussed in the remainder of this chapter.

8.4 Nitrogen Evolution from Two Component Model Fuels

Pyridine is a highly volatile and mobile compound relative to n-dodecane. When droplets of the pyridine doped model fuel are rapidly vaporized the pyridine is preferentially expelled from the droplet surface causing the surface temperature to approach the boiling point of n-dodecane. According to the boundary condition

$$\left.\frac{\partial m}{\partial r}\right|_{r=R} = \frac{\dot{m}''}{D}(m_s - m_V) \qquad 8.1$$

the more rapid the rate of vaporization
the greater will be the concentration gradient of pyridine in the liquid at the droplet surface, enhancing the transport of pyridine from the droplet core. The limit of this behavior occurs when the evolution of pyridine proceeds to completion with no loss of n-dodecane.

If diffusion is not able to transport enough low molecular weight material to satisfy the droplet vaporization requirement, the surface composition will shift towards the heavier molecular weight component, increasing its relative volatility. This is seen to happen for the acridine doped fuel. The high molecular weight of acridine results in a smaller diffusivity and lower volatility, so that the acridine is unable to dissipate itself by diffusion nor is it able to vaporize readily. Thus the surface concentration increases until the relative volatility, en-

hanced by the higher concentration and temperature at the surface, is such that the acridine participates in the vaporization process. This takes place at an extent of vaporization less than that found for equilibrium distillation. For the fuel in question the extent of vaporization at which this occurs is large since the initial acridine concentration is low and much n-dodecane must be lost before any significant surface gradients may be established, and even then only at the highest rate of vaporization (furnace temperature, 1400 K) is any departure from equilibrium evolution observed.

Quinoline and n-dodecane have comparable vapor pressure curves, thus the effects of diffusional resistance and rate of vaporization become more important. The quinoline doped fuel droplets exhibited a transitional behavior due to the competition between surface regressions, diffusional resistance, and the relative volatility. The discussion for pyridine bound the fractional evolution between the maximum evolution constraint and the equilibrium constraint. This is valid when the surface concentration remains low or constant throughout the vaporization, but if an intermediate build-up of surface concentration takes place, then a new equilibrium curve must be considered, and if any loss of the compound has taken place a new maximum evolution constraint must be designated. The competition between the several effects requires a more complete analysis to separate the contributions of each. This is provided by the theoretical development of section 6.3.

8.5 The Mathematical Model of Species Differentiation in Vaporizing Droplets

The Comparison between theoretical and experimental results is made through the equation

$$Y = 1 - (1-X)\left(1 + \frac{m_f - m_o}{m_o} \sum_{\text{all } a} B_a F_a H_a(\tau)\right) \qquad 8.2$$

in which B_a and F_a are functions of the ratio (λ/D) alone. That means that these terms are independent of volatility effects. The time dependent functions are X and $H_a(\tau)$. The extent of vaporization, X, is governed by gas phase energy transport and for the model fuels may be extracted from the "d^2-law", thus

$$X = 1 - (1+K\tau)^{3/2} \qquad 8.3$$

The effects of volatility are contained in $H_a(\tau)$

$$H_a(\tau) = (1+K\tau)^a - 1 + \sum_{r=1}^{\infty} (-1)^r \left(\frac{K}{b}\right)^r \left\{\prod_{q=0}^{r-1} (a-q)\right\} \left((1+K\tau)^{a-r} - 1 + G(\tau)\right) \qquad 8.4$$

where

$$G(\tau) = \frac{m_s - m_o}{m_f - m_o} = 1 - e^{-b\tau} \qquad 8.5$$

The value of 'b' determines how rapidly surface concentration of the component in question approaches its terminal value. For simple binary systems of the sort that are being considered here, this terminal value would be zero, unity or a stable azeotropic value. If 'b' is large, the summation term of Eq. 8.4 becomes negligible leaving only a diffusion term, $\{(1+K\tau)^a - 1\}$, in which the values of 'a' are directly derived from the ratio (λ/D). The competition between volatility and mass transport in the particle is contained in the repetitive combination in the summation term of Eq. 8.4, $\{(1+K)^a - 1 + G(\tau)\}$. Values of 'a' are always negative so that this term is zero at both as $\tau \to \infty$ and $\tau = 0$. A dominant $G(\tau)$

controls the droplet vaporization through volatility effect. When the term $\{(1+K\tau)^a - 1\}$ is dominant i.e. $\{(1+K\tau)^a - 1 + G(\tau)\} < 0$, the vaporization is mass transfer limited in the liquid phase. There is always a shift from the regime of control by volatility to control by diffusional effects, the extent at which this occurs being dependent upon the ratio (λ/D), and 'b'.

The time constant 'b' incorporates the volatility properties and is indirectly coupled to the diffusion effects and the rate of vaporization through the boundary condition Eq. 8.1. Since for a given liquid phase surface composition a unique equilibrium vapor phase composition exists, a vaporization driving force (m_s-m_v), may be generated as a function of (m_s-m_o). m_s varies monatonically from m_o to m_f, and this temporal variation is described by Eq. 8.5. Thus 'b' is a scaling parameter for the surface concentration variation to be compared against K, Eq. 8.3, the droplet lifetime scaling parameter.

8.6 Interpretation of Model Fuel Data by the Mathematical Model

The pyridine vaporization driving force continuously declines throughout the droplet vaporization. The quinoline and acridine doped fuels have a maximum in their vaporization driving force. Differences between the quinoline and acridine evolution are because quinoline passes through this maximum (m_s-m_v) at intermediate extents of vaporization, whereas the acridine does not achieve its maximum (m_s-m_v) until large extents of vaporization. The non-dimensional time scales for quinoline and acridine are approximately the same $(b\simeq\frac{1}{2})$, however it must be recognized that the non-dimensional time, τ, is more compressed for acridine. The value of 'b' for pyridine is approximately 61. Thus surface concen-

trations for quinoline and acridine vary gradually from m_o to unity over the lifetime of the droplet, whereas the pyridine surface concentration rapidly declines from m_o to zero.

8.7 A General Discussion of Interactions in Diffusionally Limited Vaporization of Two Component Fuels

For binary mixtures the evolution curve for each component during droplet vaporization is initially tangent to its equilibrium curve and terminates with a slope of unity. The more volatile component will evolve more rapidly, the less volatile component being retarded in its evolution. The loss of volatile vomponent from the surface creates concentration gradients in the droplet (negative gradients for the less volatile component and positive gradients for the more volatile component). The surface regression, caused by the loss of the more volatile component, accentuates the concentration gradients by convecting the less volatile component retained in the liquid surface towards the droplet's center. If diffusion is rapid, concentration gradients are small and the center and surface concentrations are nearly equal, thus the distillation will follow that of a well mixed system.

If concentration gradients are significant, the evolution of the components are primarily controlled by vaporization driving force. The relative volatility, as measured by the vaporization driving force, is strongly influenced by the initial concentration of the mixture as well as the vapor pressure driving force of the individual components. Thus, for a binary mixture there is a minor component and a major component, either of which may be more volatile. A volatile minor component will have very low surface concentrations. If the volatility is so great that diffusion is unable to overcome the concentration gradients, but yet is

rapid, the volatile component may still be transported from the interior of the droplet rapidly enough to satisfy the vaporization requirement; especially since the vaporization driving force favors the volatile component, even though its concentration is low, because the surface temperature is nearly that of the boiling point of the less volatile component. A volatile major component will dominate the vapor phase composition until the less volatile minor component has attained an adequate surface concentration by loss of the more volatile component and diffusional limitations. When the vapor pressures of the components are equal no separation may be effected. However, if a small vapor pressure difference exists between components, a separation by vaporization is improved by the liquid phase diffusional resistance. In all cases the more volatile component is favored initially. However, as vaporization progresses the less volatile component will have an accelerated evolution. The transition from one regime to the other is dependent upon the competition between the effects of volatility and diffusion.

The behavior described for the binary fuels is valid with a few minor inclusions to heavy fuel oils. During the course of vaporization of a heavy fuel oil droplet, light components are lost, and thus intermediate molecular weight components, which to the lost volatiles appeared to be heavy components, now behaves with respect to the heavy materials in the same way as the lost light components. The prediction of species evolution under these circumstances for which values of 'a' and 'b' are constantly changing, is a formidable task even when total knowledge of fuel composition and component properties is available.

CHAPTER 9

CONCLUSIONS

The evolution of fuel-nitrogen from vaporizing droplets of heavy fuel oils departs significantly from the equilibrium batch distillation nitrogen evolution. The differences observed in the nitrogen evolution of vaporizing droplets as opposed to equilibrium batch distillation are attributable to diffusion limitation in the liquid phase.

The extent to which diffusion limitation plays a role is influenced by the rate of vaporization and the volatility of each nitrogen containing compound with respect to all other fuel components. During the initial stages of vaporization the lower molecular weight compounds have enhanced evolutions, but after some extent of vaporization, determined by the fuel properties and environmental conditions, the heavier molecular weight compounds are evolved at accelerated rates.

A Gulf Coast No. 6 petroleum fuel oil, and Indo-Malaysian No. 6 petroleum fuel oil, and a SRC-II heavy distillate fraction fuel oil, all of which have most of their nitrogen content bound to the higher molecular weight fuel components, display rates of nitrogen evolution that were greater than equilibirum distillation results would suggest. The carbon to hydrogen ratio of the fuel residues, which was found to increase during the course of equilibrium distillation, remains uniform with increasing extent of droplet vaporization, thereby inhibiting the formation of a nitrogen rich non-distillable residue which would form a char.

Raw Paraho shale oil and SRC-II middle distillate fraction fuel oil, which have their nitrogen associated primarily with the intermediate molecular weight fuel species, exhibited an initial nitrogen free weight loss associated with the vaporization of a light fraction. This initial loss of light fraction increased with increasing rate of vaporization. When nitrogen evolution

from these fuels commences, it is in proportion to the weight loss, paralleling equilibrium nitrogen evolutions but originating at a higher extent of vaporization due to the initial nitrogen free weight loss.

The retardation in nitrogen evolution from the shale oil and SRC-II middle distillate is not so great that detrimental effects preclude staged combustion as a method to control fuel-nitrogen conversion to nitric oxide. On the other hand, the Gulf Coast No. 6 and Indo-Malaysian No. 6 petroleum fuel oils behave, both with respect to nitrogen evolution and the tendency to char formation, such that staged combustion appears to be an appropriate method to handle them.

A mathematical model, describing the "d^2-law" vaporization of droplets of binary mixtures, showed that the scaled concentration profile of a component within the droplet to be dependent upon the ratio of the vaporization rate constant and the liquid phase diffusivity. The rate of evolution is determined by the modification of surface concentration by diffusion and the volatility of the component at the surface. The change in surface composition resulting from this interaction is found to be exponential in the non-dimensional time and is totally described by a single time constant.

The application of the mathematical model to real fuels requires a knowledge of the complexities of fuel compositions and their solvent interactions, but when this information becomes available, it is quite possible to apply the mathematical model to them after some modification. Nevertheless, generalities of fuel behavior are already clarified and guidelines thereby obtained should be considered for combustor design particularly when alternate fuels are involved.

APPENDIX A

FUEL PROPPETIES AND EQUILIBRIUM BATCH DISTILLATION RESULTS FOR RAW ALASKAN PETROLEUM FUEL OIL AND H-COAL LIQUIDS

	(i)	(ii)	(iii)	(iv)
Ultimate Analysis, %:				
Carbon	85.90	90.16	90.29	91.13
Hydrogen	11.46	9.36	8.07	8.59
Nitrogen	0.49	0.52	1.04	0.73
Sulfur	1.63	0.10	0.11	0.03
Oxygen	0.61	1.10	0.81	1.11
Ash	0.03	Trace	0.04	0.01
Water and Sediment		<0.05	12.0	3.0
Flash Point, °C	102	>93	>93	>93
Pour Point, °C	3	-20	7	-18
Gross Heat of Combustion, MJ/kg	43.26	39.93	41.67	40.74
Specific Gravity @ 15°C	0.9619	1.0007	1.0575	1.0568

Table A.1

Fuel Properties of (i) Raw Alaskan Petroleum, (ii) H-Coal Low Cut, (iii) H-Coal High Cut, and (iv) H-Coal Full Range

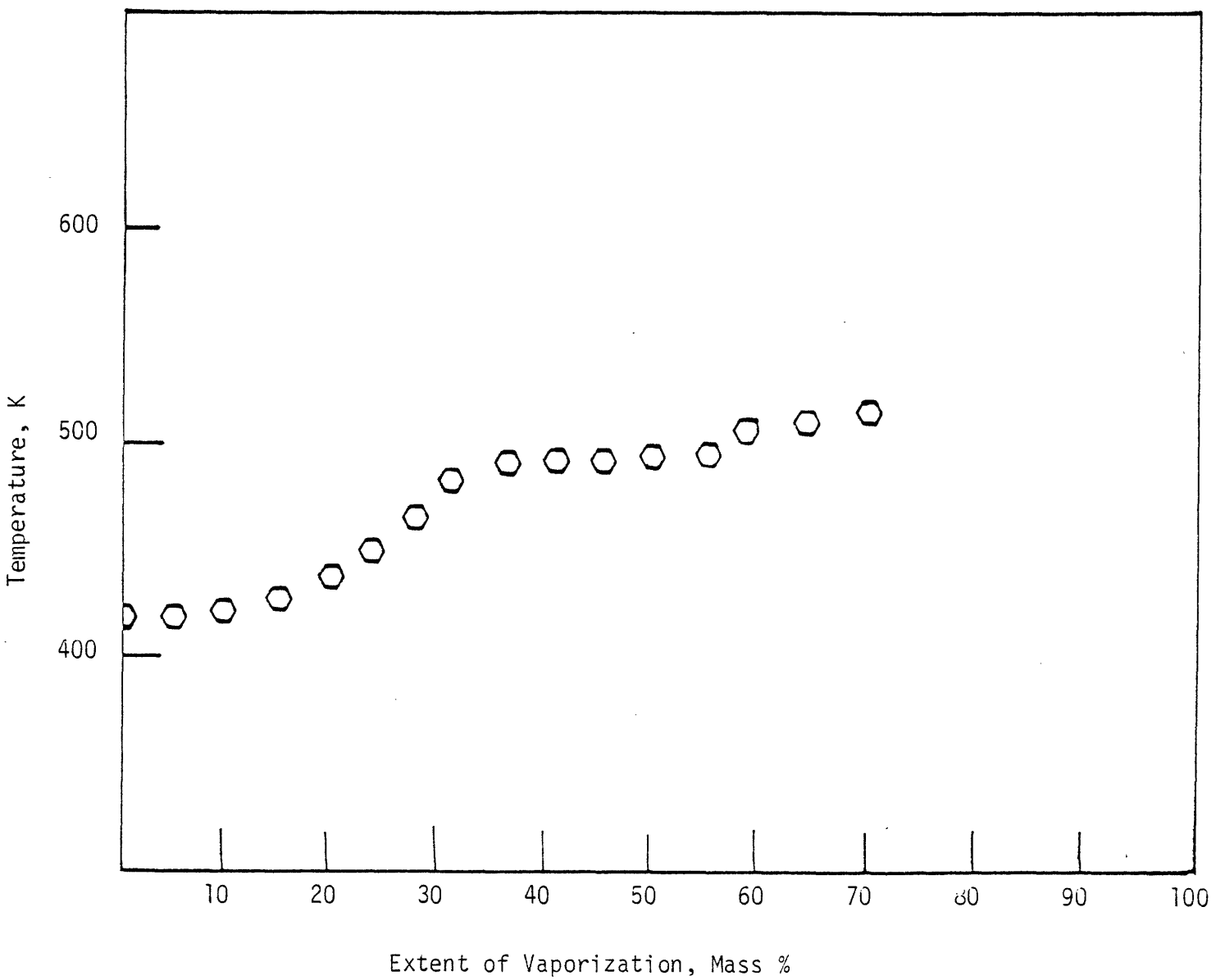

A.1 Engler-Type Boiling Point Curve of Raw Alaskan Petroleum .....

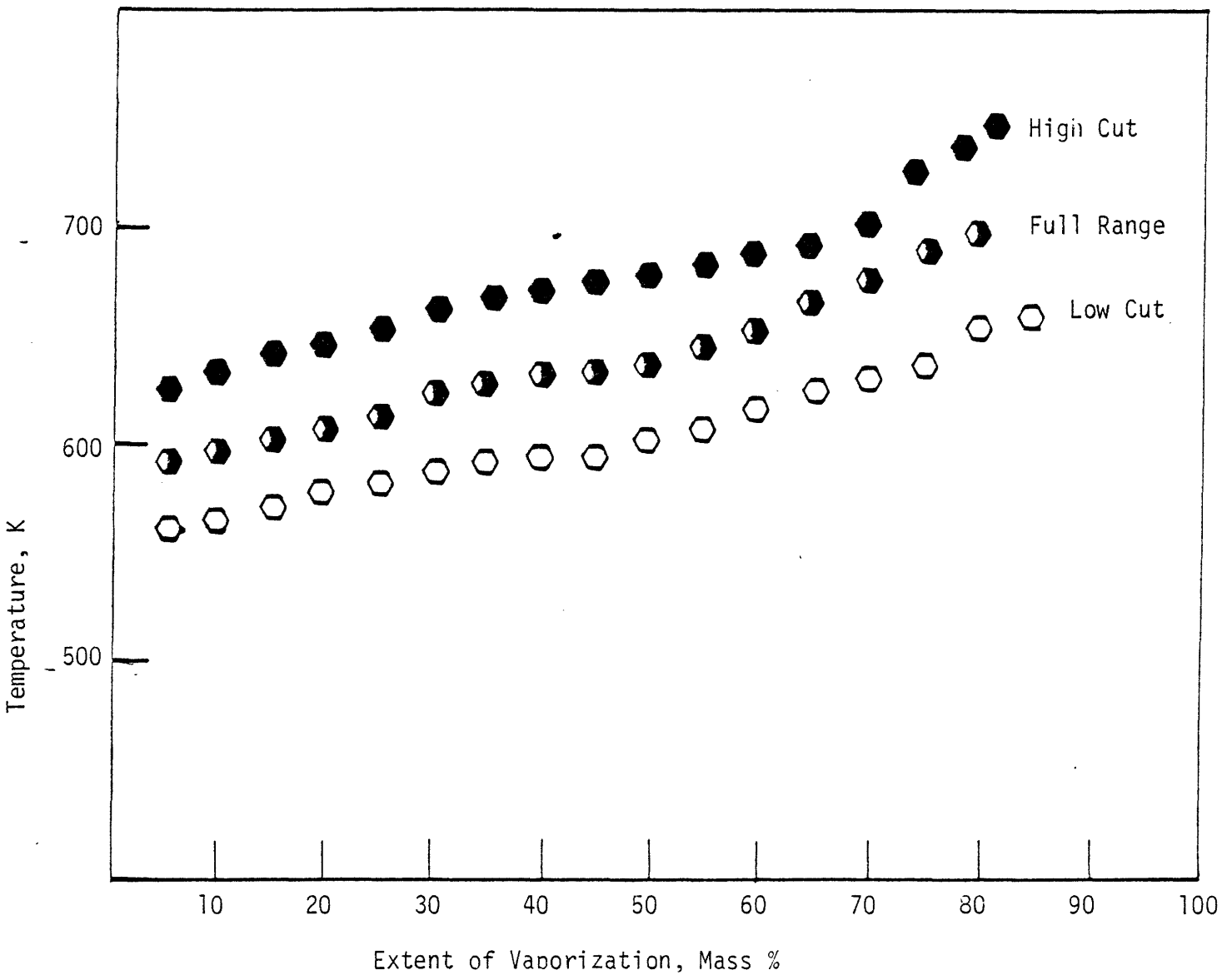

A.2 Engler-Type Boiling Point Curves of H-Coal Low Cut, H-Coal High Cut, H-Coal Full Range

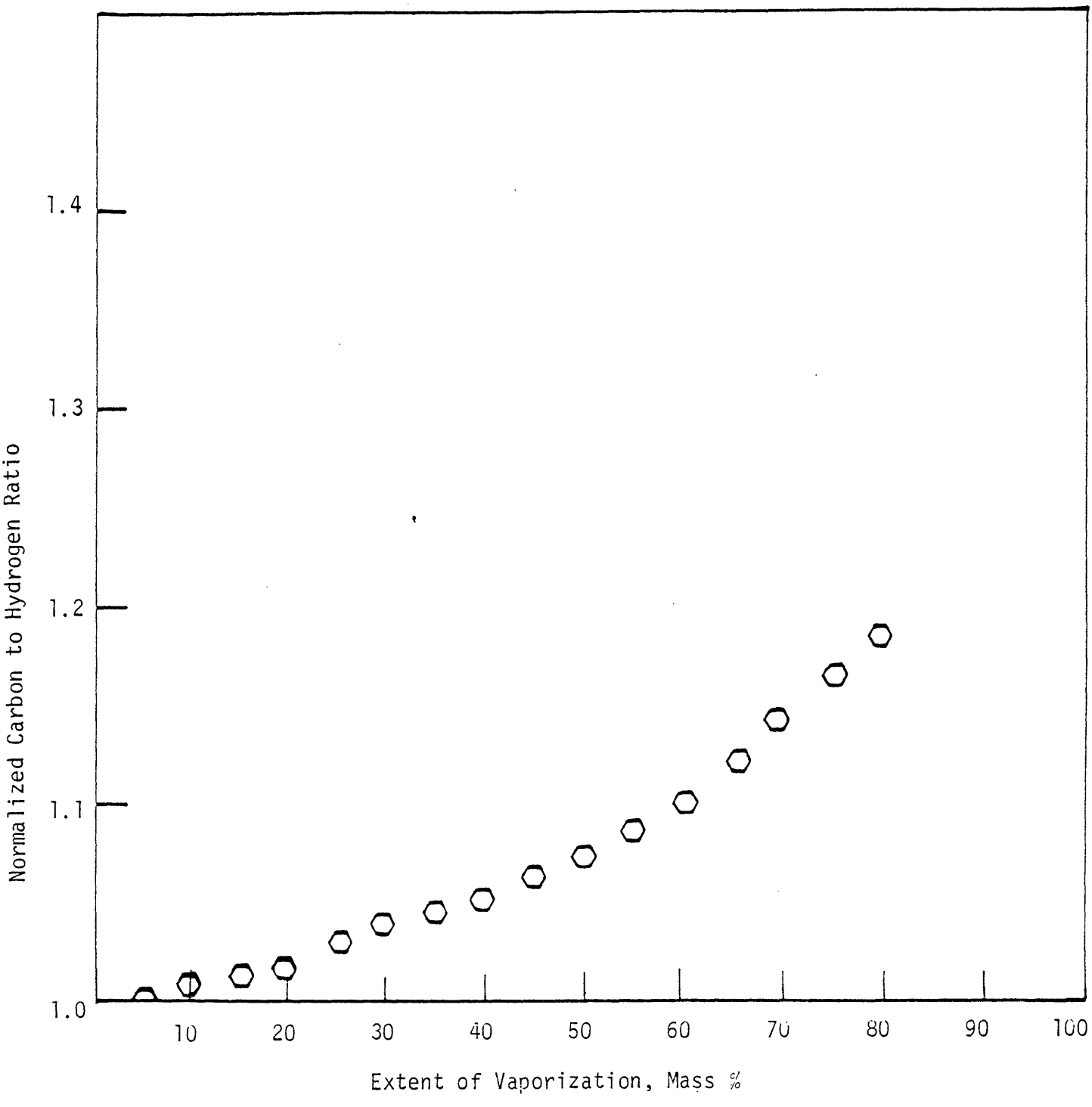

A.3 Normalized Carbon to Hydrogen Atomic Ratios of Fuel Residues During Equilibrium Batch Distillation of Raw Alaskan Petroleum

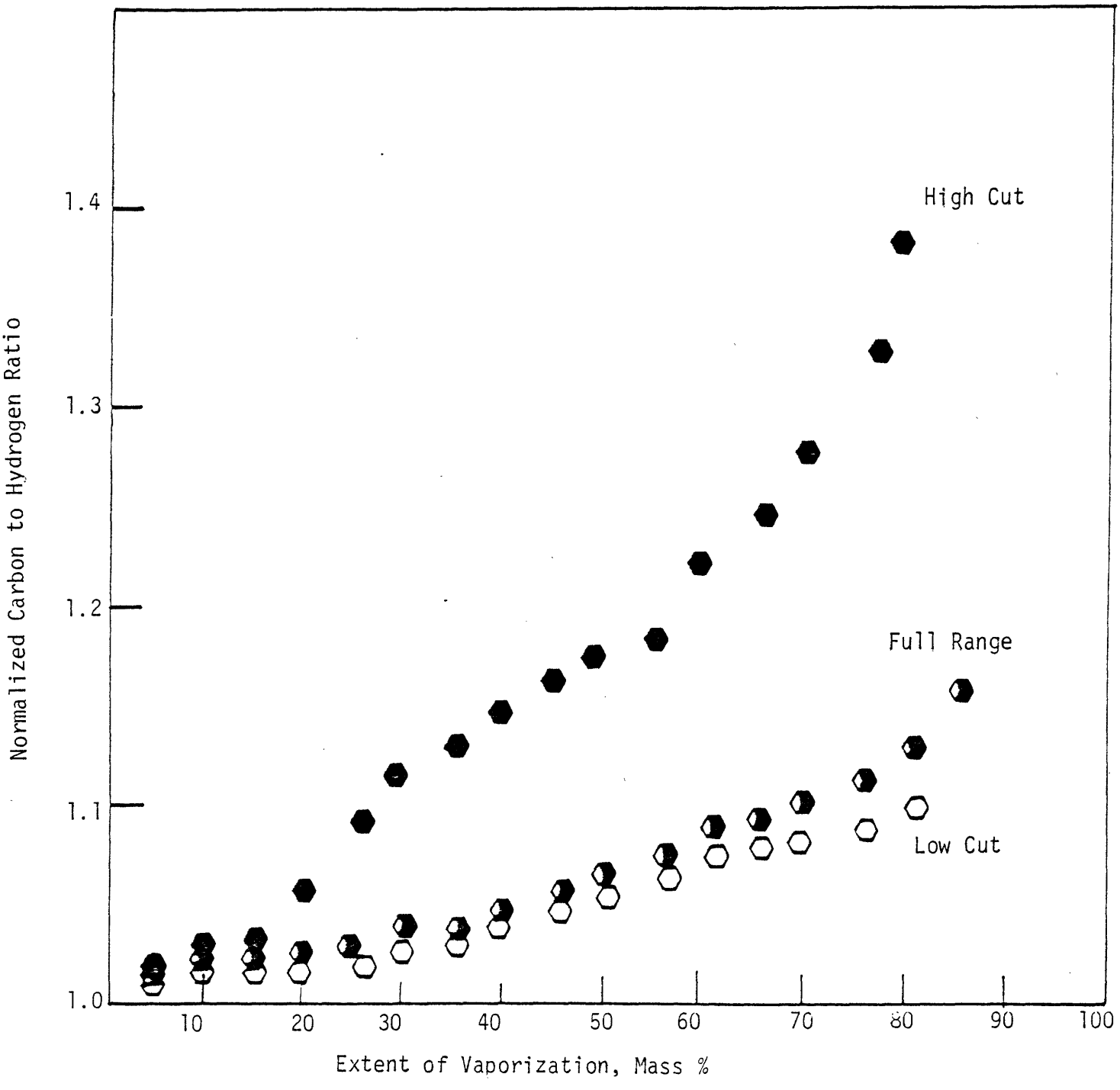

A.4 Normalized Carbon to Hydrogen Atomic Ratios of Fuel Residues During Equilibrium Batch Distillation of H-Coal Low Cut, H-Coal High Cut, and H-Coal Full Range

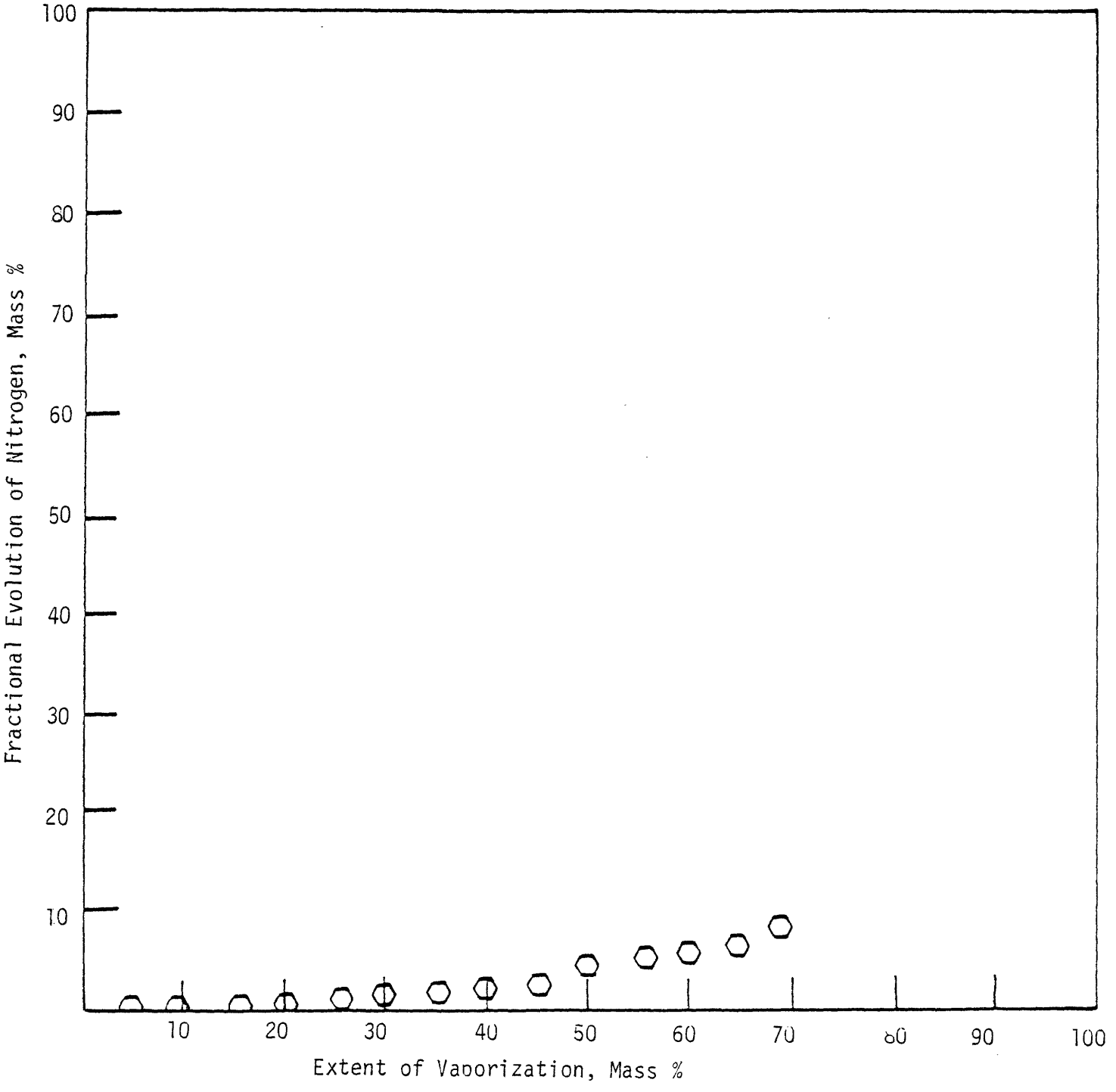

A.5 Nitrogen Evolution During Equilibrium Batch Distillation of Raw Alaskan Petroleum

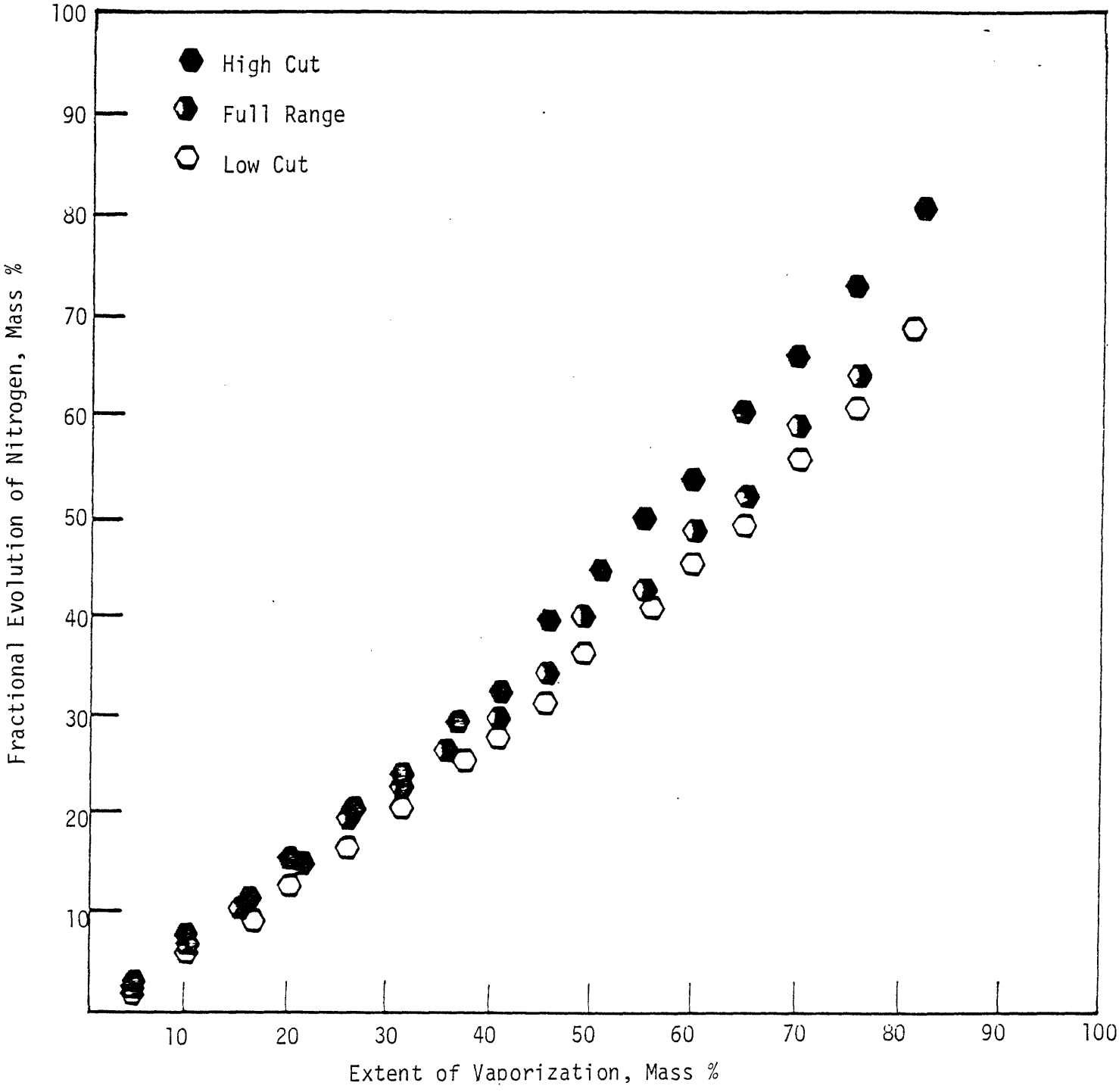

A.6 Nitrogen Evolution During Equilibrium Batch Distillation of H-Coal Low Cut, H-Coal High Cut, and H-Coal Full Range

APPENDIX B

CALCULATION OF THE MASS RATE OF VAPORIZATION FOR LINEAR DROPLET OF n-DOEDECANE

Properties for liquid n-Dodecane at its normal boiling point of 489.5 K are as follows 140:

$$\rho_\ell = 598 \quad kg/m^3$$

$$Q = 257 \times 10^3 \ J/kg$$

The gas phase properties are evaluated at a reference temperature, T_r(viz. Eq. 6.23), for Helium

T_g,K	T_s,K	T_r,K	k,W/m·K	C_{PD} J/kg·K
1000	489.5	660	0.265	5192
1200	489.5	726	0.284	5192
1400	489.5	793	0.304	5192

Sample calculation of mass vaporization rate constant (viz. Eq. 6.20, note that $\rho\alpha = k/C_p$).

$$T_g = 1000 \ K$$

$$\lambda = \frac{8(0.265)}{(598)(5192)} \ln\left(1+ \frac{5192[1000-489.5]}{257 \times 10^3}\right) \ m^2/s$$

$$\lambda = 1.656 \times 10^{-6} \ m^2/s$$

To correct for interference from other droplets in an array one must generate an array vaporization efficiency, η_A, which compares the mass vaporization rate of a droplet in an array, $\dot{m}_A$, to that of an isolated droplet, $\dot{m}_I$. Thus if a "d^2-law" applies

$$\eta_A = \frac{\dot{m}_A}{\dot{m}_I} = \left(\frac{\lambda_A}{\lambda_I}\right)\left(\frac{d_A}{d_I}\right) \qquad B.1$$

For the initial period of vaporization the ratio of diameters is close to unity and the vaporization rate constants may be directly corrected using η_A. The value of η_A given by Eq. 3.9 is for a three dimensional array. To obtain a value of η_A for a linear array Eq. 3.9 is evaluated for a three particle array which is linear, and correction is made for the influence of other particles in an infinite array upon the end particles of the finite array. Correcting for first order effects only (that would be the correction for the center particle of a five particle droplet array which results from the overlapping of three arrays of three particles), the array vaporization is η_A , where η_A is the three particle array efficiency. Higher order corrections do not provide any advantage, since the interparticle spacing obtained from measurement is a strong function of η_A. Small errors in measuring interparticle spacing cause variations in the inifinite particle array efficiency that are comparable to the higher order corrections. For the binary fuel arrays, the ratio of interparticle spacing to particle diameter was about five. Thus, to calculate η_A, let

$$N = 3$$

$$S/d = 3.5$$

$$S/S_n = 1$$

then

$$\eta_A = \frac{2-(\frac{3}{2})(3.5)-(\frac{1}{2})(1)}{3[\frac{1}{3.5} - (\frac{1}{2})(3.5)-(\frac{1}{2})(1)]} = 0.63$$

thus $\eta_A^3 = 0.25$

and $\lambda_A = 0.25\ (1.65)\ mm^2/s = 0.41\ mm^2/s$ at $T_g = 1000$ K

APPENDIX C

TRANSFORMATION DIFFERENTIALS FOR THE EQUATIONS OF LIQUID PHASE DIFFUSION IN A SHRINKING SPHERE

The following equations transform Eqs. 6.24 - 6.32 into Eq. 6.33 - 6.36. The transformation from (r,t) to (z,τ) coordinates requires the total differentials

$$\left.\frac{\partial m}{\partial t}\right|_t = \left.\frac{\partial m}{\partial z}\right|_t \left.\frac{\partial z}{\partial t}\right|_t + \left.\frac{\partial m}{\partial \tau}\right|_z \left.\frac{\partial \tau}{\partial t}\right|_r \qquad \text{C.1}$$

$$\left.\frac{\partial m}{\partial r}\right|_t = \left.\frac{\partial m}{\partial z}\right|_t \left.\frac{\partial z}{\partial r}\right|_t + \left.\frac{\partial m}{\partial t}\right|_z \left.\frac{\partial \tau}{\partial t}\right|_t \qquad \text{C.2}$$

The various parts of Eqs. C.1 and C.2 are as follows:

$$\left.\frac{\partial z}{\partial t}\right|_r = \frac{DK}{R^2} Z \qquad \text{C.3}$$

$$\left.\frac{\partial z}{\partial r}\right|_t = \frac{(KZ)^{1/2}}{R} \qquad \text{C.4}$$

$$\left.\frac{\partial \tau}{\partial t}\right|_t = \frac{D}{R^2}(1+K\tau) \qquad \text{C.5}$$

$$\left.\frac{\partial \tau}{\partial t}\right|_t = 0 \qquad \text{C.6}$$

$$\left.\frac{\partial m}{\partial z}\right|_t = \frac{(m_s-m_o)}{z^{1/2}}\left(\left.\frac{\partial \omega}{\partial z}\right|_\tau - \frac{\omega}{2z}\right) \qquad \text{C.7}$$

$$\left.\frac{\partial m}{\partial \tau}\right|_z = \frac{(m_s-m_o)}{z^{1/2}} \left.\frac{\partial \omega}{\partial \tau}\right|_z \qquad \text{C.8}$$

Substituting Eqs. C.3 - C.8 into Eqs. C.1 and C.2 yields

$$\left.\frac{\partial m}{\partial t}\right|_r = \frac{(m_s-m_o)}{Z^{1/2}} \left(\frac{DK}{R^2}\right) \left(\frac{Z\partial\omega}{\partial Z}\right)_\tau - \frac{\omega}{2} + \frac{(1+K\tau)}{K} \left.\frac{\partial\omega}{\partial\tau}\right|_Z \qquad C.9$$

$$\left.\frac{\partial m}{\partial r}\right|_t = \frac{(m_s-m_o)}{Z^{1/2}} \frac{(KZ)^{1/2}}{R} \left(\left.\frac{\partial\omega}{\partial Z}\right|_\tau - \frac{\omega}{2Z}\right) \qquad C.10$$

By the proper manipulation of Eq. C.10 and substitution into Eq. C1 the second order derivative of Eq. 6.24 may be obtained. Thus,

$$\frac{D}{r^2}\frac{\partial}{\partial r}\left(r^2 \left.\frac{\partial m}{\partial r}\right)\right|_t = \frac{KD}{4R^2Z}\frac{\partial}{\partial Z}\left\{\frac{4R^2Z}{K}\frac{(m_s-m_o)}{Z^{1/2}}\frac{(KZ)^{1/2}}{R}\left(\left.\frac{\partial\omega}{\partial Z}\right|_\tau - \frac{\omega}{2Z}\right)\right\}\Bigg|_\tau \frac{(KZ)^{1/2}}{R} \qquad C.11$$

$$\frac{D}{r^2}\frac{\partial}{\partial r}\left(r^2 \left.\frac{\partial m}{\partial r}\right)\right|_t = \frac{(m_s-m_o)}{Z^{1/2}} \frac{DK}{R^2}\left(Z \left.\frac{\partial^2\omega}{\partial Z^2}\right|_\tau + \frac{1}{2}\left.\frac{\partial\omega}{\partial Z}\right|_\tau\right) \qquad C.12$$

The above equations are all that are necessary for the transformation to (Z, τ) coordinates.

APPENDIX D

CALCULATION OF THE FRACTIONAL EVOLUTION OF NITROGEN DURING THE VAPORIZATION OF BINARY FUELS

The properties required for the performance of this calculation are the vapor pressure - temperature dependence, the liquid-vapor thermodynamic equilibrium relationships, and the diffusivities in the mixture of each fuel component. Also, the mass rate of vaporization must be known to account for the effect of surface regression in the case of droplet vaporization.

The vapor pressure euqations for the components of the binary systems studied are given in Eqs. 7.4-7.7. The thermodynamics equilibria for the doped materials were assumed to obey Raoult's Law, Eq. 6.5, since these materials were in lower concentrations for most of the lifetime of the droplets. The diffusivities were estimated using the equation[26]

$$D_{12} = 7.4\ (10^{-8})\ (\ell MW_2)^{1/2}\ \frac{T}{\mu_2 V_1^{0.6}}\quad cm^2/s \qquad D.1$$

where for n-Decane, T $\sim$ 490 K

$$\mu_2 \sim 0.2\ cp$$
$$MW_2 \sim 170$$
$$\ell \sim 1$$

and V_1 is the molal volume for the dopant material, and is estimated uding the relationship

$$V_1 = 0.285\ V_c^{1.048}$$

where V_c is the critical volume. Thus,

Dopant	V_c, $cm^3/gmole$	V_l, $cm^3/gmole$	D_{12}, mm^2/s
Pyridine	254	94.43	1.544×10^{-2}
Quinoline	405	153.98	1.151×10^{-2}
Acridine	556	214.63	0.9432×10^{-2}

The diffusivities obtained are employed in the determination of characteristic values for the orthoganal series solution, Eq. 6.55 in the term K/4 which contains the ratio λ/D. The values of λ may be calculated as done in appendix A, or, as with the following calculations, the measured values, Eq. 7.8 - 7.10, may be used. The values of K/4 so obtained are

	1000 K	12000 K	1400 K
Pyridine	1.432	2.083	2.516
Quinoline	1.921	2.794	3.375
Acridine	2.344	3.409	4.119

With these values the characteristic values, 'a', Eq. 6.55, the series constants, B_a, Eq. 6.57, and the droplet average weighting term, F_a, Eq. 6.86, may be evaluated. For example, in the case of pyridine at 1000 K, the following values are calculated

term	a	B_a	F_a
1	-1.0734	-1.5581	-1.0409
2	-6.2572	+1.0785	+0.3594
3	-14.8749	-1.0171	-0.1710
4	-26.9370	+1.0221	+0.0992
⋮	⋮	⋮	⋮

The solution so far has not considered volatility effects at the surface of the droplet. These are incorporated by the trial and error selection

of a value of 'b' that satisfies both Eq. 6.77 at Z = K/4, and Eq. 6.78. Now (m_s-m_v) is a function of m_s alone. For a binary system at equilibrium

$$m_{s1} = \frac{1}{1 + \frac{MW_2}{MW_1}\left(\frac{1}{x_1} - 1\right)} \qquad D.2$$

$$m_{v1} = \frac{1}{1 + \frac{MW_2}{MW_1}\left(\frac{1}{y_1} - 1\right)} \qquad D.2$$

Employing the equilibrium distillation equations of section 6.1

$$m_{s1} - m_{v1} = \frac{1}{\left(\frac{1}{m_s}\right) + \left(\frac{1}{m_s}\right)^2 \frac{1}{\left(\frac{1}{m_s} + \frac{MW_2}{MW_1} - 1\right)\left(\frac{P_T}{p_1} - 1\right)}} \qquad D.3$$

For an equilibrium batch distillation m_{s1} of Eq. D.2 is the mass fraction throughout the liquid phase. The evaluation of (m_s-m_v) entails the same calculation as for batch distillation but it is valid only at the droplet surface. Now, Eq. 6.6 is a function of T alone, thus Eq. D.3 must be a function of T_s alone which in turn is a function of m_s. However m_s must obey the exponential decay in concentration of Eq. 6.76. Thus, the value of 'b' which when used in Eqs. 6.77 and 6.78 produces a correspondence between (m_s-m_o) and (m_s-m_v) for all τ, that equals that obtained from Eq. D.3, is the answer. For the example of pyridine 'b' was found to be 60.6. At last, $H_a(\tau)$ may be evaluated, and Eq. 6.89 solved. Continuing the pyridine example, $m_f = 0$, so that

$$Y = 1 - (1-X)\left(1 + \sum_{\text{all } a} B_a F_a H_a(\tau)\right) \qquad D.4$$

$$\tau = \frac{(1-X)^{2/3} - 1}{K} \qquad D.5$$

Let X = 0.1, then $\tau = 1.18 \times 10^{-2}$ solving for $H_a(\tau)$ when 'b' = 60.6 and $\tau = 1.18 \times 10^{-2}$

Term	$H_a(1.18 \times 10^{-2})$
1	-0.6783
2	+0.7052
3	-0.7103
4	+0.7122
⋮	⋮

Substituting G_a, F_a, and $H_a(\tau)$ into Eq. D.4

$$Y = 1 - (1-0.1)(1-0.8782) = 0.8904$$

NOMENCLATURE

A	proportionality constant, Eq. 2.4; integration constant, Eq. 6.45
A_a	integration constant, Eq. 6.46
A_ϕ	integration constant, Eq. 6.47
a	proportionality constant, Eqs. 2.4, 3.7, 6.21, 6.22; separation constant, Eqs. 6.40 and 6.41, for characteristic values viz. Eq. 6.55
B	transfer number, Eq. 3.4; integration constant Eq. 6.45
B_a	integration constant, Eq. 6.46
B_ϕ	integration constant, Eq. 6.47
b	viz Eq. 6.76
C	Cunningham slip factor, Eq. 5.5
C_T	integration constant, Eq. 6.48
C_ζ	integration constant, Eq. 6.49
c	specific heat capacity at constant pressure.
D	mass diffusivity
$D(\tau)$	Duhamel superposition integral driving function
D_j	jet diameter at vena-contracta
D_o	orifice diameter
d	droplet diameter
d_f	flame sheet diameter
d_m	minimum resolvable diameter
d_o	initial droplet diameter
$\dot{d}$	rate of change of droplet
E	activation energy
F_a	viz. Eq. 6.86
f	relative aperture (stop number)
$G(\tau)$	viz. Eq. 6.76

H gross heat of combustion

$H_a(\tau)$ viz. Eq. 6.81

h heat transfer coefficient

i stoichiometric ratio

K viz. Eq. 6.29

k thermal conductivity

L_o initial number of moles liquid, Eq. 6.1

L_f final number of moles liquid, Eq. 6.1

l separation constant, Eqs. 6.42 and 6.43

M ambient oxygen mass fraction, Eq. 3.4; Magnification, Eqs. 5.6 and 5.7

$M(a,b,x)$ Kummer's function[137]

m mass fraction

m_f terminal liquid phase mass fraction

m_o initial liquid phase mass fraction

m_s surface liquid phase mass fraction

m_v surface vapor phase mass fraction

$\bar{m}$ volumetric average mass fraction

$\dot{m}$ mass rate of droplet vaporization in a stagnant atmosphere

$\dot{m}_c$ mass rate of droplet vaporization with convection effects

$\dot{m}''$ mass rate of vaporization per unit droplet surface area

N number of particles in array

N_∞ ambient oxygen mole fraction

P_i partial pressure, component i

P_T ambient pressure

P_i vapor pressure, pure component i

Q specific latent heat of vaporization

q index parameter

R	droplet raduis
R_a	adsorbed radiant energy per unit mass vaporized
R_F	resolving power of film
R_L	resolving power of lens
R_o	initial droplet radius
r	radius; index parameter
s	dummy variable
S	interparticle spacing
S_n	spacing between particle n and a peripheral array particle
S_o	initial inteparticle spacing
T	temperature; separation variable, Eq. 6.39
T_f	flame temperature
T_g	ambient gas temperature
T_r	reference temperature for gas phase properties
T_s	droplet surface temperature
t	time
u	object-lens distance
V_j	jet velcity at vena-contracta
V_o	gas velocity in orifice
V_r	radial velocity
$\dot{v}$	volmetric flow rate
W	transformed mass fraction, Eq. 6.32
X	extent of vaporization, Eq. 6.88
x_i	liquid phase mole fraction, component i
x_{io}	initial liquid phase mole fraction, component i
x_{if}	final liquid phase mole fraction, component i
Y	fractional evolution of nitrogen, Eq. 6.87

y_i vapor phase mole fraction, component i

Z transformed spatial coordinate, Eq. 6.30

α thermal diffusivity

Δ depth of focus

$\simeq$ separation variable, Eq. 6.39

υ frequency

ξ separation variable, Eq. 6.39

Π product

π 3.14159

ρ gas density

ρ_ℓ liquid density

ρ_p particle density

Σ summation

σ coefficient of surface tension

η_A efficiency of evaporiation for a droplet array with respect to a isolated vaporizing droplet

θ normalized mass fraction profile, Eq. 6.58

λ vaporization rate constant, Eq. 3.6

μ dynamic viscosity

τ transformated temporal coordinate, Eq. 6.31

ϕ separation variable, Eq. 6.39

χ moles of combustion product per unit mass of fuel burnt in oxygen

Ω moles of oxygen for stiochiometric combustion per unit mass of fuel.

G_r Grashoff number

L_e Lewis number

Nu_d Nussult number, droplet vaporizing in a stagnant atmosphere

$Nu_{d,fc}$	Nussult number droplet vaporizing with forced convection
Pr	Prandtl number
Re	Reynolds number
[ ]	concentration, Eq. 2.4

REFERENCES

1. Hottel, H.C. and Howard, H.B., New Energy Technology, Some Facts and Assessments, M.I.T. Press, Cambridge, MA (1971).

2. Some Useful Fact on Energy, Gulf Oil Corp. (1981).

3. Averitt, P., "Coal Resources of the United States", U.S.Gt.S. Bull. 1275 (1969).

4. Chigier, N., Energy, Combustion and Environment, McGraw-Hill, Inc., New York (1981).

5. Hubbert, M.K., "U.S. Energy Resources: A Review as of 1972", A National Fuels and Energy Policy Study, Pt. 1, U.S. 93d. Congress, 2d. Session, Senate Committee on Interior and Insular Affairs, Ser. No. 93-40 (92-75) (1974).

6. Longwell, J.P., 16th. Symposium (International) on Combustion, p. 1, The Combustion Institute, Pittsburgh, PA (1977).

7. Sarofim, A.F. and Bartok, W., "Methods for Control of Nitrogen Oxide Emissions from Stationary Sources", A.I.Ch.E. Advanced Seminar, Philadelphia (1973).

8. Mason, H.B. and Shimzu, A.B., "Briefing Document for the Maximum Stationary Source Technology Systems Program for NO_x Control," Aero Therm Final Report 74-123, EPA Contract No. 68-02-1318 (1974).

9. Sarofim, A.F. and Flagan, R.C., "NO_x Control for Stationary Combustion Sources," Internal Report, Department of Chemical Engineering, M.I.T. (1975).

10. Crawford, A.R., Manny, E.H., and Bartok, W., "Field Testing: Application of Combustion Modifications to Control NO_x Emissions from Utility Boilers," Esso Research Engineering, Report No. EPA-650/2-74-066 (1974).

11. Bartok, W., Crawford, A.R., and Piegari, G.J., "Systematic Field Study of NO_x Emission Control Methods for Utility Boilers," Esso Research and Engineeirng Co., Report No. GRU. 4GNOS.71 to the Office of Air Programs, Research Triangle Park, North Carolina (1971).

12. Cato, G.A. and Robinson, J.M., "Application of Combustion Modification Techniques to Control Pollution Emissions from Industrial Boilers," KVB Engineering, Tustin CA, Interim Report-Phase I, under EPA Contract No. 68-02-1074 (1974).

13. Cato, G.A., Buening, H.J., DeVivo, C.C., Morton, B.G., and Robinson, J.M., "Field Testing: Application of Combustion Modifications to Control Pollutant Emissions from Industrial Boilers-Phase I," KVB Engineering, Tustin CA, Report No. EPA-650/2-74-078a (1974).

14. Fenimore, C.P., Combustion and Flame, 19, p. 289 (1972).

15. Turner, D.W. and Siegmund, C.W., "Staged Combustion and Flue Gas Recycle: Potential for Minimizing NO_x from Fuel Oil Combustion," Esso Research and Engineering Co., Presented at American Flame Research Committee/EPA Flame Days, Chicago (1972).

16. Turner, D.A., Andrews, R.L., and Siegmund, C.W., A.I.Ch.E. Symp. Ser., 68, p. 55 (1972).

17. McCann, C.R., Demeter, J.J., Orning, A.A., and Bienstock, D., "NO_x Emissions at Low Excess-Air Levels in Pulverized Coal Combustion," ASME Winter Meeting, Proceedings (1970).

18. Martin, G.B. and Berkau, E.E.,A.I.Ch.E. Symp. Ser., 68, p. 45 (1972).

19. Pershing, D.W., Brown, J.W., Martin, G.B., and Berkau, E.E., "Influence of Design Variables on the Production of Thermal and Fuel NO_x from Residual Oil and Coal Combustion," Presented at the 66th Annual A.I.Ch.E. Meeting, Philadelphia, PA (1973).

20. Flagan, R.C. and Appleton, J.P., Combustion and Flame, 23, p. 249 (1974).

21. Hazard, H.R., "Conversion of Fuel Nitrogen to NO_x in a Compact Combustor, "ASME Paper No. 73-WA/GT-2, Presented at the ASME Winter Annual Meeting of the Gas Turbine Division, Detroit, MI (1973).

22. Frazer, R.P. and Eisenklam, P., Trans. Instn. Chem. Engs., 34, p. 294 (1956).

23. Putnam, A.A., Benington, F., Einbinder, H., Hazard, H.R., Kettelle Jr., J.D., Levy, A., Miesse, C.C., Pilcher, J.M., Thomas, R.E., Weller, A.E., and Landey, B.A., "Injection and Combustion of Liquid Fuels," Battelle Memorial Institute, WADC Technical Report 56-344 (1957).

24. Orr, C., Particulate Technology, MacMillan Pub. Co., New York (1966).

25. "Biblography on Sprays, 2d. Ed.," The Pennsylvania State University (1953).

26. Perry, R.H. and Chilton, C.H., Chemical Engineer's Handbook, McGraw-Hill Inc., New York (1969).

27. Chigier, N.A, Prog. Energy Combust. Sci., 2, p. 97 (1976).

28. Giffen, E. and Muraszew, A., Atomization of Liquid Fuels, Chapman and Hall, London (1953).

29. Rosin, P. and Rammler, E., J. Inst. Fuel, 7, p. 29 (1933).

30. Dombrowski, N., Biochemical and Biological Engineering Science (Vol. 2), Academic Press (1968).

31. Chang, T.Y., "Combustion of Heavy Fuel Oil," Sc.D. Thesis, M.I.T., Cambridge, MA (1941).

32. Berglund, R.N. and Liu, B.Y.H., Env. Sci. and Tech., 7, p. 147 (1973).

33. Lerner, S.L., Homan, H.S., and Sirignano, W.A., "Multicomponent Droplet Vaporization at High Reynolds Numbers: Size, Composition and Trajectory Histories," Presented at the 73rd Annual A.I.Ch.E Meeting, Chicago (1980).

34. Axworthy, A.E., Schneider, G.R., Shuman, M.D., and Dayan, V.H., "Chemistry of Fuel Nitrogen Conversion to Nitrogen Oxides in Combustion," Rocketdyne Division, Rockwell International, Canoga Park CA, Report No. EPA-600/2-76-039 (1976).

35. Combustion-Generated Pollution, Science Research Council, Her Majesty's Printing Office, London (1976).

36. Levy, J.M., Longwell, J.P., and Sarofim, A.F., "Conversion of Fuel-Nitrogen to Nitrogen Oxides in Fossil Fuel Combustion: Mechanistic Considerations," M.I.T., Cambridge, MA, prepared for Energy and Environmental Research Corporation under subcontract EER-83182 of EPA Contract No. 68-02-2631 (1978).

37. Bowman, C.T., Prog. Energy Combust. Sci., 1, p. 33 (1975).

38. Glassman, I., Combustion, Academic Press, New York (1977).

39. Fabuss, B.M. Smith, J.O., and Satterfield, C.N., "Thermal Cracking of Pure Saturated Hydrocarbons," Advances in Petroleum Chemistry and Refining (Vol. 9), Academic Press (1966).

40. Dryer, F.L. and Glassman, I., "Combustion of Chain Hydrocarbons," Project Squid Workshop on Alternative Hydrocarbon Fuels: Combustion and Chemical Kinetics, Columbia, MD (1977).

41. Golden, D.M., "Pyrolysis and Oxidation of Aromatic Compounds," Project Squid Workshop on Alternative Hydrocarbon Fuels: Combustion and Chemical Kinetics, Columbia, MD (1977).

42. Vranos, A., "Liquid-Phase Reactions of Vaporizing Hydrocarbon Fuels," Project Squid Workshop on Alternative Hydrocarbon Fuels" Combustion and Chemical Kinetics, Columbia, MD (1977).

43. Mezey, E.J., Singh, S., and Hissong, D.W., "Fuel Contaminants, (Vol. 1)." Battelle Columbus Laboratories, Report No. EPA-600/2-76-177a (1976).

44. "Coal Conversion Systems Technical Data Book," Chicago Institute of Gas Technology, Contract No. EX-76-C-01-2286 (1978).

45. Cooper, B.R., "Scientific Problems of Coal Utilization," DOE Symp. Ser., 46 (1978).

46. Considine, D.M., Energy Technology Handbook, McGraw-Hill Inc., New York (1977).

47. Beer, J.M. and Hanson, S.P., "Combustion of Coal-derived Liquids and Shale Oil in Gas Turbine Combustors," Project Squid Workshop on Alternative Hydrocarbon Fuels: Combustion and Chemcial Kinentics, Columbia, MD (1977).

48. Zeldovich, Y.B., Acta Physicochimica U.S.S.R., 21, p. 577 (1946).

49. MacKinnon, P.J., Air Pollution Control Association Journal, 24, p. 237 (1974).

50. Fenimore, C.P., Combustion and Flame, 19, p. 289 (1972).

51. Takahashi, Y., "Development of Super-Low NO_x PM Burner," Mitsubishi Technical Bulletin No. 134, Mitsubishi Heavy Industries Ltd. (1979).

52. Eberius, K.H. and Just, T., "Atmospheric Pollution by Jet Engines," AGARD Conference Proceedings No. 125, p. 16 (1973).

53. Blauwens, J., Smets, B., and Peeters, J., 16th Symposium (International) on Combustion, p. 1055, The Combustion Institute, Pittsburgh, PA (1977).

54. Sarofim, A.F., Williams, G.C., Modell, M., and Slater, S.M., "Conversion of Fuel NItrogen to Nitric Oxide in Premixed and Diffusion Flames," the 66th Annual A.I.Ch.E. Meeting, Philadelphia, PA (1973).

55. Myerson, A.L., 16th Symposium (International) on Combustion, p. 1085, The Combustion Institute, Pittsburgh, PA, (1975).

56. Haynes, B.S., Iverach, D., and Kirov, N.Y., 15th Symposium (International) on Combustion, p. 1103, The Combustion Institute, Pittsburgh PA (1975).

57. Sarofim, A.F., Pohl, J.H., and Taylor, B.R., "Strategies for Controlling Nitrogen Oxide Emissions During Combustion of Nitrogen-Bearing Fuels," Internal Report, Department of Chemical Engineering, M.I.T. (1977).

58. Perkins, H.C., Air Pollution, McGraw-Hill Inc., New York (1974).

59. Singer, J.G., Combustion: Fossil Power Systems, Combustion Engineering Inc., Winsor, CT (1981).

60. Rawdon, A.H. and Sadowski, R.S., "An Experimental Correlation of Oxides of Nitrogen Emissions from Power Boilers Based on Field Data," A.S.M.E. paper 72-WA/PWR-5 (1972).

61. "Control Techniques for Nitrogen Oxide Emissions from Stationary Sources," National Air Pollution Control Administration, Publication AP-67 (1970).

62. Godsave, G.A.E., "The Burning of Single Drops of Fuel," National Gas Turbine Establishment, Reports R87, R88 (1951).

63. Godsave, G.A.E., "The Flow of Heat and Carbon Residue in Drops of Fuel,"National Gas Turbine Establishment, Report R125 (1952).

64. Godsave, G.A.E., 4th Symposium (International) on Combustion, p. 818, The Combustion Institute, Pittsburgh, PA (1953).

65. Godsave, G.A.E., Nature, 164, p. 708 (1949).

66. Maxwell, J.C., Scientific Papers, 11, p. 629 (1890).

67. Nussult, W., "Der Verbrennungsvorgang in der Kohlenstaubfeuerung," VDl, 68, p. 124 (1924).

68. Fuchs, N.A., Evaporation and Droplet Growth in Gaseous Media, Pergamon, London (1959).

69. Long, V.D., J. Inst. Fuel, 37, p. 522 (1964).

70. Goldsmith, M. and Penner, S.S., Jet Propulsion, 24, p. 245 (1954).

71. Wise, H., Lorell, J., and Wood, B.J. 5th Symposium (International) on Combustion, p. 132, Reinhold, New York (1955).

72. Hottel, H.C., Williams, G.C., and Simpson, H.C., 5th Symposium (International) on Combustion, p. 101, Reinhold, New York (1955).

73. Spalding, D.B., 4th Symposium (International) on Combustion, p. 847, Williams and Wilkins, Baltimore (1953).

74. Spalding, D.B., Fuel, 29 (2), p. 25 (1950).

75. Kotaki, S. and Okazaki, T., Int. J. Heat and Mass Transfer, 12, p. 595 (1969).

76. Krier, H. and Wronkiewicz, J.A., Combustion and Flame, 18, p. 159 (1972).

77. Rosner, D.E. and Chang, W.S., Comb. Sci. and Tech., 7, p. 145 (1973).

78. Crespo, R. and Linãn, A., Comb. Sci. and Tech., 11, p. 9 (1975).

79. Hubbard, G.L., Denny, V.E., and Mills, A.F., Int. J. Heat and Mass Transfer, 16, p. 1003 (1973).

80. Law, C.K., Combustion and Flame, 26, p. 17 (1976).

81. Wise, H. and Ablow, C.M., J. Chem. Phys., 27, p. 389 (1957).

82. Ranz, W.E. and Marshall, W.R., Chem. Engr. Progr., 48, p. 141 (1952).

83. Agoston, G.A., Wise, H., and Rosser, W.A., 6th Symposium (International) on Combustion, p. 708, Reinhold, New York (1957).

There is no text material missing here.
Pages have been incorrectly numbered.

84. Eisenklam, P., Arunachalam, S.A., and Weston, J.A., 11th Symposium (International) on Combustion, p. 715, The Combustion Institute, Pittsburgh, PA (1967).

85. How, M.E., J. Inst. Fuel, 39, p. 150 (1966).

86. Goldstein, S., Proc. Roy. Soc. (London), 123A, p. 318 (1933).

87. Arrowsmith, A., Ph.D. Thesis, Department of Chemical Engineering and Fuel Technology, University of Sheffield (1970).

88. Carsten, J.C., Williams, A., and Zung, J.T., J. Atmospheric Sci., 27, p. 798 (1970).

89. Zung. J.T., J. Chem. Phys., 47, p. 3578 (1967).

90. Labowsky, M., Chem. Eng. Sci., 31, p. 803 (1976).

91. Ray, A.K. and Davis, E.J., Chem. Eng. Commun., 6, p. 61 (1980).

92. Williams, A.L., Carstens, J.C., and Zung, J.T., Advances, in Chemistry Series, 166, p. 54, American Chemical Society (1978).

93. Samson, R., Bedeaux, D., and Deutch, J.M., Combustion and Flame, 31, p. 223 (1978).

94. Chiu, H.H. and Liu, T.M., Comb. Sci. and Tech., 17, p. 127 (1977).

95. Newbold, F.R. and Amundson, W.R., A.I.Ch.E. J., 19. p. 22 (1973).

96. Wood, B.J. Wise, H., and Inami, S.H., Combustion and Flame, 4, p. 235 (1960).

97. Law, C.K. and Law, H.K., "A d^2-law for Multicomponent Droplet Vaporization and Combustion," AIAA 19th Aerospace Sciences Meeting (1981).

98. Law, C.K., Combustion and Flame, 26, p. 219 (1976).

99. Law. C.K., A.I.Ch.E. J., 24 (4), p. 626 (1978).

100. Landis, R.B. and Mills, A.F., "Effect of Internal Diffusional Resistance on the Evaporization of Binary Driplets," 5th International Heat Transfer Conference, Tokyo (1974).

101. Savic, P., "Circulation and Distortion of Liquid Drops Falling through a Viscous Medium," National Research Council of Canada, Mechanical Engineering Report MT-22 (1953).

102. Prakash, S. and Sirignano, W.A., "Liuqid Fuel Droplet Heating with Internal Circulation," Presented at the Central States Section meeting of the Combustion Institute, Cleveland, OH (1977).

103. Law, C.K., Chung, S.H., and Srinivasan, N., "Experimental and Theoretical Re-examination of the Classical d^2-law of Droplet Combustion," Presented at the Western States Section Meeting of the Combustion Institute, Provo, UT (1979).

104. Sirignano, W.A. and Law, C.K., Advances in Chemistry Series, 166, p. 3, American Chemical Society (1978).

105. Masdin, E.G. and Thring, M.W., J. Inst. Fuel, 35, p. 251 (1962).

106. Kobayasi, K., 5th Symposium (International) on Combustion, p. 141, Reinhold, New York (1955).

107. Bolt, J.A. and Saad, M.A., 6th Symposium (International) on Combustion, p. 717, Reinhold, New York (1957).

108. Hall, A.R. and Diederichsen, J., 4th Symposium (International) on Combustion, p. 837, Williams and Wilkins, Baltimore (1953).

109. Agoston, G.A., Wood, B.J., and Wise, H., Jet Propulsion, 28, p. 181 (1958).

110. Goldsmith, M., Jet Propulsion, 26, p. 172 (1956).

111. Graves, C.C., Proceedings of the 3rd. Midwestern Conference on Fluid Mechanics, p. 759, Minneapolis, MN (1953).

112. Spalding, D.B., Fuel, 30, p. 121 (1951).

113. Monaghan, M.T., Siddal, R.G., and Thring, M.W., Combustion and Flame, 12, p. 45 (1968).

114. Kumagai, S. and Isoda, H., 6th Symposium (International) on Combustion, p. 726, Reinhold, New York (1957).

115. Spalding, D.B., Fuel, 32, p. 169 (1953).

116. Udelson, D.G., Combustion and Flame, 4, p. 93 (1962).

117. Eisenklam, P. and Arunachalam, S.A., Combustion and Flame, 10, p. 171 (1966).

118. Burgoyne, J.H. and Cohen, L., Proc. Roy. Soc. (London), A225, p. 375 (1954).

119. Bolt, J.A. and Boule, T.A., ASME Trans., 78, p. 615 (1956).

120. Wolfehard, H.G. and Parker, W.G., J. Inst. Pet., 35, p. 118 (1949).

121. Sundokov, I.N. and Predvokitelov, A.S., 7th Symposium (International) on Combustion, p. 352, The Combustion Institute, Pittsburgh PA (1959).

122. Topps, J.E.C., J. Inst. Pet., 37, p. 535 (1951).

123. Shyu, R.R., Chen, C.S., Goudie, G.O., and El-Wakil, M.M., Fuel, 51, p. 135, (1972).

124. Chen, C.S. and El-Wakil, M.M., Proc. Inst. Mich. Eng., 184 (3J), p. 95 (1969).

125. Sakai, T., Kito, M., and Saito, M., 14th Symposium on Combustion, Japan, p. 68 (1976).

126. Archer, J.S. and Eisenklam, P., J. Inst. Fuel, 43, p. 397 (1970).

127. Braide, K.M., Isles, G.L., Jordan, J.B., Williams, A., J. Inst. Energy, 52, p. 115 (1979).

128. Schneider, J.M. and Hendricks, C.D., Res. Sci. Instrum., 35 (10), p. 1349 (1964).

129. Lindblad, N.R. and Schneider, J.M., J. Sci. Instrum., 42, p. 635 (1965).

130. Mims et al., "Laboratory Studies of Trace Element Transformations During Coal Combustion," Presented at the 87th National A.I.Ch.E. Meeting, Boston, MA (1979).

131. Connor, W.D., Air Pollut. Control Assoc. J., 16, p. 35 (1966).

132. Photography with Large-Format Cameras, Kodak publication O-18 (1977).

133. Carroll, J.S., Photographic Lab Handbook, Amphoto, Garden City, NY (1977).

134. Vogel, A.I., Elementary Practical Organic Chemistry, Longmans, London (1966).

135. Van Winkle, M., Distillation, McGraw-Hill Inc., New York (1967).

136. Reyleigh, Phil. Mag., 4 (6), p. 521 (1902).

137. Abramowitz, M. and Stegun, I.A., Handbook of Mathematical Functions, Dover Publ. Inc., New York (1965).

138. Fedoseeva, N.V., Advances in Aerosol Physics, 1, p. 21. (1971).

139. Fong, L., S.B. Thesis, M.I.T., Cambridge, MA (1980).

140. Vargaftik, N.B., Tables on the Thermophysical Properties of Liquids and Gases, Wiley, New York (1975).